UNIVERSITY OF BELGRADE

FACULTY OF MECHANICAL ENGINEERING

ABULGASEM. M. SAEED SGHAYER

FATIGUE LIFE ASSESSMENT OF DAMAGED INTEGRAL SKIN –STRINGER PANELS

DOCTORAL DISSERTATION

BELGRADE, 2018

UNIVERZITET U BEOGRADU
MAŠINSKI FAKULTET

ABULGASEM. M. SAEED SGHAYER

PROCENA ZAMORNOG VEKA OŠTEĆENIH INTEGRALNIH OPLATA-UZDUŽNICI PANELA

doktorska disertacija

Beograd, 2018

SUPERVISOR :

Dr Aleksandar Grbović, vanredni profesor,

Univerzitet u Beogradu, Mašinski fakultet

.....

BOARD OF COMMISSION

Dr Aleksandar Sedmak, redovni profesor,

Univerzitet u Beogradu, Mašinski fakultet

.....

Dr Dragan Milković, vanredni profesor

Univerzitet u Beogradu, Mašinski fakultet

.....

Dr Katarina Čolić, naučni saradnik,

IC MF Beograd

.....

Dr Gordana Kastratović, vanredni profesor Univerzitet u Beogradu,

Saobraćajni fakultet

……

Data of defence ……

Acknowledgements

This is the end of my journey in obtaining my PhD. I have not travelled in a vacuum in this journey. This thesis has been seen through to completion with the support and encouragement of numbers people including my good wishes, my friends and colleagues. At the end of my thesis, I would like to thank all those people who made this thesis possible and an unforgettable experience for me. First of all, I would like to thank to my PhD advisors, Professor **Aleksandar Grbović** for supporting me during these past three years and sharing his great knowledge and experience with me. Without his supervision and constant help this dissertation would not have been possible. Under his guidance I successfully overcame many difficulties and learned a lot.

I would also thank to Professor Aleksandar Sedmak for his guidance and suggestions as Head of Department. I appreciate the help offered by Dr. Blagoj Petroveski .

I would like to pay high regards to my father, mother, brothers, and who I love for their sincere encouragement and inspiration thorough my research work and lifting me uphill this phase of life. I owe everything to them.

Finally, my deep appreciation is addressed to my lovely wife Fadia and my sweet sons Ishaq and Yaqub for their patience during the period of my study.

ABSTRACT

Fatigue life of integral skin-stringer panels produced by laser beam welding (LBW) is analysed in this thesis. This type of panel is usually used in airframe structure where fatigue and damage tolerance are of paramount importance, since aircraft must be designed to tolerate relatively large fatigue cracks. In this work numerical models of skin-stringer panel were developed, computer simulation were carried out and results were compared to experimental values from fatigue tests of panels made of Al6156-T6/2.8 mm (LB welded). The main aim was to validate a numerical method for fatigue life prediction of damaged skin-stringer panels. This is why a fracture mechanics approach was used in the first place and why models were analyzed using the Extended Finite Element Method (XFEM) through code ABAQUS. Another methods were also used: analytical for static and fatigue strength assessment of welded joints (based on FKM guidelines) and Finite Element Method (FEM) for laser beam welding process simulation and identification of heat affected zone. Numerical simulation of LBW showed significant amount of residual stresses which must be treated before exposing skin-stringer panels to variable external load.

In order to evaluate fatigue life of damaged panels (i.e. the life of panels with crack initiated in the middle of the base metal) and consequently improve the damage tolerance performance of integral structures, Morfeo/Crack for Abaqus code was used. This code calculates coordinates of the 2D or 3D crack fronts (as cracks grow through the structure) and distribution of stress intensity factors K_I, K_{II} and K_{III} along the crack front (effective stress intensity factor K_{eff} is also calculated). Then, Paris law is used for estimation of number of cycles that will grow crack to critical length. Values of fatigue life of skin-stringer panels obtained by XFEM method were close to those obtained in the experiment, but in some cases differences were about 30%. It was discovered that difference was caused by not adequately defined mesh; this is why the influence of the element size on the fatigue life estimation was also analyzed in thesis. But, it must be emphasized that numerical models of this size (scale 1:1) were never used before, and that all fatigue life values obtained in numerical simulations were less than experimental values. This means that all predictions were conservative, i.e. on the safe side.

In order to increase life of damaged skin-stringer panels so-called clips are used. Numerical models with clips were also made, calculations carried out and results compared with experimental

values for panels without clips. Longer fatigue life was obtained in simulations with clips, justifying the use of these elements for fatigue life extension. However, experimental investigations must be carried to confirm these numerical findings, but this thesis gives basis for next steps.

Key words: finite element analysis, XFEM, stress intensity factors, crack modelling, crack propagation, laser beam welding, fatigue strength assesment

Scientific field: Mechanical Engineering

UDC number: 629.7.024: 621.791.05: 620.19 (043.3)

SAŽETAK

Zamorni vek integralnih oplata-uzdužnici panela dobijenih metodom laserskog zavarivanja jeste osnovna tema ove teze. Integralni paneli se obično koriste u vazduhoplovnim strukturama kod kojih su zamor i tolerancija oštećenja od velike važnosti, pošto letelice moraju biti projektovane tako da izdrže i pojavu rekativno velikih zamornih prslina. U ovom radu su razvijeni numerički modeli oplata-uzdužnici panela, sprovedene su kompjuterske simulacije na njima i dobijeni rezultati su upoređeni sa eksperimentalnim vrednostima iz testova na zamor panela debljine 2.8 mm od aluminijuma Al6156-T6. Cilj sprovedenih numeričkih simulacija i poređenja sa eksperimentom bio je verifikacija numeričkih modela za predviđanje veka pod zamorom oštećenih oplata-uzdužnici panela. U tu svrhu su korišćeni parametri mehanike loma, a modeli su analizirani pomoću proširene metode konačnih elemenata (PMKE) integrisane u kompjuteski kod ABAQUS. Pored ove metode korišćene su i druge: analitička, za procenu statičke i zamorne čvrstoće zavarenih spojeva (a na osnovu smernica definisanih u FKM standardima) i klasična metoda konačnih elemenata za simulaciju procesa laserskog zavarivanja i identifikaciju zone uticaja toplote. Numerička simulacija laserskog zavarivanja je pokazala da nakon samog procesa postoje zaostali naponi u materijalu koji se moraju tretirati pre nego što se oplata-uzdužnici paneli izlože spoljašnjem promenljivom opterećenju.

U svrhu procene zamornog veka oštećenih integralnih panela (tj. veka panela sa prslinom iniciranom na sredine osnove) i potom poboljšanja njihovog ponašanja sa aspekta zamora, korišćen je softverski kod Morfeo/Crack for Abaqus. Ovaj kod izračunava coordinate 2D i 3D fronta prsline kako se prslina širi kroz strukturu, a potom i raspodelu faktora intenziteta napona K_I, K_{II} i K_{III} duž fronta prsline (vrednosti efektivnog faktora intenziteta napona K_{eff} se takođe određuju). Potom se koristi Parisov zakon za procenu broja ciklusa spoljnjeg opterećenja koji će prslinu proširiti do kritičnih dimenzija. Vrednosti zamornog veka oplata-uzdužnici panela dobijene na ovaj način, korišćenjem PMKE, bile su bliske eksperimentalnim, ali je u nekim slučajevima razlika bila oko 30%. Utvrđeno je da je tolika razlika bila plod nedovoljno dobro definisane mreže konačnih elemenata; iz tog razloga je uticaj broja čvorova i elemenata mreže (tj. njene gustine) takođe analiziran u ovoj tezi. Mora se, međutim, istaći da numerički modeli ovih dimenzija (razmere 1:1) ranije nisu bili korišćeni i da su svi zamorni vekovi dobijeni u simulacijama bili kraći nego oni u

eksperimentima. To znači da su sva predviđanja dobijena numerikom bila konzervativna, odn. na strani sigurnosti.

Da bi se produžio zamorni vek oštećenih oplata-uzdužnici panela koriste se ojačanja u vidu tzv. klipova. Numerički modeli panela sa klipovima su takođe napravljeni, sprovedeni su proračuni i vrednosti broja ciklusa su upoređene sa vrednostima iz eksperimenata sa panelima bez klipova. Dobijen je veći broj ciklusa nego u eksperimentu, što opravdava korišćenje ovakvih elemenata za produženje zamornog veka oštećenih panela. Međutim, potrebna su dalja eksperimentalna istraživanja da bi se potvrdili numerički rezultati, ali ova teza daje dobru osnovu za sledeće korake u tom pravcu.

Ključne reči: analiza konačnim elementima, proširena metoda konačnih elemenata, faktori intenziteta napona, modeliranje prslina, rast prslina, lasersko zavarivanje, procena zamorne čvrstoće

Naučna oblast: mašinsko inženjerstvo

UDC broj: 629.7.024: 621.791.05: 620.19 (043.3)

Nomenclature

a Crack length

a 0 Initial crack length

E Young's modulus

F Applied force

J-integral

K Stress intensity factor

KI Mode-I stress intensity factor

$Keff$ Effective stress intensity factor

ν Poisson's ratio

C Constant (in Paris equation)

m Constant (in Paris equation)

da/dN Fatigue crack growth rate

ΔK Stress intensity factors range

R Stress ratio

N number of cycles

Abbreviations

BOAC British overseas aircraft company

FAR Federal Aviation Regulations

DSG design service goal

NTSB National Transportation Safety Board

DOC direct operating cost

SIF(s) stress intensity factor(s)

XFEM extended finite element method.

LEFM linear elastic fracture mechanics

CTOD crack tip opening displacement

FEM Finite Element Method

BEM Boundary Elements Method

BM base material

FSW Friction Stir Welding

LBW laser beam welding

SN stress level versus number of cycles (curve)

VCCT virtual crack closure technique

GDC generalized form displacement correlation method

MCCI modified crack closure integral

PUM Partition of unity method

DOF degrees of freedom

PUFEM partition of unity finite element method

FKM ForschungsKuratorium Maschinenbau

TABLE OF CONTENTS

List of Figures

List of tables

Chapter 1: INTRODUCTION

1.1Back ground

Typical riveted skin-stringers structures have been introduced in aircraft fuselage assemblies since the 1940's, and then widely used in many parts of the aircraft (as shown in Figure 1.1). It seems that it is difficult to get significant improvement in this technology because of the advancement made during the last century. Integral skin-stringer structures, which make skin and stringers as a continuum, are suitable to change the situation, even though they are poor at damage tolerance performance. Compared with the conventional riveted structures, integral skin-stringer structures have many advantages, such as lower weight and lower cost to manufacture. It is worthy of note that, fewer components mean they are easy to inspect and no holes in riveted joints improve fatigue crack initiation life.

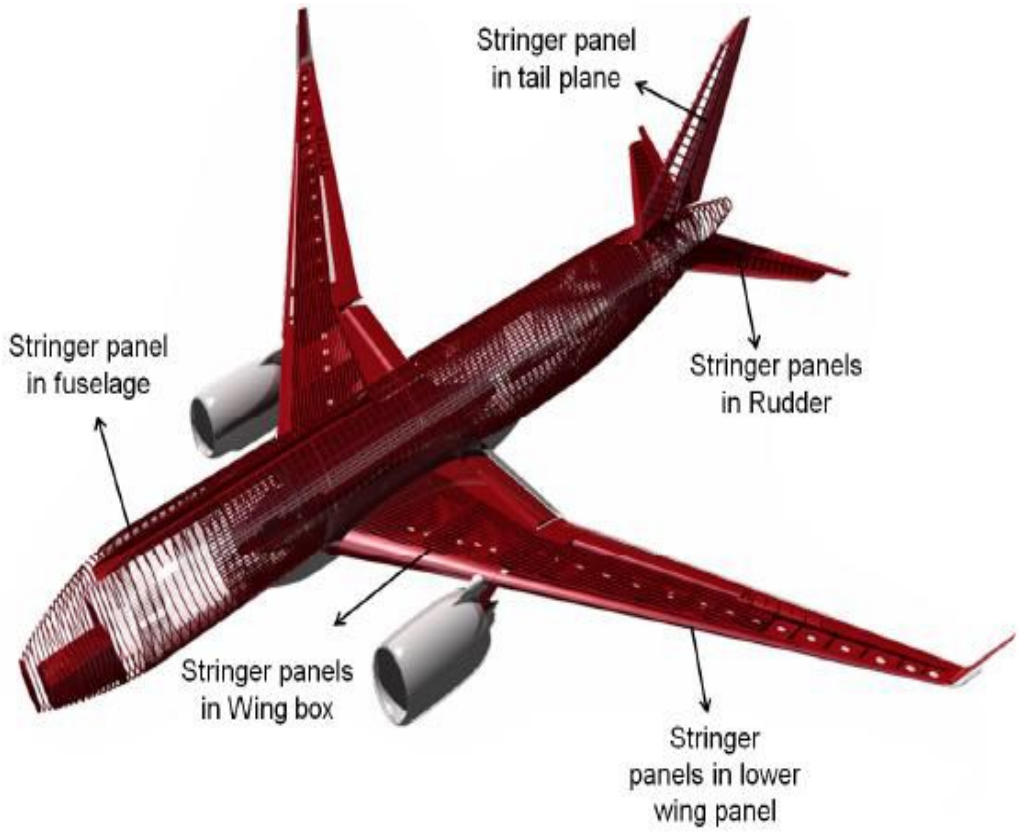

Figure 1.1 Locations of stringer panels in the aircraft

NASA began Integral Airframe Structures (IAS) Program to develop integral metallic structures in 1966 [1.1]. The purpose of the program was to design and test structures, which were lower in price than the current structures and improvement in structural weight and performance. The IAS program obtained satisfactory results with the improvement and the application of integrally stiffened fuselage structure. The configuration of integral aircraft fuselage structure and conventional fuselage structure are compared in Figure 1-2.

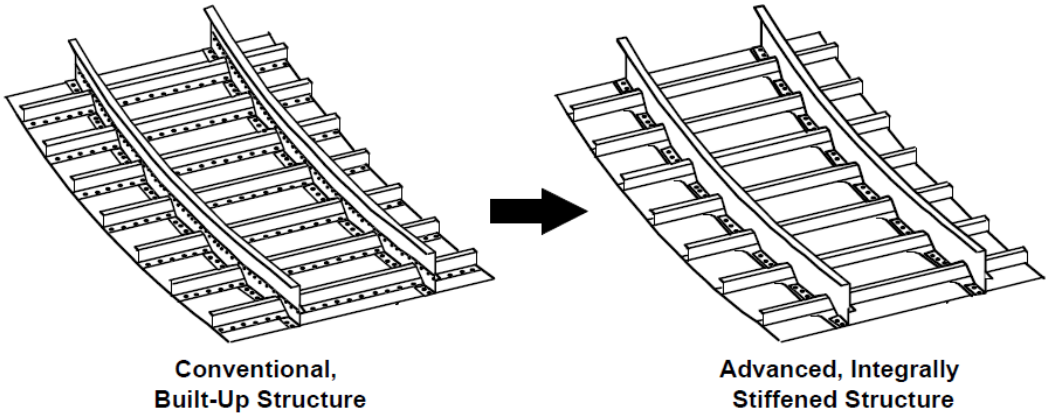

Figure 1.2 Integral aircraft structure and conventional structure [1]

In recent years, the technology of design, analysis integral structures have become one of the key technologies for the widespread use of the integral metallic skin-stringer structures in the aerospace field. Two different methods are used in order to optimize the damage tolerance performance of the integral skin-stringer panels. The first one is to apply new alloy materials with lower crack propagation rate and higher fracture toughness. Another one is to design or optimize new structure conformation. In order to achieve the latter objective, many researchers have been done research to develop efficient and reliable methods to improve the damage tolerance performance of integral skin-stringer panels [1.2].

1.2 Laser Beam Welding Joining Technology.

Riveting has been the state of the art joining technology in the aeronautical industry for decades and it has demonstrated its value and reliability. But the necessary overlap joint demands large amounts of material and its production chain is also time consuming. New processes such as LBW and Friction Stir Welding (FSW) present new solutions to overall weight savings and process time reduction. These processes are continuously under improvement and their application is still to be broadened. It has been observed in larger metallic structures of models such as in the A318, A340 and A380 that LBW has advantages compared to conventional riveted fuselages. Regarding the production of structures, LBW can be up to 20 times faster than riveting. LBW is characterized by high energy concentration with high welding speed, narrow Heat Affected Zones (HAZ), deep penetration effect and low remaining component distortion after welding [1.3]. Another advantage is that the process only requires one-sided access. Lower fuselage panels made of AA6xxx series (Al-Mg-Si-Cu) and processed with LBW as an efficient joining technology are already established in the market, figure 1.3. In fact, LBW has been applied with AA6013 and AA6056 as part of the skin and AA6110 or AA6056 for the stringer. These AA's provide higher buckling strength and lower weight compared with riveted design . High potential has also been found on the AA5xxx series for welded structures due to the ease to weld it and good properties after welding [1.4].

Figure 1.3: LBW panels in the A380 [Airbus source].

The AA2xxx series, which is a copper alloy type, is highly used for aircraft sheet construction, as is the case of AA2024 fuselages but this specific AA is not good for welding. Now it is possible to use laser-weld able AA's of the 2xxx series such as AA2198 [1.4].

Nevertheless, there are some limitations in the use of LBW. For the case of aluminum, when it is subjected to heat, it suffers large deformations which are due to its high thermal expansion coefficient and these may induce panel distortions. Low energy input is, therefore, desirable in order to reach the given production tolerances. Another limitation of welding aluminum is that it cannot be in contact with air. Helium or argon are used as shielding inert gases around the area where the welding process takes place. Another problem of welding materials with lithium is the large pore formation in laser weld seams [1.3]. As a consequence, the strength in the HAZ is reduced, sometimes by as much as 50%, due to the thermal treatment the material receives during welding. The introduction of the LBW method requires a transfer from riveted differential build up structures to laser welded integral structures, as seen in figure 1.4, and the introduction of high strength materials. One of the current challenges for LBW is to provide appropriate, crack free joints with low porosity, resulting in high mechanical performance of the welded joint [1.5].

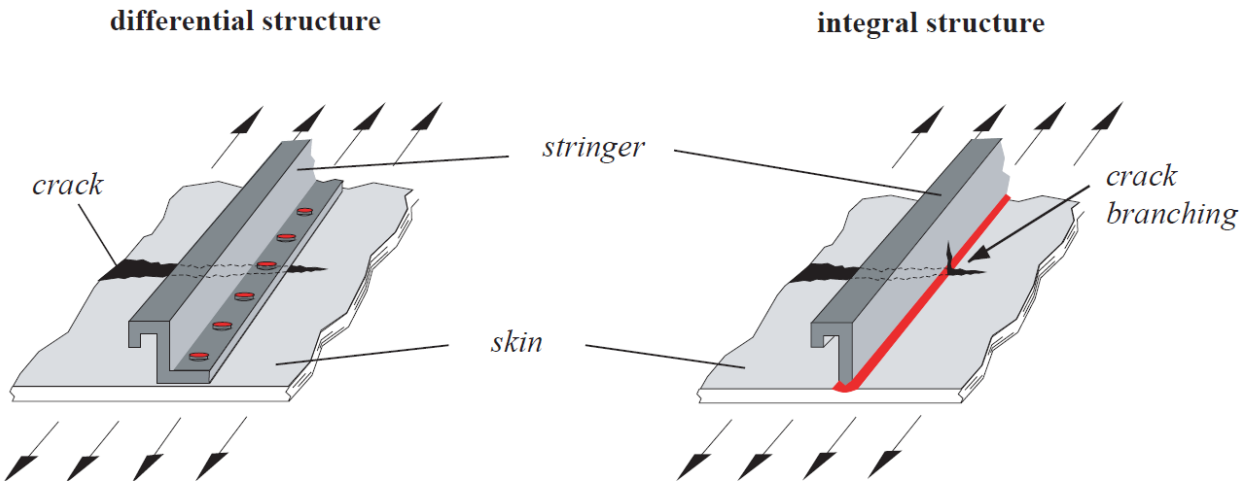

Figure 1.4: Difference between crack in a differential riveted and integral welded structures [1.6].

Despite manufacturing precautions, cracks may appear in integral skin-stringer structure and reduce its stiffness and the load-carrying capacity. The safe operation of pressurized fuselage structure is ensured through the operation of damage tolerant design and evaluation, which intended to certify that fatigue, corrosion, or other mechanisms should cause crack to grow within the operational life, so that the remaining structure can withstand reasonable loads without failure or excessive structural deformation until the damage is detected. Two types of damage most frequently associated with the structural integrity of the fuselage are longitudinal cracks under hoop stresses (induced by cabin pressurization) and circumferential cracks under stresses from vertical bending of the fuselage [1.7]. A critical element of damage tolerant design in pressurized fuselage is the ability to predict the growth rate of fatigue cracks under known applied loading.

The crack growth stage is studied by using stress intensity factor (SIF). SIF is fundamental quantity that governs the stress field near the crack tip. It depends on the geometrical configuration, crack size and the loading conditions of the body. There are many methods used in the numerical fracture mechanics for SIFs calculations. The crack opening displacement (COD) method, as well as the force method, was popular in early applications of finite element method (FEM) to fracture analysis [1.7]. The virtual crack extension (VCE) methods, proposed by Parks [1.8] and Hellen [1.9], led to increased accuracy of SIF results. The VCE method requires only one complete analysis of a given structure to calculate SIF. Both the COD and VCE methods can be used to calculate SIF for all three fracture modes. However, additional complex numerical procedures have to be applied to get results.

FEM has been used for decades for calculating SIFs, but it has some restrictions in crack propagation simulations mainly because the finite element mesh needs to be updated after each propagation step in order to track the crack path. Extended finite element method (XFEM) suppresses the need to mesh and remesh the crack surfaces and is used for modeling different discontinuities in 1D, 2D and 3D domains. XFEM allows for discontinuities to be represented independently of the FE mesh by exploiting the Partition of unity finite element method (PUFEM) [1.10]. In this method additional functions (commonly referred to as enrichment functions) can be added to the displacement approximation as long as the partition of unity is satisfied. The XFEM uses these enrichment functions as a tool to represent a non-smooth behavior of field variables.

There are many enrichment functions for a variety of problems in areas including cracks, dislocations, grain boundaries and phase interfaces. Recently, XFEM and its coupling with level set method were intensively studied. The level set method allows for treatment of internal boundaries and interfaces without any explicit treatment of the interface geometry.

Due to the relatively short history of the XFEM, commercial codes which have implemented the method are not prevalent. There are however, many attempts to incorporate the modeling of discontinuities independent of the FE mesh by either a plug-in or native support. Cenaero [1.11] has developed a crack growth prediction add-in Morfeo/Crack for Abaqus which relies on the implementation of the XFEM method available in Abaqus software. Problems involving static cracks in structures, evolving cracks, cracks emanating from voids etc., were numerically studied and the results were compared against the analytical and experimental results to demonstrate the robustness of the XFEM and precision of Morfeo/Crack for Abaqus [1.12].

The cracks are represented with the help of two signed distance functions that are discretized on the same mesh as the displacement field with first-order shape functions. Method for representing the cracks in this application is exactly the same as described in [1.13]. After each step of the propagation simulation, the SIFs are computed from the numerical solution at several points along the crack fronts. Interaction integrals are used to extract the mixed-mode SIFs with the help of auxiliary fields. After that Paris-Erdogan fatigue crack growth model [1.14] based on the range of the stress intensity factor can be used for evaluation of the number of cycles that will grow crack to the critical length. This model is chosen because of its simplicity; however, it has been used for decades as a basic framework in fracture mechanics.

1.3 Numerical simulation of weld residual stresses.

The welding simulation has proven to be an efficient aid for the determination of the residual stress condition after the welding. This leads to the possibility of obtaining important statements about the residual stress condition in places where a measurement cannot be taken for geometrical reasons. Finite element analysis together with the equations of continuummechanics and irreversible thermodynamics (non-equilibrium thermodynamics) forms the basis for a successful analysis of welding processes. In thermodynamics, a change in the thermodynamic state of a system is irreversible if the system cannot be restored to its former state by infinitesimal

changes in some property of the system without expenditure of energy. Most systems found in nature are not in thermodynamic equilibrium because they are not isolated from their environment and are therefore continuously sharing matter and energy with other systems. This sharing of matter and energy includes being driven by external energy sources as well as dissipating energy.

Goldak et al. contributed to the development of welding analysis by developing a realistic heat source model to define the distribution of the flux on the surface of the bead-on plate weld and the power density throughout the volume of the weld. The analyses usingthese models apply not only to quasi-steady state conditions but also to the transients on starting and stopping the weld. Transient computation is important because thermal strain and thermal stress are almost always more severe at the beginning and the end of the welding process. He also performed a three dimensional (3D) transient computation of stress, strain, displacement, and temperature fields around a tack weld in a 12.7 mm thick butt joint of 1020 carbon steel with nonlinear thermo-elasto-plastic finite element analysis (FEA). In the present study, a 3D transient FE analysis was performed using commercial FE code SYSWELD to analyse the welding residual stresses of the various type of clip-skin weld. Since it is a short distance weld, where run-in and run-out positions would possess different residual stresses, a transient thermal analysis was necessary. Goldak's conical heat source model was used to model the LBW accurately. Temperature field data is experimentally obtained for comparison with that obtained by simulation and hence were used to modify the heat source model to calibrate the thermal simulation.

The complexity of welding FE analysis required some development stages by several studies using different FE codes. Some investigations are related here starting with Mok et al, who studied the numerical prediction of the welding residual stresses in a thick (26 mm) Tjoint of steel specimen with the FE code ABAQUS. The heat input from the electrode was simulated using a modified version of Goldak's double ellipsoidal heat source model. Two dimensional (2D) analyses were conducted with generalized plane strain elements. During the welding simulation, the specimen was not restrained and was free to distort. A timeindependent, thermo-elastic-plastic constitutive model was assumed. Strain hardening and the Bauschinger effect were modelled by a kinematic hardening model. The effect of allotropic phase transformations was neglected. The predicted results agreed reasonably well (within 50 MPa) with neutron diffraction measurements. Also a through-thickness stress gradient was predicted which is contrary to some researchers'

assumption of constant through-thickness stress. Another thermo-mechanical analysis using ABAQUS was conducted by Cañas et al. The residual stresses were determined in gas metal arc (GMAW) butt welded plates of the aluminium alloy AA 5083-O introducing simplified thermal hypotheses which, making use of an analytical thermal solution, omitting the actual ordering in time of the thermal actions. It was claimed that the use of the envelope of temperatures permitted the maximum reduction in the input data preparation, producing excellent results. The distribution of residual stresses obtained using a plane stress model was in very good accordance with the measurements obtained by means of the blind-hole technique. This agreement confirmed that it didn't seem necessary to include factors like the phase change, the creep or the modelling of the added metal. The plane strain model was unable to fit the distribution of experimental residual stresses. An uncoupled thermomechanical analysis approach was employed by Zain-ul Abdein et al. using ABAQUS as well to predict the residual stresses in LB bead-on plate welded 6056 T4 aluminium alloy thin plate. A cone-shaped volumetric heat source with Gaussian distribution and an upper hollow sphere was used to attain the required weld pool size and temperature fields. A 3D symmetric model of the test plate and support was incorporated. A good correlation was found between experimental and simulation results.

Sarkani et al. compared the residual stress fields in a welded T-joint computed by 3D models with those computed by 2D models. It was proven that the temperature distribution in the central zone of the joint could be captured successfully by a 2D finite element model by a technique that takes into account the heat transfer balance and welding speed. The residual stresses in the plane of the 2D model computed by that method showed fairly good agreement with those computed by the 3D model. All analyses were performed with ABAQUS. Kim et al. predicted the residual stress by a numerical simulation for modified 9Cr-1Mo steel multi-pass welds of V-butt and T-plate specimens induced by gas tungsten arc welding (GTAW) processes and compared the results with the experimentally determined residual stresses. Neutron diffraction technique is used to measure the residual stresses both on the surface and in the interiror of a thickness for the welded specimens. A finite element analysis using ABAQUS was carried out to calculate the residual stress distributions for the two types of welded specimens. Two dimensional idealization of a complex three dimensional geometry was assumed and 2D axisymmetric models were used. A transient thermal analysis was performed for a sequential addition of each weld bead. The weld

passes were modelled to be added to the weld region just before a welding for each pass by using the “born and death” option in the software. The mechanical analysis was modelled similarly for a sequential addition of each weld bead. Loading was supplied from the temperature-time history of the thermal analysis. The predicted residual stresses had a closeagreement with the measured data although there some differences, quantitatively.

Wu et al. used the general purpose FE package ANSYS in a butt welded BS 4360 steel plate. A 2D FE analysis with a plane strain model was used to simulate the three dimensional welding process since a quasi-steady state was assumed to exist in certain long welds under a uniform welding speed. The model was validated by comparison of its predictions with published residual stresses from experiments and other numerical simulations. A thermal and stress analysis was performed sequentially. It was however concluded that a nonlinear transient thermal analysis was necessary to trace the rapid change of temperature with time while a static analysis could be adopted for the stress analysis. However, a significant number of time points, at which the temperature results were to be read into the stress analysis, should be defined to capture the temperature gradient and give accurate residual stress results using the load steps option. In addition, radiation and latent heat from phase transformations could be ignored to simplify the modelling procedure. In a further study , an FE simulation of fillet metal inert gas (MIG) welded T-joint of steel material was studied. The main features of the essentially 2D analysis by means of ANSYS were ramped heat input function, temperature dependent material properties and element death and rebirth technique. A parallel experimental investigation allowed the assessment of plastic properties variations in the welding area. The model was validated by temperature history data from the tests. The calculated longitudinal residual stress distributions along the surfaces of the plate were found to be good agreement with the experimentally determined patterns. Li et al. investigated residual stresses in multi-pass welding of pipe-plate structure consisting of Q345 material. A 3D finite element analysis is performed using ANSYS code. The temperature distribution and its history in the welding model were computed by the heat conduction analysis. Then, the temperature history was employed as a thermal load in the subsequent mechanical elastic plastic calculation of the residual stress field. During the thermal analysis the model change option was used to simulate the weld metal deposition. After the completion of first welding pass, new elements were added to the model to simulate the weld metal deposition during the second welding pass. In the mechanical analysis, the kinematic hardening was taken into account. It is concluded

that the maximum tensile radial and the hoop stress occurred in the weld bead, and the maximum tensile axial stress occurred in the weld toe.

Another comparative study is conducted by Keppas et al. to determine residual stresses in a 3-bead letterbox-type repair weld on a 2 ¼ CrMo low alloy ferritic steel plate using a proposed simulation based on decoupled thermal and mechanical analyses and the "birth and death of elements" technique and by neutron diffraction. Parametric studies included modelling aspects such as 2D plane strain versus 3D analysis, re-melting of weld material during sequential bead deposition, melting of base plate near the fusion line and annealing. Despite the large length of the 3-bead plates, 2D plane strain analysis is found to over-predict longitudinal stresses as compared to a full 3D simulation. Incorporating annealing in the analysis, the predicted transverse residual stresses were affected significantly however longitudinal stresses are not sensitive to this modelling aspect. Predicted stresses were compared with neutron diffraction testing data. It is concluded that numerical results were, in general, in satisfied agreement with the experimental data. Mousavi et al. performed a 3D finite element analyses by element birth and death technique to analyze the residual stresses produced in the tungsten inert gas (TIG) grooved butt welding process of 304L stainless steel material. The effect of geometry configurations on the residual stress distributions were predicted from the 3D computer analysis using a thermoelastoplastic constitutive equation and compared with the results from X-ray diffraction analysis.

Temperature dependent material properties were used and the effects of conduction, radiation and convection due to both air and inert gas flow rate were considered in the simulation. Simulation results showed that the peak of the tensile residual stress obtained for the ugrooved configuration was less than that predicted for the v-grooved configurations. The predicted residual stresses were in good agreements with those obtained by the X-ray diffraction experiments. The best agreement between the residual stress distributions and the X-ray experiments was obtained using the kinematic and isotropic hardening constitutive equations.

Preston et al. developed an FE model taking into account the history-dependence of the yield stress-temperature response of TIG bead-on plate welded 2024 T3 aluminium alloy during welding. The FE predictions were validated against high resolution X-ray synchrotron diffraction measurements of residual strain. It was shown that the effect of the temperature history was weak for that alloy. The dominant requirement for that alloy was to use an appropriate short time-scale for softening of the material in selecting the yield stresstemperature response. It was anticipated

that the effect of history could be greater in higher strength alloys and tempers, which suffer a greater degree of softening during welding. Cramer et al. also studied the residual stresses in aluminium welded joints. The residual stresses were established on selected evaluation paths not only on the surface with the radiographic procedures but also across the plate thickness with the hole drilling procedures. MIG welded complex structure of the engine mounting from the automobile industry was investigated. An FE model of half the system was elaborated and hybrid meshing was carried out with volume and shell elements. The volume elements were used in the region around the weld so that the steep three-dimensional gradients of the temperature and the stresses could be portrayed. With regard to both the longitudinal and transverse residual stresses, it is showed that a comparison of the residual stresses from the radiographic measurement and the FE calculation resulted in very good congruence not only in the level of the residual tensile stress peaks but also in their qualitative course. In addition, hole drilling procedure offered the possibility of establishing courses across the depth.

Teng et al. studied on residual stress analysis in T-joint fillet welds of SAE 1020 steel material by using thermal elasto-plastic analysis in the FEA. The technique of element birth and death was used to simulate the weld filler variation with time. Additionally the effects of flange thickness, welding penetration depth and restraint condition of welding on residual stresses were discussed. It is found that a high transverse stress and a very large stress were produced near the fillet weld toe. Moreover, the tensile residual stress near the fillet weld toe increased with increasing flange thickness. With increasing penetration depth or heat input in fillet welding, the the tensile residual stress near the fillet weld toe decreased. Lee et al. investigated the circumferential variations of residual stresses in circumferential welds of KS SPPS 42 carbon steel pipes and the effects of diameter (thickness ratio ranging from 10 to 100) on residual stress distribution using a 3D uncoupled thermo-mechanical FE analysis. It is demonstrated that the axial and hoop residual stresses were generally influenced by the pipe diameter in the thin walled pipe welds. In the thick
walled pipe welds similar tendency is expected to exist except for the complex residual stress distributions induced by the multi-pass welding, which was planned to be investigated in a

future work. As can be understood from the referred studies, the FE analyses of the welding process toyield residual stresses have been satisfactorily progressed being a powerful tool to enable the process and design optimization of the weld joints. [1.15]

1.4 Problem definition and adopted approaches.

Leight-weight welded components with high strength are of essential interest for all branches that produce moving masses , the goal is enhancing effective payload and property reliability of structures. These goals may be pursued through materials science, manufacturing techniques and design engineering. These three disciplines are mutually dependent and it is through their interaction that progress is achieved. LBW offers the possibility to manufacture joints of all light metals such as aluminium, titanium, magnesium and their combinations. The high potential of laser welding technologies has been proven through successful applications in the automotive, aeronautics and aerospace industries. Aluminium alloys are major materials for light-weight constructions especially in the transportation industry due to their good mechanical properties and low density. An appropriate joining technology is the laser beam welding process, because of its low localised energy input resulting in low distortion and high processing speeds. This concentrated heat input leads to narrow but deep weld seams. Despite the numerous advantages, LBW may suffer from statistically occurring seam imperfections like notches or holes in the seam which reduce the mechanical properties of the joint. However, using optimum process parameters and filler wire adapted to the alloy and weld geometry, weld qualities are possible, which fulfil the requirements of the aircraft industry, where estimates of risks are normally done in a most conservative way. Currently, LBW of Al-alloys of 6xxx and 2xxx grades require use of filler wire with high Si-content.

The weld zones generally exhibit “strength undermatching” which causes difficulties for the designers to fulfil the strength requirements,the safe operation of many structures and components is ensured through the operation of damage tolerant design and evaluation, which intended to certify that fatigue, corrosion, or other mechanisms should cause crack to grow within the operational life of the system, so that the remaining structure can withstand reasonable loads without failure or excessive structural deformation until the damage is detected. A critical element of damage tolerant design in many systems is the ability to predict the growth rate of fatigue cracks growing through the structure under known applied loading. Effective stress state of the welded

components considering residual stress fields, in this context, is highly significant. Residual stresses exist in many manufactured components, as a consequence of the thermal or mechanical processing applied during production. Local plastic deformation of a material will produce residual stress variation; as will rapid cooling from elevated temperatures as in the case of fusion welding, where the material's yield strength is usually significantly lower than at room temperature. It is crucial to predict quantitatively how a given residual stress field will enhance or degrade fatigue crack growth rates. When a residual stress field is present, a growing fatigue crack is likely to exhibit a different growth rate from a crack growing in residual stress free material. This has obvious implications for lifing components where a damage tolerant approach is adopted, assuming a known fatigue crack growth rate and load cycle characteristics. If not taken into account, a tensile stress field can lead to an overestimate of the component life, while a compressive residual stress could give a conservative life. The aim is to design and manufacture components with compressive residual stresses which will lead to retardation of crack growth and hence improved damage tolerance performance. This was possible to a certain extent in conventional riveted structures and should also be possible for advanced welded integral Al-alloy components or sub-structures, such as stiffened panels.[15]

The basis for this thesis is the report presented on "European Workshop on Short Distance welding Concepts for airframes - WEL-AIR" on June 2007 that is created on the basis of damage tolerance analysis of 4-stringer flat panels that are jointly made by the Airbus division in Bremen and GKSS Research Center Geesthacht (Hamburg) – Germany. By courtesy of project participants, the results of fatigue test of laser beam welded short distance clip welds using 4-stringer flat panels, were available for inspection and they were used as reference for verification of fatigue life values obtained by numerical simulations using XFEM and FKM to evaluate stress results, in particular with cyclic stresses. The FKM guideline "Analytical Strength Assessment of Components" describes a static strength assessment as well as a fatigue strength assessment. WB/FKM facilitates the evaluation of an FEM analysis by carrying out strength assessment according to the FKM guideline for the analytical models.

1.5 Thesis Outline.

This research is divided into 7 chapters, which look at achieving the above objectives; the details of each chapter are given below:

- **Chapter 1:** Introducing the importance of the development of welding technology.
- **Chapter 2:** presents a critical review of the issues affecting fatigue design approaches.
- **Chapter 3**: In this chapter introduces briefly the analysis methods for SIF (stress intensity factor) Calculation and crack growth life prediction for integral stiffened panels.
- **Chapter 4:** Analytical and numerical assessment of fatigue strength integral ,in this chapter describes a static strength assessment as well as a fatigue strength assessment
- **Chapter 5:** In this chapter, Numerical simulations of crack growth in damage integral skin stringer panel using XFEM.
- **Chapter 6:** Experimental Validation of Numerical Results (XFEM).
- **Chapter 7:** This chapter concludes the results and discussion.

Chapter 2: LITERATURE SURVEY

2.1. Historical Accidents Related To Fuselage Fatigue.

This Chapter presents a critical review of the issues affecting fatigue design approaches. The applications of damage tolerant methodology for plates with stringer reinforcement have been also presented. The design of aircraft including the development, and testing programs are mentioned. The safety is of the foremost concern to the aircraft design. The investigations normally lead to new research and development, improved design, and modified regulations.

2.1.1 Damage Tolerance Design Philosophy.

Historically, there are three different approaches to ensure the safety of an aircraft structure: Safe-life, fail-safe and damage tolerance [2.1]. Safe-life, introduced in the 1930's, takes a philosophy of safety by retirement. The life of a structure is the number of flights, landings, or flight hours during which there is a low probability that the strength will degrade below its design strength. It assumes that, throughout its entire life, all identified loads are low enough and the strength high enough to sustain them. In the fail-safe philosophy, introduced in the 1950's, a structure is capable of sustaining a certain amount of damage without catastrophic failure of the entire structure. To ensure this, the design approach considers additional load path elements in case one of the elements fails.

The specification of necessary inspection intervals is based on the service experience and does not consider the initiation and growth of cracks. Finally, introduced in 1978, the damage tolerance philosophy assumes that the structure contains an initial defect that will grow under service usage. It requires fracture mechanics based engineering evaluation of crack growth and residual strength characteristics to establish the inspection intervals. The main objective is to detect and monitor cracks in the structural elements before they propagate to failure. In the Federal Aviation Regulations (FAR), part 25, section 571, it is stated that" an evaluation of the strength, detail design and fabrication must show that the catastrophic failure due to fatigue, corrosion, or accidental damage, will be avoided throughout the operational life of the air plane" [2.2]. For all primary structures with the exception of the landing gear the damage tolerance design and evaluation is required [2.3]. A crack extending into two frame bays with the central frame also cut

is generally assumed. The structure is considered to comply with the regulations if, under the specified conditions, it arrests the skin within two frame bays.

On January 10, 1954, a British Overseas Aircraft Company (BOAC) de Havilland Comet I aircraft, on its way to London from Rome, suffered a midair disintegration at about 30,000 feet and crashed into the Mediterranean Sea off the island of Elba. At the time of the accident, the aircraft, registration number G-ALYP (known as Yoke Peter) had flown 3,680 hours and had experienced 1,286 pressurized flights [2.4]. Comet I aircraft was the first high-altitude transport jet aircraft ever flown, which enabled the aircraft to achieve a much higher altitude, therefore extending its range and increasing its efficiency. This aircraft was capable of maintaining a cabin pressure differential of almost twice that of any other aircraft in service at that time [2.4]. The Comet I fleet was grounded for modifications after the GALYP incident. Two weeks after reinstatement, on April 8, 1954, a second Comet (Yoke Yoke), on its way to Cairo from Rome, crashed near Naples. Yoke had accumulated 2,703 flight hours and 903 flight cycles. The Comet accidents were later found to be related to fatigue cracks caused by the high stresses at corners of the automatic direction-finding window. The fuselage cabin for this airplane was substantiated by static pressurization. These accidents raised concerns on how fatigue is addressed in the regulations for jet transport aircraft, and resulted in inclusion of fatigue requirements in the regulations.

2.1.2. Aloha Airlines Accident.

On 28 April 1988, Aloha airlines Flight 243, a Boeing 737-200, suffered a midflight explosive decompression while undertaking a regularly scheduled passenger flight from Hilo to Honolulu, Hawaii. The explosion, which occurred at 24,000 feet above the Pacific Ocean, caused a disintegration of a 17ft section of the crown of the fuselage.

There were 95 people on board this flight: 89 passengers, two-flight crew, three flight attendants, and an FAA air traffic controller in the jump seat. Remarkably, the only fatality was the senior flight attendant who was sucked out of the aircraft during the explosive decompression. A photo of the aircraft after the accident is shown in Figure 2.1

The aircraft had been placed in service in 1969, and had accumulated 35,496 flight hours and 89,680 flight cycles. The design service goal (DSG) of that aircraft was 75,000 cycles. The 19 year old aircraft had averaged about 13 flights a day during its time of service, and had the second

highest flight cycles in the entire B737 fleet. In the accident report [2.5], the National Transportation Safety Board (NTSB) concluded, among others, that the fuselage failure initiated at the lap joint along stringer S-10L as a result of multiple site fatigue cracking along the upper rivet row of the lap joint combined with disbonding of the lap joint. Because of the disbond, there were high stress concentrations at the knife-edges of the countersunk rivet holes, resulting in fatigue crack initiation. The NTSB concluded that the long term effects of disbonding, the associated corrosion, and fatigue cracking in lap joints was not considered in the 150,000-cycle test during certification. Response to the Aloha Airlines accident included research initiatives, industry activities, and government regulations. [2.6]

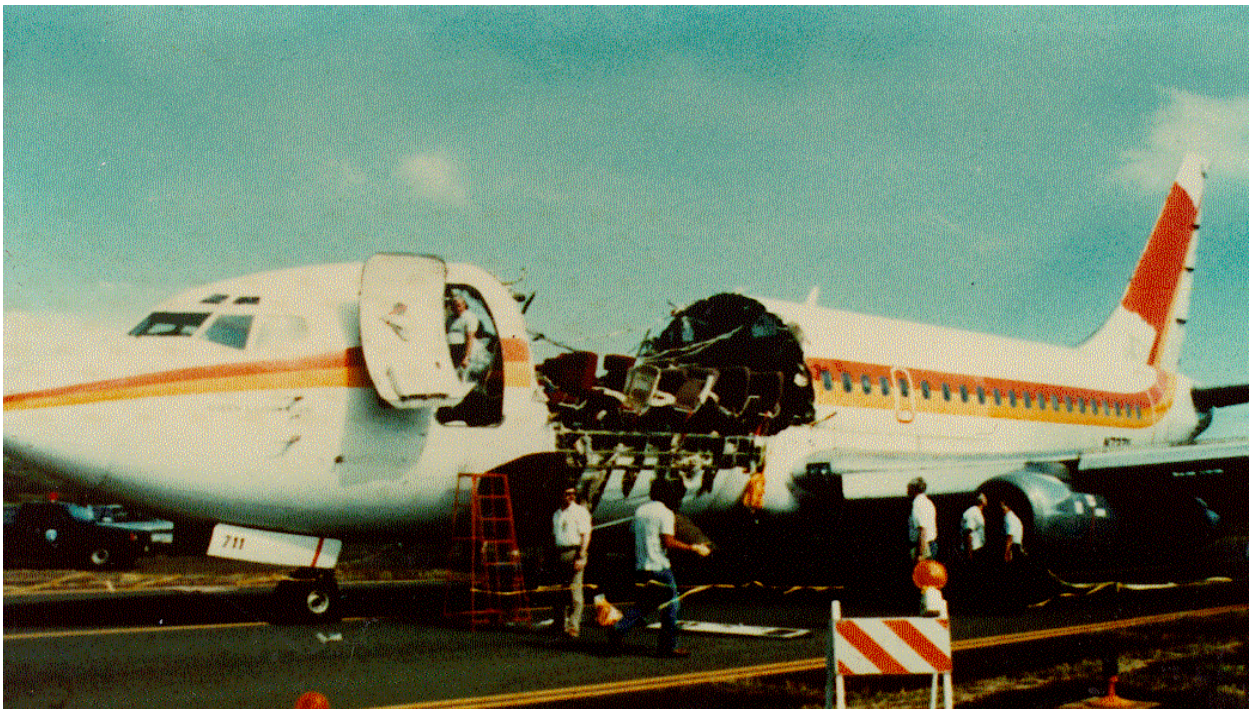

Figure 2.1. Catastrophic accident of Aloha Airlines B737.

2.1.3 Industrial revolution-1960

Fatigue is a process of local strength reduction. The phenomenon is often referred to as a process of damage accumulation in a material undergoing fluctuating loading. This process occurs in engineering materials such as metallic alloys, polymers and composites. To describe the mechanical fatigue process as result of a repeated load working on a structure, different parameters

are used, like cyclic load, stress intensity and crack growth rate. The maximum load is P_{max}, the minimum P_{min} [kN] and the ratio between the minimum and maximum load (P_{min}/P_{max}), that is often used as a measure of the mean stress, is called the load ratio R. Crack growth rate da/dN is the crack increment da per loading cycle increment dN. The stress intensity factor K [MPa√m], working on the crack tip is calculated from the applied load P and actual crack length and direction in a construction. The maximum stress intensity is Kmax, the minimum Kmin and the difference between both is ΔK, see figure 2.2. Fluctuating loads can lead to fluctuating local high stresses and microscopic small cracks may appear. Once a crack exists in a structure, it will tend to grow under cyclic loading. Even if the maximum of the cyclic load on a construction is below the elastic limit of the material, fatigue may lead to failure. Fatigue is a progressive process the damage develops slowly in the early stages and near the end of a structure's life, and it accelerates very quickly towards failure.

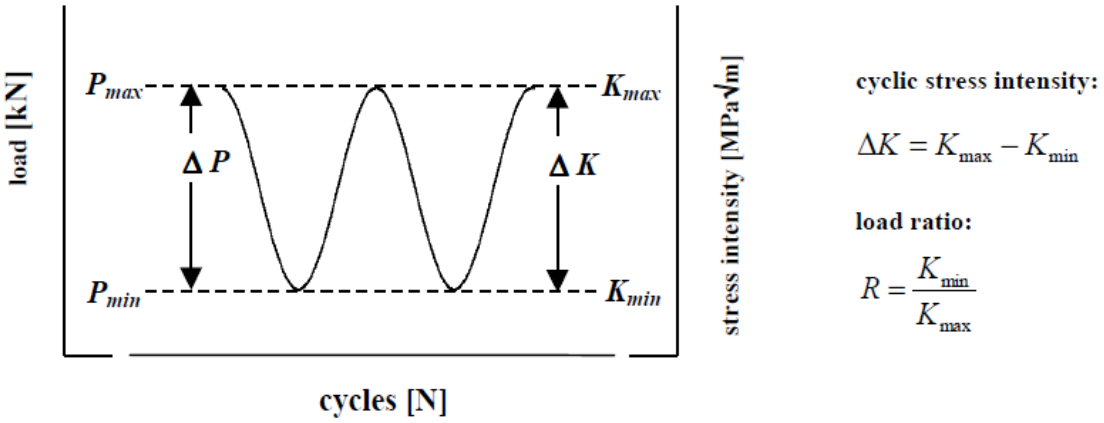

Figure 2.2. Mechanical parameters to describe the fatigue loading system.

However, details of the fatigue process may differ between materials. The fatigue process can be defined generally as [2.7] "The process of the cycle-by-cycle accumulation of local damage in a material undergoing fluctuating stresses and strains."

- **description of the phenomenon.**

Fatigue of metals in structures has been studied since the beginning of the 19th century. Railroads, bridges, steam engines: a whole gamut of new structures and machines were developed, which

were made of steel in the times of the industrial revolution. Many of them were exposed to cyclic stresses during service life and many of them failed, the origin of failure was unknown, until Albert [2.8] made the first report about failure caused by fatigue, in 1829. He observed failure of iron mine-hoist chains, caused by repeated small loads. Ten years later, in 1839, Poncelet, a professor of mechanics at the école d'application, Metz, introduced the term fatigue in his lectures. Rankine [2.9] recognized the importance of stress concentration in 1843.
He noted that fracture occurs near sharp corners. However, until then the phenomenon was described qualitatively only.

- **Systematic experiments and microscopic observations.**

Wöhler made a major step in 1860. Wöhler, a railroad engineer, started performing systematic experimental research on railroad axles. He observed that steel would rupture at stress below the elastic limit if a cyclic stress were applied. However, there was a critical value of cyclic stress, the fatigue limit, below which failure would not occur. He found a way to visualize "time to failure" for specific materials. In this S-N-curve approach the stress amplitude, σa is plotted as function of the number of cycles to failure, see figure 2.3 [2.10].

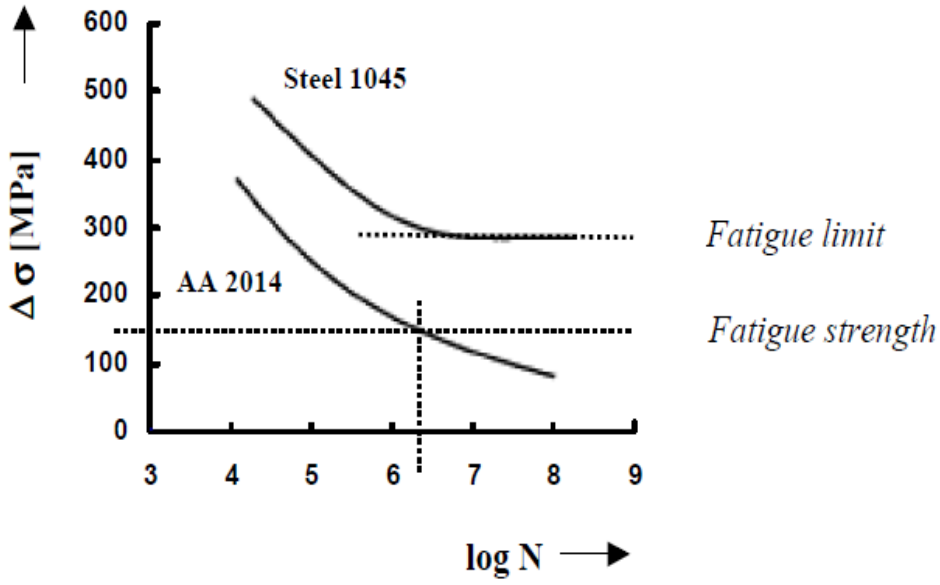

Figure 2.3. S-N curves for low-carbon steel (fatigue limit) and AA 2014 (no fatigue limit).

A logarithmic scale is used for the horizontal axis, while the stress is plotted using either a linear or logarithmic scale.

Fatigue limit: the stress below which a material can be stressed cyclically for an infinite number of times without failure.

Fatigue strength: the stress at which failure occurs for a given number of cycles.

The first crack surface investigations where made by Ewing [2.11] in 1903. He showed the nature of fatigue cracks, using a microscope, see figure 2.4.

Figure 2.4. Crack surface showed by Ewing & Humfrey, 1903

- **Explanations and predictions.**

Around 1920 Griffith investigated the discrepancy between the theoretical strength of a material, and the true value, sometimes 1000 times less than the predicted value. He discovered that many microscopic cracks and/or other imperfections exist in every material. He assumed that these small cracks lowered the overall strength. Because of the applied load, high stress concentrations are expected near these small cracks, which magnify the stresses at the crack tip. These cracks will grow more quickly, thus causing the material to fail long before it ever reaches its theoretical strength. Any voids, corners, or hollow areas in the internal area of the material also result in stress concentrations. Mostly fracture will begin in one of these areas, simply because of this phenomenon [2.12].

2.1.4 after 1960: Paris and Elber.

An important push to understand the fatigue process was made by Paris and Elber. In 1961, Paris found a more or less linear correlation on double logarithmic scales between crack growth rate da/dN and cyclic stress intensity factor ΔK for some part of the fatigue curve, see figure 2.5 [2.13]. This well-known Paris' law reads:

$$da / dN = C\Delta K^m \qquad (2.1)$$

Where $\Delta K = K_{max} - K_{min}$ and C and m are experimentally determined scaling constants

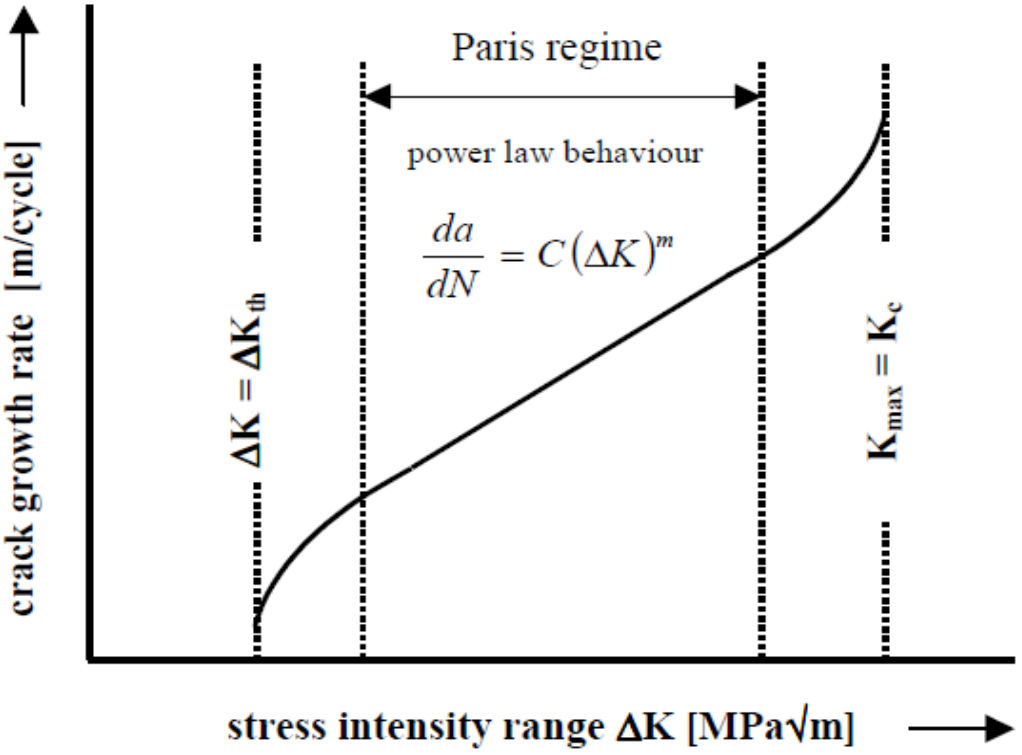

Figure 2.5. Paris' Law: linear correlation between crack growth rate da/dN and stress intensity factor _K on log-log scale.

Paris' law is generally accepted for a wide range of different materials; however, the physical meaning is limited. The major issue at that time was how to explain stress ratio effects. In 1970, Elber published a famous article titled "Fatigue Crack Closure under Cyclic Tension"

[2.14]. In this article, he assumed crack closure to be the cause of stress ratio-effects. By crack closure, he meant contact of the crack surfaces, at a load above the minimum load. Elber assumed that, when crack closure occurs, the effective cyclic stress intensity range ΔKeff that works on the crack tip, is lower than the expected or applied ΔK-range, see figure 2.6. The crack growth rate is no longer a result of the whole ΔK magnitude, but only of a part of it.

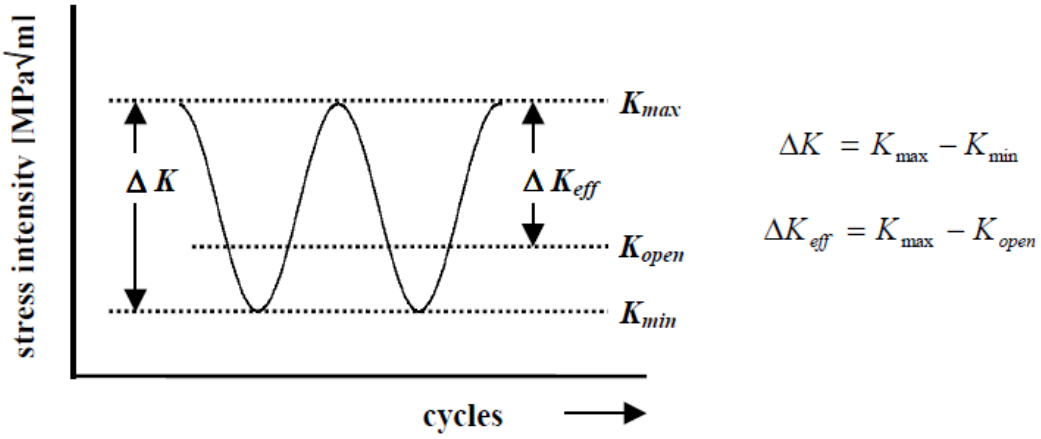

Figure 2.6. Principle of Elber's crack closure theory.

2.2 Fracture Mechanics

When performing a proof of strength, flawless components can generally be assumed. Under certain circumstances, potential discontinuities are taken into account with increased safety factors. Yet the existence of defects and cracks can fundamentally alter the strength behavior of components and structures. For example, technical products sometimes fail well below the static strength level or fatigue strength of the material). Technical fracture mechanics an interdisciplinary subject linking engineering mechanics and materials engineering, assumes the existence of cracks in components and structures as a matter of principle. Cracks can possess small dimensions in the micrometer range, but they can also be relatively large in size, e.g. in the range of a millimeter or even a meter. Typical crack types that often arise in components and structures.

The basis for fracture-mechanical concepts and methods is the investigation of circumstances in the immediate vicinity of the crack tip. By looking at local stresses in the area of the crack, stress and displacement fields appearing there, stress intensity factors and the fracture-mechanical material parameters that are relevant for cracks, concepts and methods are developed that make it possible to assess and predict stable and unstable crack growth. These basic circumstances and relationships will be described in the following.

2.2.1 Concept of Cracks.

Cracks are local separations of the material of a structure. These material separations disrupt the force flow in the component considerably. The force flow is sharply redirected, and a local singular stress field appears in the area of the crack tip or the crack front. Figure 2.7 b, c show the disturbance of the flow of force by cracks in comparison with a component without cracks, Fig. 2.7a.

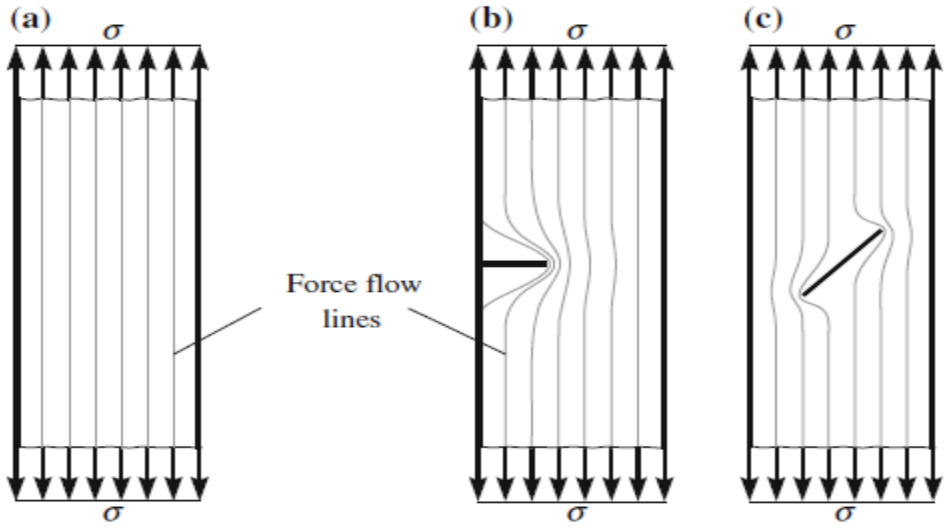

Figure. 2.7 Disturbance of the force flow path through cracks.

Force flow is defined as the transmission of forces or stresses through a component. Force flow lines can also be understood as stress level lines. Where force flow lines are sharply redirected and lie close to each other, high local stresses occur. A tensile-loaded plate without defects or cracks has a completely undisturbed force flow, Fig. 2.7 a. In a component with an edge crack, the force

flow lines are sharply diverted and compressed due to the crack, Fig. 2.7b. A stress concentration arises at the crack tip of—purely theoretically—infinitely high stresses. Figure 2.7 c shows the force flow path of a component with an inclined internal crack. Force transmission through the component has again been disturbed considerably.

However, in contrast to the force flow in Fig. 2.7 b, the force flow path is now asymmetrical with respect to the crack. Obviously, the crack (or in the vicinity of the crack) is being loaded differently in Fig. 2.7b than in Fig. 2.7c. Because of the simplicity of crack geometry—a crack is regarded as a mathematical section in fracture mechanics.

2.3 Fundamentals of Fatigue Crack Propagation.

Fatigue crack propagation, referred to as stage II in Figure 2.8, represents a large portion of the fatigue life of many materials and engineering structures. Accurate prediction of the fatigue crack propagation stage is of utmost importance for determining the fatigue life. The main objective of the fatigue crack propagation may be presented in this form: "Determine the number of the cycles N_c required for a crack to grow. from a certain initial crack size a_0 to the maximum permissible crack size a_c, and the form of this increase $a = a(N)$, where the crack length a corresponds to N loading cycles. "

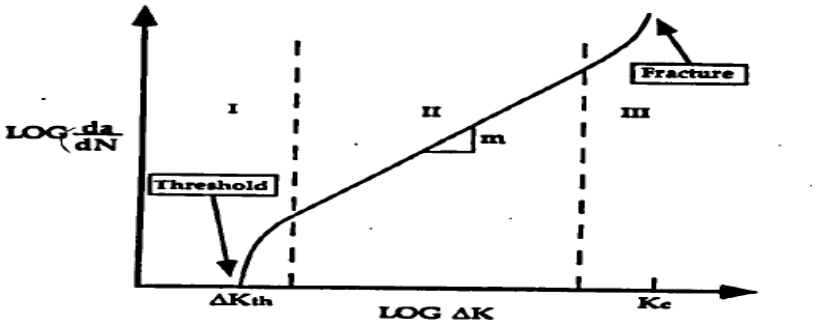

Figure (2.8) typical fatigue crack growth behavior in metals.

Fatigue crack propagation data are obtained from pre-cracked specimens subjected to fluctuating loads, and the change in crack length is recorded as a function of loading cycles. The crack length

is plotted against the number of the loading cycles for different load amplitudes. The stress intensity factor is used as a correlation parameter in analyzing

The fatigue crack propagation results. The experimental results are usually plotted in a log (ΔK) versus log (da/dN) diagram, where ΔK is the range of the stress intensity factor and da/dN is the crack propagation rate. The load is usually sinusoidal with constant amplitude and frequency. Two of the four parameters K_{max} , K_{min}, $\Delta K = K_{max} - K_{min}$ or $R = K_{min} / K_{max}$ are needed to define the stress intensity factor variation during a loading cycle.

A typical plot of the characteristic sigmoidal of a log(ΔK)- log(da/dN) fatigue crack growth rate curve is shown in Figure 2.9. Three regions can be distinguished. In region I, da/dN diminishes rapidly to a very small level, and for some materials there is a threshold value of the stress intensity factor range ΔK_{th} meaning that for $\Delta K < \Delta K_{th}$ no crack propagation takes place. In region II there is a linear log(ΔK) - log(da/dN) relation. Finally, in region III the crack growth rate curve rises and the critical stress intensity factor Kc, leading to catastrophic failure. Experimental results indicate that the fatigue crack growth rate curve depends on the ratio R, and is shifted toward higher da/dN values as R increases.

Cyclic stresses resulting from constant or variable amplitude loading can be described by two of a number of alternative parameters. Constant amplitude cyclic stresses are defined by three parameters, namely a mean stress, $\boldsymbol{\sigma}_m$., a stress amplitude, $\boldsymbol{\sigma}_a$, and a frequency ω, υ. The frequency is not needed to describe the magnitude of the stresses. Only two parameters are sufficient to describe the stresses in a constant amplitude loading cycle. It is possible to use other parameters; for example, minimum stress, $\boldsymbol{\sigma}_{min}$, and the maximum stress, $\boldsymbol{\sigma}_{max}$, to describe the stresses completely. The stress range, $\Delta\boldsymbol{\sigma} = \boldsymbol{\sigma}_{max} - \boldsymbol{\sigma}_{min}$, can also be used in combination with any of the others, except, $\boldsymbol{\sigma}_a$ In addition, another parameter is often convenient. This is the so-called stress ratio R, defined as R=. $\boldsymbol{\sigma}_{min} / \boldsymbol{\sigma}_{max}$

One of the above parameters can be replaced by the load ratio R to define the cyclic load. Any of the following combinations fully defines the stresses in a constant amplitude loading: $\Delta\boldsymbol{\sigma}$ and R, $\boldsymbol{\sigma}_{min}$ and R, $\boldsymbol{\sigma}_{max}$ and R. $\boldsymbol{\sigma}_a$ and R, and $\boldsymbol{\sigma}_m$. and R. The case of R=0 defines the condition in which the stress always rises from, and returns to 0. When R= -1, the stress cycles around zero as a mean, which is called fully reversed loading.

In order to study the parameters, which affect the fatigue crack growth a through thickness

crack is considered in a wide plate subjected to remote stressing that varies cyclically between constant minimum and maximum values, The stress range is defined as $\Delta\sigma = \sigma_{max} - \sigma_{min}$. The fatigue crack propagation rate is defined as the crack extension, Δa, during a small number of cycles, ΔN, the propagation rate is Δa / ΔN, which in the limit can be written as the differential da/dn. It has been found experimentally that provided the stress ratio $R = \sigma_{min} / \sigma_{max}$, is the same then ΔK correlates fatigue crack growth rates in specimens with different stress ranges and crack lengths and also correlates crack growth rates in specimens of different geometry. This correlation is presented in Figure 2.9. The data obtained with a high stress range, $\Delta\sigma_{high}$, commence at relatively high values of da/dN and ΔK. The data for a low stress range, $\Delta\sigma_{low}$, commence at lower values of da/dN and ΔK, but reach the same high values as in high stress range case.

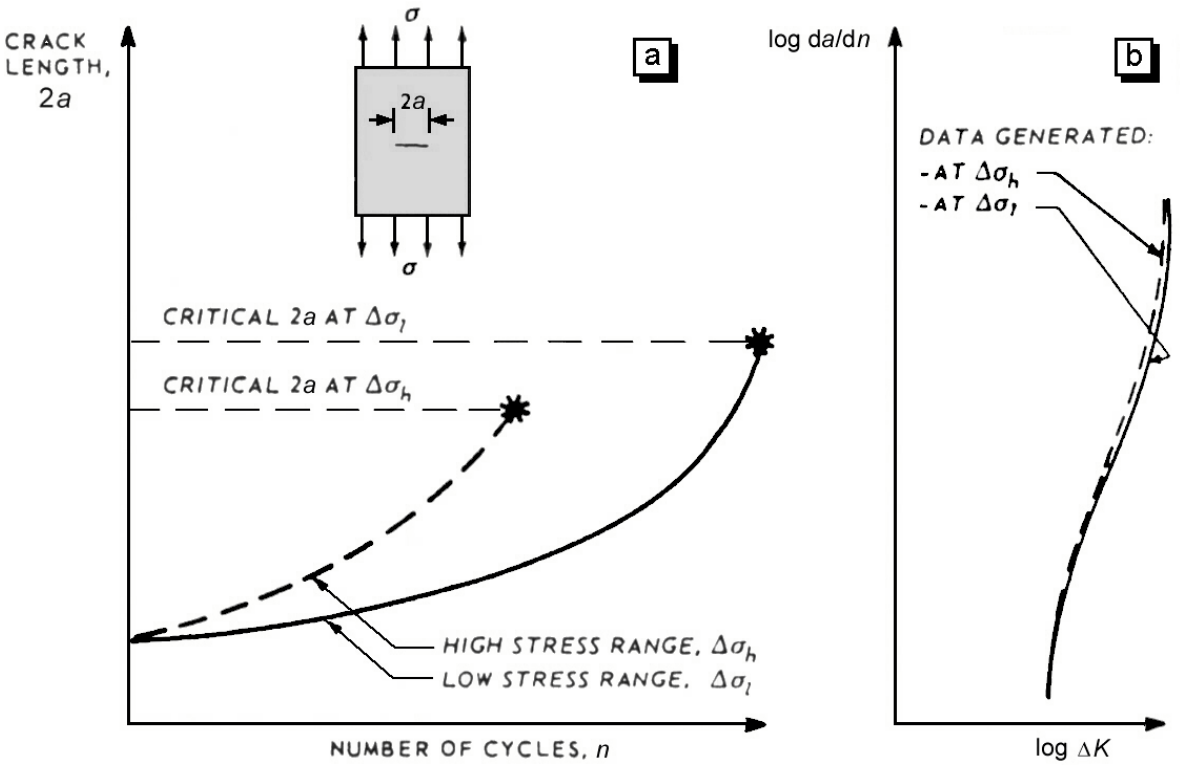

Figure (2.9) Correlation of fatigue crack propagation data by ΔKwhen the stress ratio, *R*, is the same.

In addition, the stress ratio R can have a significant influence on the crack growth behavior. In other words, besides the stress intensity factor range, ΔK, there is an influence of the relative values of K_{max} and K_{min} , since $R= \sigma_{min}/ \sigma_{max} = K_{max} / K_{min}$ .This is presented in Figure 2.10, which shows that crack growth rates at the same stress intensity range ΔK values are generally higher when the load ratio R is increasing. It is important at this point to note that the effect of the load ratio R has proved to be from the bibliography strongly material dependent. [2.16]

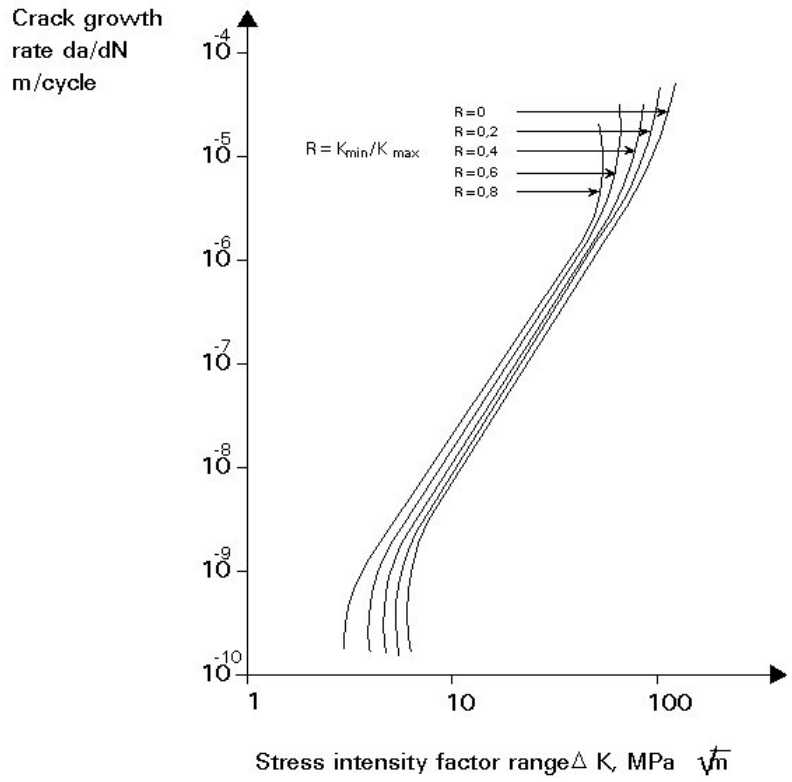

Figure (2.10) Effect of mean stress upon fatigue crack for Aluminum alloys.

A number of different quantitative continuum mechanics models of fatigue crack propagation have been proposed in the literature. All these models lead to relations based mainly on experimental data correlations. They relate da/dN to such variables as the external load, the crack length, the geometry and the material properties. One of the most widely used fatigue crack propagation laws is that proposed by Paris and Erdogan and is usually referred in the literature as the "Paris law". It has the form:

$$\frac{da}{dN} = C\,(\Delta K)^m \qquad (2.1)$$

Where $\Delta K = K_{max} - K_{min,}$ with K_{max} and K_{min} referring to the maximum and minimum values of the stress intensity factor in the load cycle. The constant C and m are determined empirically from a log(ΔK) - log(da/dN) plot. The value of **m** is usually taken equal to 4 for aluminum alloys, resulting in the so-called "4th power law" while the coefficient **C** is assumed to be a material constant. Paris Law equation represents a linear relationship between log (ΔK) and log (da/dN) and is used to describe the fatigue crack propagation. Experimental data are well predicted using Paris Law equation for specific geometrical configurations and loading conditions. The effect of mean stress, loading and specimen geometry is included in the constant C. ("Paris law") has been widely used to predict the fatigue crack propagation life of engineering components.

The crack growth mechanism shows that a fatigue crack grows by a small amount in every load cycle. Growth is the geometrical consequence of slip and crack tip blunting. Re-sharpening of the crack tip upon unloading sets the stage for growth in the next cycle. It can be concluded from this mechanism that the crack growth per cycle, Δa, will be larger if the maximum stress in the cycle is higher (more opening) and if the minimum stress is lower (more re-sharpening).The local stresses at the crack tip can be described in terms of the stress intensity factor K, where K= $\beta\sigma\sqrt{\pi a}$, if σ is the nominal applied stress. In a cycle, the applied stress varies from $_{min}$ to σ_{max} over range $\Delta\sigma$. Therefore, the local stresses vary in accordance with:

$$\mathbf{K_{min}= \beta\sigma_{min}\sqrt{\pi a}}$$

$$\mathbf{K_{max}= \beta\sigma_{max}\sqrt{\pi a}} \qquad \mathbf{(2.2)}$$

$$\mathbf{\Delta K = \beta\Delta\sigma\sqrt{\pi a}}$$

An amount of crack growth is defined as Δa in one cycle, which is expressed in m/cycle. If growth were measured over e.g. ΔN = 10000 cycles, the average growth per cycle would be $\Delta a/\Delta N$, which is the rate of crack propagation. In the limit where $N \rightarrow 1$, this rate can be expressed as the differential da/dN When a structural component is subjected to fatigue loading, a dominant crack reaches a critical size under the peak load during the last cycle leading to catastrophic failure. The basic objective of the fatigue crack propagation analysis is the determination of the crack size, a, as a function of the number of the cycles, N. Thus, the fatigue crack propagation life N_p is obtained. When the type of the applied load and the expression of the stress intensity factor are

known, application of one of the foregoing fatigue laws enables a realistic calculation of the fatigue crack propagation life of the component. As an example, consider a plane fatigue crack of the length $2a_0$ in a plane subjected to a uniform stress $\boldsymbol{\sigma}$ perpendicular to the plane of the crack. The stress intensity factor K is given by:

$$\boldsymbol{k = f(a)\sigma\sqrt{\pi a}} \qquad \textbf{(2.3)}$$

Where $f(a)$ is a geometry dependent function Integrating the fatigue crack propagation law expressed by equation (2.1) gives:

$$\boldsymbol{N - N_0 = \int_a^{a_0} \frac{da}{C(\Delta K)^m}} \qquad \textbf{(2.4)}$$

where No is the number of load cycles corresponding to the half crack length a_0 . Introducing the stress intensity factor range ΔK, where K is given from equation (2.2),
into equation (2.1) results in:

$$\boldsymbol{N - N_0 = \int_a^{a_0} \frac{da}{C\left[f(a)\Delta\sigma\sqrt{\pi a}\right]^m}} \qquad \textbf{(2.5)}$$

Assuming that the function $f(a)$ is equal to its initial value $f(a_0)$ so that

$$\boldsymbol{\Delta K = \Delta K_0\sqrt{\frac{a}{a_0}}}\ , \quad \boldsymbol{\Delta K_0 = f(a_0)\Delta\sigma\sqrt{\pi a_0}} \qquad \textbf{(2.6)}$$

Equation (2.5) gives :

$$\boldsymbol{N - N_0 = \frac{2a_0}{(m-2)C(\Delta K_0)^m}\left[1 - \left(\frac{a_0}{a}\right)^{\frac{m}{2}-1}\right]} \quad \textbf{for m} \neq \textbf{2 .} \qquad \textbf{(2.7)}$$

Unstable crack propagation occurs when

$$K_{max} = K_{IC} = f(a)\sigma_{max}\sqrt{\pi a} \quad (2.8)$$

from which the critical crack length a_0 is obtained. Then, the equation 2.5 for $a = a_0$ gives the fatigue crack propagation life $N_p = N_c - N_0$. Usually, however $f(a)$ varies with the crack length a and the integration of equation (2.5) cannot be performed directly, but only through the use of numerical methods.

2.4 Crack Closure Phenomenon in Fatigue Crack Propagation.

In the early 1960s, Paris, et al. [2.16, 2.17] demonstrated that fracture mechanics is a useful tool for characterizing crack growth due to fatigue phenomenon. Since that time, the application of fracture mechanics to fatigue problems has become almost routine. There are, however, a number of controversial issues and unanswered questions in this field. The procedures for analyzing fatigue under constant amplitude loading at small scale yielding conditions are fairly well established, although a number of uncertainties remain. The concept of similitude, when it applies, provides the theoretical basis for fracture mechanics. Similitude implies that the crack tip conditions are uniquely defined by a single loading parameter such as the stress intensity factor. Consider a growing crack in the presence of a constant amplitude cyclic stress intensity Figure 2.16. A cyclic plastic zone forms at the crack tip, and the growing crack leaves behind a plastic wake. If the plastic zone is sufficiently small, that is embedded within an elastic singularity zone, the conditions at the crack tip are uniquely defined by the current K value, and the crack growth rate is characterized by K_{min} and K_{max}. In order for the similitude assumption to be valid, the crack tip of the growing crack needs to be sufficiently far from its initial position, and external boundaries should be remote.

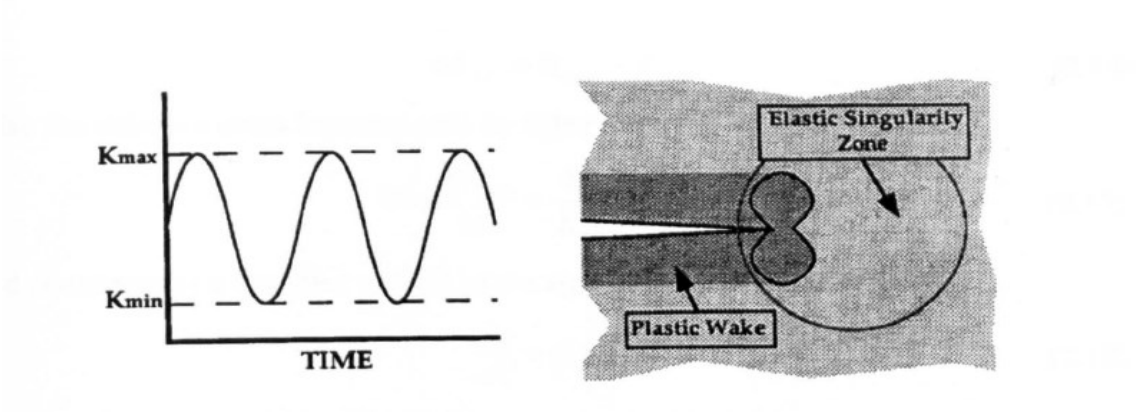

Figure 2.11 Constant amplitude fatigue crack growth under small yielding conditions.

It is convenient to express the functional relationship for crack growth in the following form:

$$\frac{da}{dN} = f_1(\Delta K, R) \qquad (2.9)$$

Where $\Delta K = (K_{max} - K_{min})$, R = K_{min}/K_{max} and $\frac{da}{dN}$ is the crack growth per cycle. The influence of the plastic zone and the plastic wake on crack growth is implicit in equation 2.9, since the size of the plastic zone depends only on K_{min} and K_{max} .A number of expressions for f_1 function have been proposed, most of which are empirical.

Soon after the Paris law gained wide acceptance as a predictor of fatigue crack growth, many researchers came to the realization that this simple expression was not universally applicable. As Figure 2.8 illustrates, a log-log plot of da/dN versus ΔK is sigmoidal rather than linear when crack growth data are obtained over a sufficiently wide range. Also, the fatigue crack growth rate exhibits a dependence on the R ratio, particularly at both extremes of the crack growth curve. A discovery by Fiber [2.18] provided at least a partial explanation for both the fatigue threshold and R ratio effect.

Elber postulated that crack closure decreased the fatigue crack growth rate by reducing the effective stress intensity range Figure 2.12. When a specimen is cyclically loaded at K_{max} and K_{min} , the crack faces are in contact below K_{op} the stress intensity at which the crack opens. Elber assumed that the portion of the cycle that is below K_{op} does not contribute to fatigue crack growth. The definition of the effective stress intensity range is:

$$\Delta K_{eff} = K_{max} - K_{op} \qquad (2.10)$$

Also the effective stress intensity ratio by Elber is:

$$U = \frac{\Delta K_{eff}}{\Delta K} = \frac{K_{max} - K_{op}}{K_{max} - K_{min}} \qquad (2.11)$$

and consequently a modified version of the equation (2.1) proposed

$$\frac{da}{dN} = C(\Delta K_{eff})^m \qquad (2.12)$$

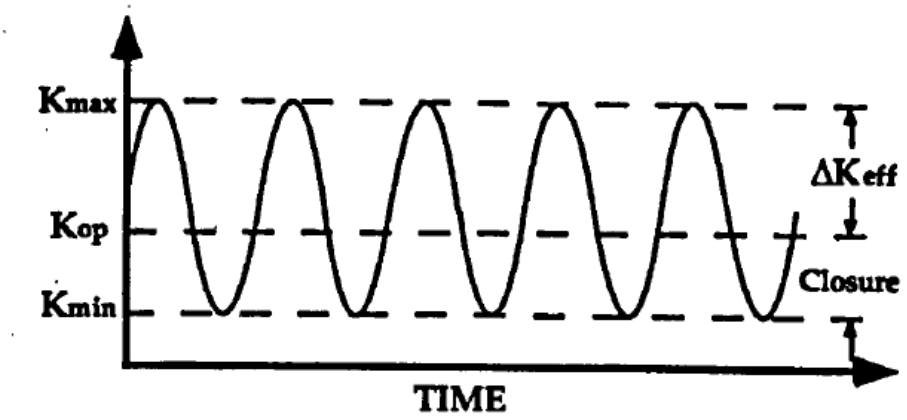

Figure (2.12) Definition of effective stress intensity range.

Crack closure occurs as a consequence of crack tip plasticity. At the tip of a growing fatigue crack, each loading cycle generates a monotonic plastic zone during increased loading and a much smaller reversed plastic zone during unloading. Approximately the reversed plastic zone size is one-quarter of the size of the monotonic plastic zone. Due to this, there is a residual plastic deformation consisting of monotonically stretched material. As the crack grows, the residual plastic deformation forms a wake of monotonically stretched material along the crack edges. Because the residual deformation is the consequence of tensile loading, the material in the crack edges is elongated normal to the crack surfaces and has to be accommodated by the surrounding elastically stressed material. This is no problem as long as the crack is open, since then the crack edges will simply show a displacement normal to the crack surfaces. However, as the fatigue load decreases, during unloading, the crack will tend to close and the residual deformation becomes important.

2.5 Effect of Residual Stresses on Crack Propagation.

Our knowledge of the relationship between residual stress and fatigue strength is perplexed due to the fact that:

- The fatigue strength depends greatly on the condition of the surface. The effect of residual stress is overshadowed by such major factors as weld geometry and surface irregularities.
- A fatigue crack may initiate in a region containing tensile residual stresses. The rate of crack growth may be increased due to the existence of tensile residual stresses. However, when the crack grows and enters regions containing compressive residual stresses, the rate of the crack growth may be reduced. As a result, it is questionable whether or not the total Effect of residual stresses on the overall crack growth is significant .

- When residual stresses are altered by a heat treatment such as peening, the metallurgical and mechanical properties of the metal are also changed. A schematic presentation of the stress field behind and in front of a crack tip under cyclic loading without welding residual stresses is illustrated in Figure 2.13

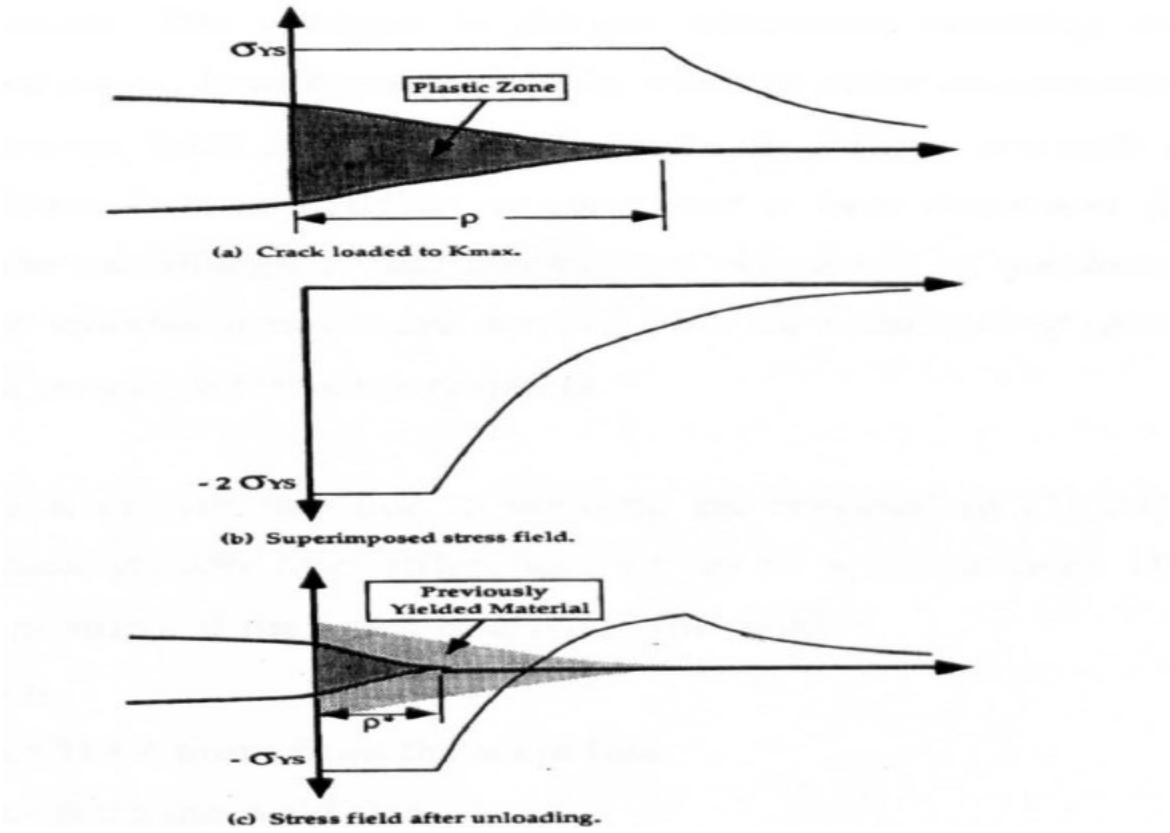

Figure 2.13 Formation of reverse plastic zone during cyclic loading, [2.19].

How residual stresses actually affect the plastic zone showed in Figure 2.13 and subsequently the fatigue strength of a welded structure is still a matter of debate. Some researchers have reported that the fatigue strength increased when specimens had compressive residual stresses, especially on the specimen surfaces, others believe that residual stresses have only a negligible effect on the fatigue strength of the weld elements. It has been suggested that in a good weld residual stresses can be ignored . Also it has been suggested that geometry affects fatigue behavior much more than residual stresses But others researchers feel that there is significant evidence that residual stresses affect the fatigue strength . Munse [2.20] summarizes as follows:

"On the basis of the available data it is believed that the effects of residual stresses may differ from one instance to another, depending upon the materials and geometry of the members, the state of stress, the magnitude of applied stress, the type of stress cycle and perhaps other factors. Many of the investigations designed to evaluate the effects of residual stress have included tests of members that have been subjected to various stress relief heat treatments. The changes in fatigue behavior resulting from these heat treatments, in some cases, have been negligible, while in other investigations, the various stress-relief treatments have produced an increase in fatigue strength of as much as twenty percent. Since it is impossible to carry out a heat treatment for stress relief without altering the metallurgical and mechanical properties of weldment, the question always arises as to whether benefits are derived from the reduction of residual stresses or from the improved properties in other respects. "

2.6 Design of integral structure.

According to NASA's research, "About a third of the airlines' direct operating cost (DOC) of an airplane is associated with the manufacturing cost, which is probably the most critical competitive parameter with regard to market share [2.21]. It means that it is an effective way to cut down the manufacturing cost to reduce the acquisition cost of an aircraft. The skin-stringers riveted structures have been used in aircraft fuselage for more than 60 years. These kind of riveted structures have advantages in damage tolerance performance and also fail-safe, since stringers gives another path for load passing, which delays the speed of crack growth. But this kind of design makes it difficult to reduce in cost significantly because they are highly refined and mature with associated construction details and fabrication processes. Nevertheless, metallic structure is well proved, and it will likely retain extensive metallic production capability and skills in the foreseeable future. Hence, the conception of designing renewed large integral metallic skin-stringer panels for aircraft fuselage for low acquisition cost and the emergence of high speed machining is imminent. A typical integral structure made by NASA's ISA program shows in Figure (2.14) .

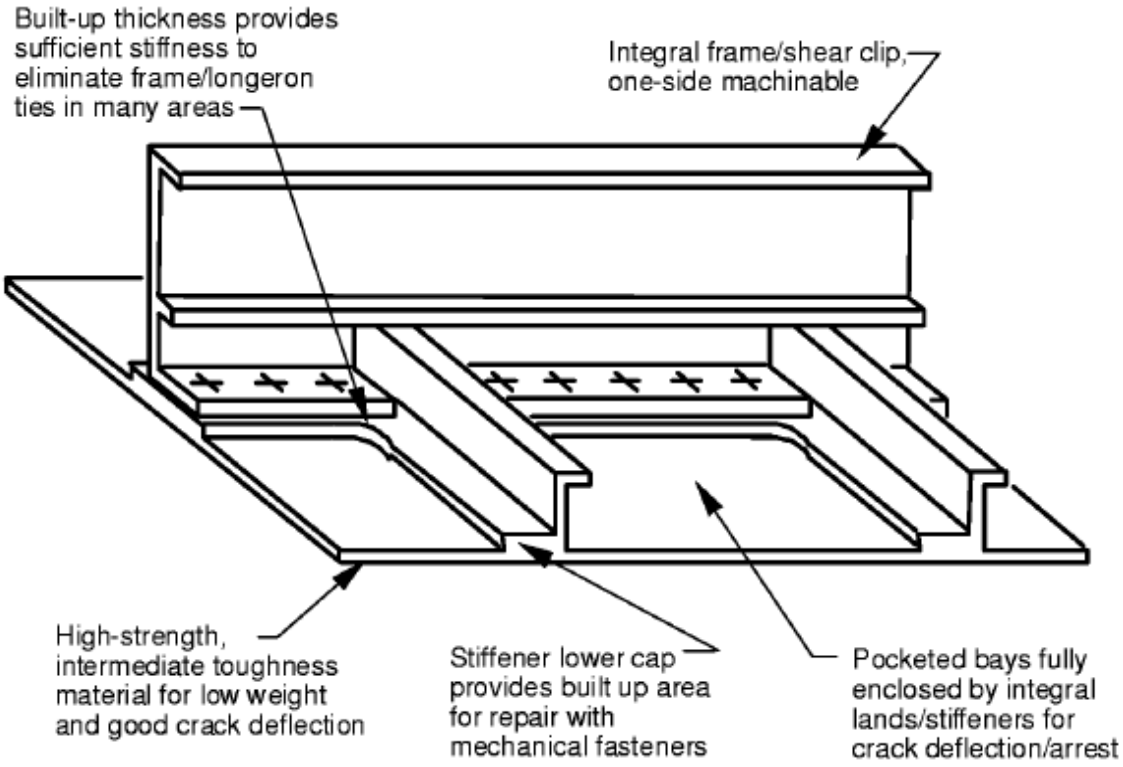

Figure 2.14 Typical integral fuselage.

The results were exciting when machined integral structures were taken into Boeing 747 fuselage. It was found to be superior in terms of part count and cost, and almost equivalent in terms of weight when compared with riveted structure. These results are summarized in Table 2-1 [2.22].

Table 2-1 Results of riveted and integral panels

Factor	Riveted Panel	Integral Panel	Integral Change From Riveted	Target Savings Over Riveted
Number of parts	78	7	91% reduction	50%
Weight	179 pounds	186 pounds	4% increase	Neutral
Estimated Cost	$33.000	$14.000	58%reduction	25%

2.7 Comparison of riveted and integral structures.

It is necessary to investigate the integral panels in details in order to ascertain the possible high benefits over riveted panels. Figure (2.15) below gives the difference between conventional riveted stringer fuselage panel and the new integral skin-stringer fuselage panel. Figure (2.16) describes the riveted stringer panel and the integral skin-stringer panel.

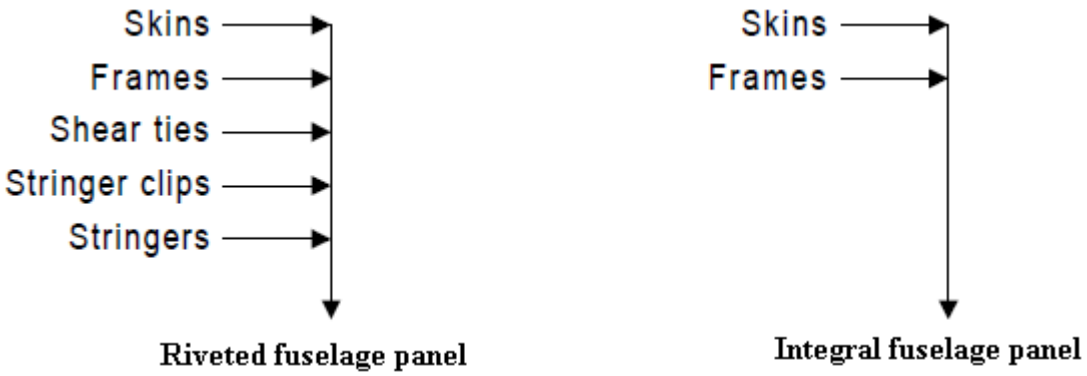

Figure (2.15) Structure of riveted panel and integral fuselage panel .

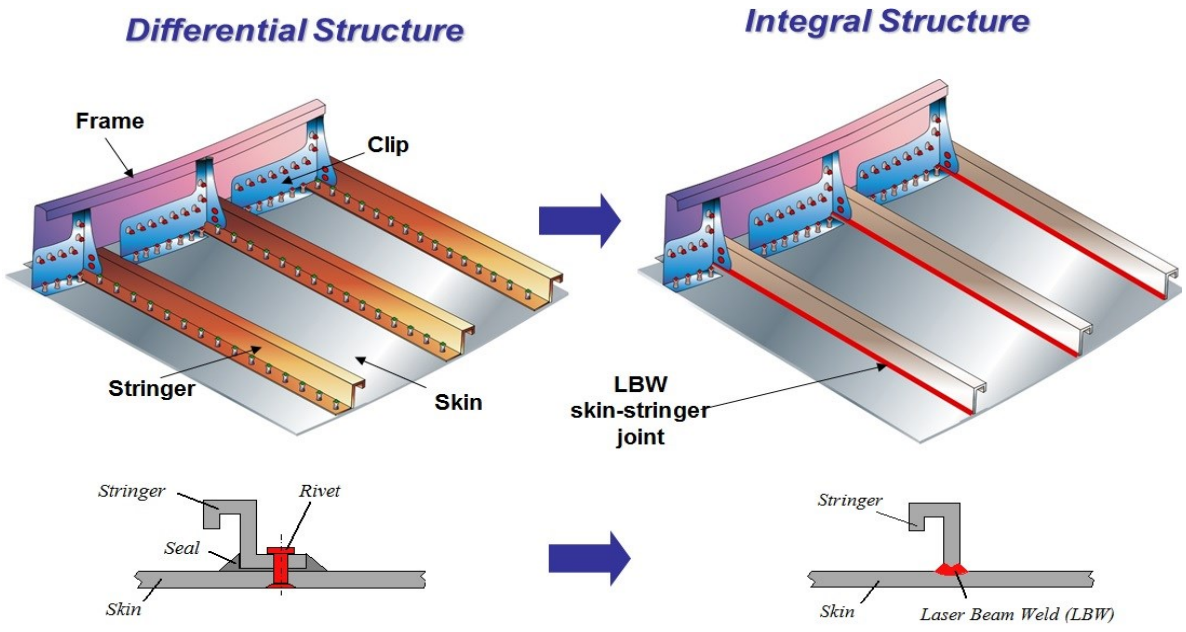

Figure (2.16) Riveted stringer panel and integral stringer panel.

[2.23] compared the damage tolerance behavior of integrally skin-stringer structures and riveted structures, and gave the pros and cons as follow: For riveted stringer panel, the pro is offering fail safety for the hard of crack going to the stiffener. The cons are causing premature initiation of fatigue cracks, thousands of fasteners to be used and the fact that they are difficult to manufacture and inspect. For integral stringer panel, the pro are reducing part count and structural complexity, automated processing and improving visual inspection capability. The cons are lacking of redundant structural members, lacking of damage tolerance behavior and increasing crack growth rates in heat affected zones.

2.8 Improvement of Integral Structures.

In order to optimize the damage tolerance performance of integral metallic structures, two particular aspects should be considered. The first one is developing new kinds of materials with a better fracture toughness property [2.24]. Although the 7000 series aluminum alloys have sensational mechanical performance, toughness sharp reduction at low temperatures which is especially dangerous for the integral metallic structures limits its use. Since 2000 series aluminum alloys are not so sensitive to very low temperature, they can be exploited to overcome the disadvantage. Another one is designing or optimizing structures. In recent years, researchers analyzed many different methods for the structure design optimization. It is an effective way to save the time and money for the prototype building through the development of methods to simulate the crack growth behavior of the components. Retarders of crack growth, which are bonded to integral metallic panels, were investigated in order to overcome the lack of a fail safety performance. In order to create a failsafe design feature, a hybrid structure bonding two different materials together is created in critical zone [2.25]. These bonded straps still have some disadvantages, even though they have advantages in delaying the fatigue crack growth. Another way for optimization is to reduce crack growth speed in the integral panels through the investigation of the optimized shapes. Stringers which play important roles in the damage tolerance behavior of integral panels are the most promising fields to analysis [2.26]. According to the research, the stress intensity factor (SIF) decreases when the crack approaches a stiffener and it increases when the stiffener has been crossed. The overall result is the crack grows slow, because

the crack growth depends on SIF variation. Besides, stiffeners increase T-stress, which may cause crack turning. Hence, it is important to build an effective model to describe the SIF evolution during the crossing of the stiffener, in an accurate way.

Chapter 3: FRACTURE MECHANICS AND XFEM (Extended Finite Element Method) CONCEPTS

3.1 Introduction.

This chapter introduces briefly the analysis methods for SIF (stress intensity factor) calculation and crack growth life prediction for integral stiffened panels. There are three types of loading that a crack can experience, as Figure 3.1 illustrates. Mode I loading, where the principal load is applied normal to the crack plane, tends to open the crack. Mode II corresponds to in-plane shear loading and tends to slide one crack face with respect to the other. Mode III refers to out-of-plane shear. A cracked body can be loaded in any one of these modes, or a combination of two or three modes. All the SIF obtained by using extended finite element method (XFEM).

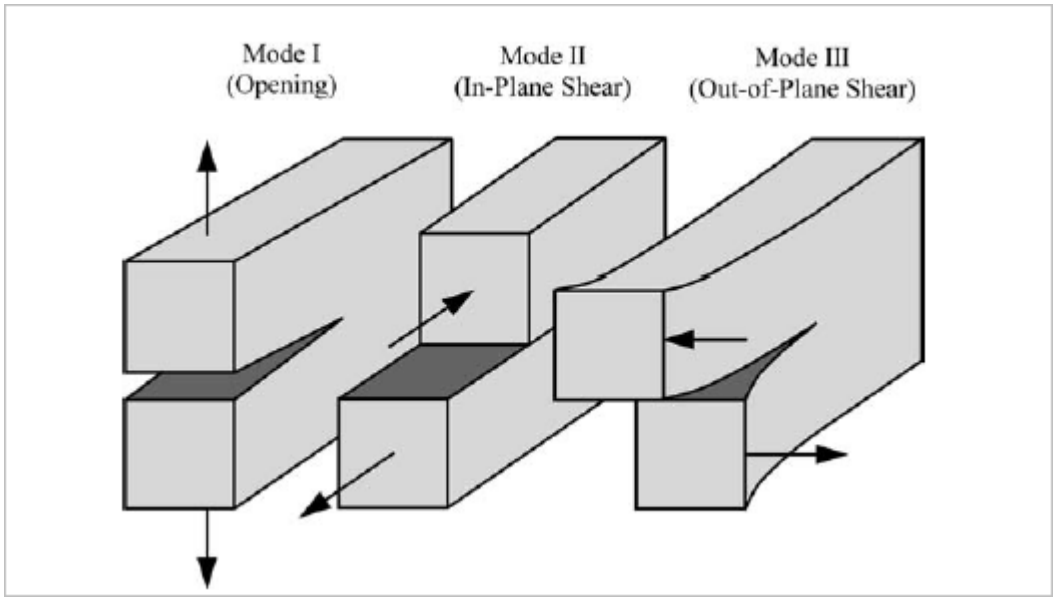

Figure 3-1 Fracture modes [3.1]

For linear elastic Materials, Griffith's approach says that a crack extends if the thermodynamic crack driving force, characterized by the energy release rate *G*, becomes equal or larger than the crack growth resistance, R (Griffith, 1921) [3.1][3.2] where as in 1956 Irwin proposed an energy approach for fracture that is essentially equivalent to the Griffith model, except that Irwin's approach is in a form that is more convenient for solving engineering problems. He postulates that

a crack grows when the crack tip stress intensity factor *K* reaches a critical value Kc.The Griffith and Irwin criteria are equivalent for linear elastic materials, since energy release rate and stress intensity factor are related. The assumptions taken in LEFM analysis is listed below [3.1]:

1. A sharp crack or flaw of similar nature already exists; the analysis deals with the propagation of the crack from the early stages.

2. The material is linearly elastic.

3. The material is Isotropic.

4. The size of the plastic zone near the crack-tip is small compared to the dimensions of the crack.

5. The analysis is applicable to near-tip region.

Linear Elastic fracture mechanics (LEFM) is valid only as long as non-linear material nonlinear material deformation is confined to a small region surrounding the crack tip. In many materials, it is virtually impossible to characterize the fracture behavior with LEFM, and an alternative fracture mechanics model is required.

Elastic-Plastic Fracture Mechanics applies to materials that exhibit time dependent, nonlinear behavior (i.e. plastic deformation) [3.2]. For crack growth in elastic-plastic materials under large scale or general yielding conditions, the common approach is to use criteria based on the crack tip opening displacement (CTOD) by Wells in 1963, Rice's J-integral in 1968 [3.1] and the energy dissipation rate by Turner and also Turner Kolednik in 1994.

3.2 Classical fracture criteria and parameters.

3.2.1 The Stress Intensity Factor.

A major activity in the design process based on fracture mechanics is the determination of the Stress Intensity Factor (in the following simply SIF). In the following sections, some of the pertinent analytical and numerical methods are discussed.

Analytical determination of SIF.

SIF can be coupled by an analytical approach in some relevant cases. Incase of an infinite plate with a central crack of length '2a', under remote stress σ_0 the calculating of SIF is as follow: (see Fig. 3.2)

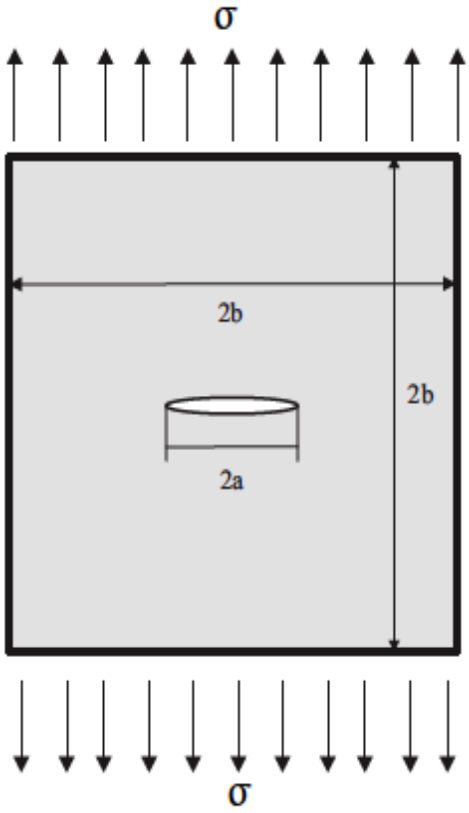

Figure 3.2: An infinite plate with a central elliptic crack [3.3]

Because the linear elastic fracture mechanics approach is based on elasticity, one can determine the effects of more than one type of loading on the crack tip stress field by linearly adding the SIF due to each type of loading. The process of adding SIF solutions for the same geometry is sometimes referred to as "principle of superposition". The only constraint on the summation process is that the SIF must be associated with the same structural geometry, including crack geometry. Thus, for the geometries shown in Fig. 3.3 the equation is as follow:

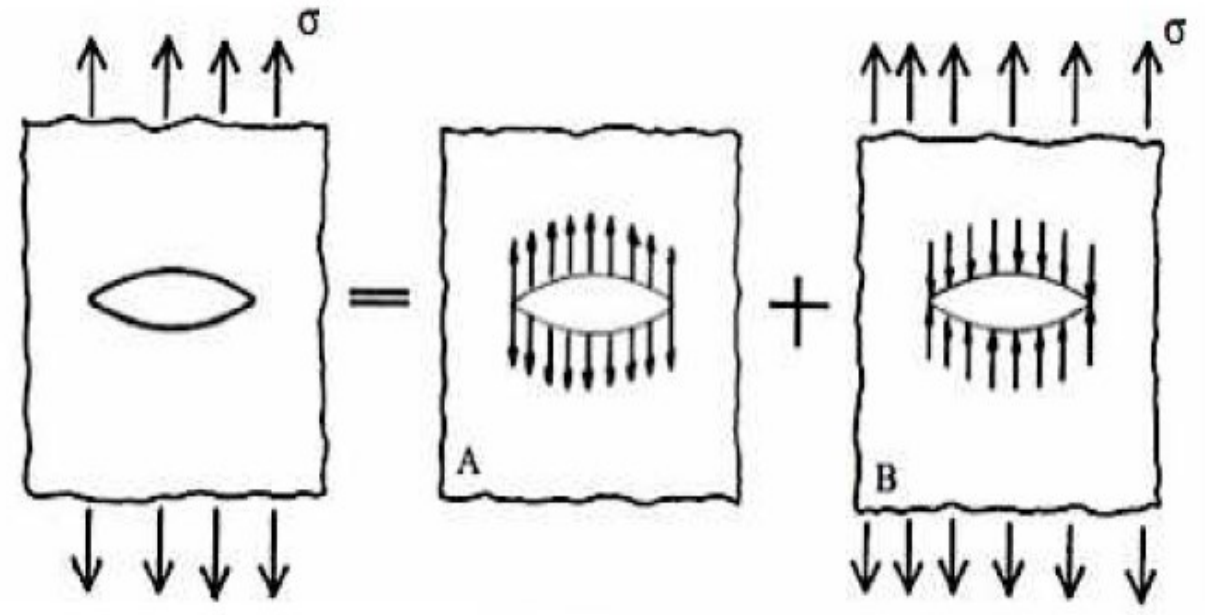

Figure 3.3: The geometries of superposition of K expression [3.4]

$$K_{IA} + K_{IB} = \sigma\sqrt{\pi a} \quad \text{3-1}$$

$$K_{IA} + 0 = \sigma\sqrt{\pi a} \quad \text{3-2}$$

$$K_{IA} = \sigma\sqrt{\pi a} \quad \text{3-3}$$

The stress distribution around the tip in mode I is described by Westergaard [3.5] as follow (Fig 3.4).

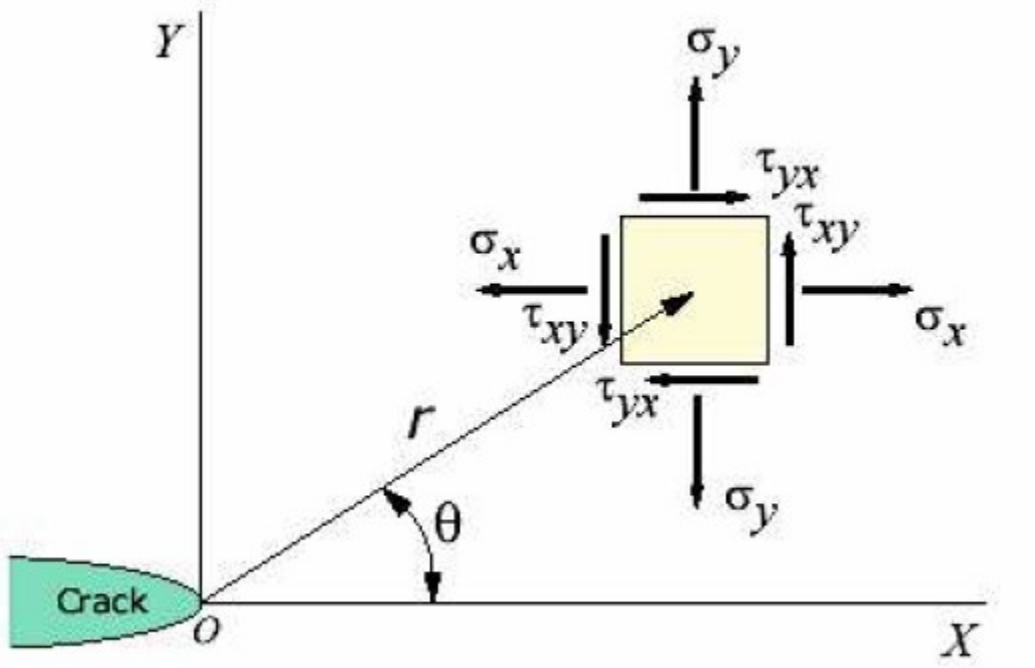

Figure 3.4: The stress distribution around the crack tip. [3.6]

$$\sigma_i = \frac{KI}{\sqrt{2\pi r}} f(\theta) \qquad 3\text{-}4$$

$$\sigma_{xx} = \frac{KI}{\sqrt{2\pi r}} cos\frac{\theta}{2}(1 - sin\frac{\theta}{2}sin\frac{3\theta}{2}) + \ \ldots\ldots \qquad 3\text{-}5$$

$$\sigma_{yy} = \frac{KI}{\sqrt{2\pi r}} cos\frac{\theta}{2}(1 + sin\frac{\theta}{2}sin\frac{3\theta}{2}) + \ \ldots\ldots \qquad 3\text{-}6$$

$$\tau_{xy} = \frac{KI}{\sqrt{2\pi r}} cos\frac{\theta}{2}cos\frac{3\theta}{2}sin\frac{\theta}{2} \ \ldots\ldots \qquad 3\text{-}7$$

For distances close to the crack tip ($r \leq 0.1a$), the second and higher order terms indicated by dots may be neglected. The I subscript is used to denote the crack opening mode, but similar relations apply in modes II and III. Above equations show three factors relevant to depict the

stress state near the crack tip: denominator $\sqrt{2\pi r}$shows the singular nature of the stress distribution; σ approaches infinity as the crack tip is approached, with a√r dependency. Depend on angle θ; it can be separated if a suitable factor is introduced. f_x = cos θ/2 ▪ (1 −sin θ/2 sin3θ/2) +…. Factor KI contains the dependence on applied stress 'σ_∞', the crack length a, and the specimen geometry. The KI factor gives the overall intensity of the stress distribution, hence its name. For the specific case of a central crack of width 2a or an edge crack of length 2a in a large sheet, KI = σα√πa and KI = 1.12σα√πa for an edge crack of length 'a' in the edge of a large sheet. Expressions for KI for some additional geometry are given in Table 3.1 The literature [3.7] contain expressions for K for a large number of crack and loading geometries, and both numerical and experimental procedures exist for determining the stress intensity factor is specific actual geometries.

Table 3.1: Expressions of KI for different geometries

Type of Crack	Stress Intensity Factor, K_I
Center crack, length 2a, in an infinite plate	$\sigma\alpha\sqrt{\pi a}$
Edge crack, length a, in a semi infinite plate	$1.12\ \sigma\alpha\sqrt{\pi a}$
Central penny shaped crack, radius a, in infinite body	$K_I = 2\ \sigma\alpha\sqrt{\pi/a}$
Center crack, length 2a in plate of width W	$\sigma\alpha\sqrt{W \tan\left(\frac{\pi a}{w}\right)}$
Two symmetrical edge cracks, each length a, in plate of total width W	$\sigma\alpha\sqrt{W \tan\left(\frac{\pi a}{w}\right) + 0.1 \sin\left(\frac{2\pi a}{w}\right)}$

These SIF's are used in design and analysis by arguing that material can withstand crack tip stresses up to a critical value of stress intensity, termed K_{Ic}, beyond which the crack propagates very fast. This critical SIF is then a measure of material toughness. The failure stress σ_f is then related to the crack length a and the fracture toughness by:

$$\sigma_f = \frac{KIc}{\alpha\sqrt{\pi a}} \qquad 3\text{-}8$$

Where α is a geometrical parameter equal to 1 for edge cracks and generally on the order of unity for other boundary conditions. Expressions for α are tabulated for a wide variety of specimen and crack geometries.

Typical values of GIc and KIc for various materials are listed in Table 3.2 [3.8, 3.9 and 3.10], and it is seen that they vary over a very wide range from material to material. Some polymers can be very tough, especially when rated on per-pound bases, but steel alloys are hard to beat in terms of absolute resistance to crack propagation.

Table 3.2: Typical values of KIC for various materials

Material type	Material	K_{IC} (MPa.$\sqrt{m}$)
Metal	Aluminum alloy (7075)	24
	Steel alloy (4340)	50
	Titanium alloy	44–66
	Aluminum	14–28
Ceramic	Aluminium oxide	3–5
	Silicon carbide	3–5
	Soda-lime glass	0.7–0.8
	Concrete	0.2–1.4
Polymer	Polymethyl methacrylate	0.7–1.6
	Polystyrene	0.7–1.1
Composite	Mullite-fibre composite	1.8–3.3
	Silica aerogels	0.0008–0.0048

3.2.2. The Energy Release Rate

By the analysis of the energy balance, the energy release rate, denoted as G, was introduced. It is defined by the energy necessary to make the crack fronts extending the crack length by

a unit length. It corresponds to the decrease of the total potential energy W_{pot} of the cracked body, when it passes from an initial configuration with a given crack length, to another configuration where the crack is increased by a unit of length "da" [3.11]:

$$\boldsymbol{G = -\frac{dW_{pot}}{da}} \qquad \textbf{3-9}$$

$$W_{pot} = W_{\varepsilon} - W_{ext} \qquad 3\text{-}10$$

Where: W_{ext} is the work of external forces and W_{pot} is the total potential energy of crack body and W_{ε} is strain energy of structure.
Using the stress field in the singular zone, one can relate G to the stress intensity factors:

$$G = \frac{(KI^2 + KII^2)}{E'} + \frac{KIII^2}{2\mu} \qquad 3\text{-}11$$

With $E' = E$ in plane stress

$E' = E/(1-\nu^2)$ in plane strain

μ : shear modulus

3.2.3 The J-Integral.

J-integral is a parameter to deal with Non-linear fracture problem, which is proposed by Rice [3.11]. J-integral is less dependent on crack tip stress singularity for it is based on the concept of conservation of energy, which means there is no need to do special treatment on the mesh around crack tip. As shown in Figure 3.5, the equation of J-integral is

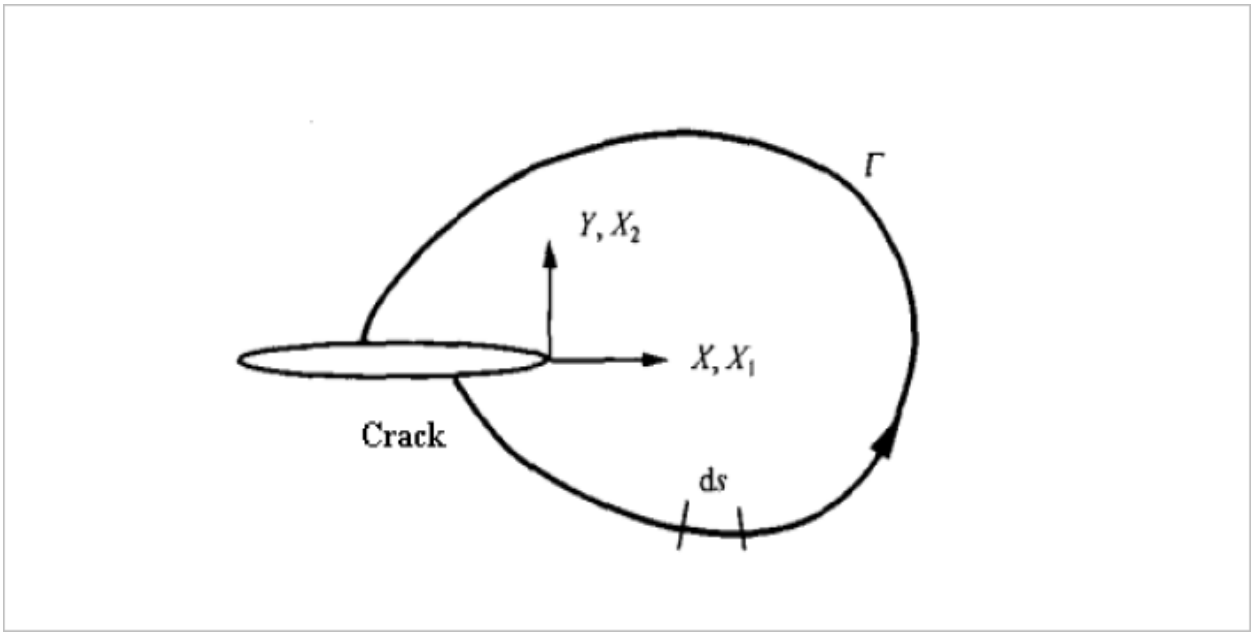

Figure 3.5 Counter clockwise loop around the crack tip.

$$J = \int_{\Gamma} \left(W dx_2 - T_i \frac{\partial u_i}{\partial x_i} \right) ds \qquad 3\text{-}12$$

Where w is the strain energy density, T_i is the traction vector, u_i is the displacement vector, ds is an element of arc along the integration contour.

- **Relation between J and K.**

In LEFM, the stress and displacement components at the crack tip are known as a function of the position relative to the crack tip. For multi-mode loading, they are characterized by the stress intensity factors KI, KII and KIII. Because the J-integral is path-independent, the integration path can be chosen to be a circle with the crack tip as its center. Integration over this circular path reveals that the J-integral is related to the SIF. For Mode I loading of the crack, it follows immediately that the J-integral is equivalent to the energy release rate G. This means that J-integral can be used in the crack growth criteria of LEFM as a replacement for K and G [3.11].

Plane stress $J = \frac{1}{E} K_I^2$ 3-13

Plane strain $J = \frac{(1-\nu^2)}{E} K_I^2$ 3-14

- **J-integral crack growth criterion**

J-integral can replace the energy release rate in LEFM and is related to the SIF. where the material behavior is described by the general Ramberg-Osgood relation [3.12], the J integral characterizes the stress at the crack tip. It is thus obvious that it can be used in acrack growth criterion. Calculation of its value is easily done, due to the fact that the integration path can be chosen arbitrarily. Critical values have to be measured according to normalized experiments

$J = Jc$ 3-15

3.2.4 Crack Tip Opening Displacement (CTOD).

In LEFM the displacement of material points in the region around the crack tip can be calculated With the crack along the x-axis, the displacement u_y in y-direction is known as a function of r (distance) and θ (angle), both for plane stress and plane strain. Displacement of points at the upper crack surface results for θ = π and can be expressed in the coordinate x, by taking:

$$r = a - x \tag{3-16}$$

Where a is the half crack length. The origin of this xy-coordinate system is at the crackcenter. The crack opening (displacement) (COD) δ is two times this displacement. It can be easily appreciated that the opening at the crack tip (CTOD), δt, is zero [3.13].

$$u_y = \frac{\sigma\sqrt{\pi a}}{2\mu}\sqrt{\frac{r}{2\pi}}\left[\sin\left(\frac{\theta}{2}\right)\left(k + 1 - 2\cos^2\left(\frac{\theta}{2}\right)\right)\right] \tag{3-17}$$

Displacement in crack plane θ = π; r = a – x:

$$u_y = \frac{(1+\nu)(k+1)}{E}\frac{\sigma}{2}\sqrt{2a(a-x)} \tag{3-18}$$

Crack Opening Displacement (COD):

$$\delta x = 2u_y(x) = \frac{(1+\nu)(k+1)}{E}\,\sigma\sqrt{2a(a-x)} \tag{3-19}$$

Crack Tip Opening Displacement (CTOD):

$$\delta t = \delta(x = a) = 0 \tag{3-20}$$

This CTOD can be used in a crack growth criterion (Fig 3.6), when plasticity at the crack tip is taken into account and the actual crack length is replaced by the effective crack length.

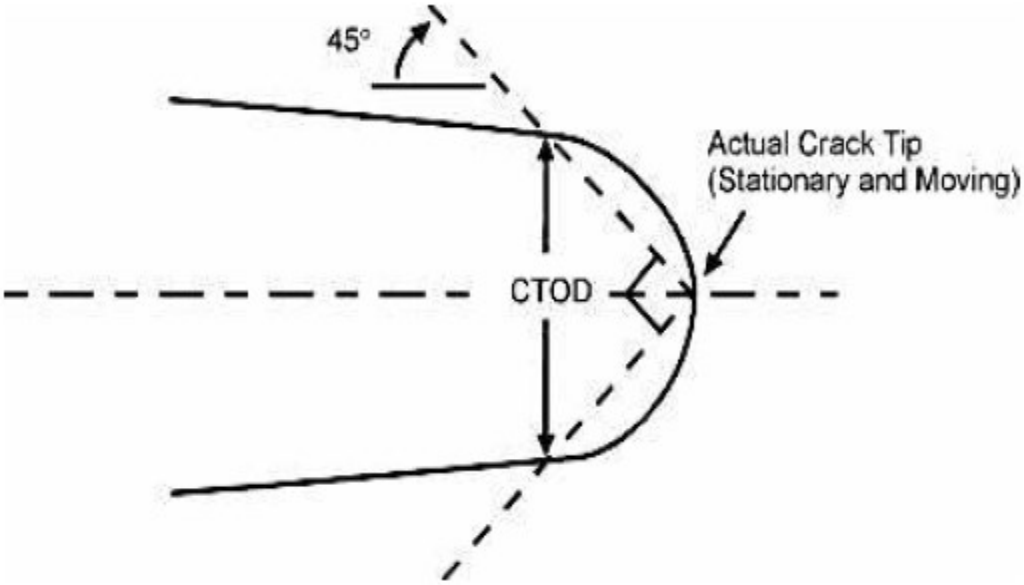

Figure 3.6 Definition of the Crack Tip Opening Displacement (CTOD).

3.3 Numerical tools.

There are many numerical approaches currently available to solve the problems concerning LEFM and to calculate the SIF. Research activity in this domain has produced a very large number of papers and it would be extremely difficult, and perhaps useless in the frame of this thesis, to extensively review all the literature on this subject. Therefore, following state of the art only briefly includes some of the basic references and proposes a classification of proposed methods by defining categories.

a) The Finite Element Method (FEM).

Usually, displacement-type finite elements (based on the virtual work principle) are widely used. According to the so-called "direct approach", the SIF are deduced from the displacement field, this is the case of the Crack Opening Displacement method (COD). In the "energy approach" which is generally more precise, the SIF are deduced from the energy distribution in the proximity of the crack tip, either from the energy release as in the method of the Virtual Crack Extension or from the J-integral as in the Equivalent Domain Integral Method [3.14]

b) The Boundary Elements Method (BEM).

In this method, only the boundaries of the solid are discretized. The partial differential equations of the Theory of Elasticity are transformed into integral equations on the boundaries of the domain. Basically, the primary unknowns of the numerical problem are the displacements. This is the case for the "crack Green's function method", the "displacement discontinuity method" and the "sub regions method". In dual method has been developed, which the surface tractions as primary unknowns [3.15].

c) The Mesh less method.

This method has been applied to fracture mechanics since 1994 and, subsequently, different improvements have been introduced, for example to couple this approach with the finite element method, to ensure the continuity of displacements in the vicinity of crack and improve the representation of the singularity at the crack tip, by using an arbitrary Lagrangian-Eulerian formulation to enrich the displacement approximation near the crack tip or to enrich the weighting functions [3.16].

d) **The Extended Finite Element Method**.

The Extended Finite Element Method (XFEM) allows some discontinuities in the assumed displacement field. Discontinuities can be due to the presence of cracks and do not have to coincide exactly with the finite element edges: they can be located anywhere in the domain independently

of the finite element mesh [3.17]. This approach is extremely used in the recent literature of fracture mechanics and is highly supported by the ABAQUS © code.

3.3.1 The Finite Element Method.

Many issues of structural integrity can be cast as problem of linear elastic fracture mechanics (LEFM). These can include fatigue crack propagation and life prediction, other types of sub-critical crack growth, residual strength estimation, and brittle fracture. In these and other related problems, it is essential to be able to predict the onset of crack growth, and its rate, shape, and stability. The finite element method, as performed within modern high-performance and low cost computing environments, is a natural tool for analyzing such LEFM problems.

A) Singular finite elements.

A fundamental difficulty when modeling linear elastic fracture mechanics (LEFM) problems through FEM is that polynomial basis functions used for most conventional elements cannot represent the singular crack-tip stress and strain fields predicted by the theory. This means that mesh doesn't assure the numerical convergence to the theoretical solution, although it is highly refined around the crack tip.

A significant improvement in the use of FEM for LEFM problems was the simultaneous, and independent, development of the quarter -point element. Crack tip displacement, stress and strain fields are modeled by standard quadratic order isoparametric finite elements if one simply moves the elements mid-side node to the position one quarter of the way from the crack tip to the far end of the element. This procedure introduces a singularity into the mapping between the element's parametric coordinate space and the Cartesian space [3.18]. The quadratic quarter-point element is illustrated in Fig 3.7.

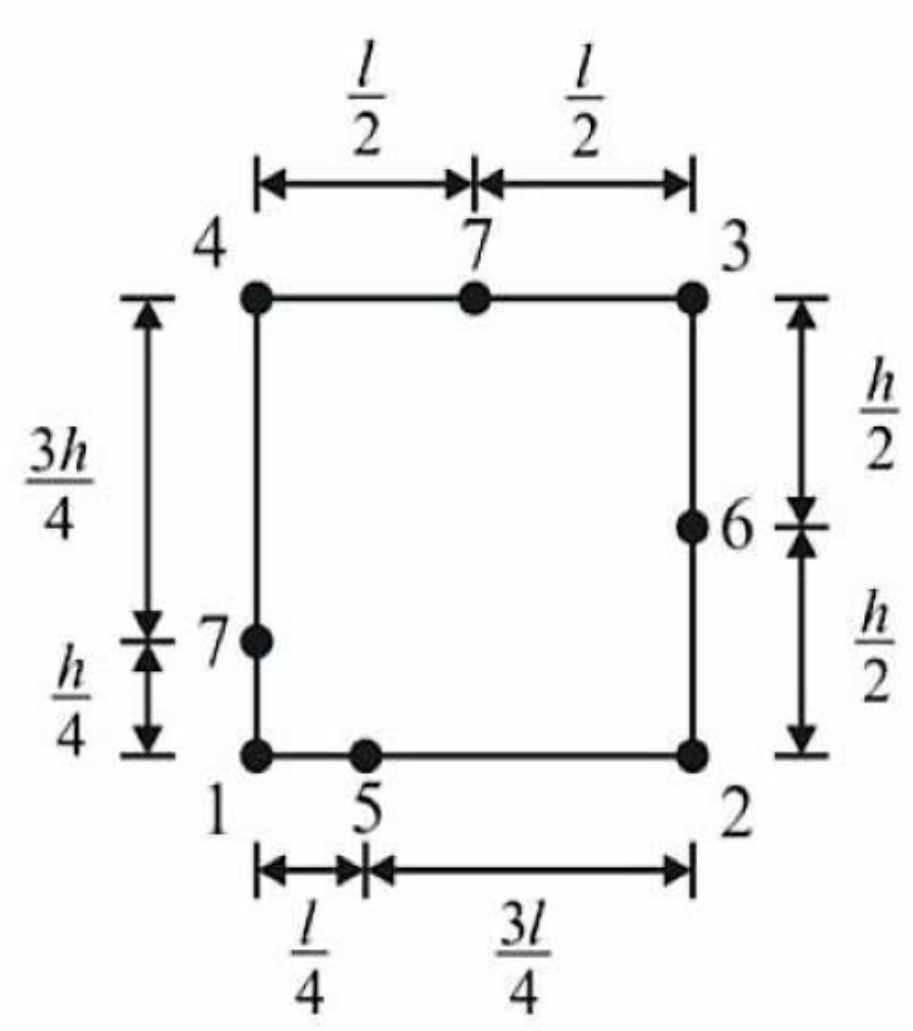

Figure 3.7 the quadratic quarter-point element

The introduction of quarter-point elements was a significant milestone in the development of finite element procedures for LEFM. With these elements standard and widely available, finite element programs can be used to model crack tip fields accurately, with only minimal preprocessing required.

B) Extracting SIF and Energy Release Rate from FEM.

Under LEFM assumptions, the stress, strain and displacement fields in the near crack-tip region are determined by the SIF. Therefore, extraction of accurate SIF is a fundamental task of FEM modeling. [3.19]. There are Four techniques very often applied: displacement correlation, virtual cracks extension, modified crack closure integral and the J-integral, these techniques look more accurate and simples. It is worthy motivated that techniques for extracting SIF's fall into one of two categories above-mentioned. Some belong the direct approaches, which correlate the SIF's with FEM results directly and energy approach, which compute the energy release rate. In general, the energy approaches are more accurate and should be used preferentially. However, the direct approaches are especially useful as a check on energy approaches because expressions are simple enough to handle the calculations. a brief description of four mentioned techniques follow:

Generalized Displacement correlation method is one of the simplest first techniques proposed to extract SIF's from the FEM displacements for a node of the mesh, by substituting directly displacement value into the analytical expressions for near-tip displacement, after subtracting the displacements of the crack tip. Usually, a node on the crack face where the displacements will be greatest is selected and thus the relative error in the displacements is expected to be smallest. A generalized form displacement correlation method (GDC) can use any linear or quadratic finite element type with homogeneous meshing without local refinement. These two features are critical for modeling dynamic fracture propagation problems where locations of fractures are not known a priori. Because regular finite elements' shape functions do not include the square-root terms, which are required for accurately representing the near-tip displacement field, the GDC method is enriched via a correction multiplier term. The proposed method using quadratic elements is accurate for mode-I and mode-II fracturing, including for very coarse meshes. An alternative formulation using linear elements is also demonstrated to be accurate for mode-I fracturing, and acceptable mode-II results for most engineering applications can be obtained with appropriate mesh resolution, which remains considerably less than that required by most other methods for estimating stress intensities [3.20]. The configuration for this simple approach is shown in Fig 3.8.

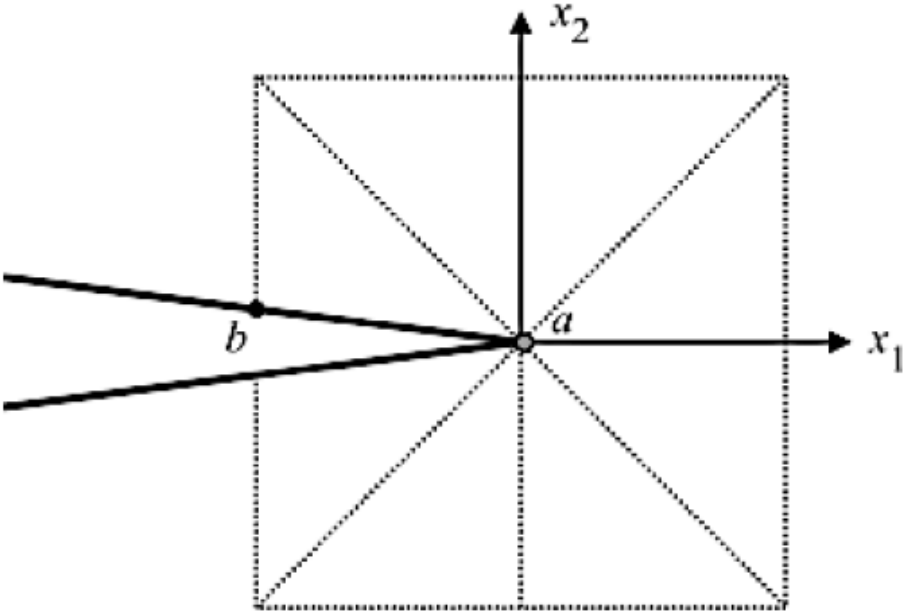

Figure 3.8 Possible sample point location for simple displacement correlation

The virtual crack extension method is an energy approach that computes the rate of change in the total potential energy of a system for a small extension of the crack. Under LEFM assumption, this is equal to the energy release rate. In general the virtual extension crack is more accurate than the displacement correlation approach for a given finite element mesh. However, as originally proposed, only a total energy release rate is computed. It is not separated for the three modes of fracture [3.21].

The modified crack closure integral (MCCI) technique was originally proposed by Rybicki and Kanninen [3.22], They observed that Irwin's crack closure integral could be used as computational tool (Fig 3.9). Release the energy release rate to the crack-tip stress and displacement fields for a small crack increment.

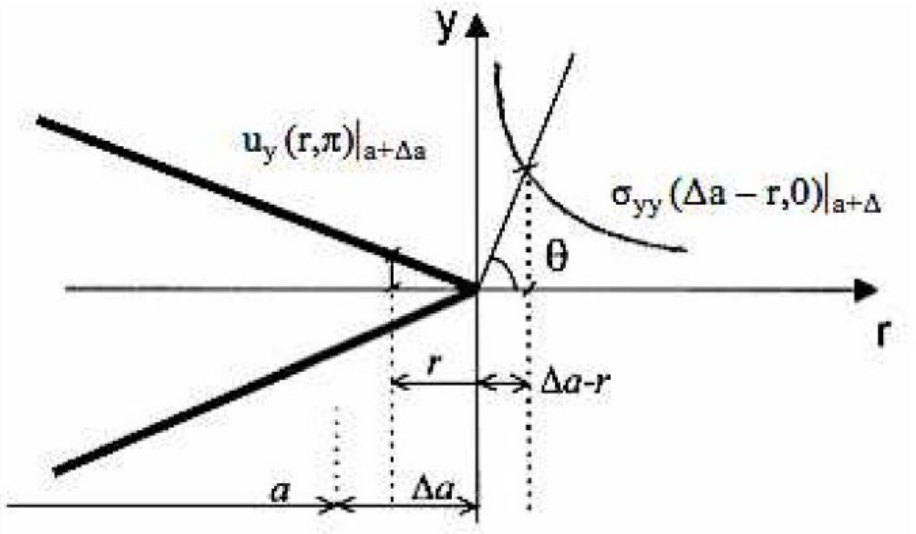

Figure 3.9 Crack-tip stress and displacement fields used in Irwin crack closure integral

The MCCI procedure has been extended for use with higher order element. Of particular interest is its formulation for quadratic-point elements is insensitive. These elements express the crack-tip displacement and stress fields in terms of second order polynomials that were consistent with the quarter- point behavior.

In general, for a given mesh the MCCI technique yields SIF's that are more accurate than the displacement correlation approach, but less accurate than the J- integral approach. However, it gives surprisingly accurate results for its simplicity and requires nodal forces and displacements only, which are standard outputs from many finite element programs.

The J-integral is well-known parameter of nonlinear fracture mechanics. Under linear elastic material assumptions, the J- integral can be interpreted as being equivalent to the energy release rate, G. In its original formulation, it relates the energy release rate of a two dimensional body to a contour integral. The contour integral in the simple form can be shown to be path-independent providing there are no body forces inside the integration area, there are no tractions on the crack surface and the material behavior is elastic [3.23].

Life prediction Methods: - the fatigue life as a whole can be divided into three parts: crack initiation, crack propagation, and final failure. Several conventional fatigue analysis methods are used in first phase life estimation such as the S-N curve approach and detail fatigue-rating approach. A small crack is assumed in the beginning of fatigue life calculation. Although the small flaw may not be fracture critical under static loads, it will gradually increase under cyclic loads. Therefore, the ability of the prediction of a component under cyclic loads becomes particularly important. During the crack propagation process, stress intensity factor plays a decisive role. It is assumed that the crack growth rate is determined by the stress intensity factor range, and different cracks have same rate of propagation if they have the same stress intensity factor. Thus, the crack propagation rate, da/dN has the relationship with stress intensity factor range,

$$\Delta K = K_{\max} - K_{\min} \tag{3-21}$$

$$da / dN = f(\Delta K) \tag{3-22}$$

Paris Equation Paris, etc were the first to find the relationship between the crack growth rate and the SIF, and began to compare it with test data [3.24]. They gave the equation in the following form:

$$da / dN = C(\Delta K)^n \tag{3-23}$$

This is Paris law, where C and n were constants related to the material.

Forman's Equation Forman's law is also a kind of life prediction method, which considers the mean stress effect of a fatigue stress cycle [3.25]. The equation is in the following form:

$$\frac{\mathrm{da}}{\mathrm{dN}} = \frac{\mathrm{C}(\Delta\mathrm{K})^{\mathrm{n}}}{(1-\mathrm{R})\mathrm{K}_{\mathrm{c}} - \Delta\mathrm{K}} \tag{3-24}$$

Where R= S_{min} / S_{max} reflects the mean stress effect. K_c is the fracture toughness which describes the effect when K_I near to K_{IC}.

As the result of fatigue testing experience, ΔK_{th} is also related to the stress ratio and material property. Hence, Forman's equation can be modified as follow:

$$\frac{da}{dN} = \frac{C(\Delta K - \Delta K_{th})^n}{(1-R)K_c - \Delta K} \qquad 3\text{-}25$$

C) Available tools and software.

In the FEM, the structure is subdivided into discrete elements. Different Element types can be used to cover the problem. Elements are connected at node, where continuity of displacement field is imposed. Displacements at nodes depend on the element stiffness and computational of the nodal forces. For structural problems, numerical solution consists of computing nodal displacements. Stress and strain distributions throughout the body, as well as the crack parameters such as SIF, can be inferred from the nodal displacements. A number of commercial FEM packages have the ability of crack modeling and performing the fracture mechanics calculations. There is also some noncommercial code, as the FRANC2D, which is developed by the Cornell University, being surprisingly easy to learn and offering many capabilities. Finite element analysis can be carried out by several available software like ABAQUS, ANSYS, and LS- DYNA etc. These software's are user friendly and give a wide range of analysis options. Static, dynamic, fluid, thermal and electromechanical problems can be analyzed by means of those codes.

In this thesis, the ABAQUS© was used, it can solve linear and nonlinear problems. It was designed to be able to investigate many links of nonlinearities such as geometrical material or multi-physic domains. Some specialized modules allow investigation of several behavior of material in presence of plasticity, buckling, electromechanical coupling and even fracture. Numerical tools are evaluated to solve nonlinear problems by an automatic updating of the set-up to assure the numerical convergence and an accurate result.

3.3.2 Extended Finite Element Method (XFEM)

The standard finite element method (FEM) provides substantial advantages in dealing with continuous field problems. However, for discontinuous field problems, it is computationally

expensive to obtain accurate solutions with polynomial approximations. Alignment of mesh with discontinuity becomes a major difficulty when treating problems with evolving discontinuities where the mesh must be regenerated at each step, i.e. re-meshing is needed continuously [3.26]. Modeling of cracks in structures and especially involving cracks requires the FEM mesh to conform the geometry of the crack and hence needs to be updated each time as the crack grows. This not only computationally costly and cumbersome but also results in loss of accuracy as the data is mapped from old mesh to the new mesh [3.27]**.**

A re-meshing technique is traditionally used for modeling cracks within the framework of finite element method where a re-meshing is done near the crack to align the element edges with the crack faces [3.28].

The Extended finite element method (XFEM), also known as generalized finite element method (GFEM) or Partition of unity method (PUM) is a numerical technique that extends the classical finite element method (FEM) approach by extending the solution space for solutions to different equations with discontinues functions. It was first introduced by Bolyteschko and Black[3.29].

The extended finite element method (XFEM) has proved to be a competent mathematical tool [3.30] since it is an extension of partition of unity; allows the presence of discontinuities in an element by enriching degrees of freedom with special displacement functions. [3.31]

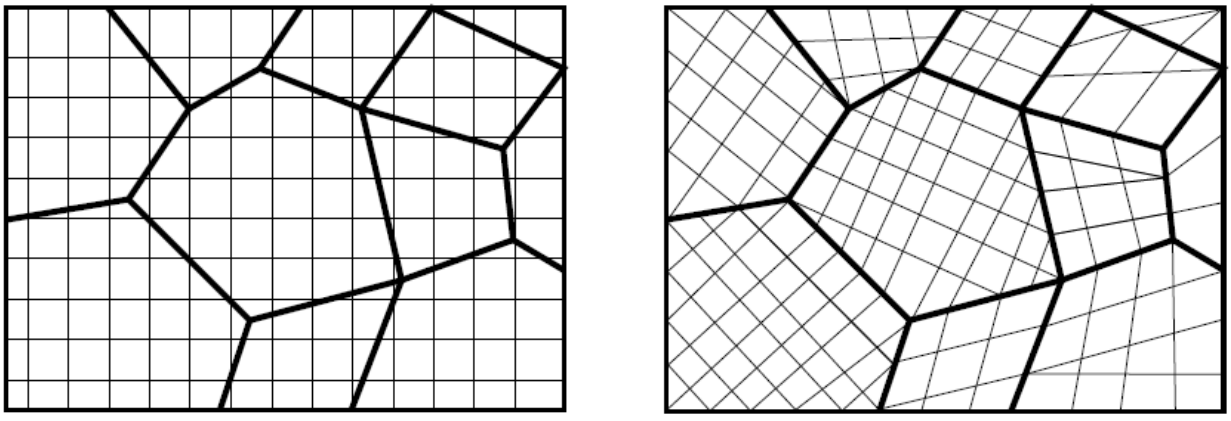

Figure 3.10: Mesh discretization in XFEM (left) and FEM (right) [3.34].

In comparison to the classical finite element method, the XFEM provides significant benefits in the numerical modeling of crack propagation. The traditional formulation of the FEM, the existence of crack is modeled by requiring the crack to follow element edges. In contrast, the crack geometry in the XFEM need not to be aligned with the element edges, which provides flexibility and versatility in modeling.

The Extended Finite Element Method (XFEM) can dramatically simplify the solution of many problems in material modeling such as the propagation of cracks, the evolution of dislocations, the modeling of grain boundaries and the evolution of phase boundaries [3.32].

The method is based on enrollment of the FE model with additional degrees of freedom (DOF) that are tied to the nodes of the elements intersected by the crack [3.32][3.34]. In this manner, the discontinuity is included in the numerical model without modifying the discretization, as the mesh is generated without taking into account the presence of the crack. Therefore, only a single mesh is needed for any crack length and orientation. In addition, nodes surrounding the crack tip are enriched with DOFs associated with functions that reproduce the asymptotic LEFM fields. This enables the modeling of the crack discontinuity with in the crack tip and substantially increases the accuracy in the computation of the stress intensity factors (SIFs).

3.3.3 Partition of Unity Finite Element Method, PUFEM

Partition of unity is a set R of continuous functions from X to the interval [0, 1] such that for every point x ε X There is a neighborhood of x where all but one finite number of the functions of Rare 0,

The sum of all the function values at x is 1, $\sum_{i=1}^{n} f_i(X) = 1$

Partitions of unity are useful because they often allow extending local constructions to the whole space. They are also important in the interpolation of data, in signal processing, and the theory of spline functions [3.34].

To improve a finite element approximation, the enrichment procedure may be applied. In other words, the accuracy of solution can be improved by including the analytical solution of the problem in the finite element formulation. In fracture mechanics problem, if the analytical fracture tip

solution can be added to the framework of the finite element discretization, predicting fracture tip fields may be improved. This will results in increase in the number of degrees of freedom.

The partition of unity finite element method (PUFEM) using the concept of enrichment functions along with the partition of unity property, can help to obtain the following approximation of the displacement within a finite element.

$$u^h(x) = \sum_{j=1}^{m} N_j(x)(u_j + \sum_{i=1}^{n} P_i(x)a_{ji} \qquad 3\text{-}26$$

Where, Pi(x) are the enrichment functions and a_{ji} are the additional unknowns or degrees of freedom associated to the enriched solution m and n are the total number of nodes of finite elements and the number of enrichment functions Pi.

3.3.4 Enrichment Function

In two-dimensional problems, fracture modeling is characterized using of two different types of enrichment functions:

1. **The Heaviside Function .**

For the elements completely cut by the fracture, The Heaviside function H(x) is applied for enrichment. The splitting of the element by the fracture results in a jump in the displacement field and the Heaviside function provides a simple mathematical approach to model this kind of behavior.

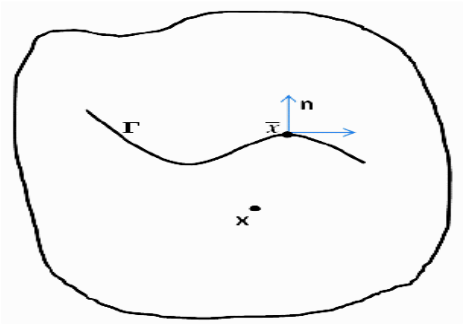

Figure 3.11 Evaluation of Heaviside function

For a continuous curve Γ representing a fracture within the deformable body Ω, we can consider a point x(x, y) in Ω. The objective is to determine the position of this point with respect to the fracture location. If the closest point belonging to Γ is$\bar{x}\,(\bar{x},\bar{y})$and the outward normal vector to Γ in$\bar{x}$ is n, the Heaviside function might be defined as follows:

$$H(x,y)=\begin{cases}1 \text{ for } (x-\bar{x}).n>0\\ -1 \text{ for } (x-\bar{x}).n<0\end{cases} \qquad 3\text{-}27$$

This function introduces the discontinuity across the fracture faces.

2. Asymptotic Near-Tip Field Functions.

For those elements that are not completely fractured and containing fracture tip, the Heaviside function cannot be used to approximate the displacement field in the entire element. For the fracture tip, the enrichment functions originally introduced by Fleming for use in the element free Galerkin Method. These four functions describe the fracture tip displacement field. The first function is discontinuous at the fracture tip.

$$[F_\alpha(r,\theta),a=1]=\begin{cases}\sqrt{r}\sin\left(\frac{\theta}{2}\right)\\ \sqrt{r}\cos\left(\frac{\theta}{2}\right)\\ \sqrt{r}\sin\left(\frac{\theta}{2}\right)sin\theta\\ \sqrt{r}\cos\left(\frac{\theta}{2}\right)sin\theta\end{cases} \qquad 3\text{-}28$$

In this formulation r,θ are polar coordinate defined at the fracture tip. The above functions can reproduce the asymptotic mode I and mode II displacement fields in LEFM, which represent the near-tip singular behavior in strains and stresses. These functions significantly improve the accuracy of calculation of KI and KII.

The term$\sqrt{r}\sin\left(\frac{\theta}{2}\right)$is discontinuous and therefore can represent the discontinuous behavior at the fracture tip. The remaining three functions are used to enhance approximation of the solution in the neighborhood of the fracture tip.

The circled nodes are the nodes of elements completely cut by the fracture and therefore enriched with Heaviside function. The nodes with Green Square are containing fracture tip and are enriched by fracture tip special function mentioned in equation above.

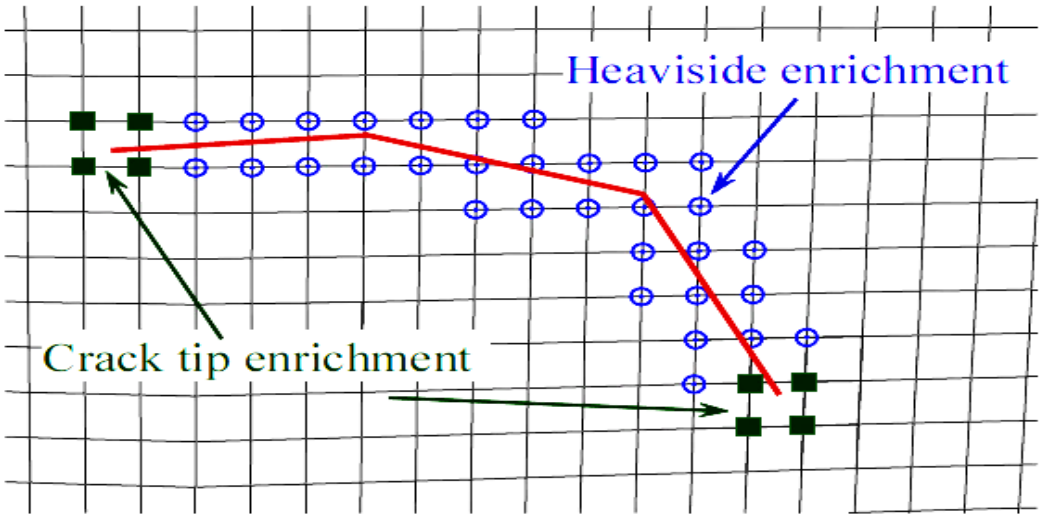

Figure 3.12 Enriched nodes in the XFEM. Circles: nodes with 2 additional DOFs. Squares: nodes with 8 additional DOFs [3.33].

Generally, for the purpose of fracture analysis, the enrichment functions typically consist of the near tip asymptotic functions that capture the singularity around the crack tip and a discontinuous function that represents the jump in displacement across the crack surfaces. The approximation for a displacement vector function with the partition of unity enrichment [3.29][3.31][3.32][3.35].

$$u = \sum_{I=1}^{N} N_I(X)[u_I + H(X)a_I + \sum_{a=1}^{4} F_a(X)b_I^a \qquad 3\text{-}29$$

Where **u** is the displacement vector.

N1(x) is the shape functions which applies to all nodes in the model

H(x) is the jump function and applies to nodes whose shape function support is cut by the crack interior.

a_I is the nodal enriched degrees of freedom vector.

Fα(x) is the asymptotic crack tip functions.

b_I^a is the nodal enriched degree of freedom vector.

The third term in the right side is applies to nodes shape function support is cut by the crack tip.

3.3.5 Level set Method for Modeling Discontinuities

In some cases, numerical simulations include moving objects, such as curves and surfaces on a fixed grid. This kind of modeling and tracking is difficult and requires complex mathematical procedure. The Level set Method (LSM) is a numerical technique that can help solving these difficulties. The key point in this method is to represent moving object as a zero level set function. To fully characterize a fracture, two different level set functions are defined:

1. A normal function, φ(x)
2. A tangential function, ψ(x)

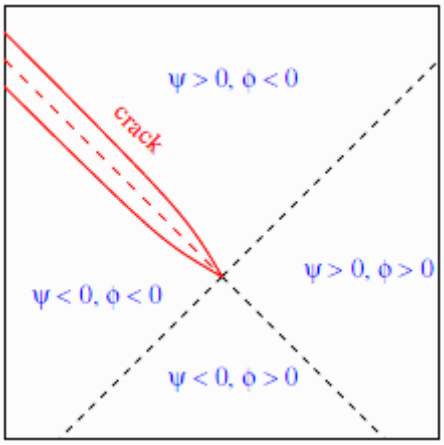

Figure 3.13 Construction of level set functions [3.32]

For the evaluation of the signed distance functions, assume Γ_c be the fracture surface and x the point we want to evaluate the φ(x) function. The normal level set function can be defined as

$\varphi(x) = (x - \bar{x}).n$ Where $\bar{x}$ and n are defined previously

The tangential level set function $\psi(x)$ is computed by finding the minimum signed distance to the normal at the fracture tip. In case of an interior fracture, two different functions can be applied. However, a unique tangential level set function can be defined as.

$$\Psi(x) = \max(\Psi_1(x), \Psi_2(x)) \qquad 3\text{-}30$$

In conclusion, referring the figure above it may be written as follows:

$$\begin{cases} \text{for } x \in \Gamma_{cr}\ (x = 0) & \text{and } \Psi(x \leq 0) \\ \text{for } x \in \Gamma_{tip}\ (x = 0) & \text{and } \Psi(x = 0) \end{cases}$$

Where Γ_{tip} indicates the fracture tips location.

3.3.6 Implementation of XFEM in Abaqus.

In ABAQUS when the crack propagation is simulated using XFEM, the near tip asymptotic singularity (the third term in the equation above) is not needed, and only the displacement jump across a cracked element (the second term in equation above) is considered. Therefore, the crack-tip has to propagate across an entire element at a time to avoid the need to model the stress singularity [3.35]. Level set method in ABAQUS is a numerical technique for describing a crack and tracking the motion of the crack. It couples naturally with XFEM and makes possible the modeling of 3D arbitrary crack growth without re-meshing [3.34]. Phantom nodes, which are superimposed on the original real nodes, are used to represent the discontinuity of the cracked elements. The phantom node iscompletely constrained to its corresponding real node when the element is intact; while the phantom node splits from the real node when the element is cut through by a crack. [3.35]

XFEM in ABAQUS makes crack modeling easy and accurate and allows cracks to be modeled independent of the mesh. Allows simulation of initiation and propagation of discrete crack along an arbitrary, solution-dependent path without requirement of re-meshing and it supports contour integral evaluation for stationary cracks [3.31].

The fracture surfaces and the fracture tip location in Abaqus are identified with a numerical procedure based on Level se Method. Once the mesh discretization has been created, each node of the finite element grid is characterized with its three coordinates with respect to the global coordinate system and two additional parameters, called PHILSM and PSILSM. These parameters are nonzero only for the enriched elements and they might be easily interpreted as the nodal coordinates of the enriched nodes in a coordinate system centered at the fracture tip and whose axes are, respectively, tangent and normal to the fracture surfaces at the fracture tip [54].

In ABAQUS, the two cracks states can be predictable [3.31][3.34][3.35]. These are:

1. Stationary cracks
2. Propagating cracks.

There are two distinct types of damage modeling for propagating cracks within an XFEM framework. These are:

1. Cohesive Segment Approach, and

2. Linear Elastic fracture mechanics (LEFM) Approach based on Virtual Crack Closure Technique (VCCT).

1. **Cohesive Segment Approach.**

It can be used for brittle or ductile material fracture application. Uses traction separation laws and it follows the general framework for surface based cohesive behavior. The damage properties (Criteria) are specified as part of the bulk material definition.

The pressure over closure relationship governs the behavior when the crack is “closed” and cohesive behavior contributes to the contact normal stress when the crack is “open”. [3.36]

Crack initiation refers to the beginning of degradation of the cohesive response at an enriched element. The process of degradation begins when the stresses or the strains satisfy specified crack initiation criteria [3.36] [3.37] [3.38]. Crack initiation criteria in ABAQUS are available based on the stress and strain. These are:

Maximum principal stress (MAXPS) and Maximum principal strain (MAXPE)

Maximum nominal stress (MAXS) and Maximum nominal strain (MAXE)

2. **Virtual Crack Closure Technique (VCCT)**

This method is more appropriate for fracture propagation problems in brittle materials. In this method, only the displacement jump function in cracked element is considered and the fracture has to propagate the entire element at once to avoid the need to model the stress singularity. The strain energy release rate at the fracture tip calculated based on the modified virtual crack closure Technique (VCCT). Using this approach fracture propagation along an arbitrary path can be simulated without the need to fracture path being known a priori.

The modeling technique is similar to the XFEM-based cohesive segment approach. In this method also phantom nodes are introduced to represent the discontinuity of the enriched elements. The fracture criterion satisfied when the equivalent strain energy release rate exceeds the critical strain energy rate at the fracture tip in the enriched element [3.34].

Chapter 4: ANALYTICAL AND NUMERICAL ASSESSMENT OF FATIGUE STRENGTH OF INTEGRAL SKIN-STRINGER PANELS

4.1 Introduction.

For components subjected to mechanical loadings FKM Guideline "Analytical Strength Assessment of Components in Mechanical Engineering" [4.1] allows an analytical assessment of the static strength and of the fatigue strength, the latter as an assessment of the fatigue limit, of the constant amplitude fatigue strength or of the variable amplitude fatigue strength, according to the service stress conditions. The FKM Guideline is valid for components produced with or without machining or by welding of steel, iron or aluminum materials that are intended for use under normal or elevated temperature conditions, and in detail:

- For components with geometrical notches,
- For components with welded joints,
- For static loading,
- For fatigue loading with more than about 10^4 constant or variable amplitude cycles,
- For milled or forged steel, also stainless steel, cast iron materials as well as aluminum alloys or cast aluminum alloys,
- For component temperatures from - 40°C to 500°C for steel, from - 25°C to 500°C for cast iron materials and from - 25°C to 200°C for aluminum materials,
- For a non-corrosive environment.

Basis of the FKM Guideline "Analytical Strength Assessment of Components in Mechanical Engineering" are the former TGL-Standards, the former VDI-Guideline 2226, as well as the German regulations DIN 18 800, the IIW-Recommendations and Eurocode 3. Moreover, the guideline was developed to the current state of knowledge by considering the results of more recent investigations.

In general, an assessment of the static strength is required prior to an assessment of the fatigue strength. Before applying the guideline, it has to be decided what cross-sections or structural detail of the component shall be assessed and what service loadings are to be considered. The service loadings are to be determined on the safe side, that is they should – with a sufficient

probability – be higher than most of the normally occurring loadings. The strength values are supposed to correspond to an anticipated probability of 97.5 % (average probability of survival P_0 = 97.5 %).

The procedure of calculation for an assessment of the static strength is presented in Figure 4.1, and almost identical procedure for an assessment of the fatigue strength in Figure 4.2. At the assessment stage (box at bottom of either Figure) the characteristic values of service stress occurring in the component (box at top on the left) and the component strength values derived from the mechanical material properties and the design parameters (middle column) are compared by including the required safety factors (box at bottom on the right). In specifying component fatigue strength values the mean stress and the variable amplitude effects are regarded as essential factors of influence. The assessment of strength is successful if the degree of utilization is less or equal 1.00 (or 100%), where the degree of utilization is defined by the ratio of the characteristic service stress to the component strength value that has been reduced by the safety factor.

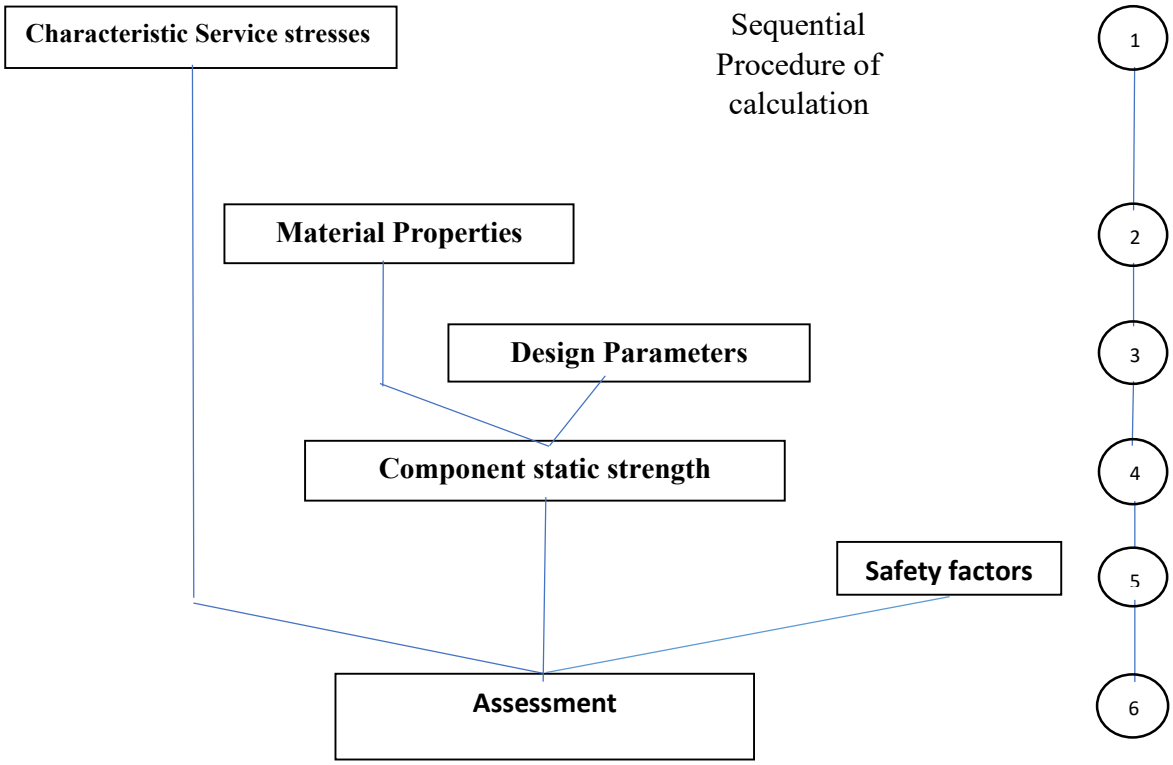

Figure 4.1 Procedure of calculation for an assessment of the static strength

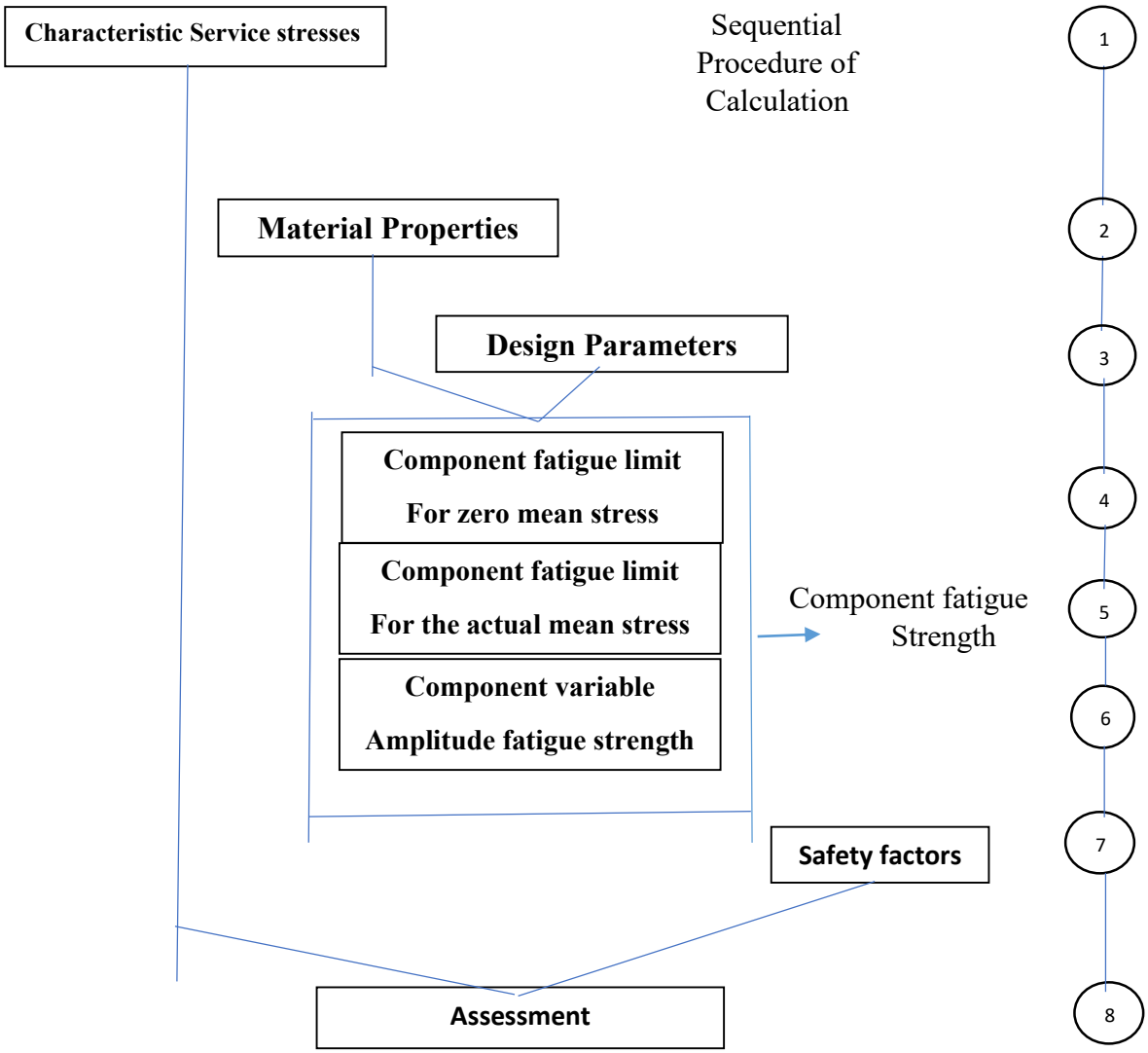

Figure 4.2 Procedure of calculation for an assessment of the fatigue strength

4.2 Service stresses.

For an application of the guideline the stresses resulting from the service loadings have to be determined for the so-called reference point of the component, that is the potential point of fatigue crack initiation at the cross section or at the component under consideration. In case of

doubt, several reference points are to be considered, for example in the case of welded joints the toe and the root of the weld. There is a need to distinguish the names and subscripts of the different components or types of stress that may act in rod-shaped (1D), in shell-shaped (2D) or in block-shaped (3D) components, respectively. The stresses are to be determined according to known principles and techniques: analytically according to elementary or advanced methods of theoretical mechanics, numerically after the finite element or the boundary element method, or experimentally by measurement.

All stresses, except the stress amplitudes, are combined with a sign; in particular, compressive stresses are negative. To perform an assessment, it is necessary to decide about the kind of stress determination for the reference point considered: the stresses can be determined as nominal stresses, as elastically determined local stresses, effective notch stresses or structural (hot spot) stresses. Correspondingly, the component strength values are to be determined as nominal strength values or as local strength values of the elastic local stress, of the effective notch stress or of the structural stress. With the procedures of calculation structured uniformly for both types of stress determination it is intended that more or less identical results will be obtained from comparable strength assessments based on either nominal stresses or local stresses.

The procedure of calculation using nominal stresses is to be preferred for simple rod-shaped (1D) and for shell shaped (2D) components. The procedure of calculation using local stresses has to be applied to block-shaped (3D) components, and moreover in general, if the stresses are determined by a finite-element or a boundary-element calculation, if there are no well-defined cross-sections or no simple cross-section shapes, if stress concentration factors or fatigue notch factors are not known, or (concerning the assessment of the static strength) in the case of brittle materials.

4.3 Assessment of the fatigue strength using local stresses.

Relevant local characteristic service stresses are the largest stress amplitudes in connection with the respective stress spectra and the related mean stress values. They are determined for the individual stress components or types of stress, e.g. amplitudes and mean values of the local normal (axial and/or bending) stress, σ_a and σ_m, and so forth.

The relevant material properties are determined as for nominal stresses. Design parameters to be considered in particular are the K_t–K_f ratios, allowing for the design of the component (shape and size), as well as the roughness factor and the surface treatment factor, by which the respective surface properties are accounted for. By specific combination of all these factors a summary design factor is calculated. The local values of the component fatigue limit for completely reversed stresses follow from the derived fatigue limit values of the material, divided by the respective design factors.

The conversions to the amplitude of the component fatigue limit and to the amplitude of the component variable amplitude fatigue strength are as for nominal stresses. The safety factors are to be determined as for nominal stresses. The assessment by means of the degree of utilization is as for nominal stresses, but with the respective local values of the characteristic stress amplitude and the value of the component fatigue limit or of the component variable amplitude fatigue strength. The assessment is carried out by means of the degree of utilization as for nominal stresses, but with the respective local values of the characteristic service stress and the local component strength values. For welded components the assessment of the static strength using local stresses is carried out using structural stresses (not with notch root stresses), for the weld toe as for non-welded components, for the root of the weld using an equivalent structural stress, that is to be derived from the structural stress components acting in the weld seam. For the assessment of the fatigue strength of welded components using structural stresses or effective notch stresses the same basic fatigue limit values for completely reversed stresses apply as for nominal stresses. They hold for effective notch stresses without conversion, but for structural stresses they have to be converted by factors given for some typical weld details. The combined effect of mean stress and of residual stresses in welded components is to be considered as for nominal stresses by means of a mean stress factor together with a residual stress factor.

4.4 WB/FKM-Weld software (FKM inside ANSYS).

The software WB/FKM-Weld (FKM inside ANSYS) allows strength assessments based on the FKM Guideline “Analytical Strength Assessment of Components in Mechanical Engineering”. As mentioned above, the guideline covers assessments of static strength and fatigue strength for components under mechanical loading. Results of CAE simulations are commonly

used to determine the local stresses for the assessment. WB/FKM-Weld performs assessments based on the FKM Guideline for all selected welds of a component. In a graphical user interface, user defines additional settings required for the weld assessments. The necessary model information is used from ANSYS Workbench. Load combinations are automatically defined based on the load steps and loading types defined in ANSYS Workbench. The software analyzes the worst load combination for every node of the finite element mesh. The result of the assessment, the degree of utilization, is visually shown on the finite element mesh in ANSYS Workbench, **but obtained values are result of analytical procedure**. WB/FKM-Weld eliminates the need to preselect critical hot-spots in an assessment and most of the manual data entries required with other software tools. Result interpretation is simplified by visualizing the degree of utilization together with the relevant load combination and other data in one plot. This allows users to identify critical hotspots as well as areas allowing material savings.

4.4.1 Modeling types and weld line definition

WB/FKM-Weld is capable to work with different representations of weld lines within the model. Depending on the representation, the definition of the weld line is based on various kinds of selections:

- Welded parts are within one body, and no weld line is defined
- Welded parts are separate bodies connected with contacts, and no weld line is defined
- Welded parts are within one body, weld line is modeled
- Welded parts are separate bodies connected with contacts, weld line is modeled.

A weld line is defined by one or more weld toes which represent the border between weld line and part. A weld toe may consist of one or more geometrical edges. Some assessment parameter can be associated separately to each edge, others to the complete weld line. The following Figure 4.3 show weld toes and geometrical edges, if the weld line is modeled and not modeled.

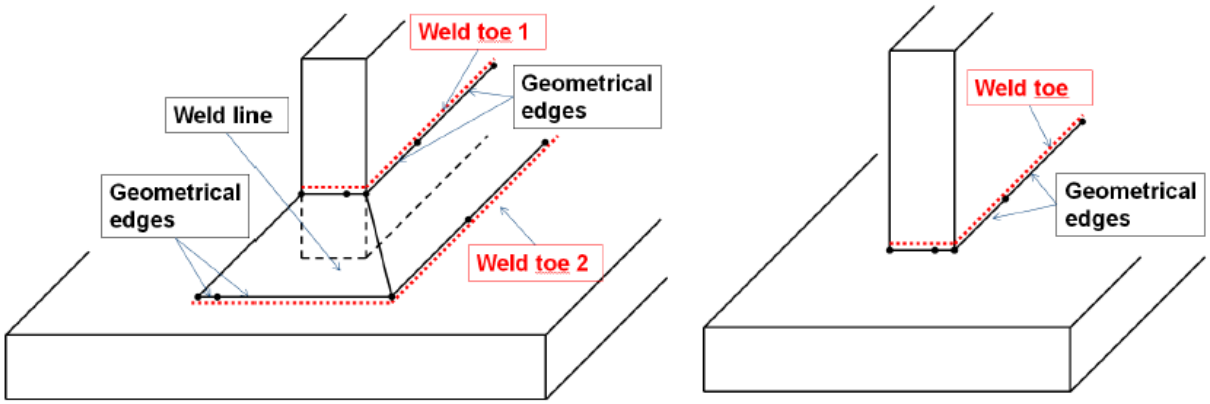

Figure 4.3 Weld toes and geometrical edges

In addition, the extrapolation surfaces attached to the weld toes have to be defined (Figure 4.4). An extrapolation surface might be associated to more than one geometrical edge of the weld toe.

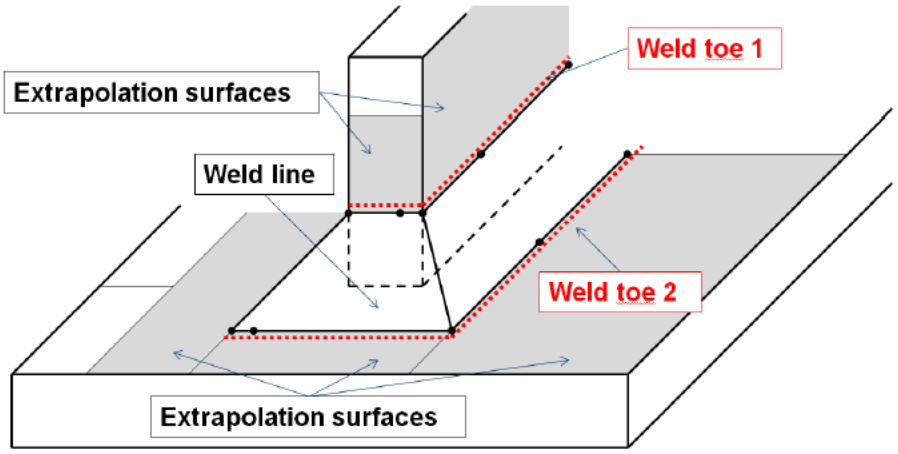

Figure 4.4 Weld toes and extrapolation surfaces

Geometry that was analyzed using WB/FKM-Weld is shown in Figure 4.5 and has exactly the same dimensions as real skin-stringer panel experimentally and numerically analyzed (shown later in Chapters 5 and 6). Loads and boundary conditions applied matched those used in numerical and experimental analysis. Connection between base plate and stringers was obtained using laser beam welding. Simulation of this process is presented later in this Chapter.

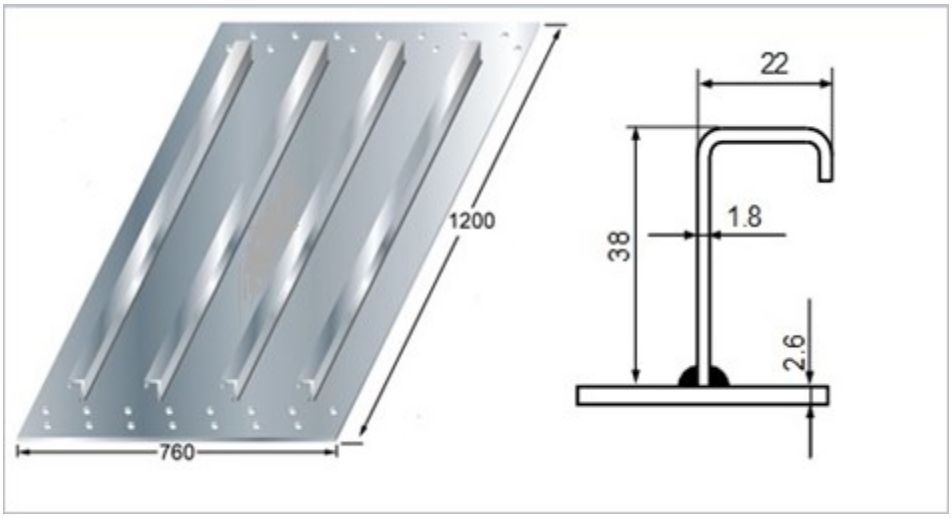

Figure 4.5 Dimensions of the 4-stringer panel made of 6156-T6 aluminum

4.5 Static and fatigue strength assessment of 4-stringer plate.

Model of four stringers welded to a base metal made of 6156 T6 aluminum with generated mesh is shown in Figure 4.6. Details of mesh can be seen in Figure 4.7.

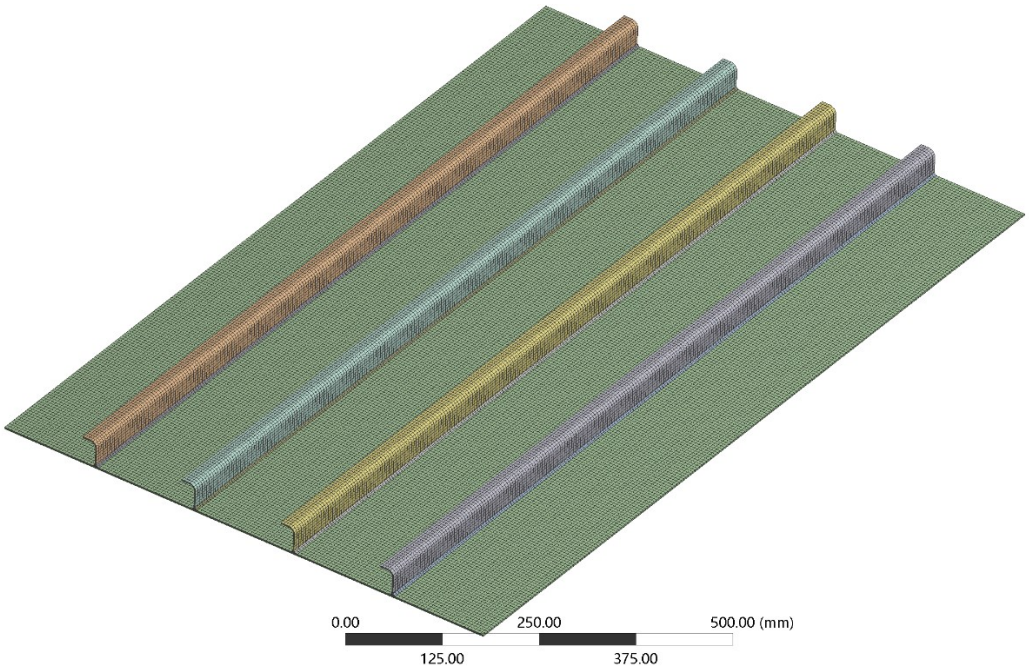

Figure 4.6 Finite element model of the 4-stringer panel made of 6156 T6 aluminum

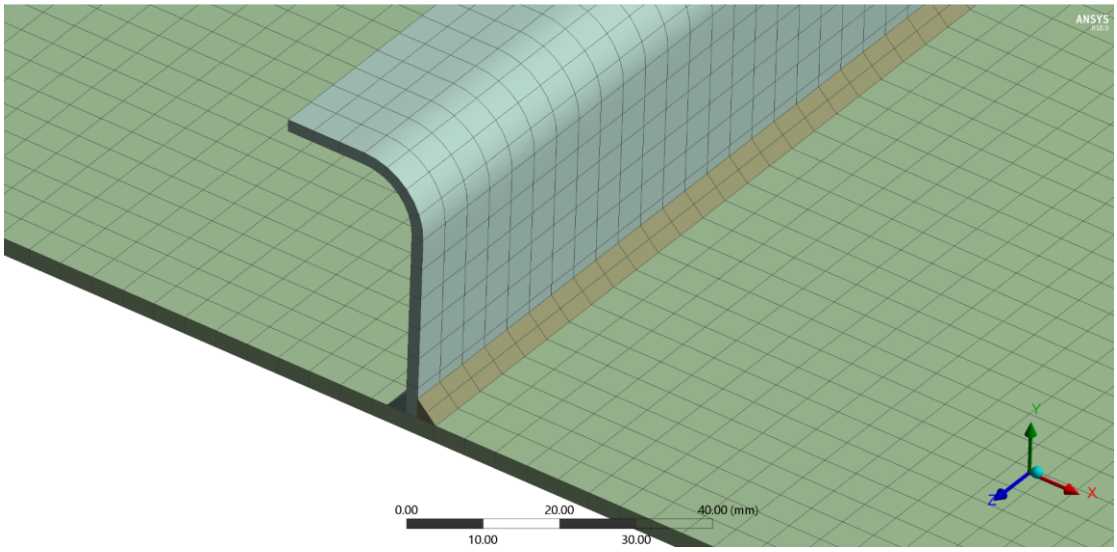

Figure 4.7 Details of mesh of 4-stringer model. Weld line is also presented.

In order to perform static and fatigue strength assessment of welded structure, welded toes, lines and extrapolations surfaces had to be defined, according to Figure 4.4. Figures 4.8 to 4.9 shows defined toes and surfaces for stringer and base metal. Toes, lines and surfaces had been defined for each stringer in the manner showed in Figures 4.8 and 4.9. Figure 4.10 shows definition of all weld connections and settings of weld lines, as well as construction properties, weld type and quality, and properties of S-N curve of material used for welding. In fatigue assessment of weld joint number of cycles used was 5e6. Figure 4.11 shows additional fatigue properties.

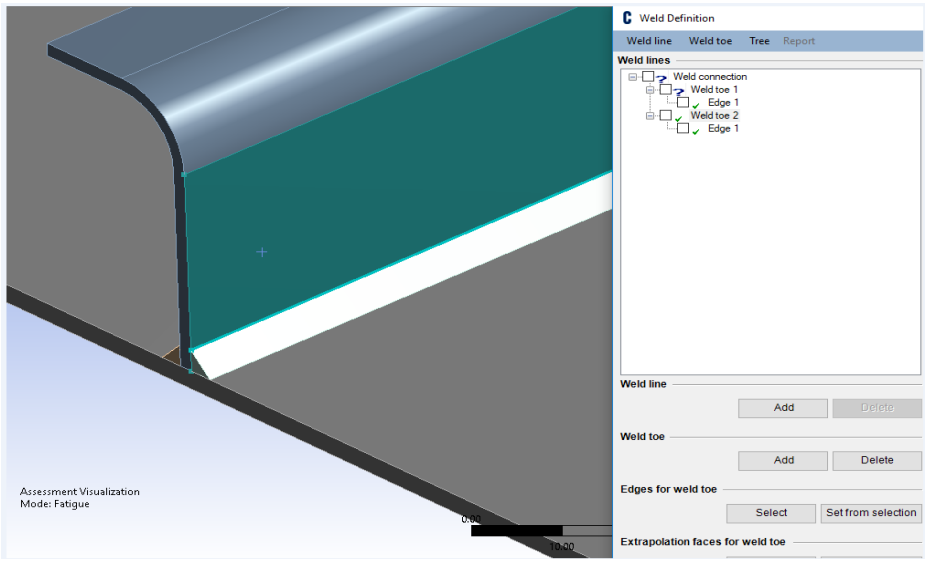

Figure 4.8 Weld toe and extrapolation surface defined on stringer

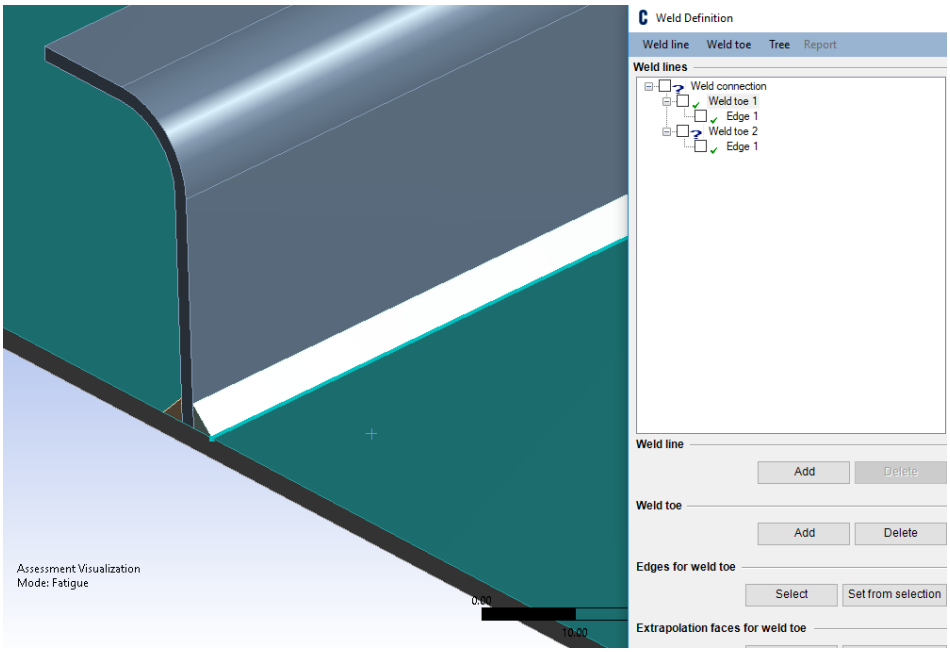

Figure 4.9 Weld toe and extrapolation surface defined on base metal

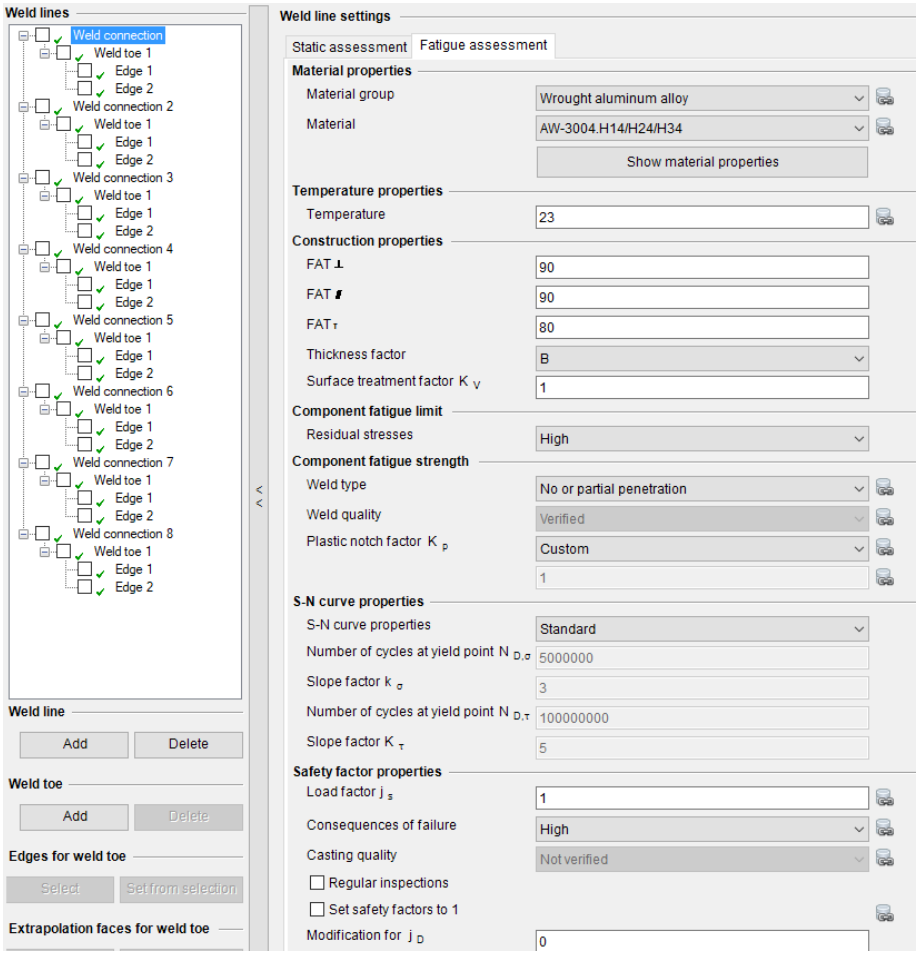

Figure 4.10 Weld definition

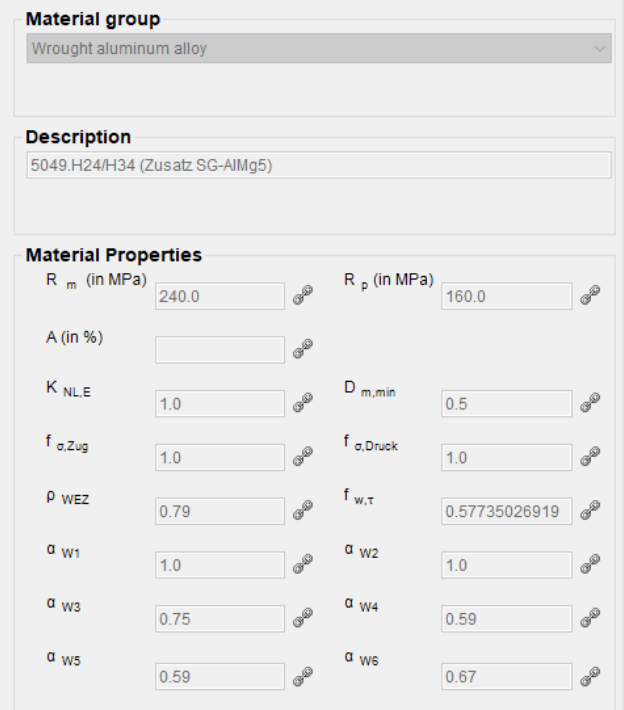

Figure 4.11 Fatigue properties of welding material

After completely defining weld lines, external force (magnitude 115000N) and boundary conditions were applied (Figures 4.12, 4.13 and 4.14 respectively) to match conditions in experiment with real skin-stringer plate.

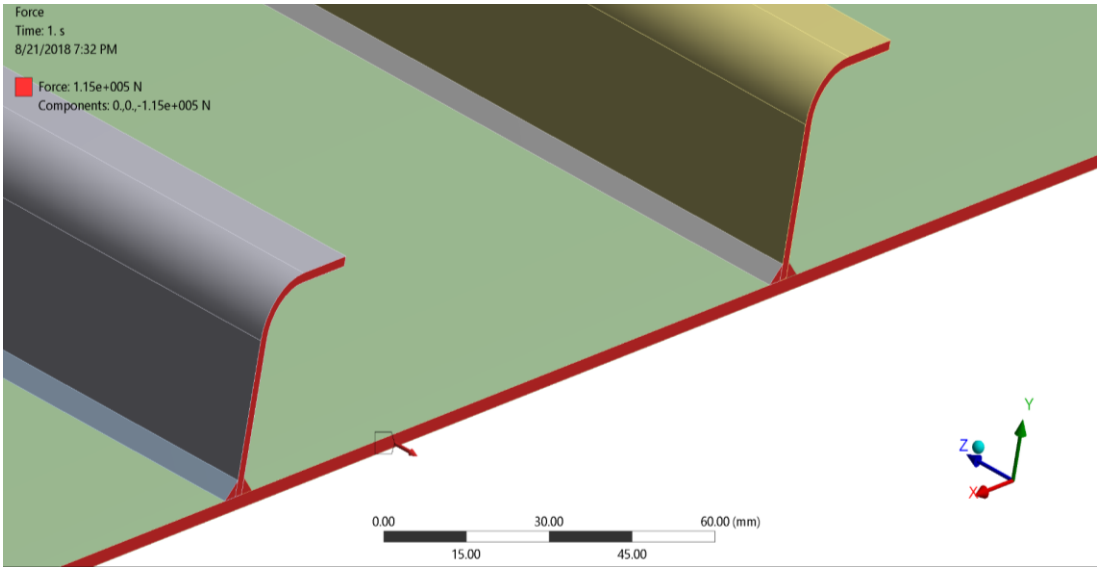

Figure 4.12 Force of magnitude 115000N applied in z direction

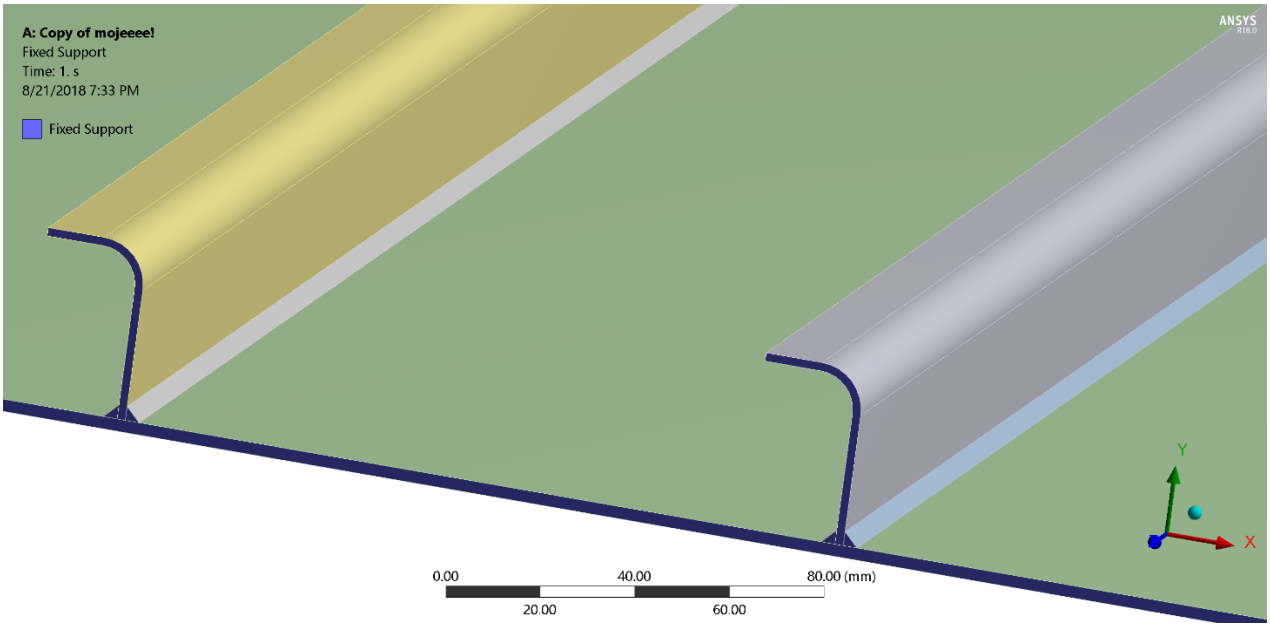

Figure 4.13 One end of the base metal and stringers is fixed

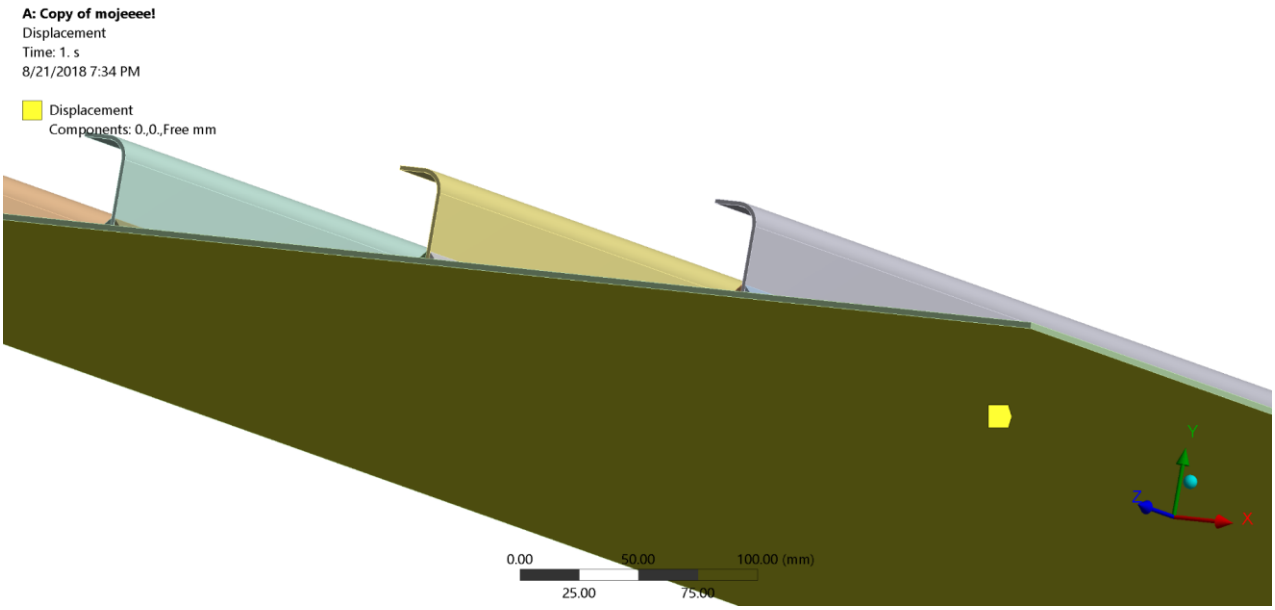

Figure 4.14 Displacement applied on bottom surface of base metal (free motion in z direction)

Figure 4.15 shows deformation obtained in numerical simulation, while Figure 4.16 presents stress distribution. Deformation obtained in simulation was compared to deformation measured in experiment and very good match was detected. This was the proof that numerical model was well defined. Immediately after this confirmation, fatigue analysis of model was conducted in Ansys Workbench with variable load (stress ratio R=0.1 was taken from experiment)

to see is there possibility of crack initiation on skin-stringer plate under presumed load. Analysis showed no evidence of crack initiation after 1e9 cycles (Figure 4.17). Nevertheless, in Chapters 5 and 6 skins-stringer plates with initial cracks were investigated, because cracks might be result of extreme loads or damage caused by unforeseen circumstances.

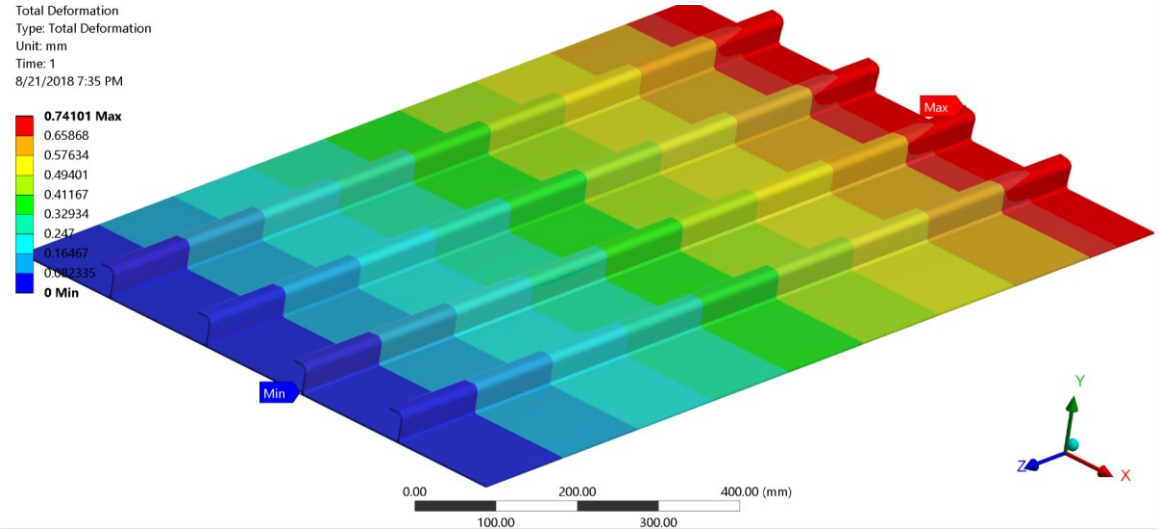

Figure 4.15 Values of skin-stringer plate deformation

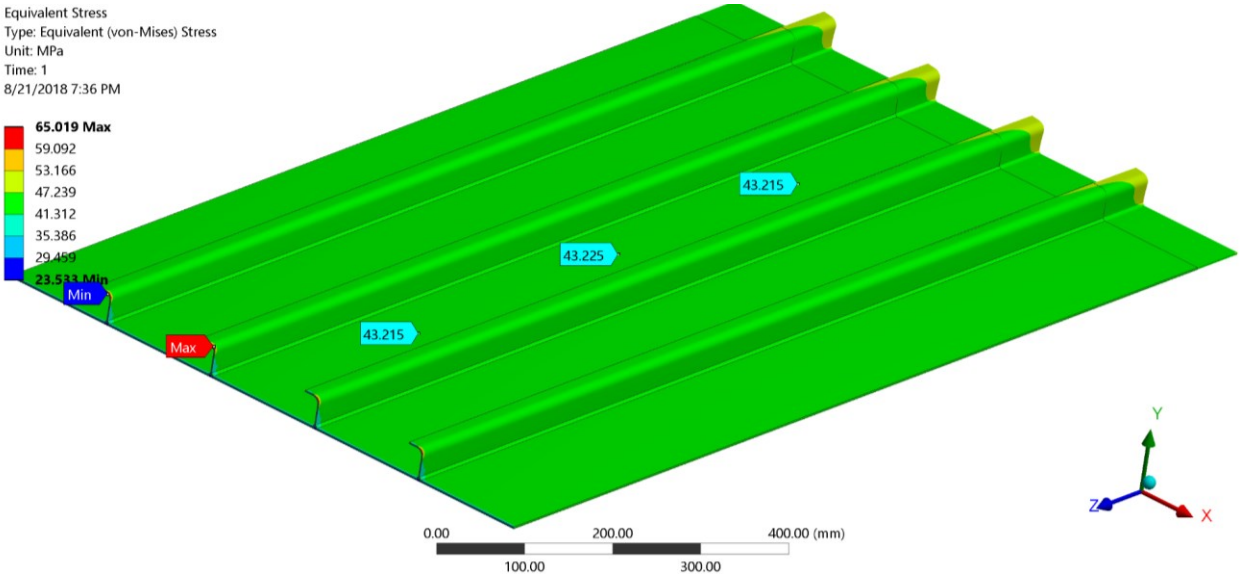

Figure 4.16 Von Mises Equivalent stresses. Uniform distribution in the middle of the plate is obtained as expected

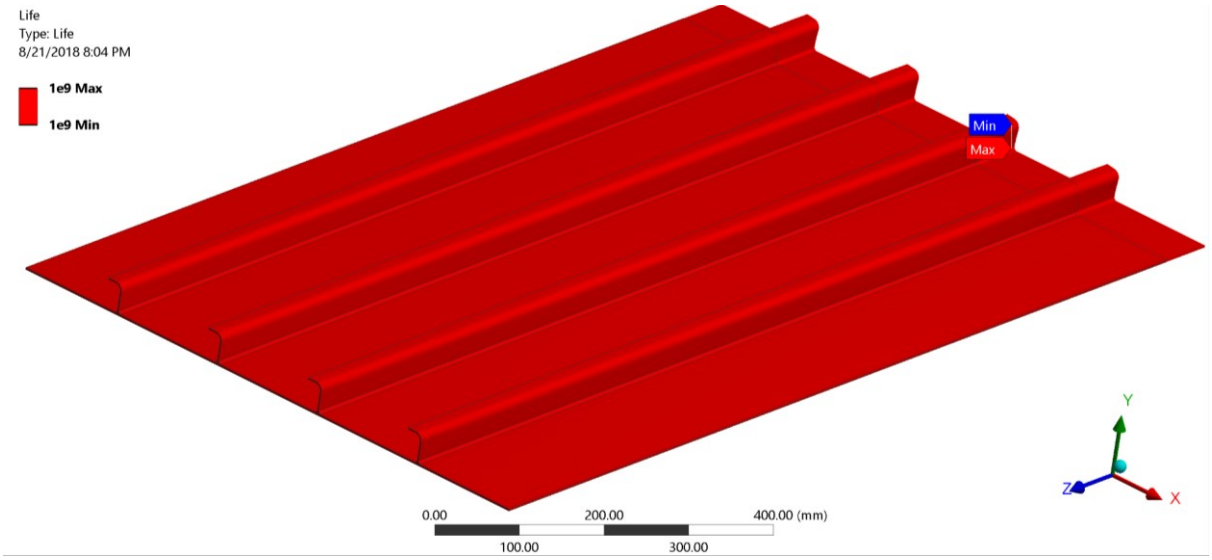

Figure 4.17 No evidence of crack initiation after 1e9 cycles of applied load (R=0.1)

Finally, results of WB/FKM-Weld analysis (static and fatigue strength assessment) are shown in Figures 4.18 to 4.20 (detailed report is presented in the appendix of this thesis). Static strength of welded joints is satisfactory because maximum obtained value is 43.74%, which is more than two times less than limit value. On the other hand, value for fatigue strength assessment is close to 100% (approximately 92%), but it is still below the defined limit, which implies that this weldment (all weld lines) will survive 5 million cycles of applied load.

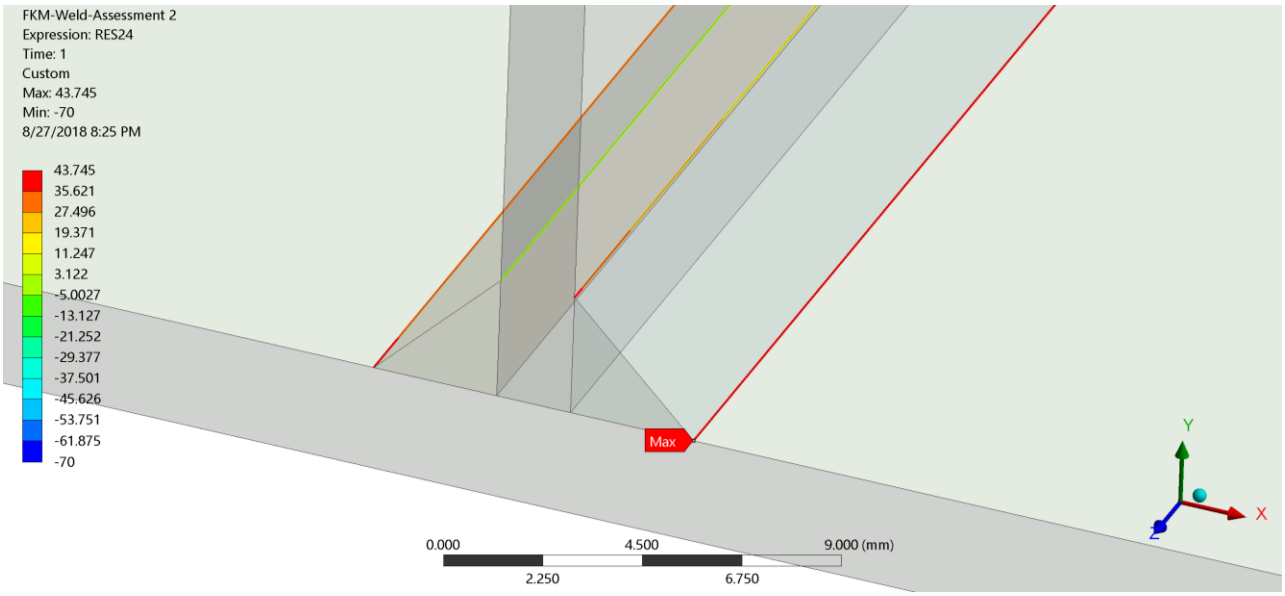

Figure 4.18 Static strength assessment of weld lines

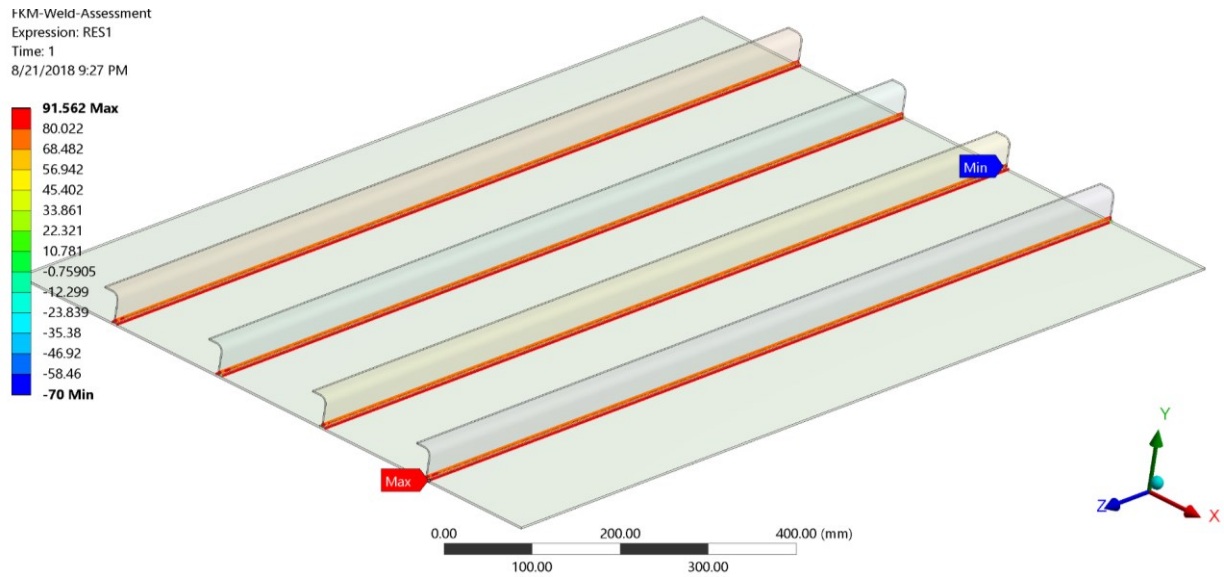

Figure 4.19 Fatigue strength assessment of all weld lines

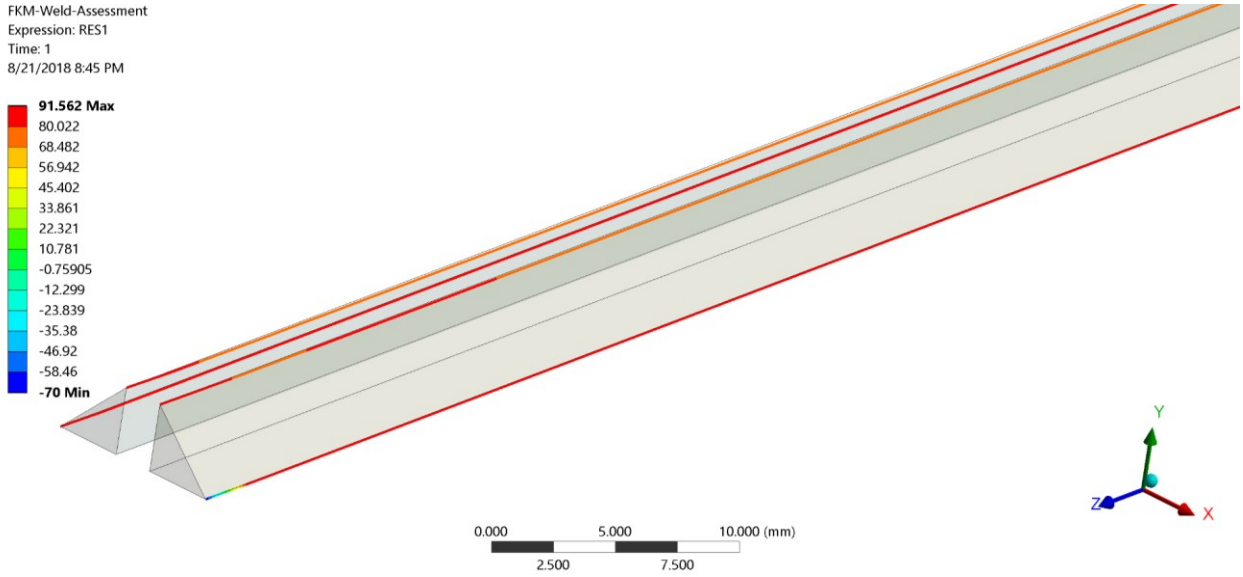

Figure 4.20 The most critical weld line

In next part of this Chapter finite element simulation of laser beam welding will be presented as a tool for heat affected zone identification and evaluation of residual stresses which can influence fatigue life of welded joints.

4.6 Finite element simulation of laser beam welding

The aircraft production industry has a high demand for lightweight solutions. In this context, the joining methods play a significant role in enabling the lightweight construction. Specifically, the use of aluminum alloys for structural components or body panels (like one presented in this thesis) is a major challenge for joining technologies. Aluminum alloys AA6xxx are very susceptible to hot cracks during fusion welding. As laser beam welding is increasingly used for welding aircraft components, special techniques are required to avoid hot cracks in weld seams. The impact of the adapted intensity on the process characteristics, e.g., the temperature field, the temperature gradients, or the molten pool geometry, can be determined by using numerical model. Here, we demonstrate possibilities of numerical simulation of laser beam welding.

For that purpose, simulation of welding process for one stringer is presented. Dimensions of the stringer are the same as dimensions of four stringers used in fatigue strength assessment. Geometry and mesh is presented in Figure 4.21, while boundary conditions are presented in Figure 4.22. It is important to emphasize that all initial connections between stringer, base metal and weld lines were modeled as frictional (coefficient of friction was 0.2) because in reality these element are not connected at all before welding.

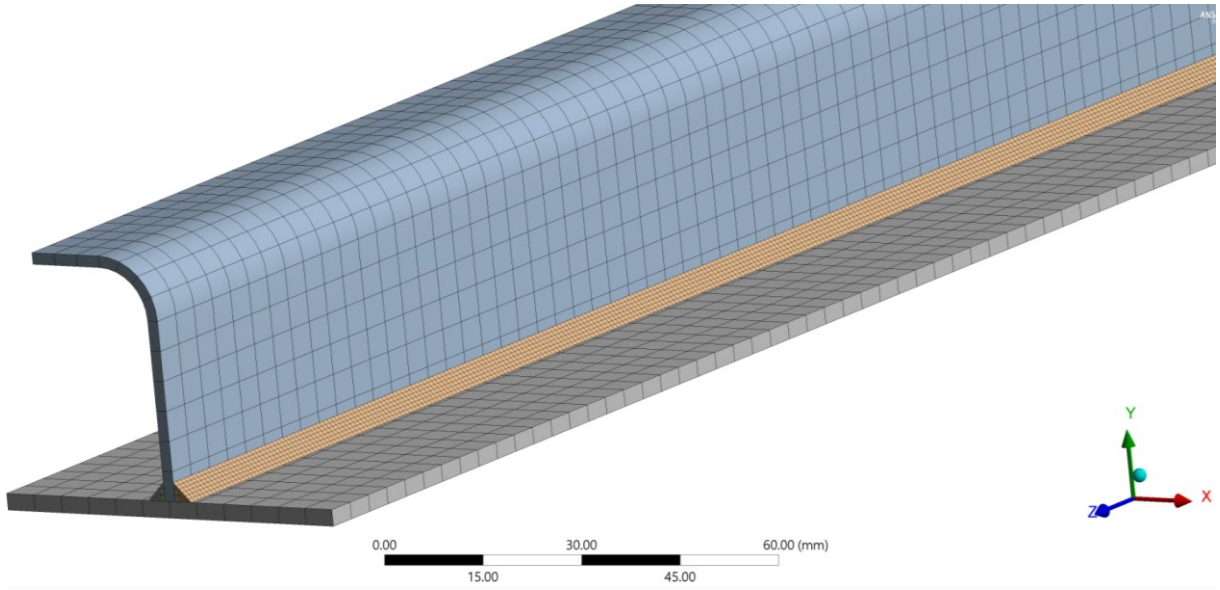

Figure 4.21 Mesh of stringer, weld lines and base metal

To simulate contact change, since after welding they will be firmly connected, command shown in Figure 4.23 was used to tell software to change type of contact from frictional to bonded (i.e. welded) when temperature reaches 150^0C. The contact status will remain bonded for the rest of the analysis, even if the temperature subsequently decreases below the critical value.

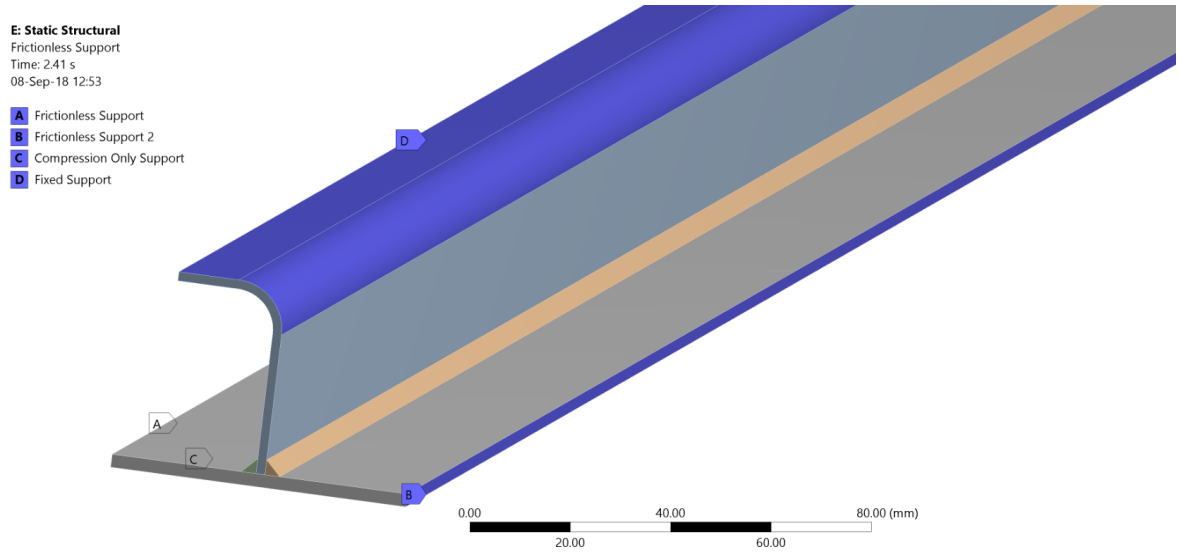

Figure 4.22 Boundary conditions used in laser beam welding simulation

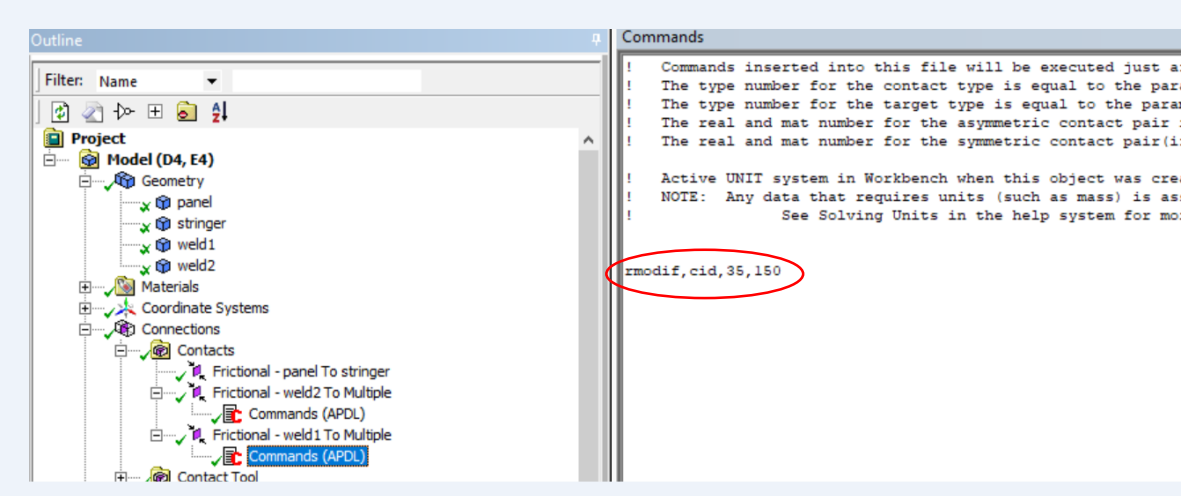

Figure 4.23 Command for defining critical bonding temperature of 150^0C

All the parts in the model were assigned the same material properties of Al6156-T6. For simplicity, no temperature dependent properties were considered. Also material was considered to be linear elastic. Welding process simulation involves two steps: (1)

Transient thermal and (2) Thermal Stress analysis. To simulate the thermal field produced by the welding process, it is necessary to model the heat source accurately and for that purpose "Moving Heat Flux" ACT extension – available for download from ANSYS support website – must be used. Also, change of convection coefficient with temperature for aluminum must be defined (Figure 4.24), as well as velocity of laser beam (5mm/s in our case) and Gaussian heat flux constant (7.5W/mm^2).

Figure 4.25 shows temperature distribution during laser beam welding simulation, while Figure 4.26 presents heat affected zone formed during the welded process.

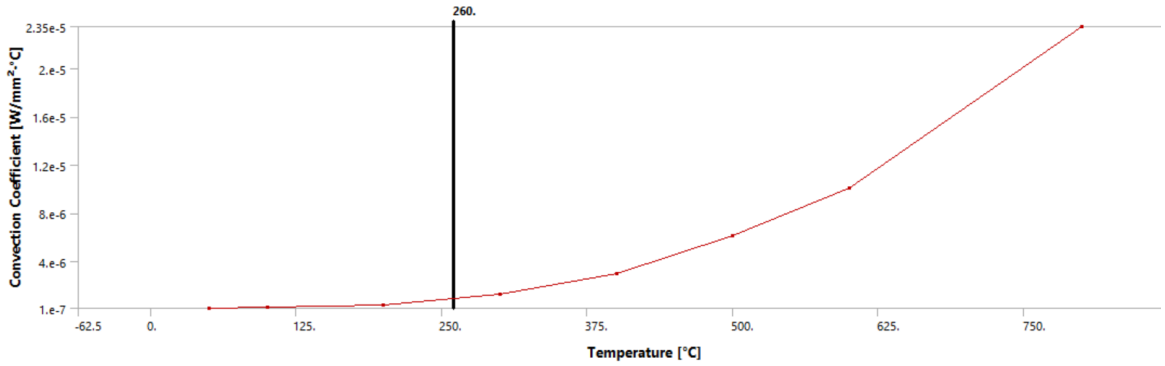

Figure 4.24 Convection coefficient vs. temperature for aluminum

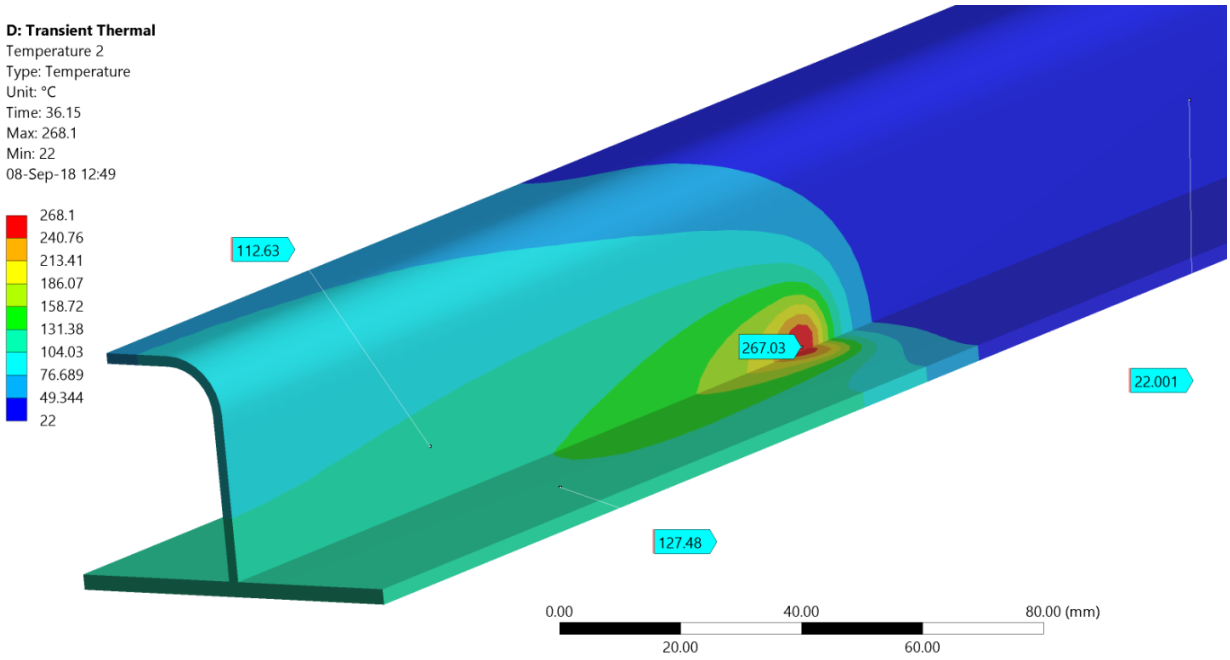

Figure 4.25 Temperature distribution 36.15s after welding started

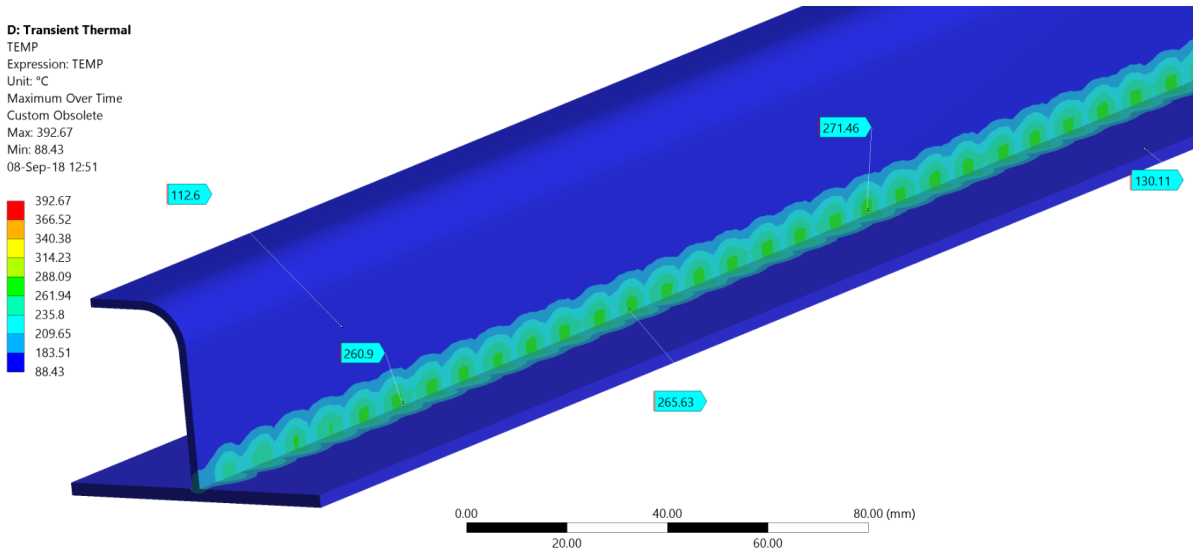

Figure 4.26 Heat effected zone

After the thermal analysis, temperatures can be imported to static structural analysis for all time instants (Figure 4.27) to perform thermal stress analysis. Values of total deformation and von Mises stress distribution at the end of the welding process simulation are shown in Figures 4.28 and 4.29.

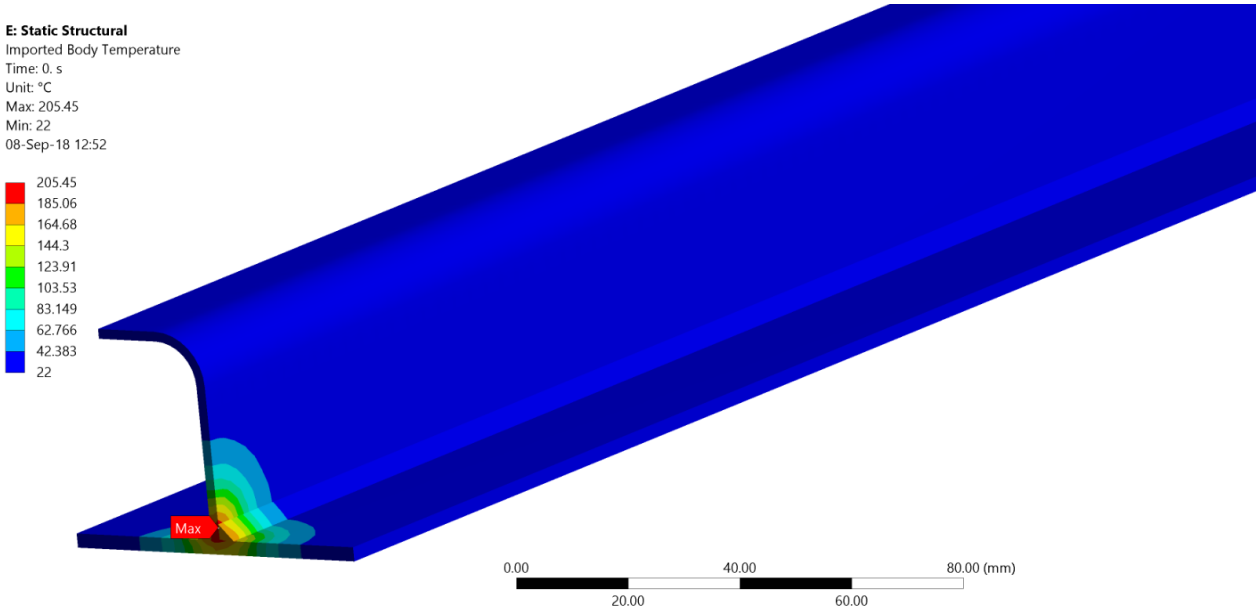

Figure 4.27 Imported temperature at initial time (t=0s)

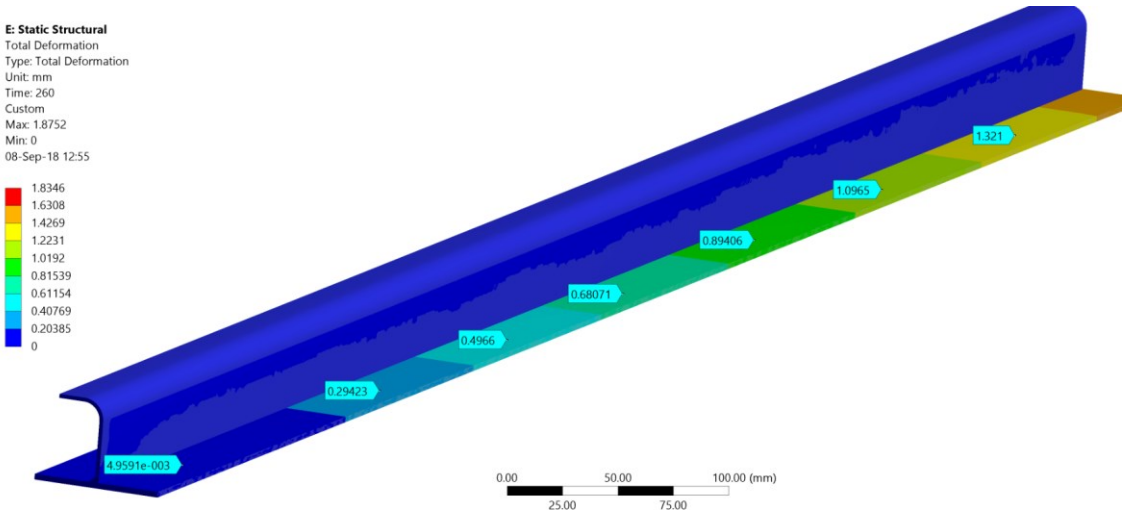

Figure 4.28 Total deformation of base plate after welding

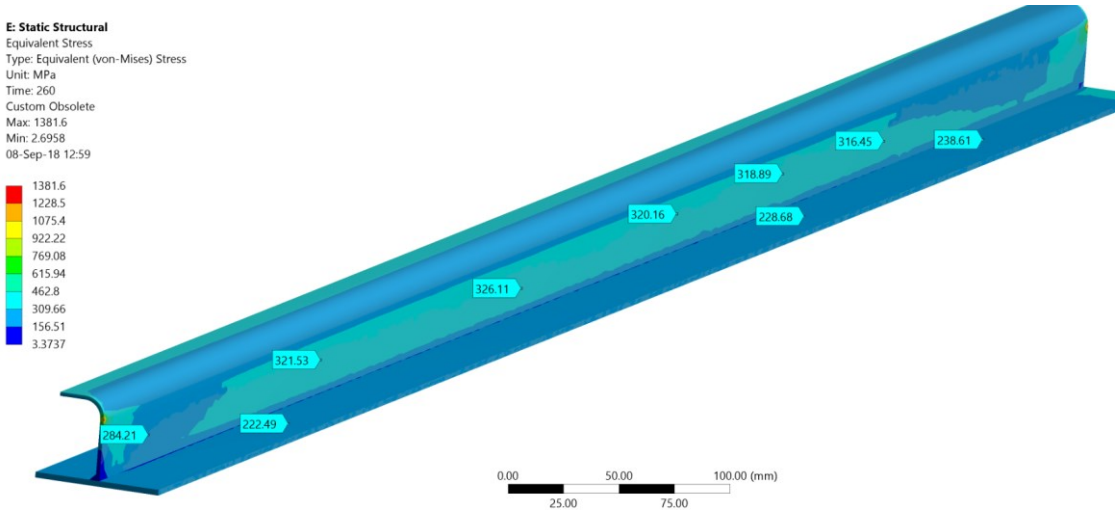

Figure 4.29 Equivalent von Mises stress 20 s after welding ended

As can be seen in Figure 4.29, thermal stresses obtained in numerical simulation of laser welding were higher than 290 MPa (value representing the yield stress of Al6156-T6), which means there is a possibility of small plastic deformation of stringer in reality. To prevent this, heat source must provide less power than 7.5W/mm^2. Nevertheless, there is significant amount of residual stress after welding that later can affect fatigue strength of welded joint. This is why some thermal or mechanical treatments must be applied for stress relief of skin-stringer plate.

Chapter 5: NUMERICAL SIMULATIONS OF CRACK GROWTH IN DAMAGE INTEGRAL SKIN STRINGER PANEL USING XFEM.

5.1 Morfeo/crack for Abaqus.

5.1.1 Introduction.

Morfeo/Crack is a software product for the computation of the stress intensity factors (SIFs) along the front of three-dimensional cracks and the prediction of crack propagation under fatigue loading using the extended finite element method (XFEM). XFEM is an extension of the finite element method that allows the presence of cracks inside the elements and offers a high precision on the stress singularity at the crack front with special enriched degrees of freedom.

Morfeo/Crack for Abaqus is built upon the implementation of XFEM available in Abaqus since version 6.10. The functionality of Abaqus for SIF computation is however limited to the calculation of stationary cracks. Morfeo/Crack for Abaqus enhances Abaqus and is capable of performing crack propagation simulations in complex geometries. The method is based on calling Abaqus/Standard at each propagation step.

Between each step, it reads the Abaqus solution, recovers an richer, improved XFEM solution in a small area surrounding the crack using a tailored integration rule, accurately computes the stress intensity factors which determine the crack advance and updates the Abaqus input file with the new crack position. Moreover, Morfeo/Crack for Abaqus profits from the nice and intuitive user interface Abaqus/CAE since it is integrated in the latter as a plug-in for the definition of the initial crack position and the specific data for fatigue crack propagation. Finally, Morfeo/Crack for Abaqus offers the choice between post-processing the results in Abaqus/CAE as usual or in a freely available post-processor (gmsh), which renders the solution at the crack tip. [5.1].

5.1.2 Number of cycles and SIF calculations (ABAQUS).

In this article, software ABAQUS is used for Number of cycles and SIF calculation. The whole data input includes Part, property, load and so on. The modules of ABAQUS are described in the Figure 5.1

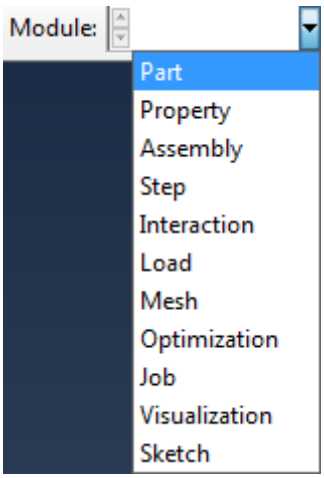

Figure 5.1 Modules in ABAQUS/CAE

There are 6 main steps of creating a model in ABAQUS

1. Create 3D model (shape and dimensions) .
2. Defining the materials, mechanical properties for all different zones.
3. Introducing the initial crack within the structure, including its shape and location.
4. Introduce the loading including its intensity, type and location within the structure.
5. Defining the boundary conditions,
6. Generating the final mesh, refined around the initial crack and in the regions were the crack expected to grow.

The X-FEM that provided by Morfeo was used for numerical simulation of fatigue crack growth.

5.2 Numerical model

5.2.1 Model I (base metal).

The main idea of numerical modeling was to test XFEM. This is done by making FE model of base metal plate with initial crack (as shown in Figure 5.2). The real loads from experiment data were used in the simulation. The number of cycles obtained numerically (obtained by the simulation) were compared with the number of cycles obtained experimentally. Base metal plate was chosen because it had simple geometry and the calculated values of SIF could be verified using other methods or can be even found in the literature.

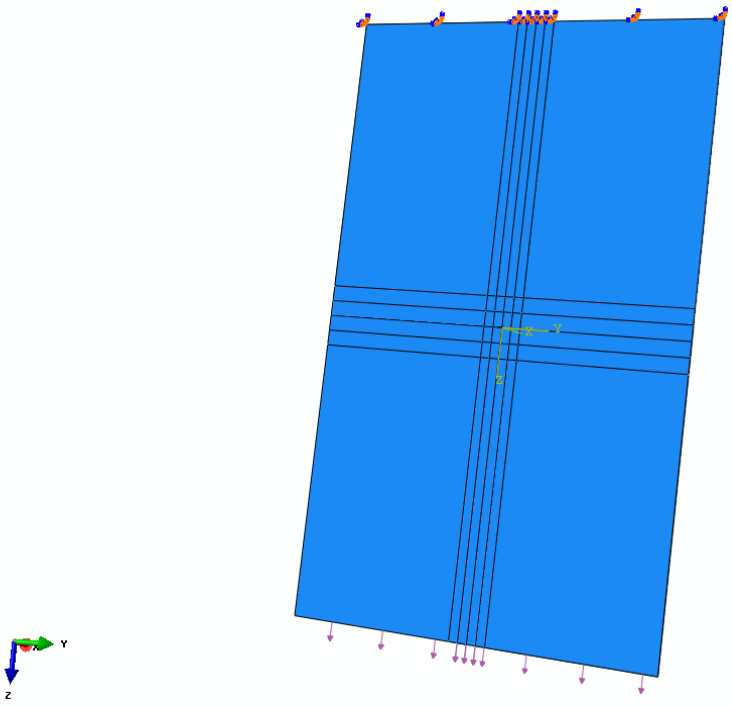

Figure 5.2 FE model of base metal plate with initial crack

In this simulation aluminum alloy AA6156 T6 was used (Young's modulus E = 71000 MPa, Poisson's ratio ν = 0.33).

The loads used in simulation were equal to average values of maximum tensile forces over time measured in experiments (obtained due to the courtesy of researchers from GKSS Research Center, Geesthacht). For base metal plate average maximum force was F_{max}=112.954 KN, while the load

ratio R=0.146 was determined on the basis of average minimum tensile force measured. Coefficients for Paris equations were adopted on the basis of the values obtained in tests with base metal plates: m = 3.174 and C=1.77195E-012 MPa mm$^{1/2}$.

Initial crack in the 1st simulation was propagated to length 2a=275 mm, and Figure 5.3 shows its shape after the last growth step.

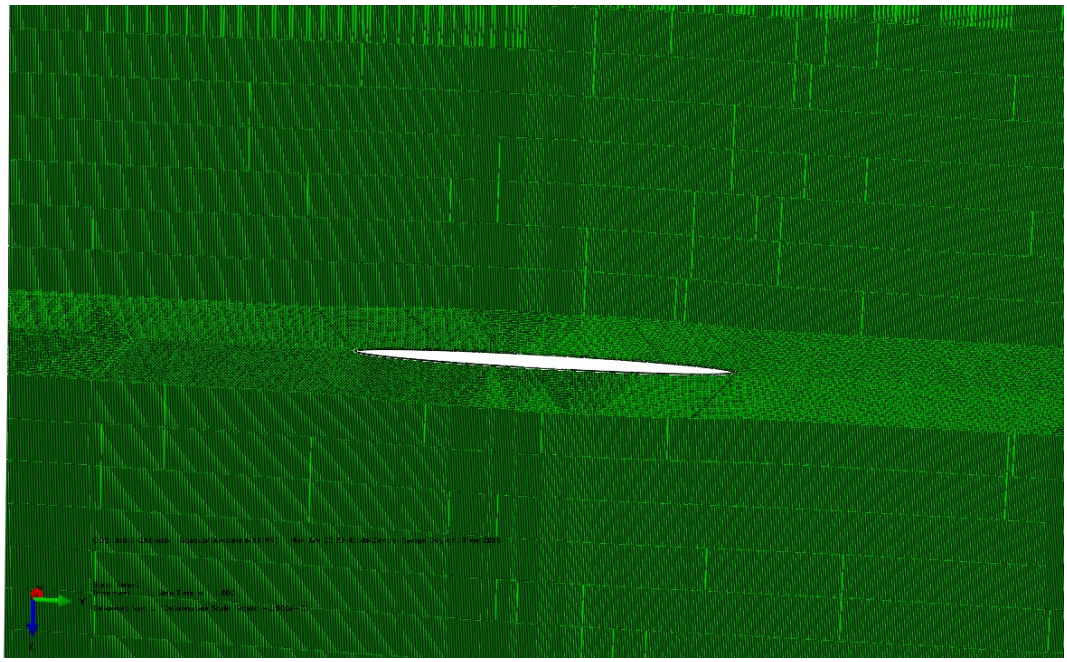

Figure 5.3 Crack on base metal plate after 260 steps of propagation (2a=275 mm)

5.2.2 Model II (4-stringer with 1mm size of mesh). AA6156 T6.

After successful numerical simulation of crack growth on base metal plate, the second has been performed on more complex geometry of 4-stringer plate previously analyzed in Chapter 4 (here shown in Figure 5.4).

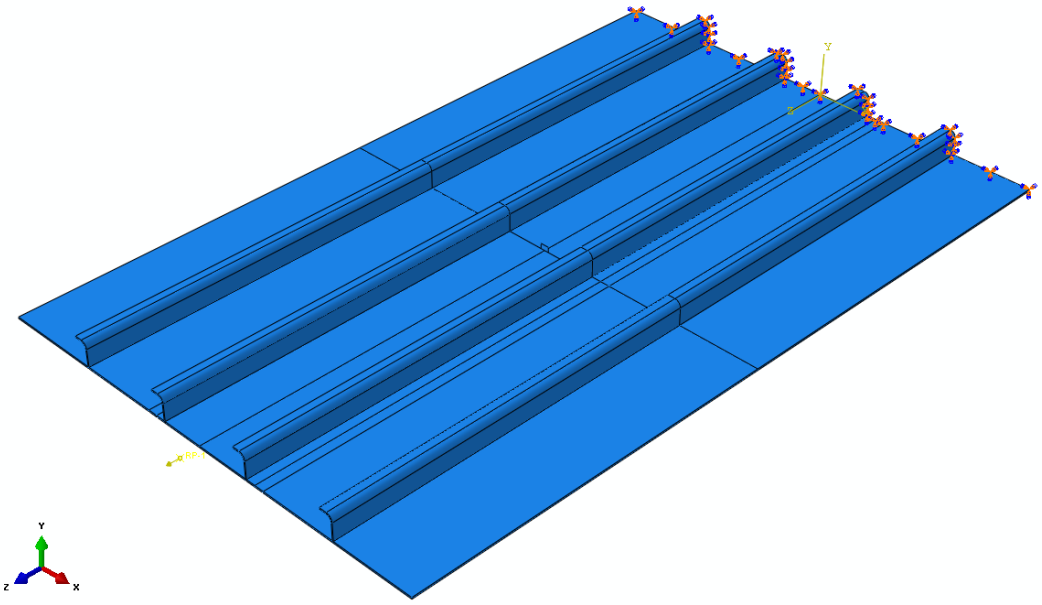

Figure 5.4 Model of 4-stringer plate with 3D crack used in simulation

The central crack of the length a0=14 mm was initiated and the load identical to that used for base metal plate was applied. The crack was propagated in the total of 173 steps (in each step crack length increased by 2 mm) and after 68 steps, it reached the wall of the left stringer and began to spread along it (Figure 5.5).

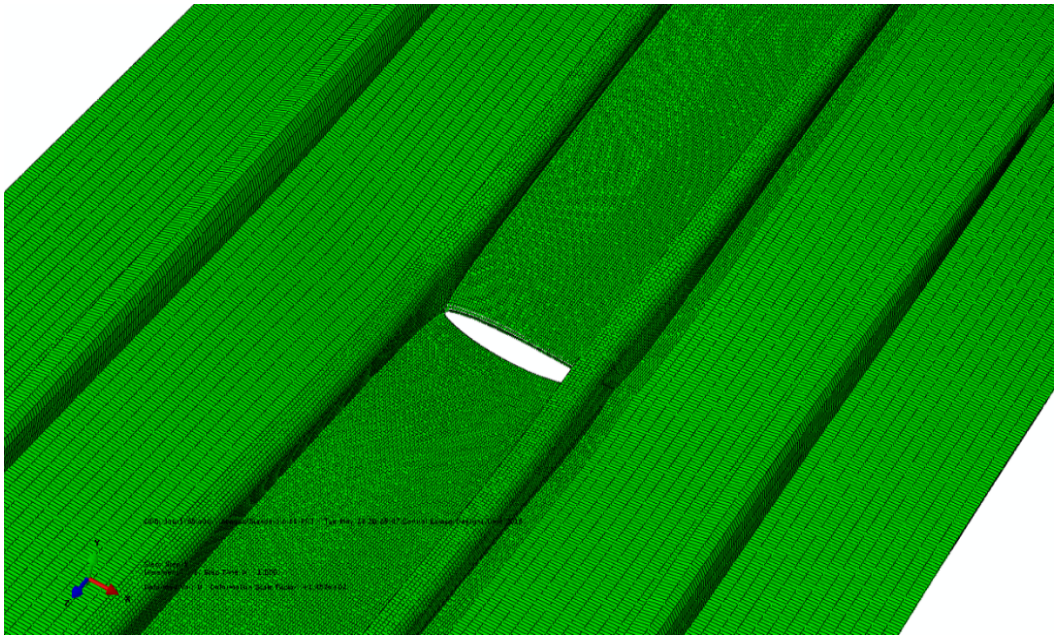

Figure 5.5 Crack in 4-stringer plate after 68 steps of propagation

At the same time crack continued to spread through the base metal plate, reaching the wall of the right stringer after 78th step (Figure 5.6) and beginning to spread along that stringer.

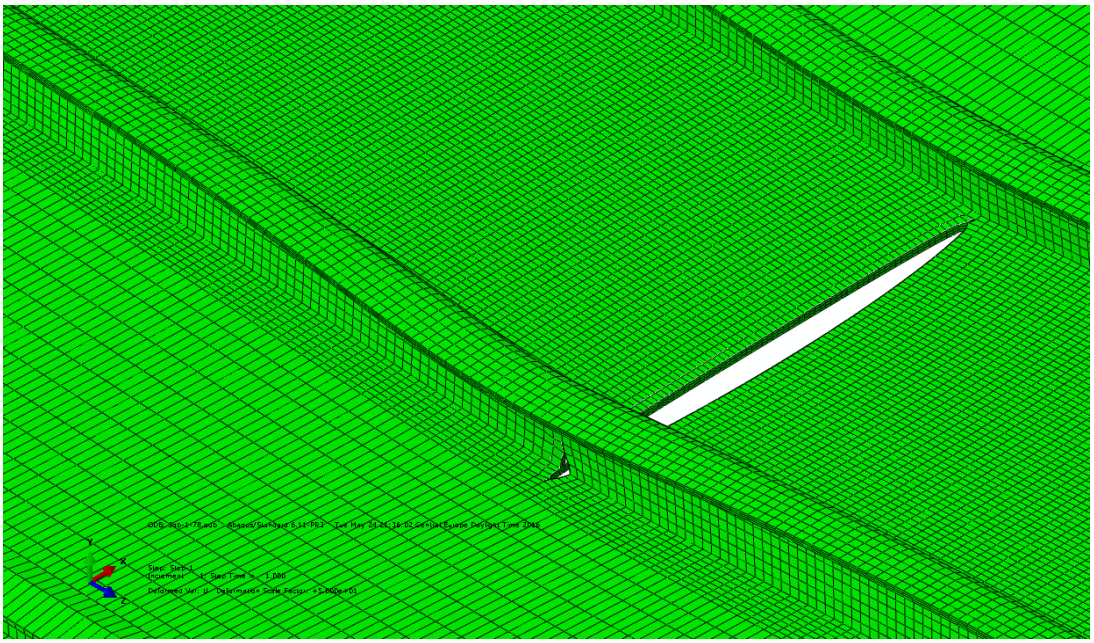

Figure 5.6 After 78 steps crack begins to spread along the stringer.

The crack is continuing spreading along the base metal to completely damage the both stringers after 130 steps. This can be clearly shown from (Figure. 5.7).

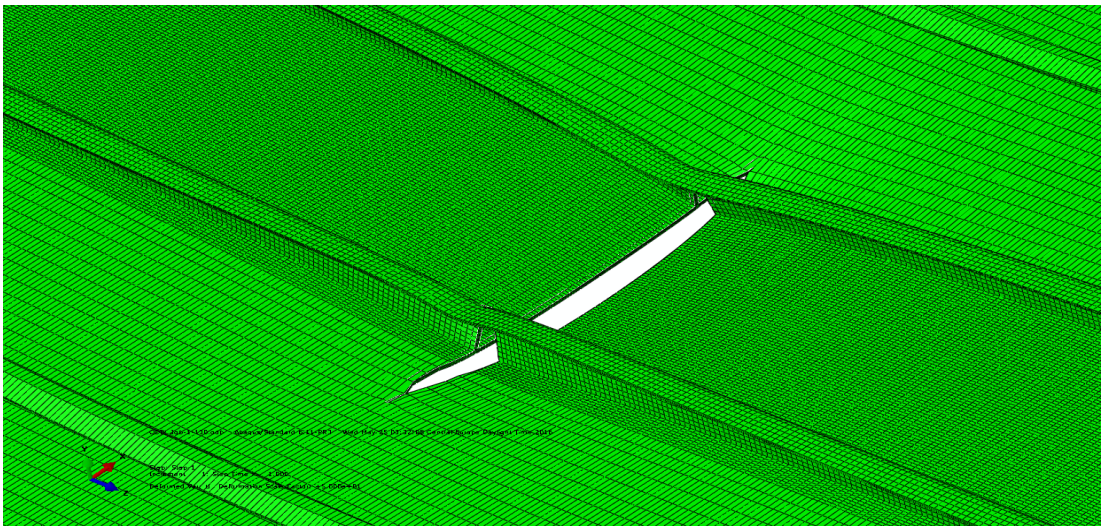

Figure 5.7 Crack after 130 steps of propagation: both stringers are highly damaged.

During the 160th step complete failure of the left stringer occurred (Figure 5.8), after which the crack continued to spread along the right stringer and through the base metal plate. Simulation of the crack growth stopped after 173 steps because the number of load cycles necessary to propagate the crack by one millimeter dropped under 100, which was the sign that crack started to propagate rapidly and that 4-stringer plate is under complete failure.

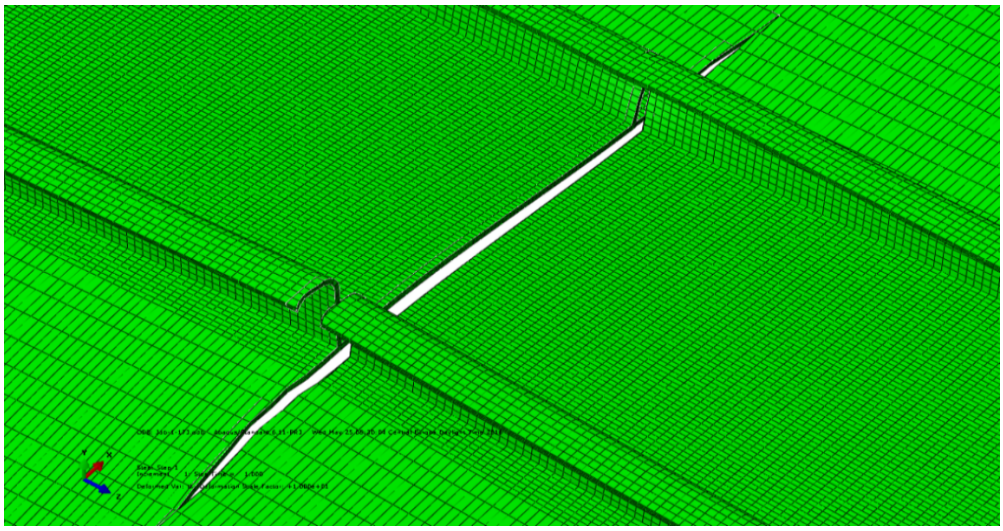

Figure 5.8 Crack after 160 steps of propagation.

5.2.3 Model III (4-stringer with 1mm size of mesh). AA6156 T4.

In this simulation aluminum alloy AA6156 T4 were used (Young's modulus E = 71000 MPa, Poisson's ratio ν = 0.33) just we had changed Coefficients for Paris equations were adopted on the basis of the values obtained in tests with base metal plates: m = 3.042 and C=4.7.E-011 MPa mm$^{1/2}$. The central crack of the length a_0=14 mm was initiated and the load identical to that used for the same pervious model was applied. The crack was propagated in the 48 steps (in each step crack length increased by 2 mm). as shown in figure 5.9

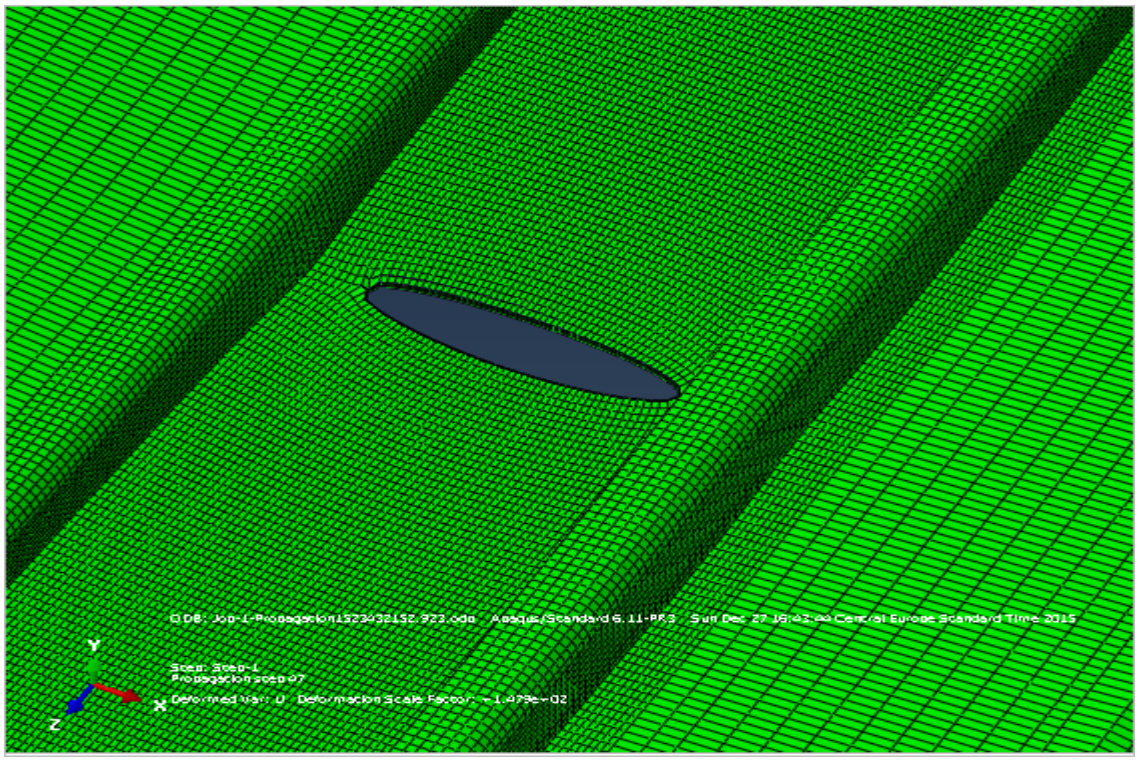

Figure 5.9 Crack after 48 steps of propagation for 4-stringers AA6156 T4

5.3 Effect of mesh size on fatigue crack propagation behavior for 4-stringers AA6156 T6.

In these models, we changed size of mesh for previous model II (4-stringer 1mm) around crack to 2mm and 4mm.

5.3.1 Model I (4-stringer with 2mm size of mesh).

In this model the central crack of the length a_0=14 mm was initiated and the load identical to that used for 4-stringes was applied and changed size of mesh. The crack was propagated in the total of 117steps (in each step crack length increased by 2 mm, 1mm left and 1mm right) and after 60 steps, it reached the wall of the left stringer (Figure 5.10) and began to spread along it.

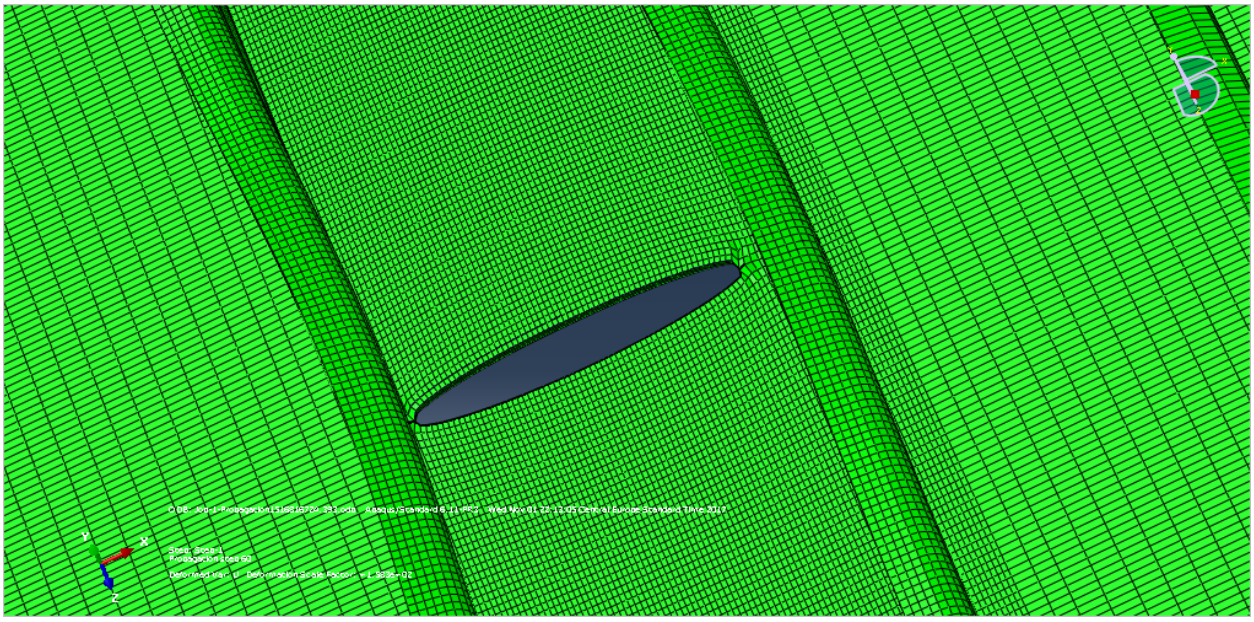

Figure 5.10 Crack in 4-stringer plate with 2mm size of mesh after 60 steps of propagation.

At the same time crack continued to spread through the base metal plate, reaching the wall of the left stringer after 80 step (Figure 5.11) and beginning to spread along that stringer.

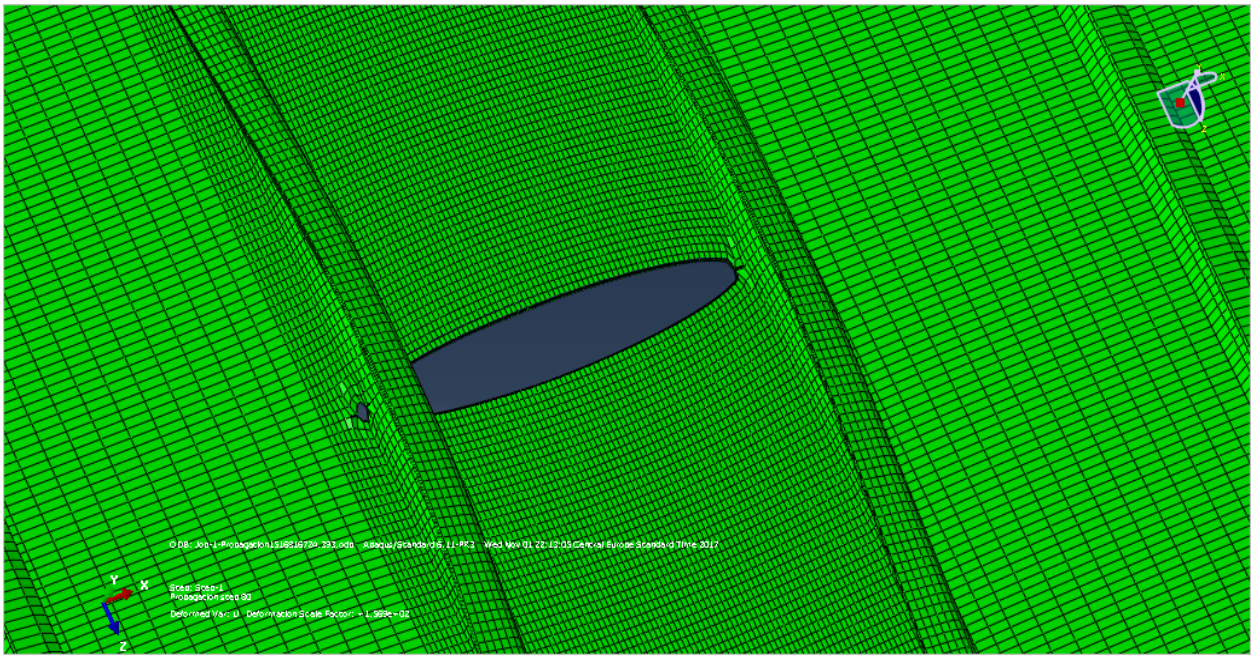

Figure 5.11 After 80 steps crack begins to spread along the stringer.

After 93 steps of propagation for both stringers, we noticed that in figure (5.12) and (5.13)

For left stringer is highly damaged compared to right stringer is began to damage.

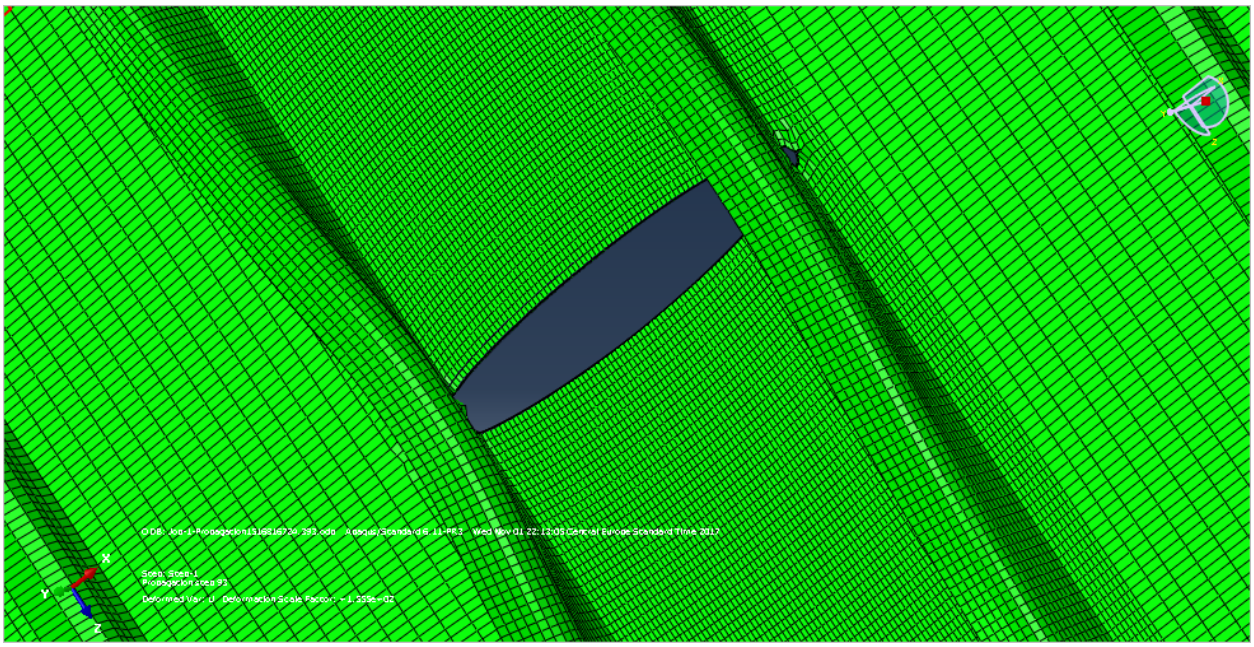

Figure 5.12 Crack after 93 steps of propagation: right stringer began to damage.

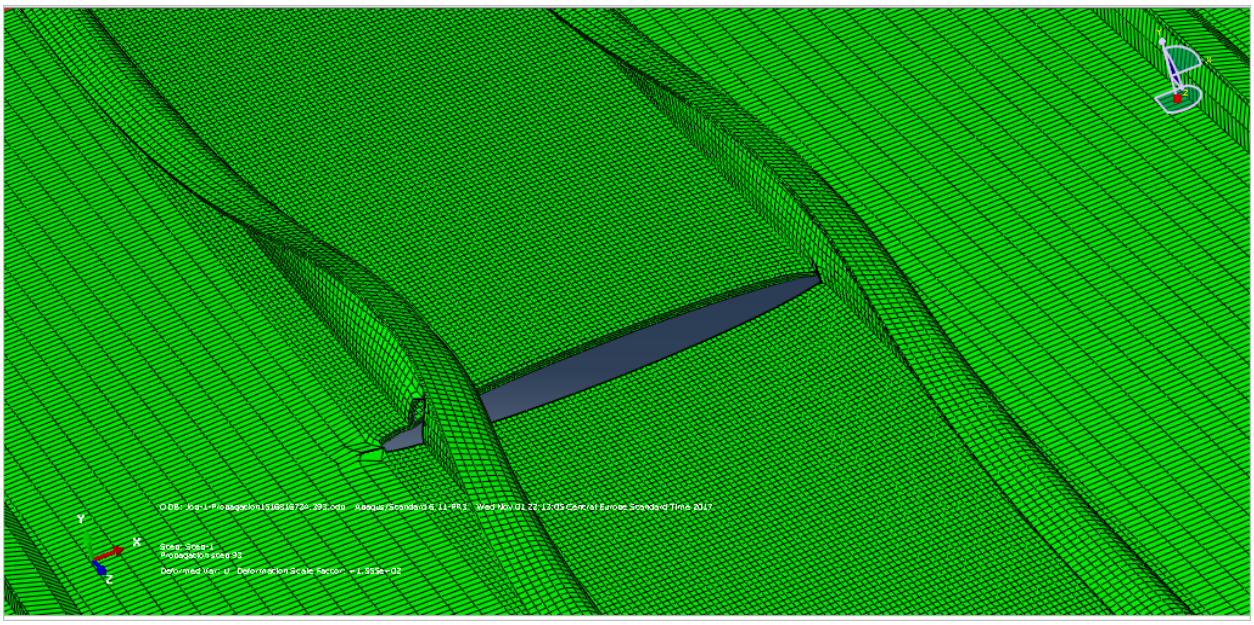

Figure 5.13 Crack after 93 steps of propagation: left stringer is highly damaged.

After 100-step complete failure of the left stringer occurred Figure 5.14, after which the crack continued to spread along the right stringer and through the base metal plate. Simulation of the crack growth stopped after 117 steps in figure 5.15 4-stringer plate is under complete failure.

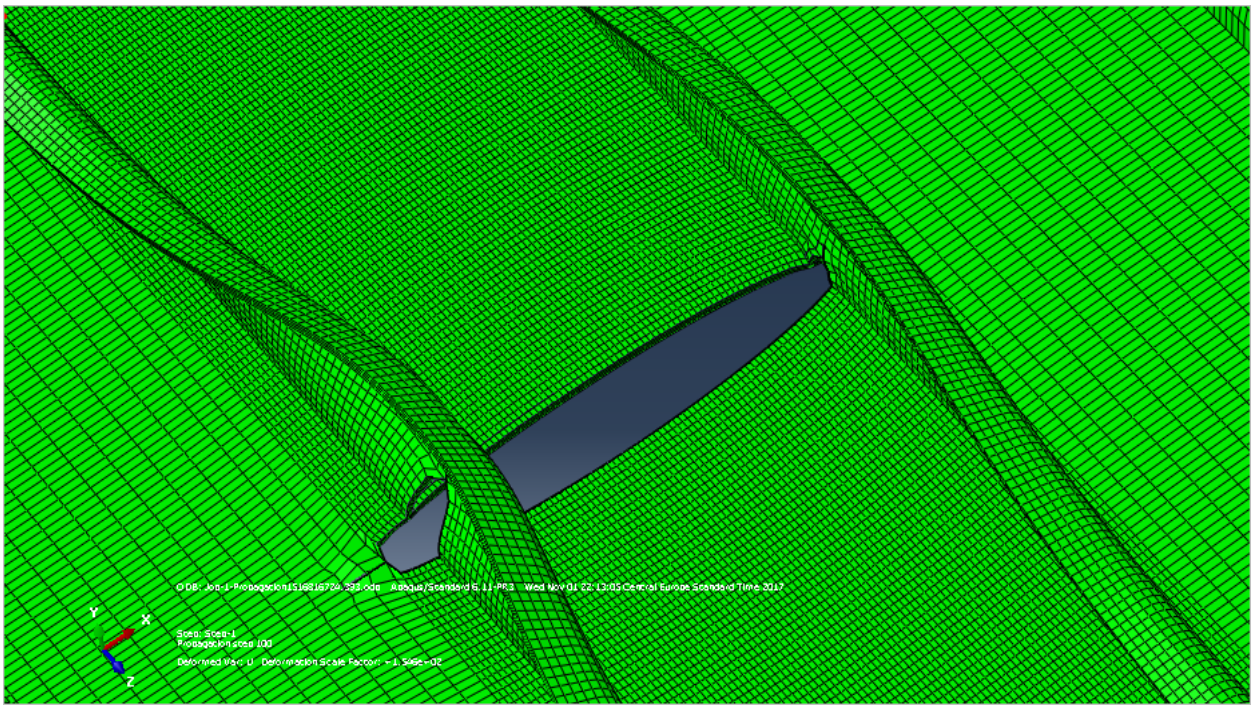

Figure 5.14 Crack after 100 steps of propagation: left stringer completely damage.

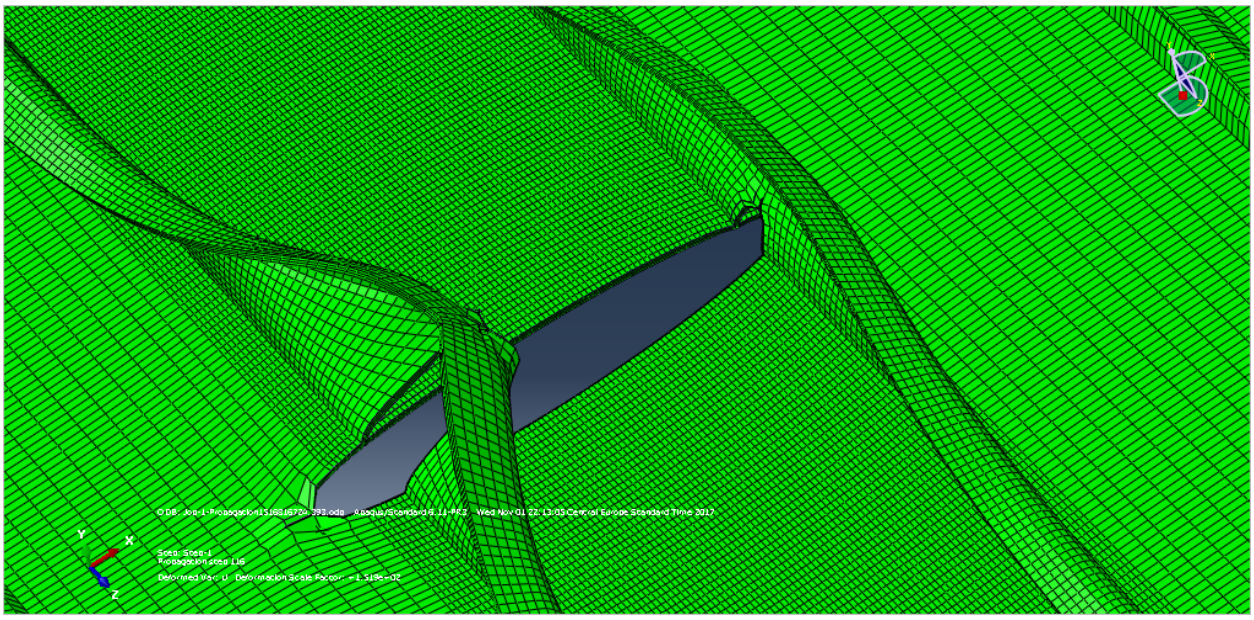

Figure 5.15 Crack after 117 steps of propagation

5.3.2 Model II (4-stringer with 4mm size of mesh).

The crack propagated in the total of 279steps. After 76 steps, it reached the wall of the left and right stringers as shown in (Figure 5.16) and began to spread both of them

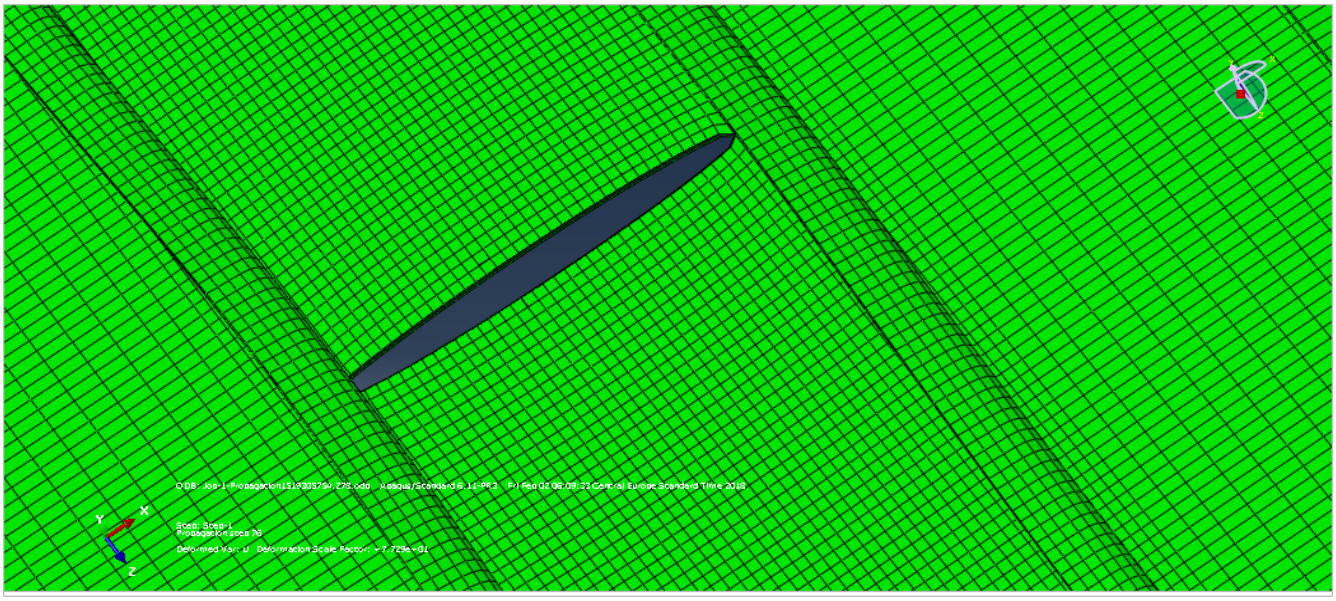

Figure 5.16 Crack in 4-stringer plate with 4mm size of mesh after 76 steps of propagation.

At the same time crack continued to spread through the base metal plate. After 88 steps, the crack began to spread along the left and right stringers as shown in (Figure 5.17).

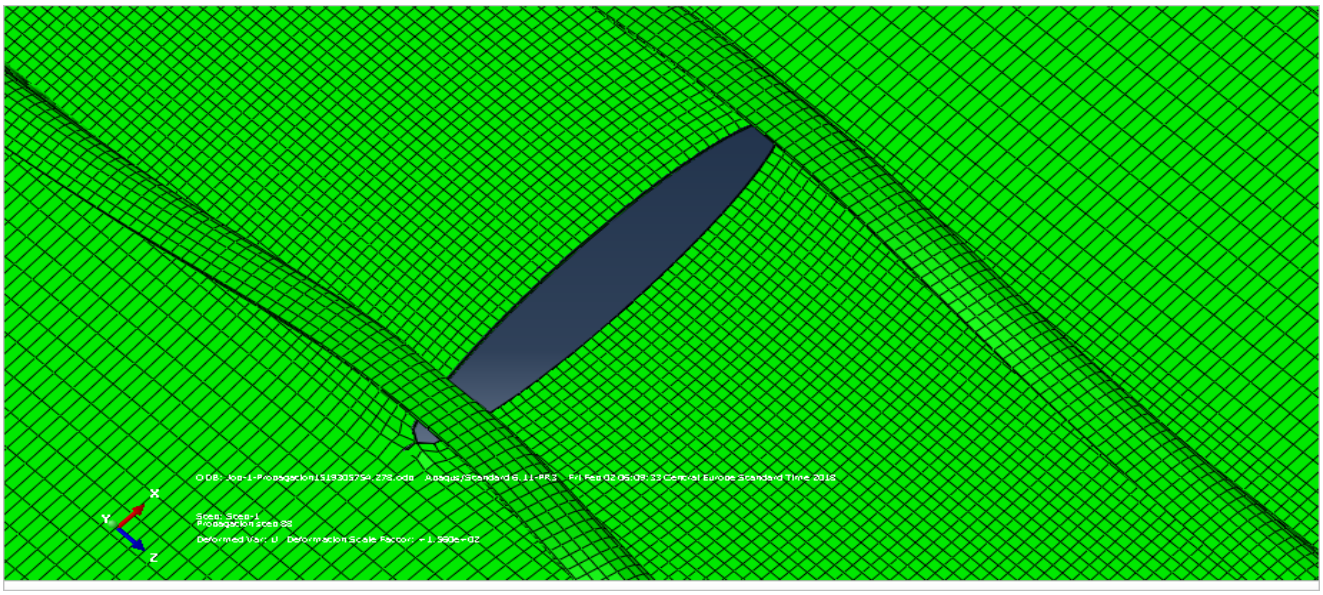

Figure 5.17 After 88 steps crack begins to spread along the stringer.

After 166-step, both stringers left and right were completed failure and destroyed. (First and second stringers in model) as shown in Figure 5.18, after that, the crack continued to spread and reached the third stringer.

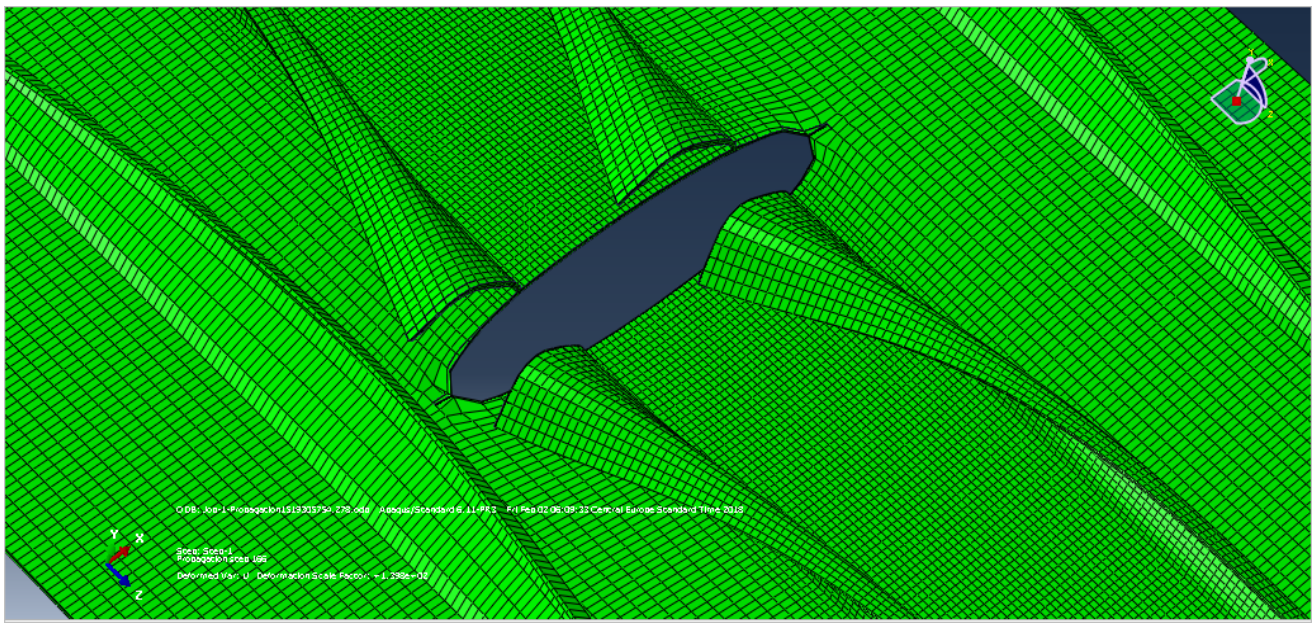

Figure 5.18 After 166 steps completed failure and destroyed first and second stringers.

After 212-steps, third stringer began to damage. After that, the crack continued to spread along the base metal toward the third and fourth stringers as shown Figure 5.19.

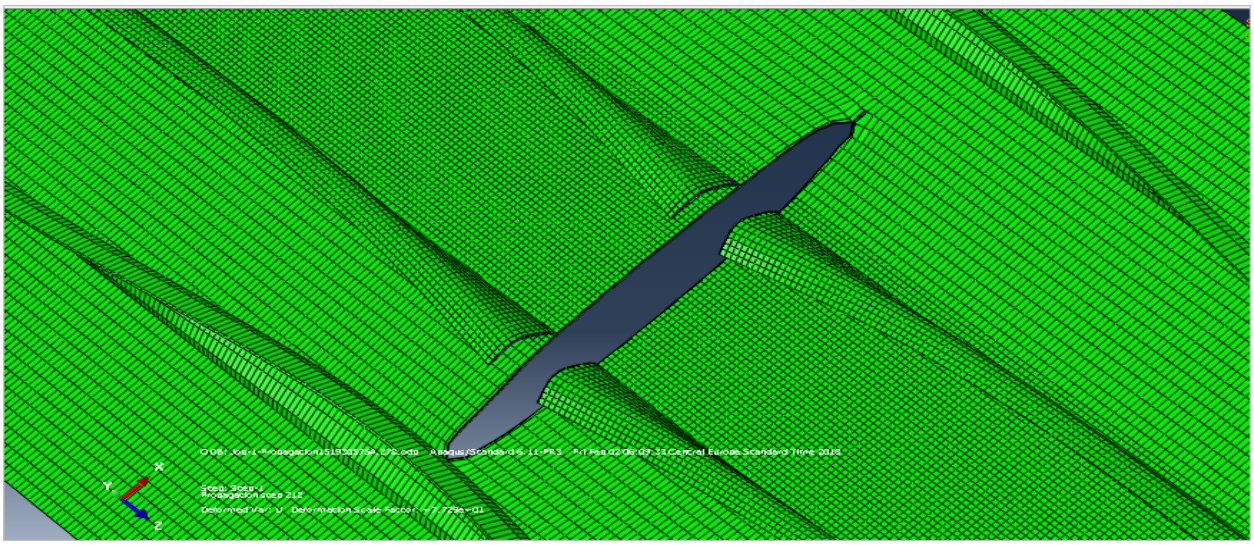

Figure 5.19 After 212 steps third stringer began to damage.

The Simulation of the crack growth stopped after 278 steps as shown in Figure 5.20. The 4-stringer plate with 4mm size of mesh was completed failure.

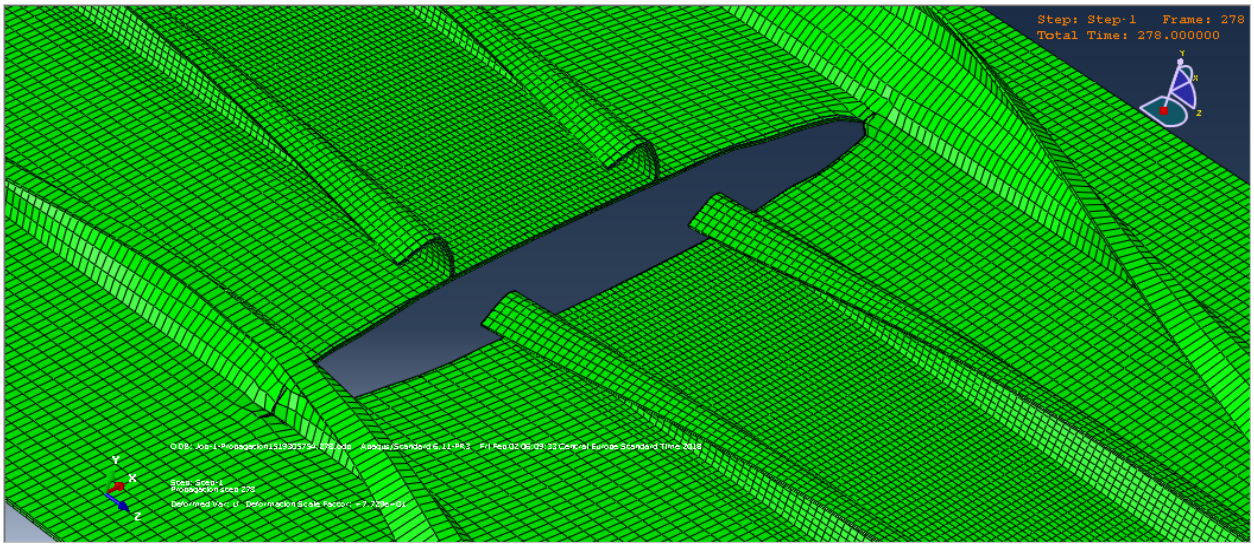

Figure 5.20 After 278 steps third and fourth stringers began to damages.

5.3.3 Model III (4-stringer with 2mm size of mesh and ((toe)).

This model was same as the previous models with a small changing. The materials and the dimensions were remains same. This model has a (LBW) welding. The dimension of the LBW welding was 2mm for both the sides. The initial crack length was 14 mm in a symmetrical position. The load ratio was R=0.146.

Figure 5.21 shows **LBW** welded stiffened panels. Figure 5.22 shown the Model III of 4-stringer plate.

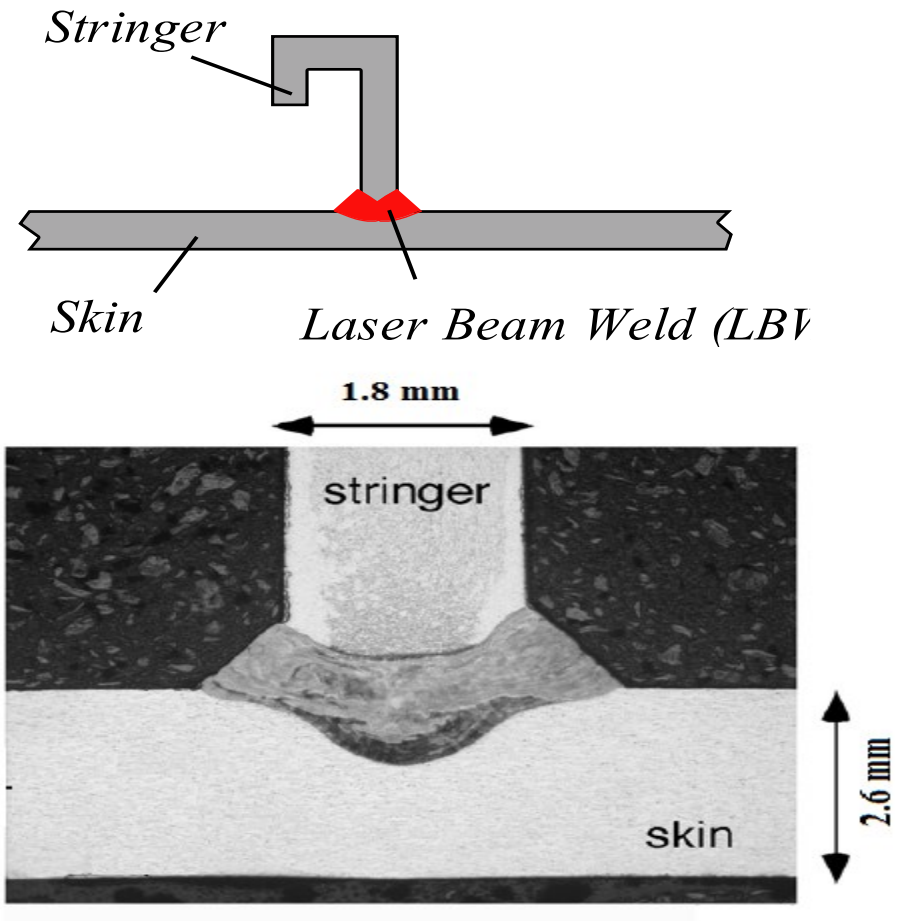

Figure 5.21 LBW welded stiffened panels

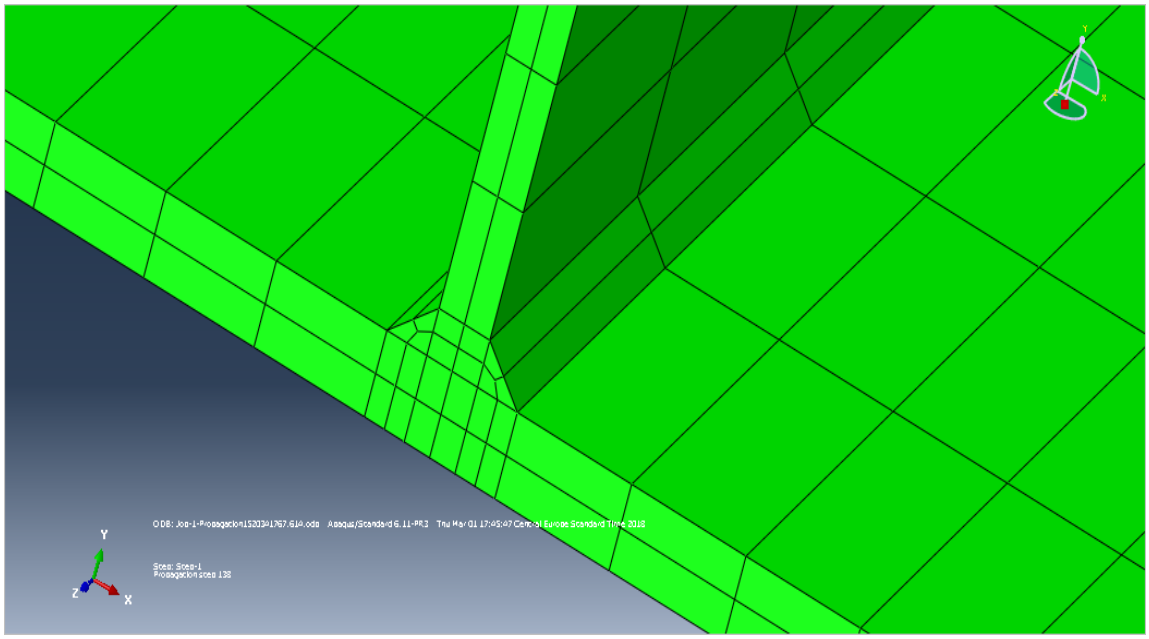

Figure 5.22 Model of 4-stringer plate with (toe) .

The crack propagated in the total of 139 steps. After 30 steps, it reached the wall of the left and right stringers as shown in (Figure 5.23) and began to spread both of them.

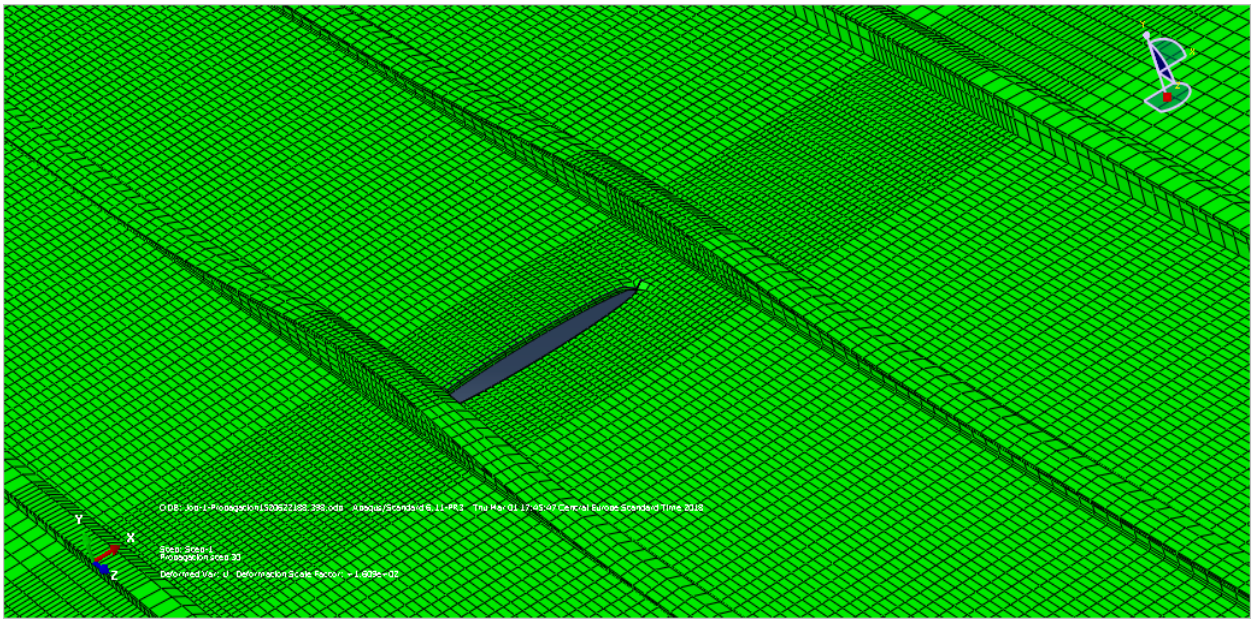

Figure 5.23 Crack in 4-stringer plate with 2mm size of mesh with toe after 30 steps of propagation.

At the same time crack continued to spread through the base metal plate. After 88 steps, the crack began to spread along first and second stringer as shown in figure (5.24).

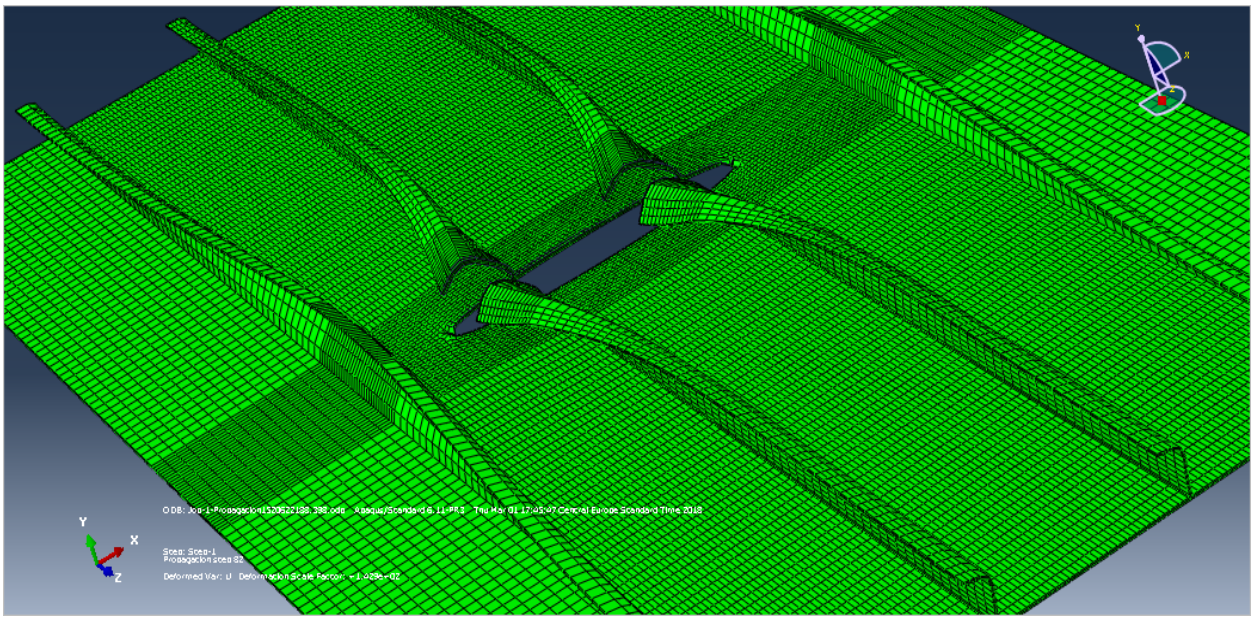

Figure 5.24 After 88 steps completed failure first and second stringers.

After 103-steps, third stringer began to damage, and continued to spread along the base metal toward the fourth stringer as shown Figure 5.25.

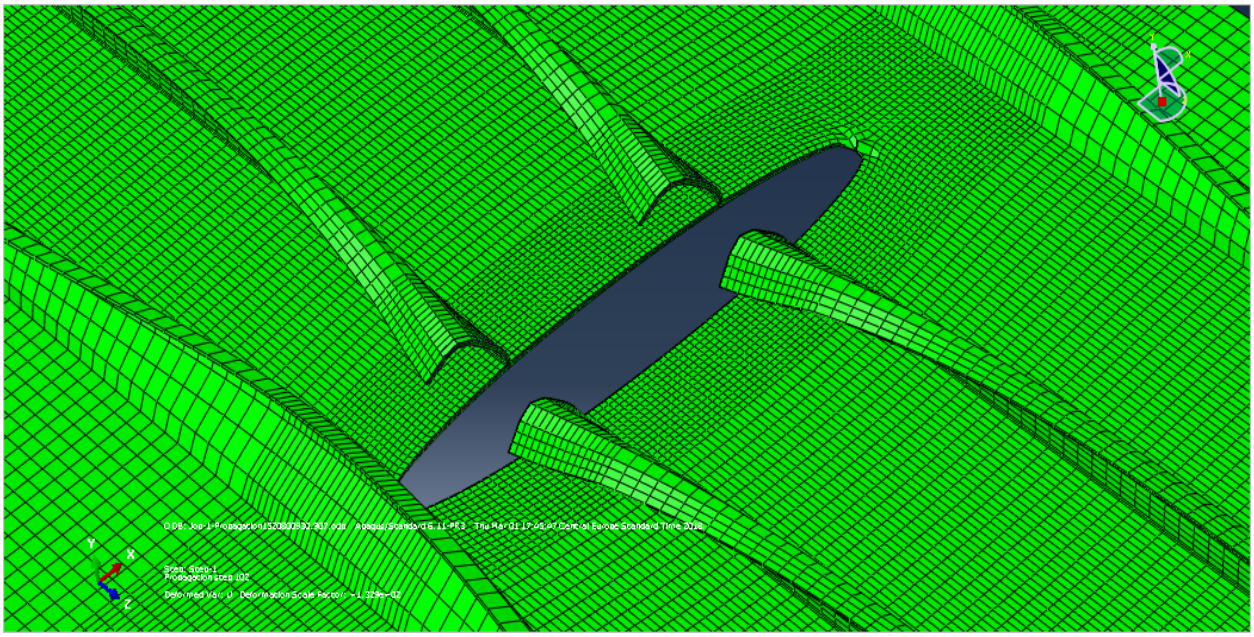

Figure 5.25 After 103 steps crack propagated toward third and fourth stringers.

The Simulation of the crack growth stopped after 138 steps as shown in Figure 5.26. The 4-stringer plate with 2mm size of mesh with (toe) was completed failure.

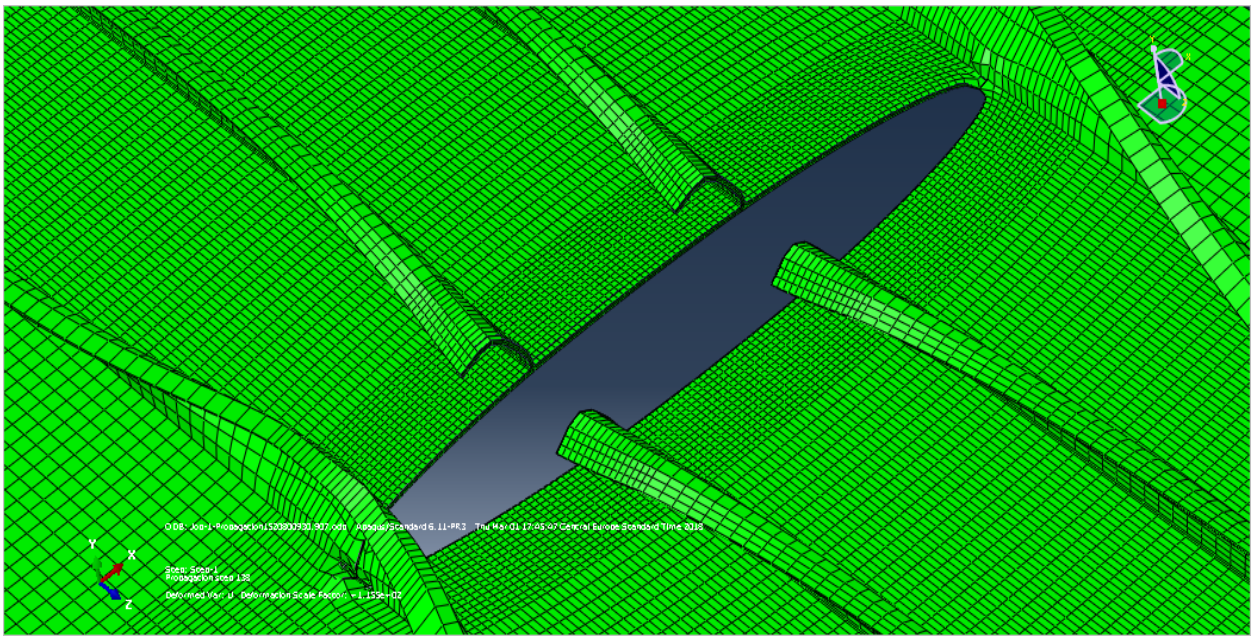

Figure 5.26 Crack after 138 steps of propagation.

5.4. XFEM ABAQUS RESULTS.

The crack growth results data we got it by XEFM for different sizes of mesh for 4-stringer panel and base metal configurations was done by Excel considering the variation of the Number of cycles (N) VS Crack length (a_{mm}).

Typical constant amplitude crack growth data are shown in Figure 5.27 the load cycles for crack length around (275 mm) is about (169030 cycles) .

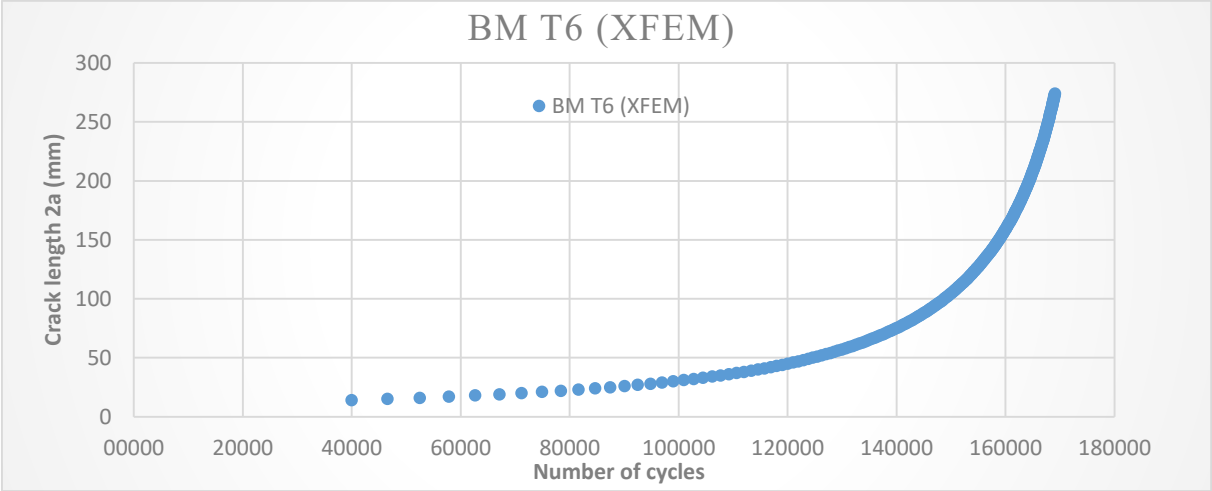

Figure 5.27 Figure 4 Crack propagation vs. cycle number N for base metal (XEFM).

In Figure 5.28, it can be noticed that load cycles for crack length around 358mm is about (254175cycles) for 4-stringer (1mm) (XEFM). The reason for the increase in number of load cycles is the (stringer) effect. The stringer can increase the life of the component comparing with base metal components.

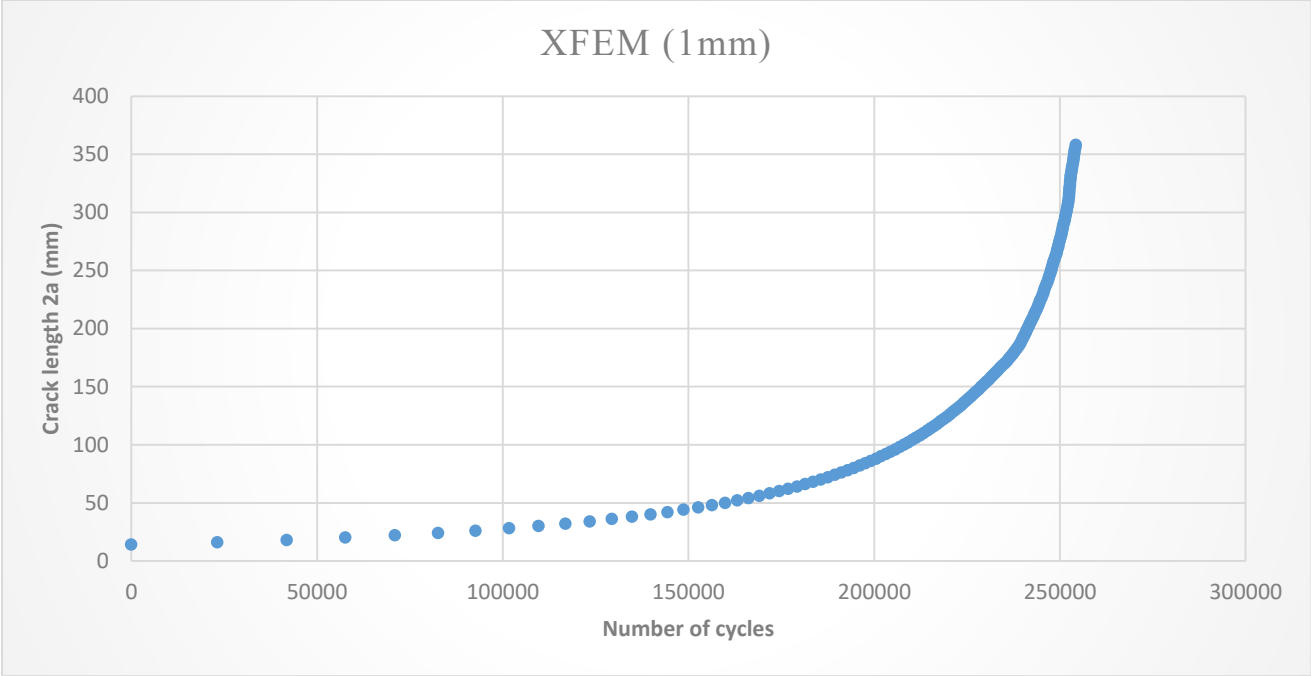

Figure 5.28 Crack propagation vs. cycle number N 4-stringer (1mm) (XEFM).

In figure 5.29 shows aluminum alloy AA6156 T4 , the number of load cycles for crack length around 107 mm is about (495644 cycles) .

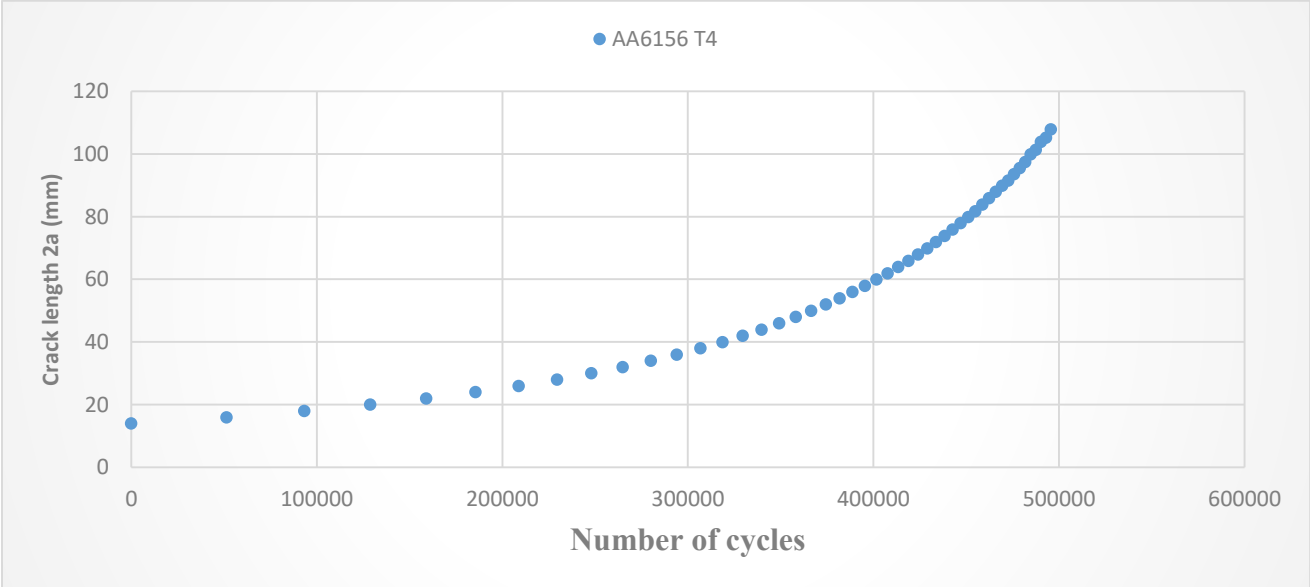

Figure 5.29 Crack propagation vs. cycle number N, 4-stringer (1mm) T4 (XEFM).

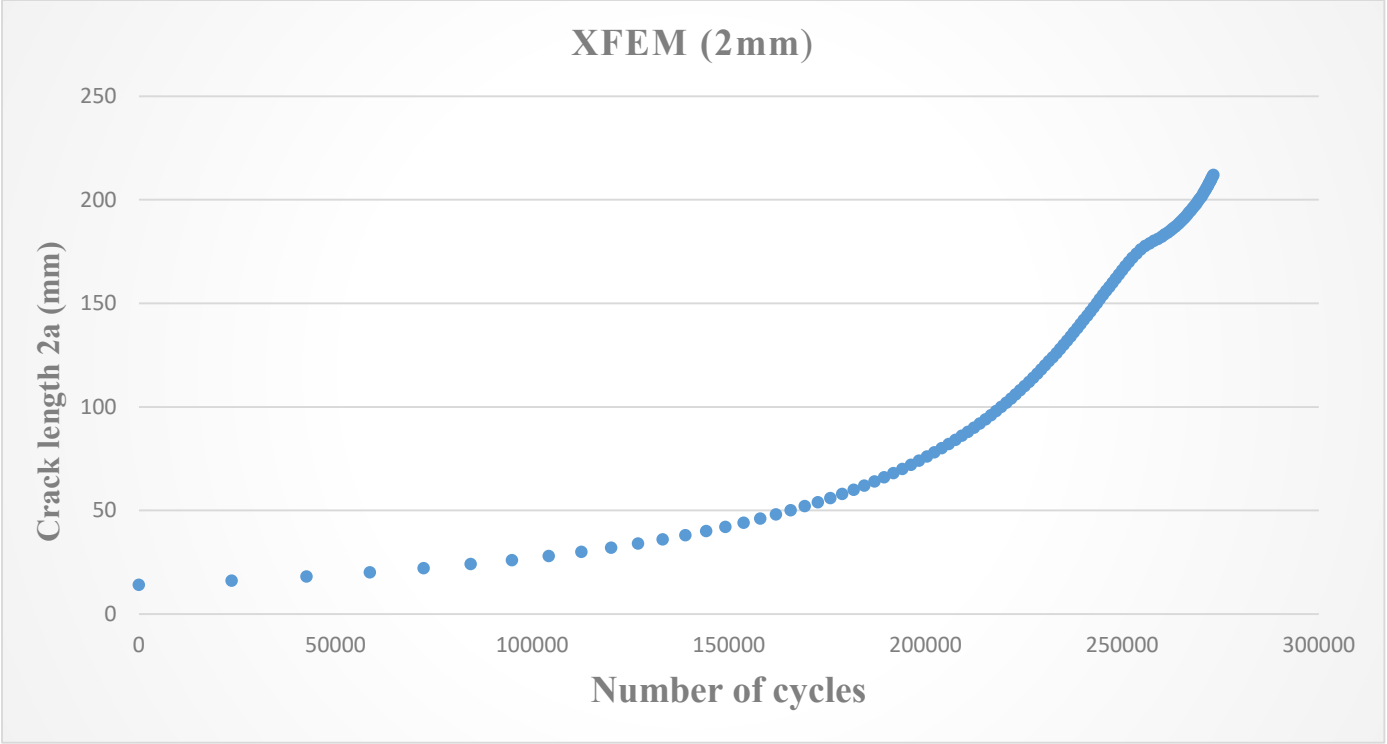

Figure 5.30 Crack propagation vs. cycle number N 4-stringer (2mm) (XEFM).

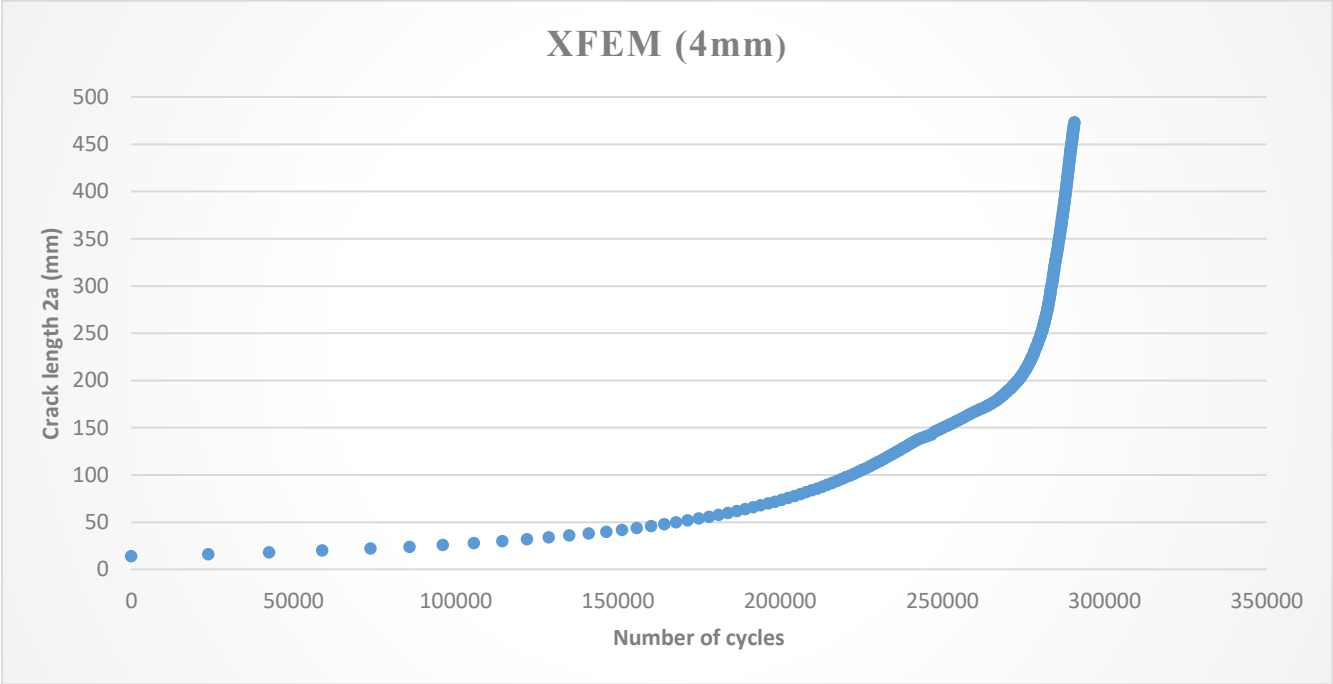

Figure 5.31Crack propagation vs. cycle number N 4-stringer (4mm) (XEFM).

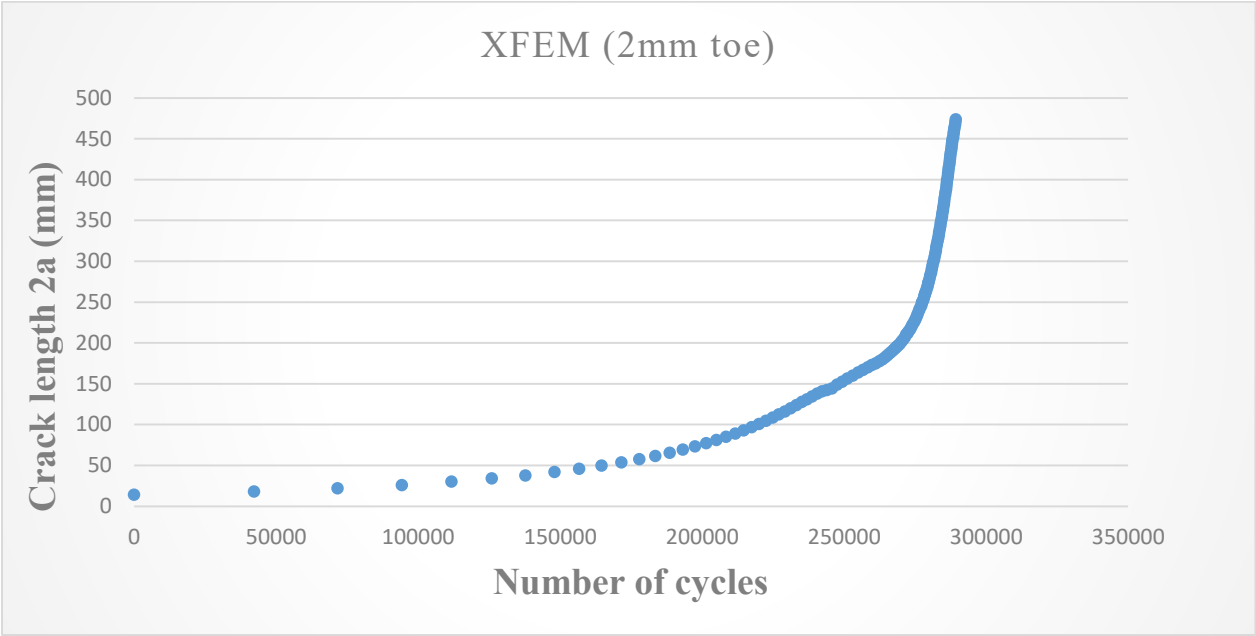

Figure 5.32 Crack propagation vs. cycle number N for 4-stringer (2mm) with toe (XEFM)

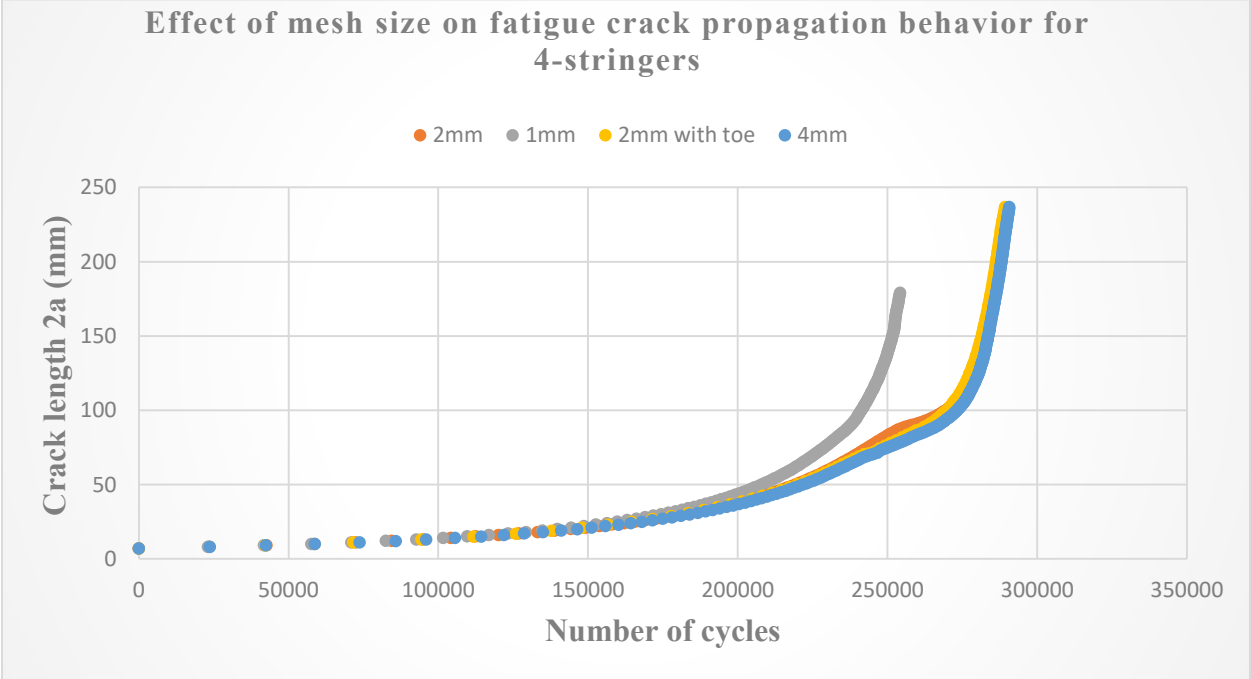

Figure 5.33 Effect of mesh size on fatigue crack propagation behavior for 4-stringers.

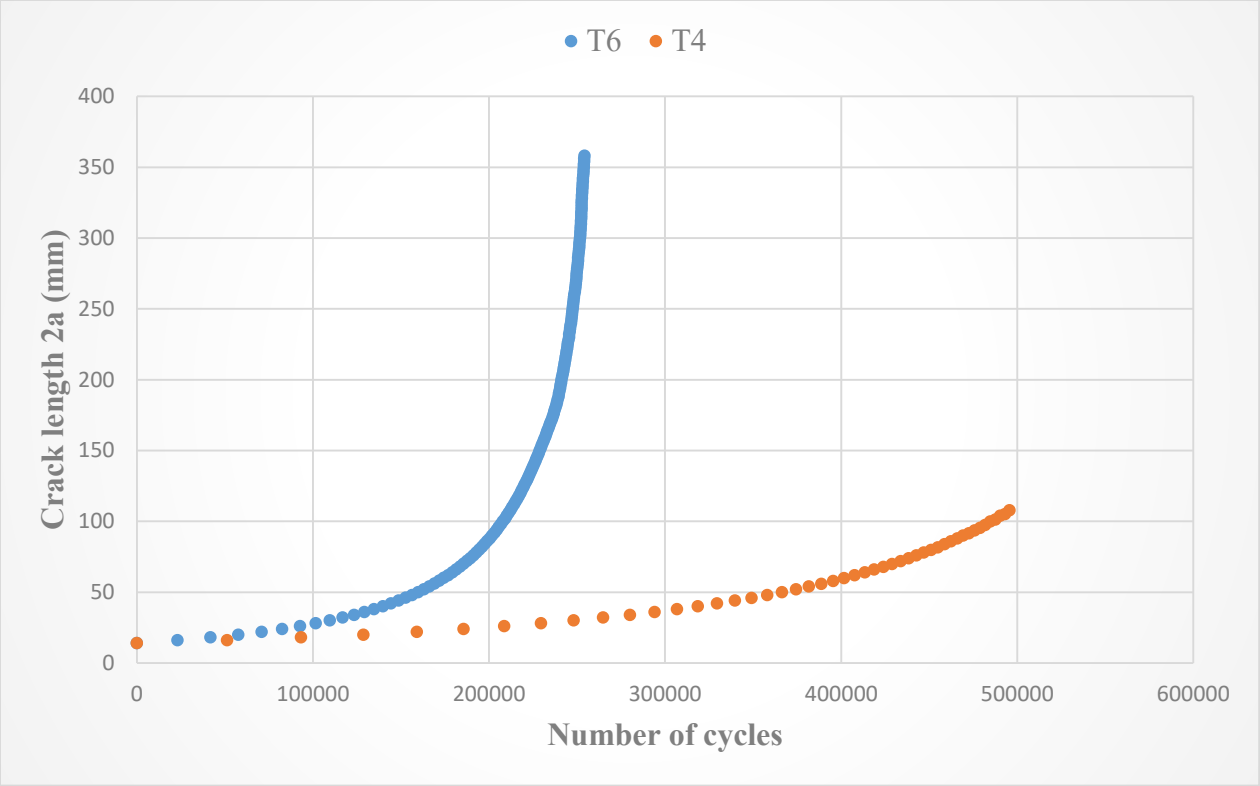

Figure 5.34 Crack propagation vs number of cycle N for T6 and T4 alloy.

All simulation analyzes are performed using ABAQUS/Morfeo software, the previous figures show that relation between the number of cycles VS crack length. ALL models in which the effected of the size of mesh give better results than the model with 1mm size of mesh as shown in figure (5.33). The results were obtained for fatigue life of the cracked structural for models are conservative. This is good in practical design and analysis with respect to fracture mechanics and life estimations.

In Figure (5.34), it can be noticed that the fatigue life for A6165 T4 is higher than A6165 T6 that's mean how Coefficients for Paris equations C and m are effected on fatigue life.

5.5 4-stringer with 3- clips 2mm size of mesh.

The geometry of the 3-clips structure shown in (Figure 4.35), was modelled after numerical simulation of 4-stringer plate with different size of meshes, in this part we also had performed much geometry for 3-clips with different meshes but we had mentioned only one model 3-clips with 2mm size of mesh, The central crack of the length a_0=17 mm was initiated and the load identical to that was used for 4-stringer plate applied. The crack was propagated in the total of 91 steps (in each step crack length increased by 2 mm) and after 14 steps, as shown in (Figure 4.36) first clip began to deformed along it. At the same time, crack continued to spread through the base metal plate, reaching the wall of the right, left stringers after 91 steps as shown in (Figure 4.37), and beginning to spread along those stringers.

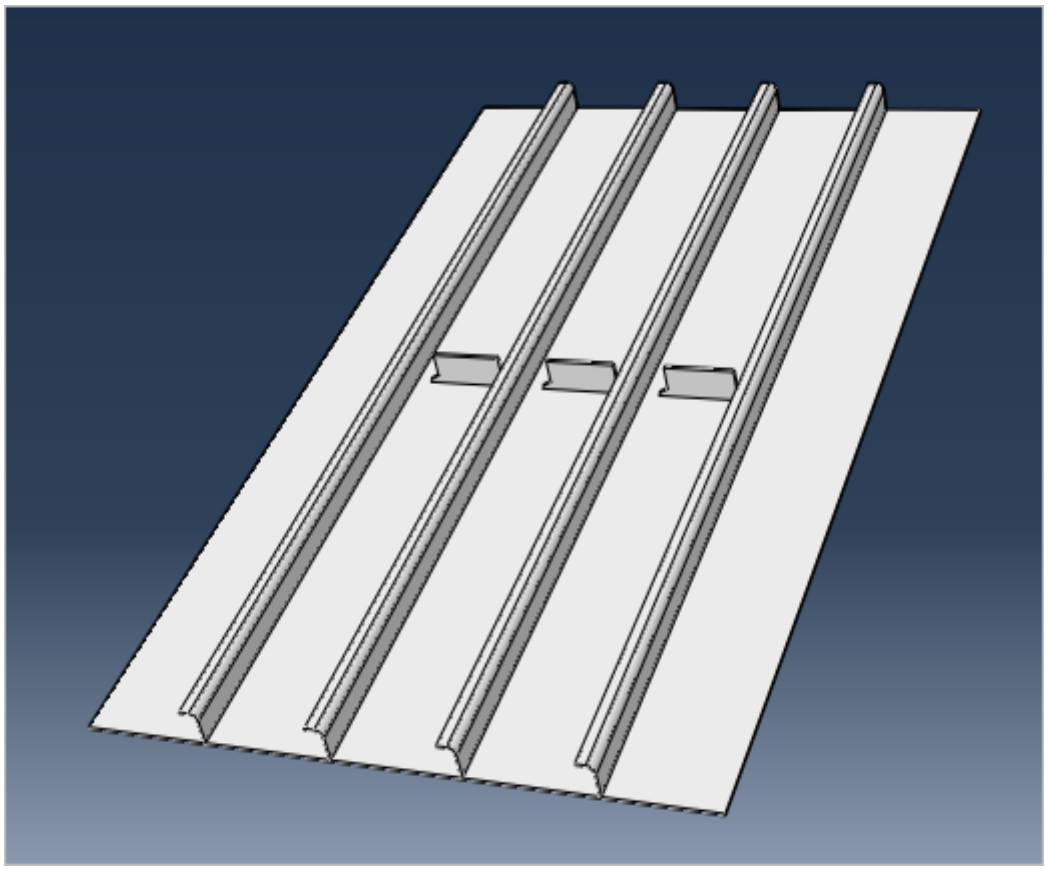

Figure 5.35 geometry of 4-stringer plate with 3-clips

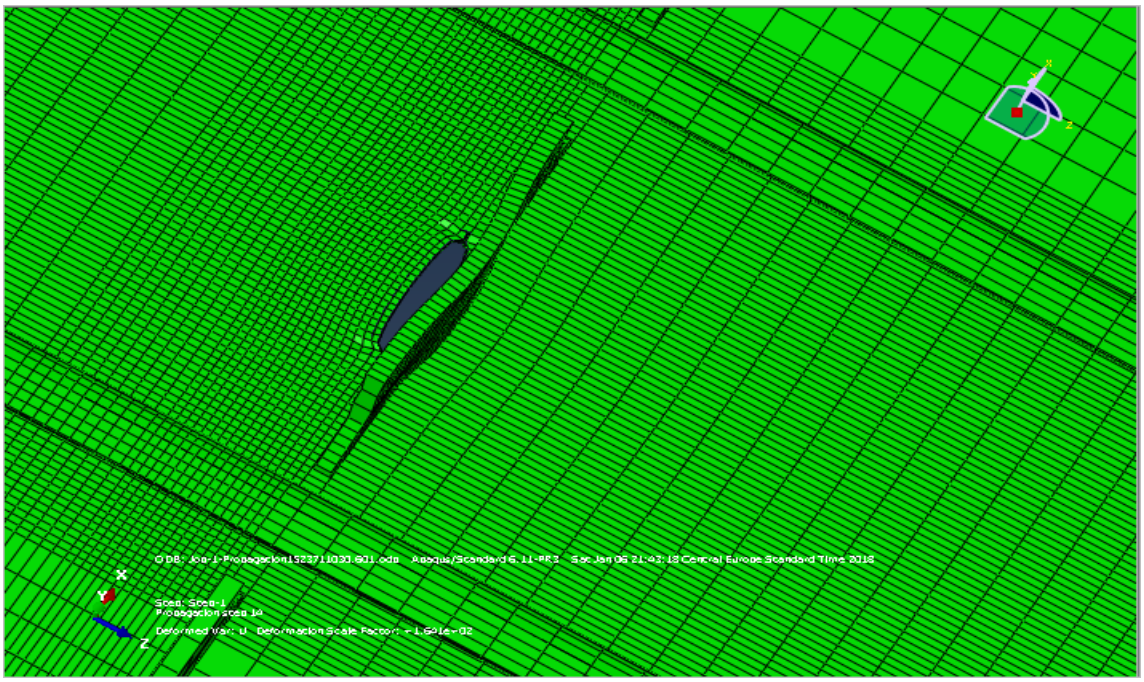

Figure 5.36 Crack after 14 steps of propagation for 4-stringers with 3-clips

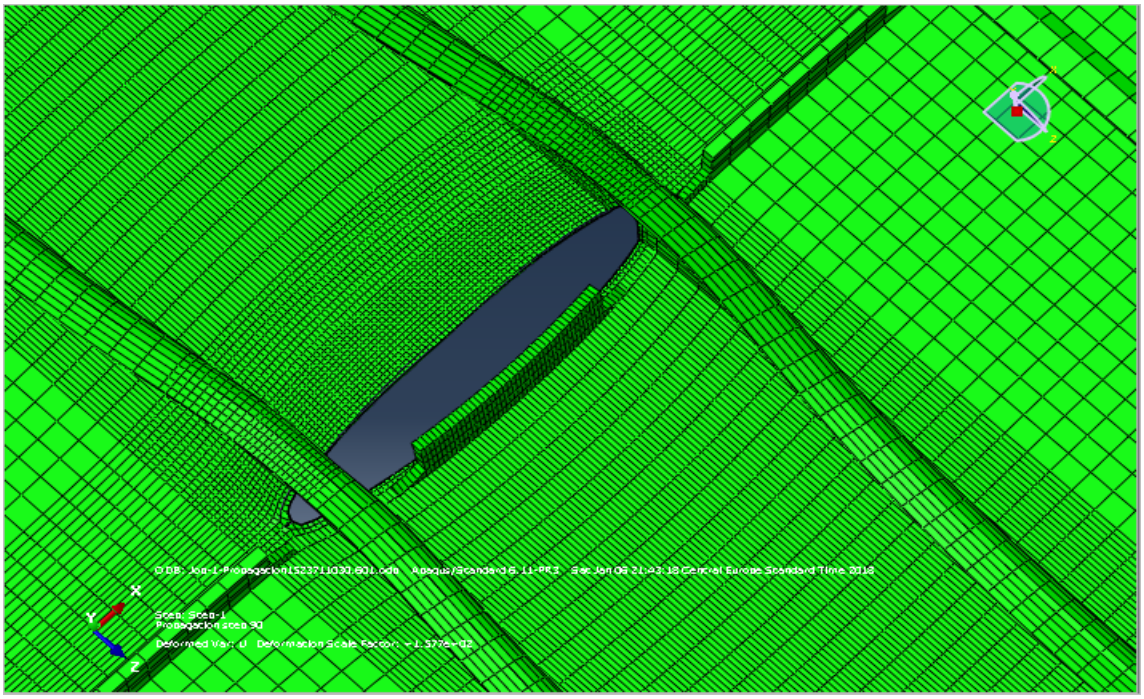

Figure 5. 37 Crack after 91 steps of propagation: left, right stringers are damaged and 1-clip deformed.

It can be noted that in figure (5.38) after modelled 4-stringer plate with 3-clips, XFEM simulation number of cycles for 3-clips is higher than 4-stringer, (278476.44 cycles versus 264958.27) cycles, which is a difference of about. 13518.17 cycles (4.85%). This difference in Number of cycles, which can lead us to enhance fatigue life.

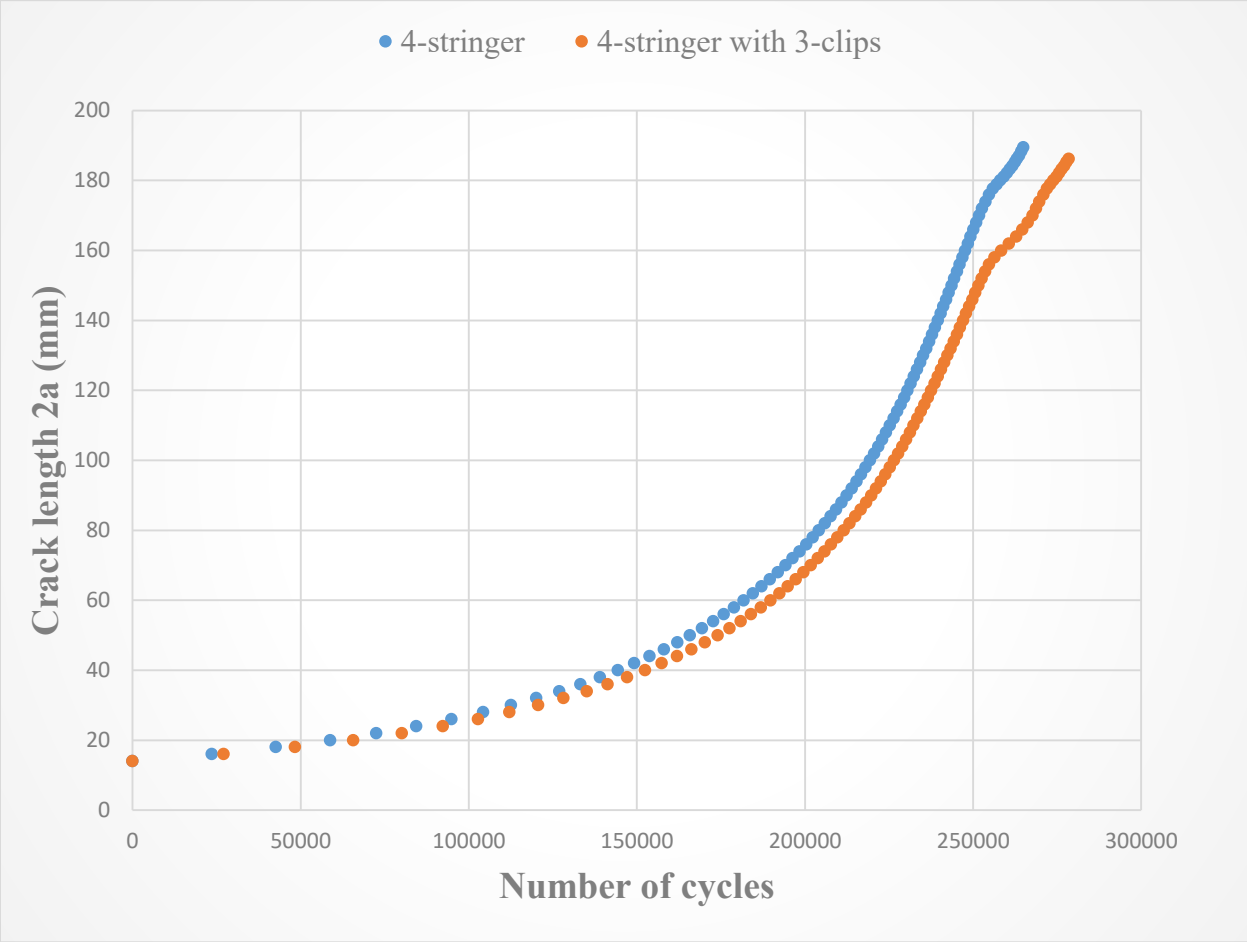

Figure 5.38 Crack propagation vs. number of cycle 4-stringer with 3-clips

Chapter 6 : EXPERIMENTAL VALIDATION OF NUMERICAL OF RESULTS (XFEM).

6.1 Introduction.

This chapter will start by introducing the material compositions as well as the literature experimental data for the base metal and four-stringer panel integral structure. All experimental results are here presented as a reference from Bremen and GKSS research Centre.
It will also describe the techniques that were applied to analyze the data obtained from the experimental procedures. The experimental procedure and the results obtained are presented and discussed. This chapter is concerned only with experimental data while the modelling work was described in the previous Chapter.

6.1.1 Materials and its properties.

AA6156 is an improved AA6056 endowed with an enhanced damage tolerance similar to the one showed by alloys of the 2xxx series, due to impurity reduction and narrower allowed composition range of alloying elements. In T4 temper, AA6156 presents a good formability while aged to T6 develops an improved toughness and a high resistance to fatigue crack growth. To assure high corrosion resistance, especially to the intergranular corrosion at high temperature [6.1]

Table 6.1 chemical composition (wt-%) of AA6156.

		Si	Fe	Cu	Mn	Mg	Ti	Cr	Zn	others	Al
AA6156	min	0.7	0	0.7	0.4	0.6	-	0	0.1	0	balance
	max	1.3	0.2	1.1	0.7	1.2	-	0.25	0.7	0.15	balance

6.1.2 Literature experimental data.

The reference of experimental data is taken from Bremen and GKSS research center. This report presented on "European Workshop on Short Distance WELding Concepts for AIRframes - WEL-AIR" on June 2007 that is created on the basis of damage tolerance analysis of 4-stringer flat panels that are jointly made by the Airbus division in Bremen and GKSS Research Center Geesthacht (Hamburg) – Germany. By courtesy of project participants, the results of fatigue test of laser beam welded short distance clip welds using 4-stringer flat panels [6.2] were available for inspection and they were used as reference for verification of fatigue life values obtained by numerical simulations using XFEM.

The main idea of the project was to perform fatigue testing of integral structures that should replace the conventional differential structures (Figure 6.1) where joints are obtained using rivets. Panels with stringers are traditionally used in fuselage production; therefore, Airbus has decided to test this type of geometry.

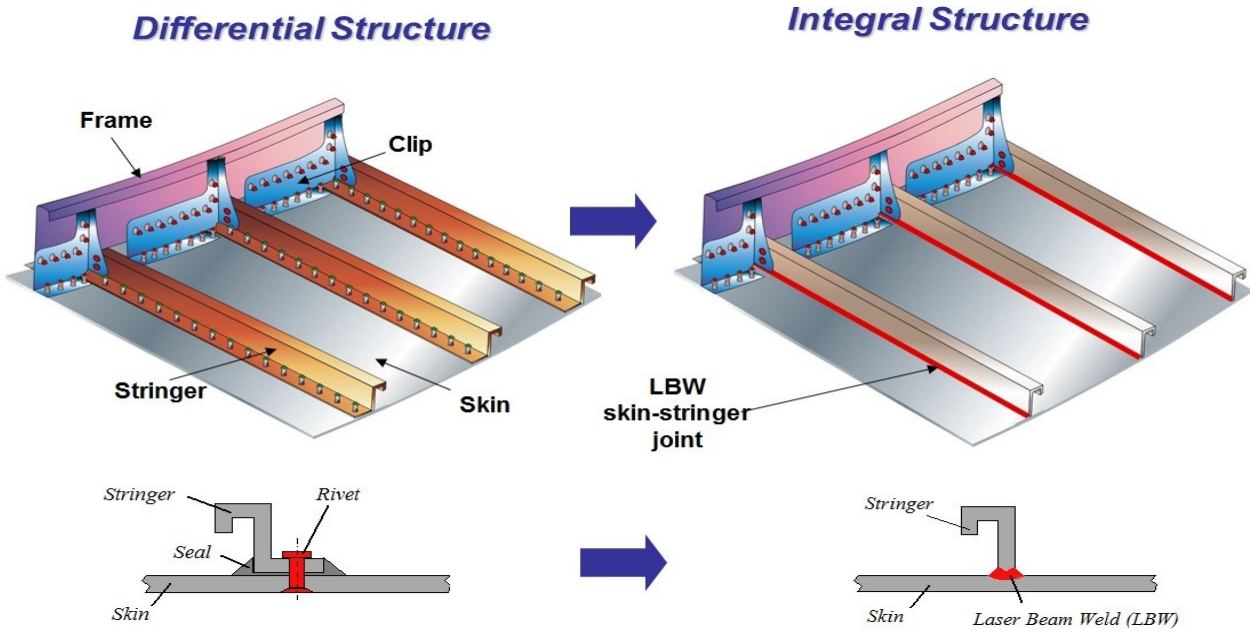

Figure 6.1 Differential vs. integral structure of the fuselage.

6.2 AA6156 T6 base Metal .

The investigated for base metal was configurations with a thin sheet .The geometry and the dimensions of the base metal given in (Figures 6.2) sizes of 760 mm × 1200 mm and 2.6 mm thickness. For base metal plate average maximum force was F_{max}=112.954 KN, while the load ratio R=0.146 was determined on the basis of average minimum tensile force measured. Coefficients for Paris equations were adopted on the basis of the values obtained in tests with base metal plates (Figure 5.3): m = 3.174 and C=1.77195E-012 MPa mm$^{1/2}$.

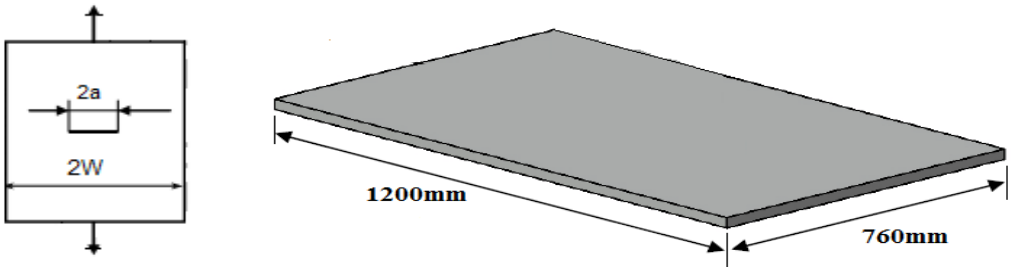

Figure (6.2) Geometry of the base metal.

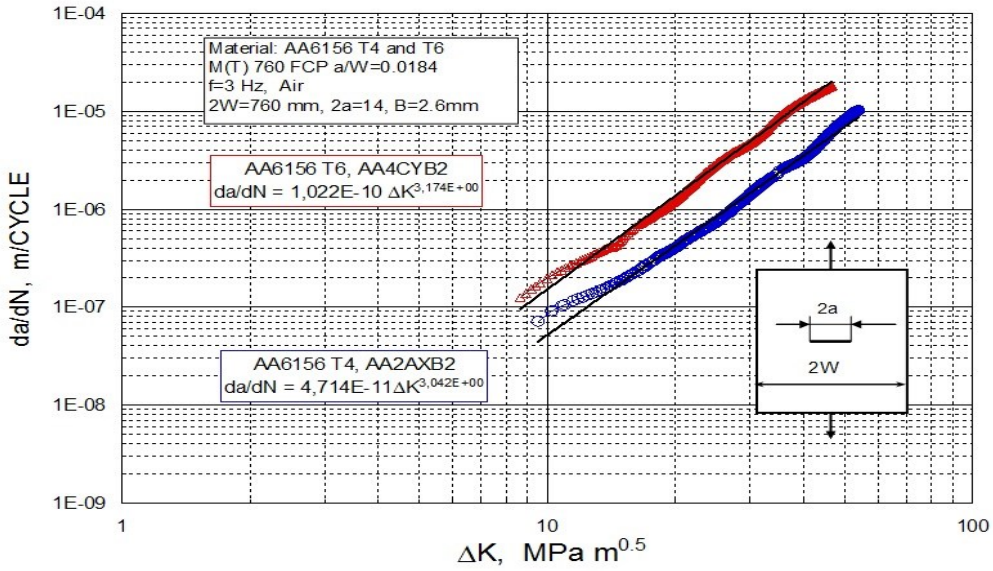

Figure 6.3 Determination of Paris coefficients on base metal plate

Table 6.3 X-FEM and Experimental data for base metal.

Number of steps	XFEM				Experiment		
	Crack length 2a mm	Stress intensity factor, KI MPa√mm	Number of cycles	Crack growth rate, da/dN (m/cycle)	Crack length (2a),mm	Cycle-Machine	da/dN, m/cycle
1	14	243.395	18249.8	5.46751E-08	14	0	1.79E-07
2	15.99773	267.984	32979.8	6.78506E-08	14.05676	40382.25	1.44E-07
3	17.99721	276.794	45404.6	8.03192E-08	15.63731	45321	1.44E-07
4	19.99512	299.566	55919.4	9.46761E-08	15.63796	45323.25	1.44E-07
5	21.9906	306.088	65081.89	1.09108E-07	15.63904	45327	1.25E-07
6	23.9903	327.81	73051.86	1.24781E-07	19.868	62304	1.38E-07
7	25.9848	332.914	80141.07	1.41059E-07	21.20155	67391.25	1.53E-07
8	27.9838	353.873	86434.25	1.57758E-07	22.50439	71885.25	1.65E-07
9	29.9766	357.848	92124.28	1.75746E-07	23.60461	75348	1.65E-07
10	31.9756	377.901	97250.77	1.93895E-07	23.60535	75350.25	1.65E-07
11	33.9695	380.859	101935.1	2.13476E-07	23.61131	75368.25	1.77E-07
12	35.9649	400.751	106209.1	2.318E-07	24.60689	78277.5	1.97E-07
13	37.9556	402.895	110155.6	2.53388E-07	26.46336	83244	2.14E-07
14	39.9522	422.059	113789.2	2.72845E-07	28.10147	87234	2.28E-07
15	41.9436	423.575	117168.2	2.9594E-07	29.69737	90845.25	2.41E-07
16	43.9389	442.432	120303.5	3.16109E-07	31.12246	93882	2.53E-07
17	45.93	443.2	123236.9	3.40903E-07	32.62743	96927	2.66E-07
18	47.9239	461.947	125976.6	3.61472E-07	34.22269	99998.25	2.74E-07
19	49.9141	461.917	128553.9	3.87991E-07	35.29641	101985	2.84E-07
20	51.9065	480.593	130974.2	4.09047E-07	36.5476	104226	2.95E-07
21	53.8965	480.05	133260.8	4.37334E-07	38.00129	106737	3.04E-07
22	55.8887	498.605	135418.1	4.58568E-07	39.12366	108612	3.11E-07
23	57.878	497.824	137463.5	4.88911E-07	40.09364	110190	3.21E-07

6.2.1 Results and discussion.

As it can be seen in Figure 6.4, the number of cycles predicted by Paris equation incorporated into Morfeo/Crack for ABAQUS software is comparable to the number of cycles obtained in one of the experiments with base metal plate (different values of number of cycles were obtained in series of experiments; however, the deviation was not greater than 15%).

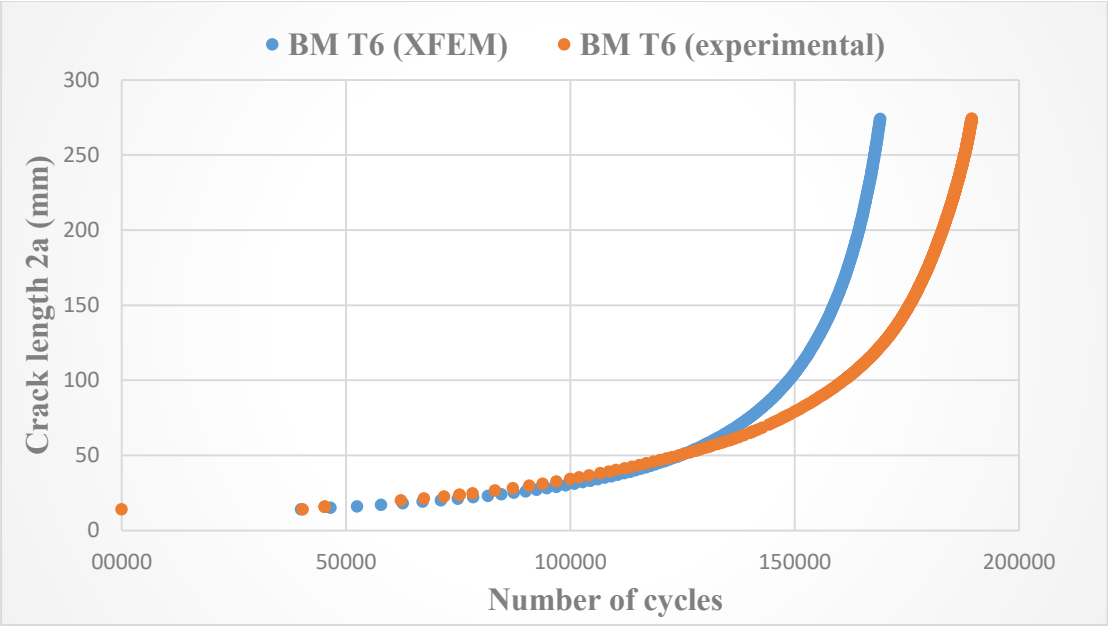

Figure 6.4. Numbers of cycles obtained in experiment and XFEM simulation (base metal T6).

Figure 6.4 shows that in XFEM simulation number of cycles to critical crack length is less than that obtained in experiment (169076 cycles versus 189514 cycles, which is a difference of about 10%); however, under crack length 2a=60mm (almost linear growth) the numbers of cycles differ insignificantly. This was also confirmed by comparing SIFs values obtained by XFEM and by software NASGRO [6.3] (Figure 6.5). It is evident that.

Morfeo/Crack for Abaqus calculates higher Mode I SIFs compared to NASGRO and due to that fact the predicted fatigue life is shorter; however, the number of cycles to critical crack length is on the safe side – predicted life is shorter than that obtained in experiment. (It is important to mention that NASGRO calculates SIFs at the tip of the 2D crack, while Morfeo/Crack for Abaqus calculates SIFs at the nodes of 3D crack front.

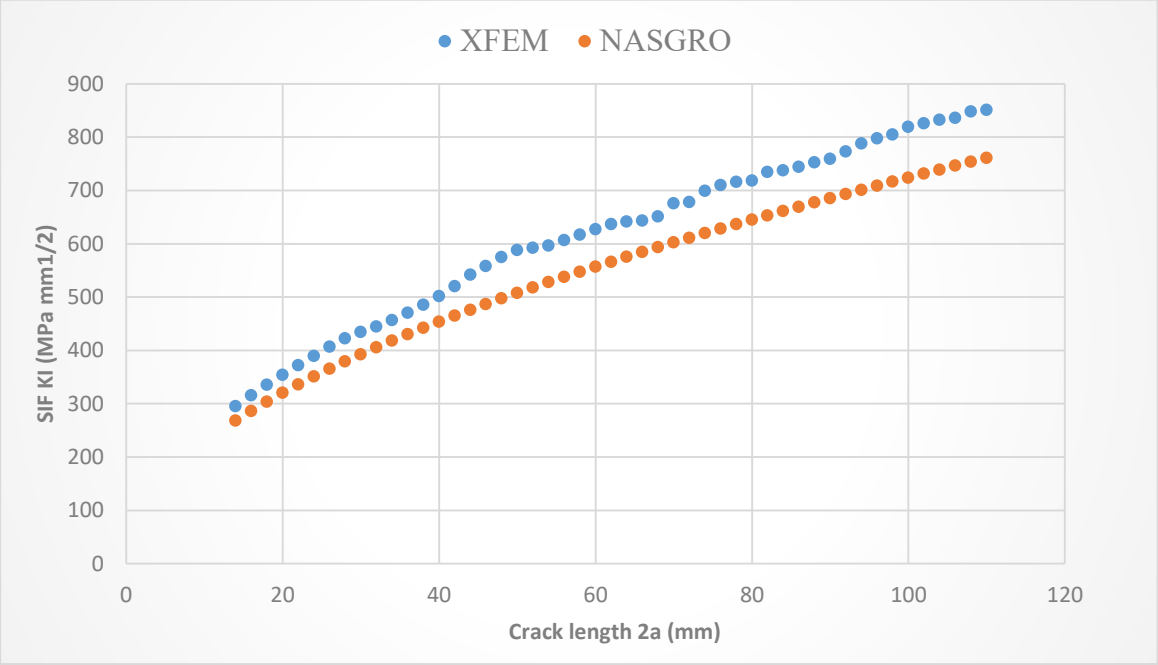

Figure 6.5 SIF values obtained in NASGRO software and XFEM simulation (base metal T6)

6.3 AA6156 T6 Four-stringer panel.

Integral skin-stringer structure is obtained using laser beam welding (LBW), and fatigue life testing was performed on panel under tension containing growing damage perpendicular to the stringer weld joint (circumferential crack, as shown in Figure 6.6). Panel geometry with stringers and their dimensions are presented in (Figure 6.7).

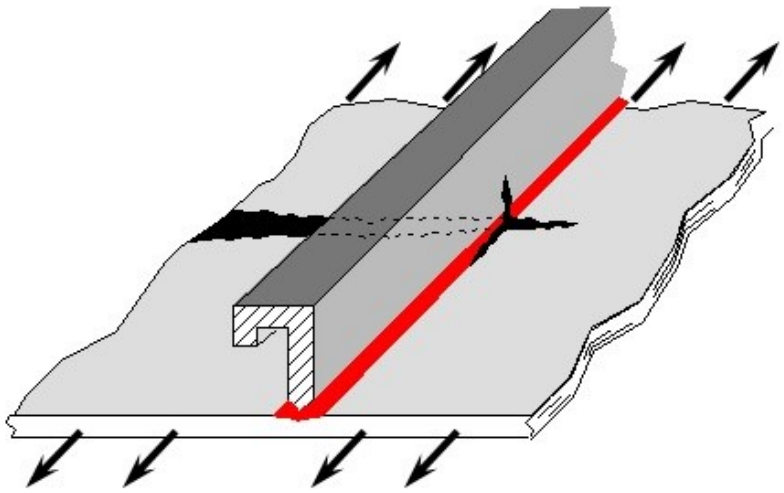

Figure 6.6 Circumferential crack on the panel under tension.

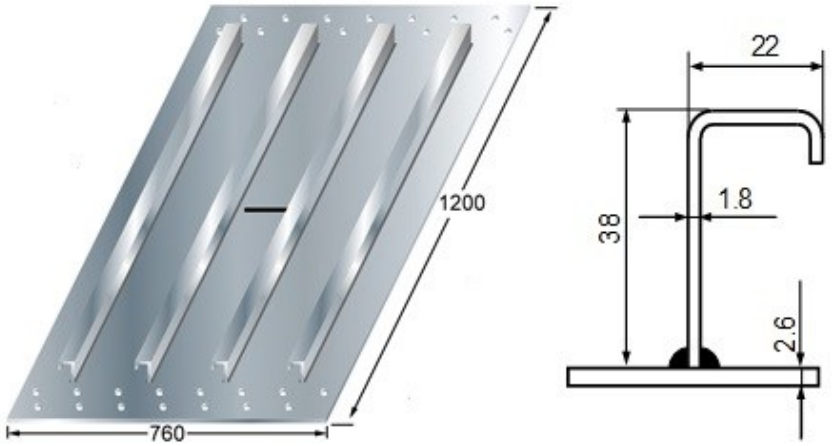

Figure 6.7 Dimensions of the 4-stringer panel made of 6156 T6 (LB welded by AIRBUS).

4-stringer panels were tested carried out at room temperature on a servo –hydraulic testing machine of 2500 KN maximum capacity shown in Figure 6.8. To ensure a pure Mode I loading, buckling was prevented by two steel beams . The initial crack length was 14 mm. The values of maximum applied tensile force (with constant amplitude and stress ratio) were varied. In tests, different aluminum alloys (6156T6, 2139T8, 6156T4) were used. The fatigue characteristics,

(represented by Paris coefficients) were determined by testing the base metal panels without stringers (Figure 6.3). Base metal panels dimensions, tension force and initial crack lengths were identical to dimensions of 4-stringer panel. The fatigue crack lengths during testing were measured using remote optical microscope as shown in figure (6.9).

Figure 6.8 Equipment used in fatigue testing.

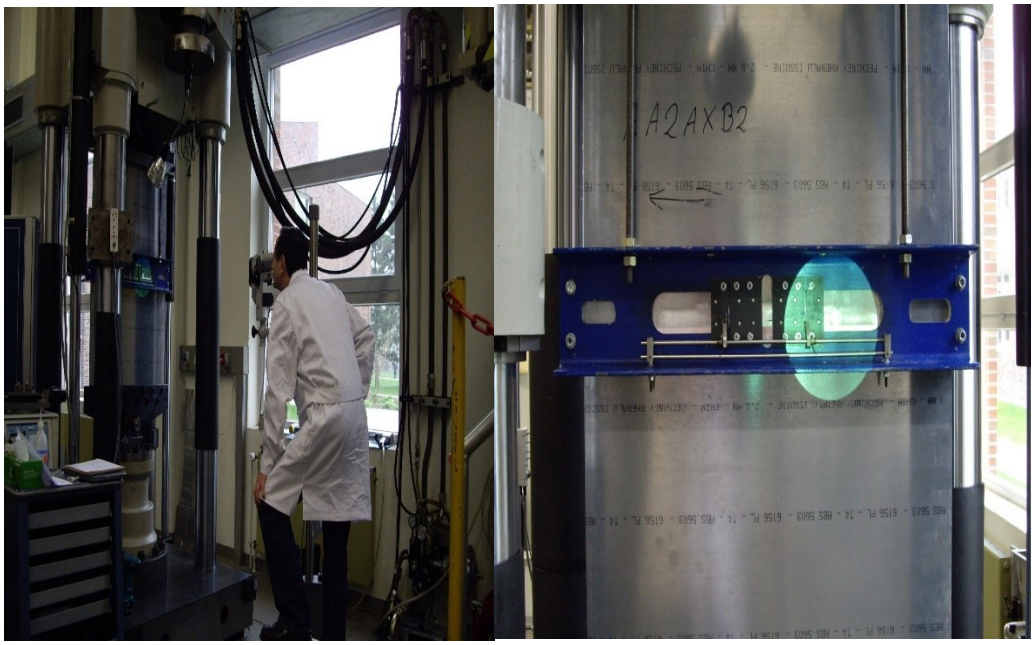

Figure 6.9 Fatigue Crack length Maseurment using Remote Optical Microscope on Panels with Anti-Buckling Guide

Figure 6.10 4-stringer Panel with 3LB welded Clips with Anti-Buckling Guide (Skin-Loading) Using Loading System I

The identical anti-buckling guide was used on the flat side of the stiffened panels with the same instrumentation as for the unstiffened panels , in figure (6.10) It was necessary to support the guides in order to prevent the out –of –plane bending caused by the asymmetry resulting from the stringers

6.3.1 Model I (4-stringer with 1mm size of mesh).

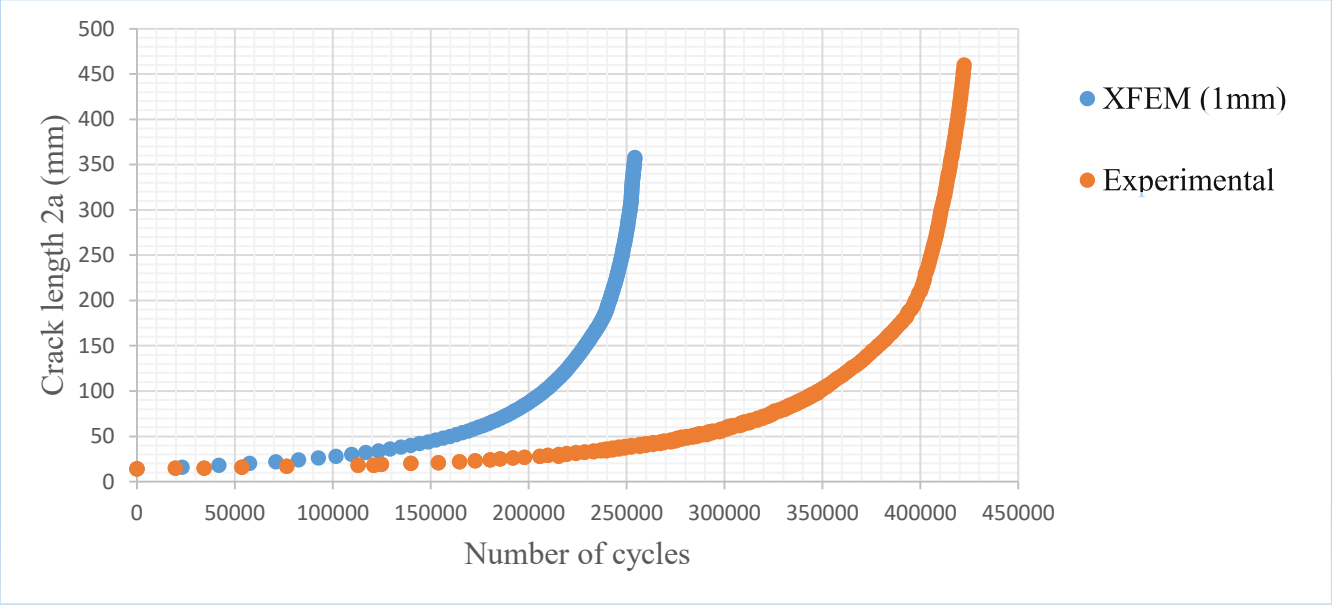

Figure 6.11. Numbers of cycles obtained in experiment and XFEM simulation (4-stringer 1mm).

Figure 6.11 shows that in XFEM simulation number of cycles to critical crack length is less than that obtained in experiment (254273 cycles versus 422328 cycles, which is a difference of about 40 %).

Having in mind that the researchers from GKSS Research Center have also investigated 4-stringer plates with crack, but the results were not completely accessible; in order to validate the results of simulation we compared the values of crack growth rate obtained by XFEM to available experimental crack growth rate values (Figure 6.12).

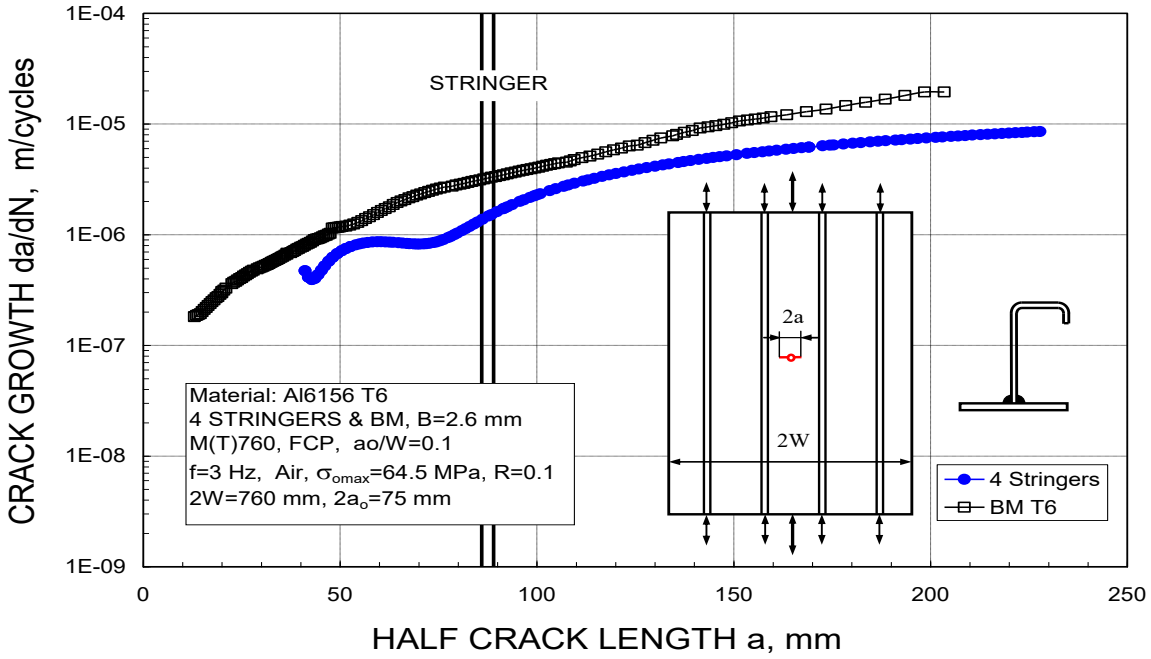

Figure 6.12 Comparison of the crack growth rate for the base metal plate (black dots) and 4-Stringer plate (blue dots) obtained in the experiment.

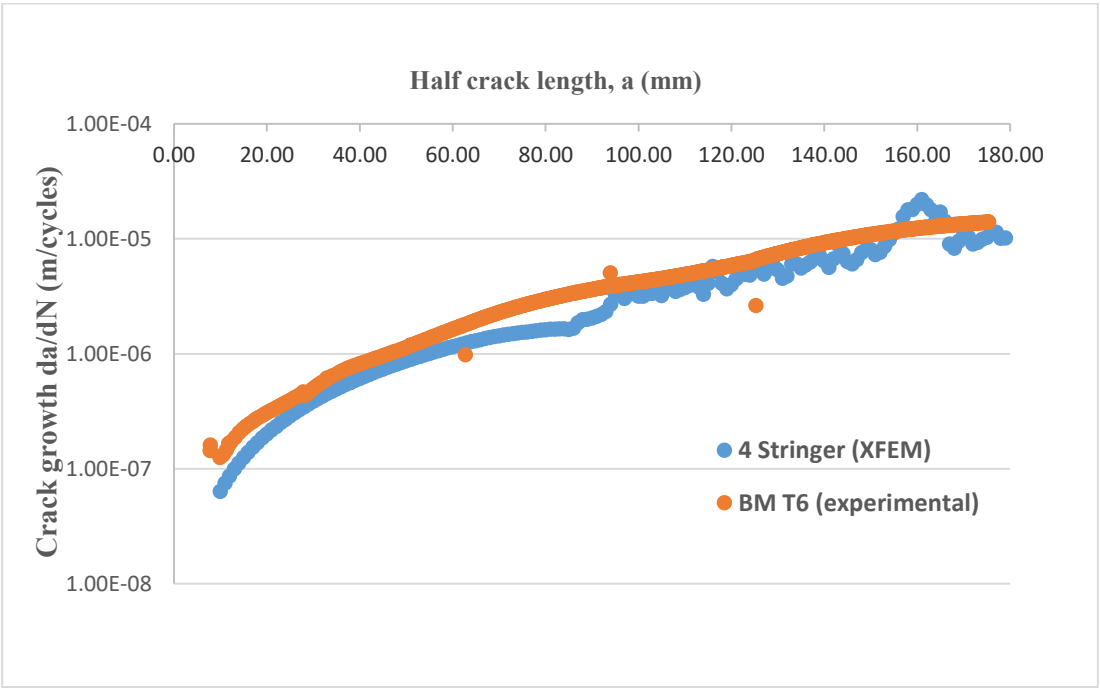

Figure 6.13 Comparison of the crack growth rate for the base metal plate obtained in the experiment and 4-stringer plate obtained in simulation with XFEM.

As it can be seen in (Figure 6.13), shows that the growth is almost logarithmic and that rate tends to the value (da/dN = 1×10–5 m/cycle), while Figure 6.11 shows certain variability in values of crack growth rate obtained using XFEM, although logarithmic trend is evident.

This is more or less expected as the values of SIFs obtained using Morfeo/Crack for Abaqus depend on the density and quality of FE mesh, but it is evident that during one growth period (155 mm < a < 165 mm) crack growth rates in simulation are slightly above the crack growth rates for base metal plate (the order of magnitude of the differences is 8×10–6 m/cycle. The reason for that (see Fig. 6.5) Morfeo/Crack for Abaqus gives somewhat higher SIFs values compared to experimental .

6.3.2 Model II (4-stringer with 2mm size of mesh).

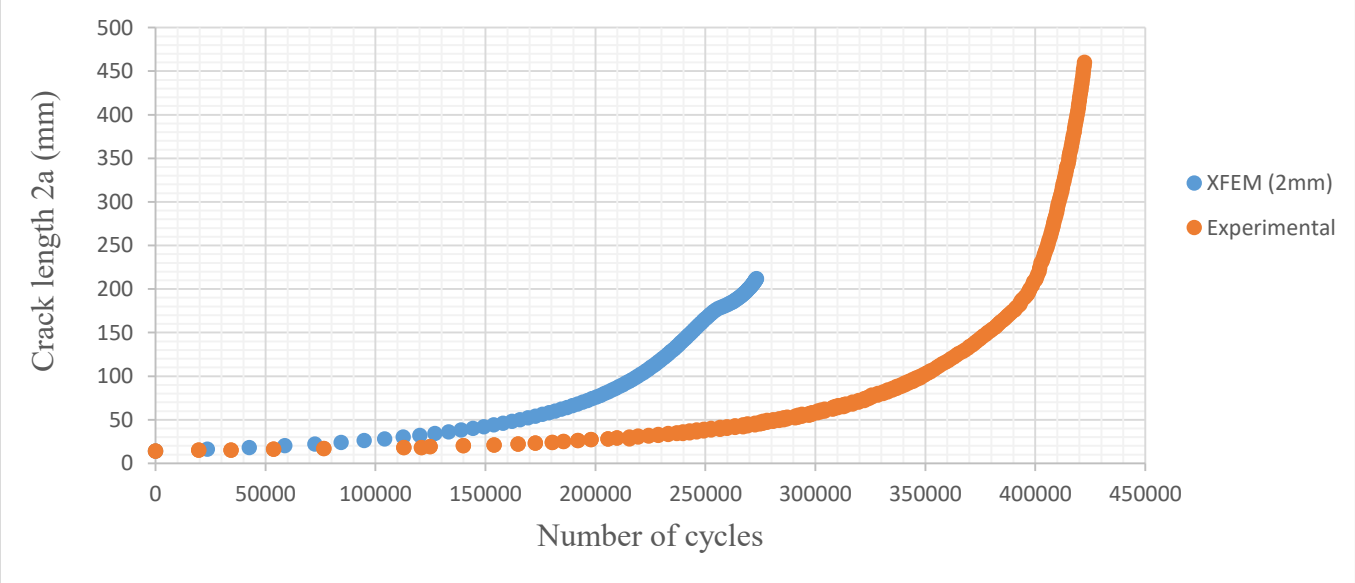

Figure 6.14. Numbers of cycles obtained in experiment and XFEM simulation (4-stringer 2mm).

Figure 6.14 shows the number of cycles to critical crack length (XFEM) is less than from number of cycles obtained in experiment (273230 cycles versus 422328 cycles, which is a difference of about 35 %).

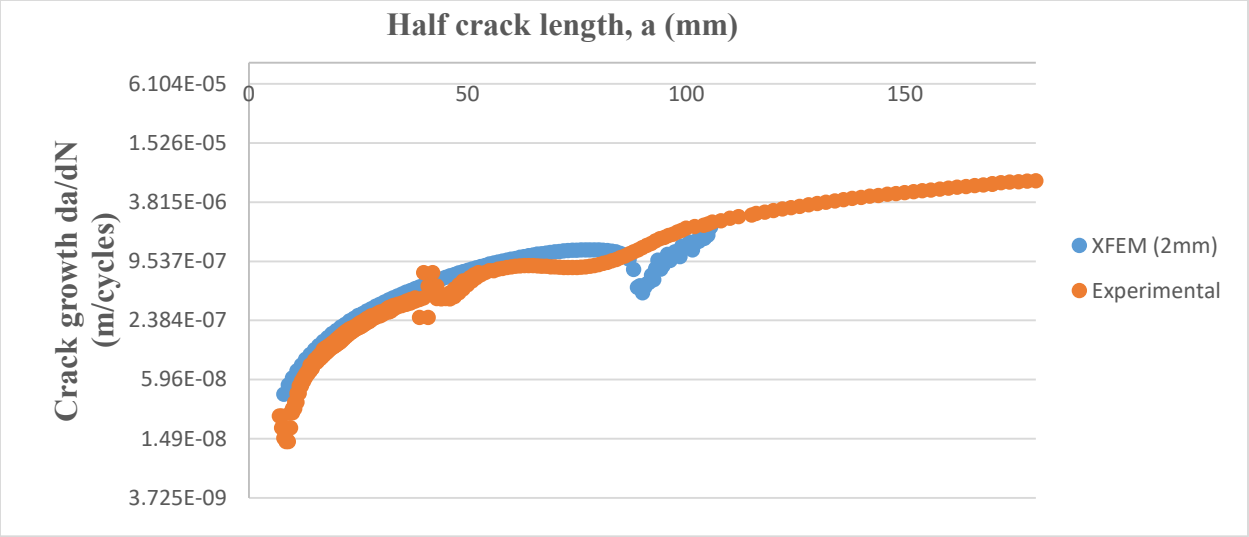

Figure 6.15 Comparison of the crack growth rate for 4-stringer obtained in the Experiment and 4-stringer plate (2mm) obtained in simulation with XFEM.

6.3.3 Model III (4-stringer with 4mm size of mesh).

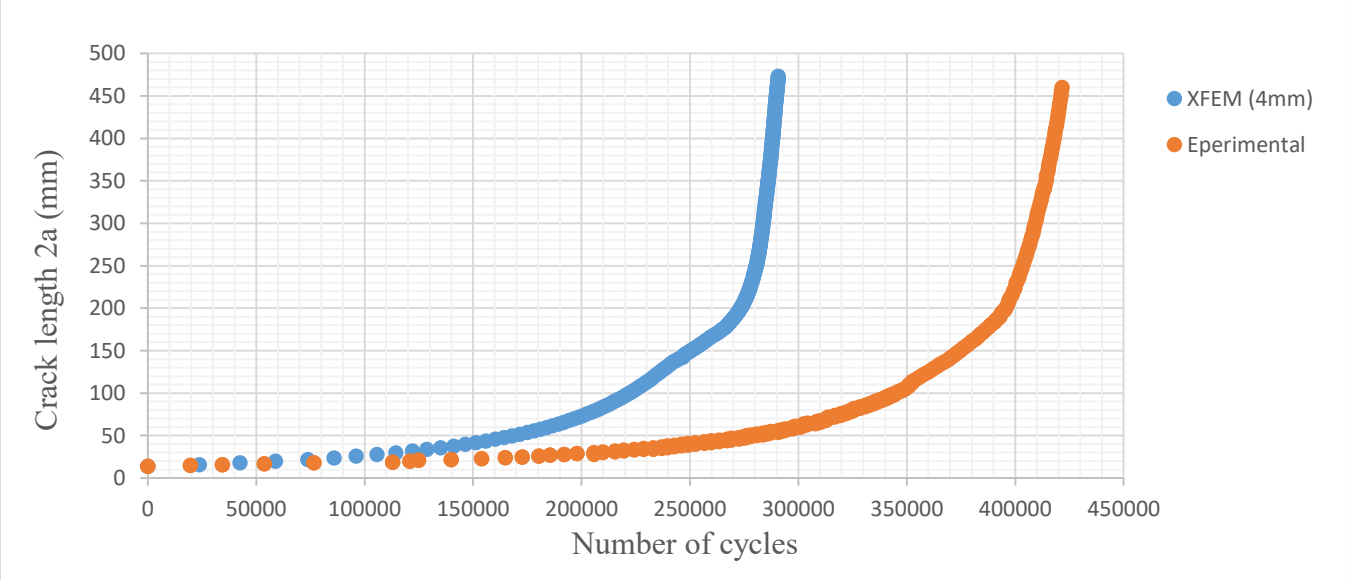

Figure 6.16. Numbers of cycles obtained in experiment and XFEM simulation (4-stringer 4mm).

As Figure 6.16, shows the number of cycles to critical crack length (XFEM) is still less than from number of cycles obtained in experiment (290743 cycles versus 422328 cycles, which is a difference of about 31 %).

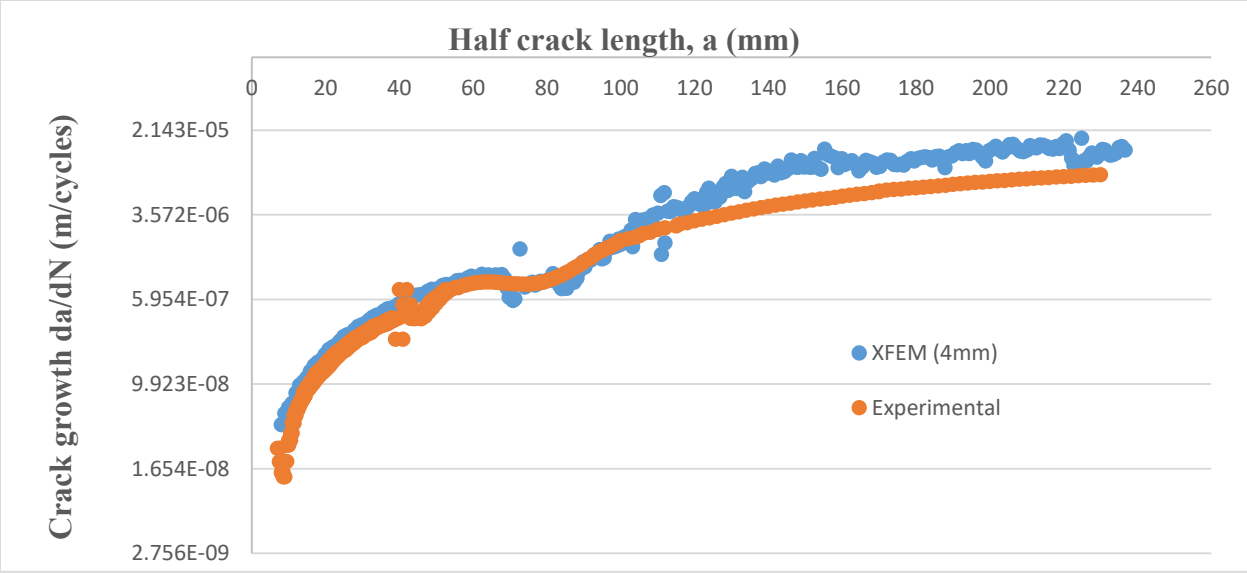

Figure 6.17 Comparison of the crack growth rate for 4-stringer obtained in the Experiment and 4-stringer plate (4mm) obtained in simulation with XFEM.

6.3.4 Model IV (4-stringer with 2mm size of mesh and (toe)).

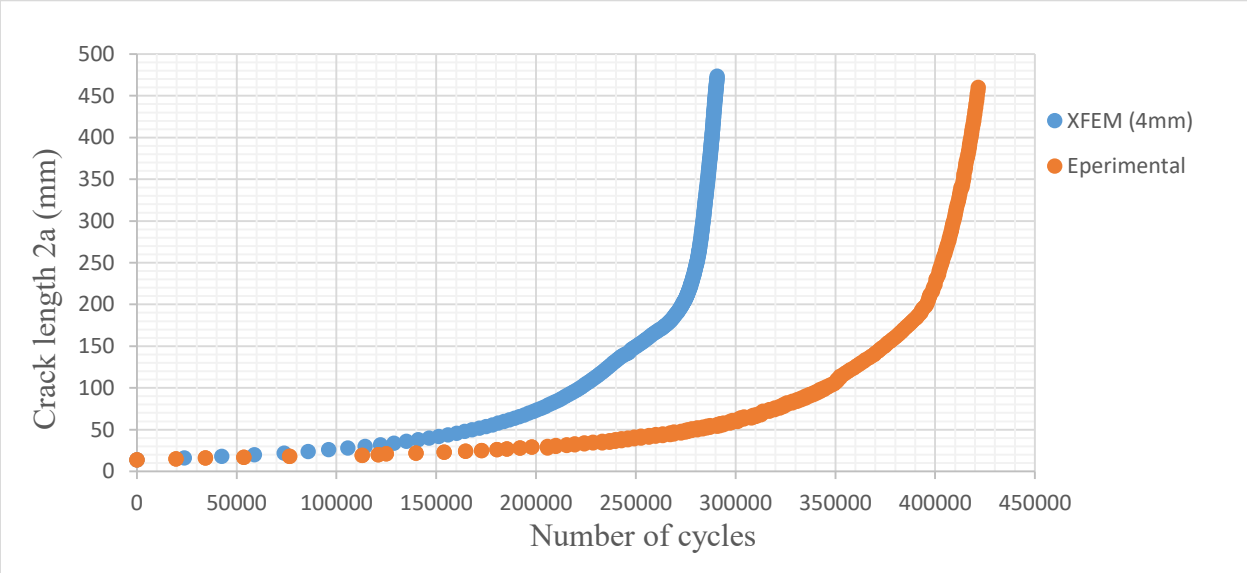

Figure 6.18. Numbers of cycles obtained in experiment and XFEM simulation (4-stringer 4mm).

As Figure 6.18 shows the number of cycles to critical crack length (XFEM) is still less than from number of cycles obtained in experiment (290743 cycles versus 422328 cycles, which is a difference of about 31 %).

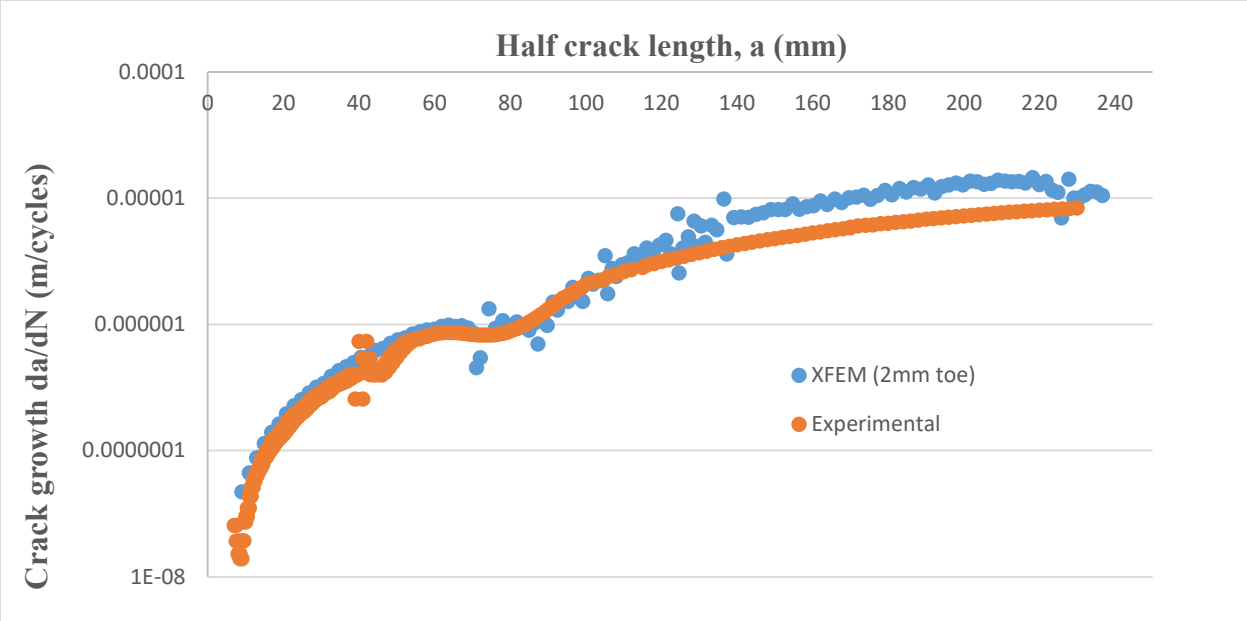

Figure 6.19 Comparison of the crack growth rate for 4-stringer obtained in the experimental and 4-stringer plate (2mm with toe) obtained in simulation with XFEM

Figure 6.19 shows comparison of experimental and 4-stringer plate (2mm with toe) numerical model values obtained in simulation with XFEM. It can be seen that cracks' speeds are almost the same until approximately 120 mm crack length. After that, crack in simulation grows slower. This length of 120mm coincides with the front reaching first stringer, after which it splits into 2 fronts. Morfeo/Crack for Abaqus calculates SIF for all 4 fronts (two on each end of the crack), and then takes maximum SIF values for number of cycle estimation. There are four stress concentrations here and this is why mesh configuration is very important to catch realistic values.

Chapter 7 CONCLUSIONS AND FURTHER WORK

The main goal of this dissertation aims to solve problems of estimation the fatigue life of integral aircraft structures, as well as fatigue crack growth phenomena. Until the development of XFEM and its integration in existing FE software packages, the numerical simulations of crack propagations through complex 3D structures were practically impossible or – in the best case very complex and with limited choice of crack shape. In addition, there was a problem with meshing, because after each step of the crack propagation new FE mesh around the crack front had to be generated which affected the accuracy of results and calculation time, especially for growth simulations of very long cracks.

XFEM can play a significant role in this subject and may reduce to a minimum the number of experimental verifications.

There are several cases analyzed. These cases are concluded in the following paragraphs:

- The first case is the base metal model. This model was simulated by using XFEM. The relation between the number of cycles and the critical crack length is less than that obtained in experiment results. The number of cycles obtained by XFEM method are 169 076 cycles. The number of cycles obtained by the experimental are 189 514 cycles. The difference between the two results are about 10%. **The XFEM method is a reliable method for the crack growth because it provides more save values compared with the experimental values. However, attention must be paid on mesh definition, because results are mesh sensitive.**
- The second case is the 4-stringers models. Due to the successful numerical simulation of crack growth on base metal plate, a more complex geometry of the 4-stringers plate were analyzed. The first model in this case is one mm size of mesh (1mm). The number of cycles obtained in this model are 254273 cycle. The number of cycles obtained by the experimental results are 422328 cycle**. The difference between the two results are about 40%.** To see the effect of size mesh, a different mesh size are analyzed. A two mm mesh size is the second model of this case. The number of cycles obtained in this model (2 mm

mesh size) are 273230 cycle. The number of cycles obtained by the experimental results is 422328 cycles. **The difference between the two results is about 35%. The deference percentage between the XFEM results and the experimental results reduced with increasing the mesh size. This is a positive point of the results.** Due to this positive result, a four mm mesh size (4 mm mesh size) is analyzed. The number of cycles obtained in this model (4 mm mesh size) was 290743 cycle. The number of cycles obtained by the experimental results is 422328 cycle. **The difference between the two results is about 31%, but from the results of second case it can be seen that, by increasing the mesh size the deference percentage decreases.** Further investigations confirmed gradual increase in number of cycles with increase in element size. This can be explained by the fact that smaller mesh size is more sensitive to stress concentration, and as a result stress intensity factors will be greater and, consequently, predicted fatigue life will be shorter.

- On the other hand, in all number of cycles calculations basic Paris law was used, and accuracy of these predictions is questionable. Better equations for estimation of number of cycles exist, like NASGRO equation, but to use them additional properties of material are needed and more experimental investigations are necessary. However, shape of the crack in simulation and damage produced on stringers and plate were almost identical to damage that appeared in experiment. **This implies that with well-defined fatigue properties of material, XFEM model – along with good crack growth equation – can estimate fatigue life with higher accuracy.** This can be good in practical design and analysis with respect to fracture mechanics and total life estimations.
- The third case is the 4-stringer with the 3-clips structure. A one model is analyzed in this case. There is no experimental verification for this model. The number of cycles obtained in this model (3-clips model) is 278476 cycle. **The number of cycles in numerical simulations are increased when clips are used,** for the same mesh density**.** This can be seen in Figure 5.38 where numbers of cycles were compared for mesh size 1mm.
- Finally, an attempt was made to assess static and fatigue strength of welded joint itself. Chapter 4 dealt with FKM regulations, and idea was to show that finite element method can be used in conjunction with analytical method in order to estimate fatigue strength. This should be the first step in fatigue analysis of welded parts used in aircraft design, because if fatigue strength of welded joint is not satisfactory, integral structure will fail

much before crack appearance. Analytical approach showed satisfactory fatigue strength, but obtained value (approx. 92%) **can be reduced by different geometry of weldment**. But, this reduction was not the goal of this thesis.

- Chapter 4 also contains FE simulation of laser beam welding. Significant residual stress was identified, as well as heat affected zone. This can influence fatigue life if no residual stress removal is performed. In simulation of crack growth this residual stress was not taken into account, because aluminum of skin-stringer panels was treated with heat before experimental work started. Stress in some areas of model after LBW was higher than yield stress; to eliminate **these higher stress different speed of laser should be used, as well as heat source with less power**.
- This work has shown that, the benefits of using both softwares (ABAQUS (Morfeo) AND ANSYS (WB/FKM)) in the integrity assessment of the structure are reflected in the following: saving time and money, which are important from an economic point of view. So skilled and experienced software user – in the framework that replaces expensive laboratory measurements, modeling the structure, introducing the initial crack in the structure, and then calculating the stress intensity and the deformation, as well as crack propagation simulation with all relevant parameters of fracture mechanics – can replace number of engineers of different specialties and can reduce time to final product.

Further work

Guidance for further research investigations in order to study more closely the phenomenon of initial stiffened structures including welded joint plates obtained by Laser beam welding are:

- Experimental testing for clips with 4-stringer skin should be conducted and then experimental values will be available for comparison.

REFERENCES

[1.1]. J.Munroe, K.Wilkins, and M.Gruber, “Integral Airframe Structures (IAS)—Validated Feasibility Study of Integrally Stiffened Metallic Fuselage Panels for Reducing Manufacturing Costs”, NASA/CR-2000-209337, May 2000.

[1.2]. Chen CS, Wawrzynek PA, Ingraffea AR. “Crack growth simulation and residual strength prediction in airplane fuselages”. NASA/CR-1999-209115; 1999 .

[1.3]. J. Enz, S. Riekehr, V. Ventzke, and N. Kashaev, “Influence of the local chemical composition on the mechanical properties of laser beam welded al-li alloys,” Physics Procedia, vol. 39 (2012), pp. 51 –58, 2012.

[1.4]. N. Kashaev, S. Chupakhin, J. Enz, V. Ventzke, A. Groth, M. Horstmann, and S. Riekehr, “Fatigueand fatigue crack propagation of laser beam-welded aa2198 joints and integral structures,” AdvancedMaterials Research, vol. 891-892 (2014), pp. 1457–1462, 2014.

[1.5].D. Dittrich, J. Standfuss, J. Liebscher, B. Brenner, and E. Beyer, “Laser beam welding of hard to weld al alloys for a regional aircraft fuselage design - first results,” Physics Procedia, vol. 12 (2011),pp. 113 – 122, 2011.

[1.6]. E. Seib, Residual strength analysis of laser beam and friction stir welded aluminium panels for aerospace application. PhD thesis, GKSS, 2006.

[1.7] Venkatesha B. K., Suresh B. S., Girish K. E., Analytical Evaluation of Fatigue Crack Arrest Capability in Fuselage of Large Transport Aircraft, International Journal on Theoretical and Applied Research in Mechanical Engineering, Vol.1, Issue 1, pp. 13-22, 2012.

[1.8] Parks D.M., A stiffness derivative finite element technique for determination of crack tip stress intensity factors. Int. J. Fract. 10 (1974), pp. 487–501.

[1.9] Hellen T.K., The finite element calculations of stress intensity factors using energy techniques, 2nd International Conference on Structural Mechanics in Reactor Technology, Paper G5/3, Berlin, 1973.

[1.10] Babuska I., Melenk J. M., The partition of unity method, Int. J. Numer. Meth. Eng., 40, pp. 727-758, 1998.

[1.11] Cenaero Morfeo, available at http://www.cenaero.be (last accesed on 4th Septembar 2016), 2016.

[1.12] Grbović A., Investigation of fatigue life in superalloys structural components, PhD Thesis (in Serbian), Faculty of Mechanical Engineering, University of Belgrade, Serbia, 2012.

[1.13] Moës N., Gravouil A., Belytschko T., Non-planar 3D crack growth by the extended finite element and level sets — Part I: Mechanical model. International Journal for Numerical Methods in Engineering, 53:2549–2568, 2002.

[1.14] Paris P. C., Erdogan F. A., Critical analysis of crack propagation laws, Jounal of Basic Engineering, TRANS ASME, 85(Series D), pp. 528–534, 1963.

[1.15] Funda Şeniz Bayraktar Analsys of residual stress and fatigue crack propagation behaviour in laser welded aerospace aluminum T-joints Phd Thesis (in Technical University Hamburg Harburg, Germany) 2011.

[2.1] R. C. Alderliesten, "Design and certification approach: Safe life, fail safe, damage tolerant." TUDelft Class video and presentation, 2011. http://collegerama.tudelft.nl/Mediasite.

[2.2] "Faa federal aviation regulations (far), part 25, section 571 damage - tolerance and fatigue evaluation of structures," 2005.

[2.3] H.-J. Schmidt and B. Schmidt-Brandecker, Fatigue and Damage Tolerance Course for Metal Structure- Lecture Notes. AeroStruc, Aeronautical Engineering, 2012.

[2.4] Swift, T., "Damage Tolerance in Pressurized Fuselages," Proceedings of the14th Symposium

of the International Committee on Aeronautical Fatigue, (Ottawa, Canada, June 8-12, 1987), Engineering Materials Advisory Services, Cradley Heath, Warley, West Midlands, U.K., 1987, pp 1-77.

[2.5] “Aircraft Accident Report – Aloha Airlines, Flight 243, Boeing 737 – 200, N73711, near Maui, Hawaii, April 1988”, NTSB/AAR-89/03, National Transportation Safety Board, Washington, D.C. 20594, June 1989.
[2.6] Hoggard, A.W., “Fuselage Longitudinal Splice Designs”, Structural Integrity of Aging Airplanes, Editors S.N Atluri, S.G. Sampath, and P. Tong. Springer-Verlag, New York, 1991.
[2.7] A. Almar-Næss, Tapir, Fatigue Handbook, Trondheim, Norway, 1985.
[2.8] W. A. J Albert, Über treibseile am Harz, Archive für Mineralogie Geognosie Bergbau und Hüttenkunde, Volume 10, pages 215-34, 1838
[2.9] W. J. M. Rankine, A Manual of Applied Mechanics, Charles Griffin and Company, Glasgow, 1858
[2.10] H.W. Hayden, W.G. Moffatt and J. Wulff, The structure and properties of Materials, Volume III, John Wiley, United Kingdom, 1965
[2.11] J.A. Ewing, Classic historic discovery of role of microscopic cracks in fatigue of metals, Philosophical Transactions of the Royal Society, 1903
[2.12] A.A. Griffith, The phenomena of rupture and flow in solids, Philosophical Transactions of the Royal Society of London, Series A, 221, pages 163-198, 1920.
[2.13] P.C. Paris, M.P. Gomez and W.E. Anderson, A rational theory of fatigue, The Trend in Engineering, Volume 13, pages 9-14, 1961
[2.14] W. Elber, Fatigue Crack Closure Under Cyclic Tension, Engineering Fracture Mechanics, Volume 2, pages 37-45, 1970
[2.15] Ewalds, H. L. and Wanhill, R. J. H., Fracture Mechanics, Edward Arnold, USA, 1989
[2.16] Paris, P. C., Gomez, M. P. and Anderson, W. P., A Rational Analytic Theory of Fatigue, The Trend in Engineering, 13,1961,9-14.
[2.17] Paris, P. C. and Ergogan, F., A Critical Analysis of Crack Propagation Laws, J. of Basic Engineering, 85,1960,528-5344
[2.18] Elber, W., Fatigue Crack Closure Under Cyclic Tension, Eng. Fracture Mechanics, 2(1), July 1970,37-44.
[2.19] Anderson, T. L., Fracture Mechanics Fundamentals and Applications, CRC Press, 1991.
[2.20] Munse, W. H., Fatigue of Welded Steel Structures, Welding Research Counci, 1964.

[2.21] R.G.Pettit, J.J.Wang, and C.toh,"Validated Feasibility Study of Integrally Stiffened Metallic Fuselage Panels for Reducing Manufacturing Costs", NASA/CR-2000-209342, May 2000.

[2.22] J.Munroe, K.Wilkins, and M.Gruber, "Integral Airframe Structures (IAS)—Validated Feasibility Study of Integrally Stiffened Metallic Fuselage Panels for Reducing Manufacturing Costs", NASA/CR-2000-209337, May 2000.

[2.23]. Grigory I. Nesterenko TsAGI, Russia "Comparison of Damage Tolerance of Integrally Stiffened and Rivetted Structures", ICAS 2000 Congress.

[2.24]. Der Veen V, Eherstrom JC, Muzzolini R. "Monolithic airframe structure: materials and methods for reduced cost reduced weight and improved damage tolerance". In: Proc. 44th AIAA materials and structures conference, paper AIAA-2003-1457; April 2003.

[2.25]. Zhang X, Boscolo M, Figueroa-Gordon D, Allegri G, Irving PE. "Fail-safe design of integral metallic aircraft structures reinforced by bonded crack retarders". Engng Fract Mech 2009;76:114–33.

[2.26] . Heinimann M, Bucci RJ, Kulak M, Garratt M. "Improving damage tolerance of aircraft structures through the use of selective reinforcement". In: 23rd ICAF symposium, Hamburg; June 2005.

[3.1]. T.L. Anderson, Fracture Mechanics: Fundamentals and Application 3rd Edition, Taylor and Francis group, 2005.

[3.2]. N.K. Simha, F.D. Fischer, G.X. Shan, C.R.Shan, C.R.Chen, O.Kolednik, J-integral and crack driving force in elastic-plastic materials, Journal of Fracture Mechanics and Physics of solids 56(2008) 2876-2895.

[3.3]. M.J. Patr´ıcio Dias. "Crack propagation on highly heterogeneous composite

materials". Doctoral Thesis, TechnischeUniversiteit Eindhoven, 2008.

[3.4] H.A. Wood and R.M. Engle. "USAF Damage Tolerance Design Handbook". Report AFFDL-TR-79-3021, United Air Force, Ohio, 1971.

[3.4] H.M. Westergaard. "Bearing Pressures and Cracks", Journal of Applied Mechanics, Vol. 6, pp.49-53, 1939.

[3.6]. http://www.efunda.com
[3.7] S. Al Laham. “Structural Integrity Branch, Stress Intensity Factor and Limit Load”. British Energy Generation Ltd. Handbook, United Kingdom, 1998.
[3.8] http://en.wikipedia.org/wiki/Fracture_toughness
[3.9] A.R. Boccaccini, S. Atiq, D.N. Boccaccini, I. Dlouhy and C. Kaya. “Fracture behaviour of mullitefibre reinforced-mullite matrix composites under quasi-static and ballistic impact loading”. Composites Science and Technology, 65, pp. 325–
[3.10] J. Phalippou, T. Woignier and R. Rogier. “Fracture toughness of silica aerogels”. Journal de Physique Colloques, 50, C4–191, 1989.
[3.11] N. Recho. “Fracture mechanics and crack growth”. Editions: John WILEY. ISBN: 978-1-84821-306-7, Mars 2012, and Rice J R, “A Path Independent Integral and the Approximate Analysis of Strain Concentration by Notches and Cracks”, Journal of Applied Mechanics, 1968, 35, 379-386.
[3.12]. W. Ramberg and W.R. Osgood. “Description of stress-strain curves by three parameters.” Technical Note, National Advisory Committee For Aeronautics, Washington DC, 1943.
[3.13] M. Fashang, D. Xiaomin, A. Micheal. “Sutton and James Newman. A CTOD
[3.14]. Y.M. Desai, T.I. Eldho and A.H. Shah. “Finite Element Method with applications in engineering”. Pearson Education India , 2011.
[3.15]. Y. Liu. “An Introduction to the Boundary Element Method (BEM) and Its Applications in Engineering”. CAE Research Lab, University of Cincinnati Cincinnati, Ohio, U.S.A. 2013
[3.16]. S.R. Idelsohn , E. Oñate , N. Calvo and F. Pin. “The meshless finite element method”. Iternational Journal for Numerical Methods in Engineerin. vol. 58-4, 2003.
[3.17]. A. Ahmed. “eXtended Finite Element Method (XFEM)- Modeling arbitrary discontinuities and Failure analysis”. Master Thesis, Universit a degliStudi di Pavia, 2009.
[3.18]. L. Gavete, F. Michavila, F. Díez. “A new singular finite element in linear elasticity”. Computational Mechanics, Volume 4, Issue 5, pp 361-371, 1989.
[3.19]. D. Potyondy, P. Wawrzynek, and A. Ingraffea, “Discrete crack growth analysis

methodology for through cracks in pressurized fuselage structures," Int J Numerical Meth Engng, 38, pp. 1611-1633, 1995.

[3.20]. F. Pengcheng, S.M. Johnson, R.R. Settgast and C.R. Carrigan. "Generalizeddisplacement correlation method for estimating stress intensity factors".Engineering Fracture Mechanics, Volume 88, pp. 90–107, 2012.

[3.21]. D.M. Parks. "The virtual crack extension method for nonlinear materialbehavior". Computer Methods in Applied Mechanics and Engineering, Volume12, pp. 353–364, 1977.

[3.22]. E. F. Rybicki and M. F. Kanninen. "Finite-element calculation of stress intensity factors by a modified crack closure integral". Engineering Fracture Mechanics, 9(4), pp. 931-938, 1977.

[3.23]. N. Recho. "Fracture mechanics and crack growth". Editions: John WILEY. ISBN: 978-1-84821-306-7, Mars 2012.

[3.24]. Paris, P C and Erdogan,F, "A critical Analysis of Crack Propagation Laws", Journal of Basic Engineering, Vol.85, 1960, 528-534.

[3.25]. Forman, R G, Keary, V E, and Engle, R M, "Numerical Analysis of crack Propagation in Cyclic-Loaded Structures", Journal of Basic Engineering, Vol.89, 1967, 459-464.

[3.26]. Krishna Lok Singh, Kamal Keswani and MallikarjunVaggar, Crack growth simulation of stiffened fuselage panels using XFEM techniques, Indian Journal of Engineering and Materials science (Vol.2), August 2014, 418-428.

[3.27]. Awas Ahmed, Extended Finite Element Method (XFEM)-Modeling arbitrary discontinuous and failure analysis, MSc thesis, University of studi da Pavia, April, 2009.

[3.28]. DibakarDatta, Introduction to Extended Finite Element (XFEM) Method, Erasmus MSc in computational mechanics (No: 080579k), France.

[3.29] Chao Zhang, Peng Cao, Yixiang Cao, Jianbo Li, Using Finite Element software to simulation Fracture Behaviour of Three-point Bending Beam with Initial crack, Journal of software, Vol.8, No.5, May 2013.

[3.30]. Vineet Kumar, IndraVir Singh, Bhanu Mishra, XFEM, Crack Growth Examination of Cryo-Rolled (CR) 6082 Al alloys, International Journal of Emerging Technology and Adavced Engineering (Vol.4) Special Issue 1, February 2014.
[3.31]. Zhen-Zhong Du, Extended Finite Element Method (XFEM) in Abaqus, Dessault system simulia.
[3.32]. Ted Belytschenko, Robert Gracie, Giulio Ventura, A review of Extended/Generalized finite element Methods for Material modelling.
[3.33]. E.Giner, N.Sukumar, J.E. Tarancon, F.J. Fuenmayor, An Abaqus implementation of the Extended finite element method, Engineering Fracture Mechanics, October 24, 2008,22.
[3.34]. Jay Sepheri, Application of Extended Finite Element (XFEM) to simulate Hydraulic Fracture Propagation from Oriented Perforations, MSc. Thesis1 Texas Tech university, May 2014.
[3.35]. Hao Wang and Jian Wang, Numerical analysis of surface crack propagation in Flexible Pavements using XFEM and Cohesive Zone Model, International Journal of Pavement research and Technology 7(3), 178-184, May 2014.
[3.36]. Adam Bevan et al, Development and validation of a wheel wear and rolling contact fatigue damage model, University of Huddersfield, Institute of Railway Research, 2013, UK.

[3.37]. J.J Kalker; Wheel-Rail Rolling Contact theory; Wear, 144(1991) 243-261; Netherlands.
[3.38]. MatinShahzamanianSichani, Wheel-Rail Contact Modelling in Vehicle Dynamics Simulation, Licentiate Thesis, KTH Engineering Science, Stockholm, Sweden, 2013. 58

[4.1].Analytical strength assessment of components [made of steel ,cast iron and aluminum materials in mechanical engineering] FKM guideline 6th edition 2012 VDMA velag

[5.1]. http://www.cenaero.be/Page_Generale.asp?DocID=27331

[6.1] https://www.researchgate.net/...AA6156.../Mechanical-characterization-by-DOE-analysis.

[6.2] Koçak M., Petrovski B., Palm V. F., Kocik R., Syassen F., Damage Tolerance Analysis of Laser Beam Welded Short Distance Clip Welds using 4-Stringer Flat Panels, European Workshop on Short Distance WELding Concepts for AIRframes - WEL-AIR, GKSS Research Center, Geesthacht (Hamburg) – Germany, 13 - 15 June 2007.

[6.3] NASGRO, http://www.swri.org/4org/d18/mateng/matint/nasgro/ (last accessed on 4th September 2016), 2016.

APPENDIX

FKM inside ANSYS - WB/FKM-Weld - Report

Global Assessment Parameters

This section contains parameters which are identical for all calculated assessment points.

General Assessment Parameters

Description	Value
Static assessment enabled	Yes
Fatigue assessment enabled	Yes
Fatigue assessment computation method	Fatigue limit
Overload case	F2: Constant stress ratio

Assessment Parameters

Description	Value
Use the equivalent mean stress for the mean stress factor calculation	Yes
Evaluate multiple path directions at corners	Yes
Angle between path directions	30.0 °
Warning threshold for path curvature	20.0 °
Contact detection radius	0.1 mm

Load Cases

The load cases were imported as proportional stresses. The stresses at the element nodes were not averaged for this calculation.

Load Case	Name	Stress Ratio	Scaling Factor
0	Static Structural Load case 1	0.1	1.0

Load Combinations

Load combinations analyzed in this assessment are created from the imported load cases. The following table lists the factors by which the stress tensors of each load case are multiplied before they are added to the load combination.

Load Combination	Load Case 0
1	0.1
2	1.0

Assessment Parameters and Results for "Weld connection"

This section starts with the input parameters for this weld, followed by the results of the selected weld nodes.

Weld Parameters

Description	Symbol	Value
Weld type		No or partial penetration
Weld quality		Verified
Residual stresses		High
Thickness factor		B
Plastic notch factor definition method		Manual
Plastic notch factor	K_p	1.0
Surface treatment factor	K_V	1.0
FAT class (perpendicular)	$FAT_{\perp}$	90.0
FAT class (parallel)	$FAT_{\parallel}$	90.0
FAT class (shear)	FAT_{τ}	80.0

Material Parameters

The material "AW-5049.H24/H34 (Zusatz SG-AlMg5)" from the group "Wrought aluminum alloy" was assigned.

Description	Symbol	Value
Component value of tensile strength	R_m	240 MPa
Component value of yield strength	R_p	160 MPa
Elongation at break	A	-
Tensile strength factor	$f_{\sigma,tension}$	1.0
Compression strength factor	$f_{\sigma,compression}$	1.0
Shear fatigue strength factor	$f_{W,\tau}$	0.577

Description	Symbol	Value
Grey cast iron factor	$K_{NL,E}$	1.0
Lower limit of effective damage sum	$D_{m,min}$	0.5
Softening factor	ρ_{WEZ}	0.79
Weld factor, full penetration or back welded, compression	$\alpha_{W,1}$	1.0
Weld factor, full penetration or back welded, tension, verified	$\alpha_{W,2}$	1.0
Weld factor, full penetration or back welded, tension, not verified	$\alpha_{W,3}$	0.75
Weld factor, full penetration or back welded, shear, verified	$\alpha_{W,4}$	0.59
Weld factor, full penetration or back welded, shear, not verified	$\alpha_{W,5}$	0.59
Weld factor, partial penetration or fillet weld	$\alpha_{W,6}$	0.67

Temperature Parameters

Description	Symbol	Value
Temperature	T	23.0 °C
Long-term temperature effect		No
Duration of exposure at temperature		1.0 h

S-N Curve Parameters

Description	Symbol	Value
Number of cycles at first knee point of the S-N curve (type I and II)	$N_{D,\sigma}$	5000000
Number of cycles at second knee point of the S-N curve (type II)	$N_{D,II,\sigma}$	-
First exponent of the S-N curve (type I and II)	k_{σ}	3.0
Second exponent of the S-N curve (type II)	$k_{II,\sigma}$	-
Number of cycles at first knee point of the S-N curve (type I and II)	$N_{D,\tau}$	100000000
Number of cycles at second knee point of the S-N curve (type II)	$N_{D,II,\tau}$	-
First exponent of the S-N curve (type I and II)	k_{τ}	5.0
Second exponent of the S-N curve (type II)	$k_{II,\tau}$	-

Safety Parameters

Description	Symbol	Value
Consequences of failure		High
Casting quality		Not verified
Regular inspections		No
Load occurs with high probability		Yes
Manual modification of the total static safety factor		0.0
Manual modification of the total fatigue safety factor		0.0
Basic safety factors set to 1.0		No
Load factor	Load factor j_S	1.0

Assessment Results for "Weld Toe 1"

Assessment Results for Node 15,897

Static strength assessment

The degree of static strength utilized is 41.1 %.

The assessment result details for the critical load combination 2 are listed in the following table.

Description	Symbol	Value
Normal stress, perpendicular	$\sigma_\perp$	20.5 MPa
Shear stress, parallel	τ	-0.7 MPa
Equivalent stress	σ_{vw}	20.5 MPa
Component value of tensile strength	R_m	240 MPa
Component value of yield strength	R_p	160 MPa
Local strain factor	K_w	1.0
Plastic notch factor	K_p	1.0
Section factor	n_{pl}	1.0
Weld factor	α_W	0.67
Component static strength	$\sigma_{SK,w}$	84.7 MPa
Temperature factor	$K_{T,m}$	1.0
Temperature factor	$K_{T,p}$	1.0
Temperature factor	$K_{T,tm}$	-
Temperature factor	$K_{T,tp}$	-
Basic safety factor for tensile strength	j_m	2.0
Basic safety factor for yield strength	j_p	1.5
Basic safety factor for creep strength	j_{mt}	1.5

Description	Symbol	Value
Basic safety factor for creep limit	j_{pt}	1.0
Load factor	Load factor j_S	1.0
Total safety factor (static)	j_{ges}	1.695
Degree of utilization for equivalent stress	$a_{SK,w}$	0.411

The following warning messages were recorded for this assessment:

- At least two extrapolation points are in the same element.

Fatigue strength assessment

The degree of fatigue strength utilized is 86.3 %.

The assessment result details for the critical oscillation between load combination 1 and load combination 2 are listed in the following table.

Description	Symbol	Value for $\sigma_\perp$	Value for $\sigma_\parallel$	Value for τ
Stress amplitude	σ_a	-9.2 MPa	-22.5 MPa	0.3 MPa
Mean stress	σ_m	11.3 MPa	27.4 MPa	-0.4 MPa
FAT class	FAT	90.0	90.0	80.0
FAT conversion factor	f_{FAT}	0.368	0.368	0.229
Plate thickness for thickness correction	t	1.0		
Thickness factor	f_t	1.1		
Component fatigue limit for completely reversed stresses	σ_{WK}	36.5 MPa	36.5 MPa	20.1 MPa
Mean stress factor	K_{AK}	1.0	1.0	1.0
Component fatigue limit	σ_{AK}	36.5 MPa	36.5 MPa	20.1 MPa
Variable amplitude fatigue strength factor	K_{BK}	1.0	1.0	1.0
Component variable amplitude fatigue strength	σ_{BK}	36.5 MPa	36.5 MPa	20.1 MPa
Local strain factor	K_w	1.0		
Plastic notch factor	K_p	1.0		
Section factor	n_{pl}	1.0		
Weld factor	α_W	0.67	0.67	0.67
Maximum value of the component variable amplitude fatigue strength	$\sigma_{BK,max}$	63.5 MPa	63.5 MPa	63.5 MPa
Temperature factor	$K_{T,D}$	1.0		
Basic safety factor	j_F	1.4		
Load factor	Load factor j_S	1.0		

Description	Symbol	Value for $\sigma_\perp$	Value for $\sigma_\parallel$	Value for τ
Total safety factor (fatigue)	j_D	1.4		
Cyclic degree of utilization for individual components	a_{BK}	-0.354	-0.862	0.022
Combined degree of utilization	$a_{BK,\sigma v}$	0.863		

The following warning messages were recorded for this assessment:

- At least two extrapolation points are in the same element.

Assessment Results for Node 17,564

Static strength assessment

The degree of static strength utilized is 39.3 %.

The assessment result details for the critical load combination 2 are listed in the following table.

Description	Symbol	Value
Normal stress, perpendicular	$\sigma_\perp$	19.5 MPa
Shear stress, parallel	τ	2.8 MPa
Equivalent stress	σ_{vw}	19.7 MPa
Component value of tensile strength	R_m	240 MPa
Component value of yield strength	R_p	160 MPa
Local strain factor	K_w	1.0
Plastic notch factor	K_p	1.0
Section factor	n_{pl}	1.0
Weld factor	α_W	0.67
Component static strength	$\sigma_{SK,w}$	84.7 MPa
Temperature factor	$K_{T,m}$	1.0
Temperature factor	$K_{T,p}$	1.0
Temperature factor	$K_{T,tm}$	-
Temperature factor	$K_{T,tp}$	-
Basic safety factor for tensile strength	j_m	2.0
Basic safety factor for yield strength	j_p	1.5
Basic safety factor for creep strength	j_{mt}	1.5
Basic safety factor for creep limit	j_{pt}	1.0
Load factor	Load factor j_S	1.0
Total safety factor (static)	j_{ges}	1.695
Degree of utilization for equivalent stress	$a_{SK,w}$	0.393

The following warning messages were recorded for this assessment:

- At least two extrapolation points are in the same element.

Fatigue strength assessment

The degree of fatigue strength utilized is 89.1 %.

The assessment result details for the critical oscillation between load combination 1 and load combination 2 are listed in the following table.

Description	Symbol	Value for $\sigma_\perp$	Value for $\sigma_\parallel$	Value for τ
Stress amplitude	σ_a	-8.8 MPa	-22.9 MPa	-1.2 MPa
Mean stress	σ_m	10.7 MPa	27.9 MPa	1.5 MPa
FAT class	FAT	90.0	90.0	80.0
FAT conversion factor	f_{FAT}	0.368	0.368	0.229
Plate thickness for thickness correction	t	1.0		
Thickness factor	f_t	1.1		
Component fatigue limit for completely reversed stresses	σ_{WK}	36.5 MPa	36.5 MPa	20.1 MPa
Mean stress factor	K_{AK}	1.0	1.0	1.0
Component fatigue limit	σ_{AK}	36.5 MPa	36.5 MPa	20.1 MPa
Variable amplitude fatigue strength factor	K_{BK}	1.0	1.0	1.0
Component variable amplitude fatigue strength	σ_{BK}	36.5 MPa	36.5 MPa	20.1 MPa
Local strain factor	K_w	1.0		
Plastic notch factor	K_p	1.0		
Section factor	n_{pl}	1.0		
Weld factor	α_W	0.67	0.67	0.67
Maximum value of the component variable amplitude fatigue strength	$\sigma_{BK,max}$	63.5 MPa	63.5 MPa	63.5 MPa
Temperature factor	$K_{T,D}$	1.0		
Basic safety factor	j_F	1.4		
Load factor	Load factor j_S	1.0		
Total safety factor (fatigue)	j_D	1.4		
Cyclic degree of utilization for individual components	a_{BK}	-0.336	-0.877	-0.087
Combined degree of utilization	$a_{BK,\sigma v}$	0.891		

The following warning messages were recorded for this assessment:

- At least two extrapolation points are in the same element.

Assessment Parameters and Results for "Weld connection 2"

This section starts with the input parameters for this weld, followed by the results of the selected weld nodes.

Weld Parameters

Description	Symbol	Value
Weld type		No or partial penetration
Weld quality		Verified
Residual stresses		High
Thickness factor		B
Plastic notch factor definition method		Manual
Plastic notch factor	K_p	1.0
Surface treatment factor	K_V	1.0
FAT class (perpendicular)	$FAT_{\perp}$	90.0
FAT class (parallel)	$FAT_{\parallel}$	90.0
FAT class (shear)	FAT_{τ}	80.0

Material Parameters

The material "AW-5049.H24/H34 (Zusatz SG-AlMg5)" from the group "Wrought aluminum alloy" was assigned.

Description	Symbol	Value
Component value of tensile strength	R_m	240 MPa
Component value of yield strength	R_p	160 MPa
Elongation at break	A	-
Tensile strength factor	$f_{\sigma,tension}$	1.0
Compression strength factor	$f_{\sigma,compression}$	1.0
Shear fatigue strength factor	$f_{W,\tau}$	0.577
Grey cast iron factor	$K_{NL,E}$	1.0
Lower limit of effective damage sum	$D_{m,min}$	0.5
Softening factor	ρ_{WEZ}	0.79
Weld factor, full penetration or back welded, compression	$\alpha_{W,1}$	1.0

Description	Symbol	Value
Weld factor, full penetration or back welded, tension, verified	$\alpha_{W,2}$	1.0
Weld factor, full penetration or back welded, tension, not verified	$\alpha_{W,3}$	0.75
Weld factor, full penetration or back welded, shear, verified	$\alpha_{W,4}$	0.59
Weld factor, full penetration or back welded, shear, not verified	$\alpha_{W,5}$	0.59
Weld factor, partial penetration or fillet weld	$\alpha_{W,6}$	0.67

Temperature Parameters

Description	Symbol	Value
Temperature	T	23.0 °C
Long-term temperature effect		No
Duration of exposure at temperature		1.0 h

S-N Curve Parameters

Description	Symbol	Value
Number of cycles at first knee point of the S-N curve (type I and II)	$N_{D,\sigma}$	5000000
Number of cycles at second knee point of the S-N curve (type II)	$N_{D,II,\sigma}$	-
First exponent of the S-N curve (type I and II)	k_{σ}	3.0
Second exponent of the S-N curve (type II)	$k_{II,\sigma}$	-
Number of cycles at first knee point of the S-N curve (type I and II)	$N_{D,\tau}$	100000000
Number of cycles at second knee point of the S-N curve (type II)	$N_{D,II,\tau}$	-
First exponent of the S-N curve (type I and II)	k_{τ}	5.0
Second exponent of the S-N curve (type II)	$k_{II,\tau}$	-

Safety Parameters

Description	Symbol	Value
Consequences of failure		High
Casting quality		Not verified
Regular inspections		No

Description	Symbol	Value
Load occurs with high probability		Yes
Manual modification of the total static safety factor		0.0
Manual modification of the total fatigue safety factor		0.0
Basic safety factors set to 1.0		No
Load factor	Load factor j_S	1.0

Assessment Results for "Weld Toe 1"

Assessment Results for Node 21,433

Static strength assessment

The degree of static strength utilized is 38.9 %.

The assessment result details for the critical load combination 2 are listed in the following table.

Description	Symbol	Value
Normal stress, perpendicular	$\sigma_\perp$	19.2 MPa
Shear stress, parallel	τ	2.7 MPa
Equivalent stress	σ_{vw}	19.4 MPa
Component value of tensile strength	R_m	240 MPa
Component value of yield strength	R_p	160 MPa
Local strain factor	K_w	1.0
Plastic notch factor	K_p	1.0
Section factor	n_{pl}	1.0
Weld factor	α_W	0.67
Component static strength	$\sigma_{SK,w}$	84.7 MPa
Temperature factor	$K_{T,m}$	1.0
Temperature factor	$K_{T,p}$	1.0
Temperature factor	$K_{T,tm}$	-
Temperature factor	$K_{T,tp}$	-
Basic safety factor for tensile strength	j_m	2.0
Basic safety factor for yield strength	j_p	1.5
Basic safety factor for creep strength	j_{mt}	1.5
Basic safety factor for creep limit	j_{pt}	1.0
Load factor	Load factor j_S	1.0
Total safety factor (static)	j_{ges}	1.695
Degree of utilization for equivalent stress	$a_{SK,w}$	0.389

The following warning messages were recorded for this assessment:

- At least two extrapolation points are in the same element.

Fatigue strength assessment

The degree of fatigue strength utilized is 88.6 %.

The assessment result details for the critical oscillation between load combination 1 and load combination 2 are listed in the following table.

Description	Symbol	Value for $\sigma_\perp$	Value for $\sigma_\parallel$	Value for τ
Stress amplitude	σ_a	-8.7 MPa	-22.7 MPa	-1.2 MPa
Mean stress	σ_m	10.6 MPa	27.8 MPa	1.5 MPa
FAT class	FAT	90.0	90.0	80.0
FAT conversion factor	f_{FAT}	0.368	0.368	0.229
Plate thickness for thickness correction	t	1.0		
Thickness factor	f_t	1.1		
Component fatigue limit for completely reversed stresses	σ_{WK}	36.5 MPa	36.5 MPa	20.1 MPa
Mean stress factor	K_{AK}	1.0	1.0	1.0
Component fatigue limit	σ_{AK}	36.5 MPa	36.5 MPa	20.1 MPa
Variable amplitude fatigue strength factor	K_{BK}	1.0	1.0	1.0
Component variable amplitude fatigue strength	σ_{BK}	36.5 MPa	36.5 MPa	20.1 MPa
Local strain factor	K_w	1.0		
Plastic notch factor	K_p	1.0		
Section factor	n_{pl}	1.0		
Weld factor	α_W	0.67	0.67	0.67
Maximum value of the component variable amplitude fatigue strength	$\sigma_{BK,max}$	63.5 MPa	63.5 MPa	63.5 MPa
Temperature factor	$K_{T,D}$	1.0		
Basic safety factor	j_F	1.4		
Load factor	Load factor j_S	1.0		
Total safety factor (fatigue)	j_D	1.4		
Cyclic degree of utilization for individual components	a_{BK}	-0.333	-0.873	-0.084
Combined degree of utilization	$a_{BK,\sigma v}$	0.886		

The following warning messages were recorded for this assessment:

- At least two extrapolation points are in the same element.

Assessment Results for Node 23,596

Static strength assessment

The degree of static strength utilized is 40.6 %.

The assessment result details for the critical load combination 2 are listed in the following table.

Description	Symbol	Value
Normal stress, perpendicular	$\sigma_{\perp}$	20.3 MPa
Shear stress, parallel	τ	0.4 MPa
Equivalent stress	σ_{vw}	20.3 MPa
Component value of tensile strength	R_m	240 MPa
Component value of yield strength	R_p	160 MPa
Local strain factor	K_w	1.0
Plastic notch factor	K_p	1.0
Section factor	n_{pl}	1.0
Weld factor	α_W	0.67
Component static strength	$\sigma_{SK,w}$	84.7 MPa
Temperature factor	$K_{T,m}$	1.0
Temperature factor	$K_{T,p}$	1.0
Temperature factor	$K_{T,tm}$	-
Temperature factor	$K_{T,tp}$	-
Basic safety factor for tensile strength	j_m	2.0
Basic safety factor for yield strength	j_p	1.5
Basic safety factor for creep strength	j_{mt}	1.5
Basic safety factor for creep limit	j_{pt}	1.0
Load factor	Load factor j_S	1.0
Total safety factor (static)	j_{ges}	1.695
Degree of utilization for equivalent stress	$a_{SK,w}$	0.406

The following warning messages were recorded for this assessment:

- At least two extrapolation points are in the same element.

Fatigue strength assessment

The degree of fatigue strength utilized is 85.6 %.

The assessment result details for the critical oscillation between load combination 1 and load combination 2 are listed in the following table.

Description	Symbol	Value for $\sigma_{\perp}$	Value for $\sigma_{\parallel}$	Value for τ
Stress amplitude	σ_a	-9.1 MPa	-22.3 MPa	-0.2 MPa
Mean stress	σ_m	11.2 MPa	27.3 MPa	0.2 MPa
FAT class	FAT	90.0	90.0	80.0
FAT conversion factor	f_{FAT}	0.368	0.368	0.229
Plate thickness for thickness correction	t	1.0		
Thickness factor	f_t	1.1		
Component fatigue limit for completely reversed stresses	σ_{WK}	36.5 MPa	36.5 MPa	20.1 MPa
Mean stress factor	K_{AK}	1.0	1.0	1.0
Component fatigue limit	σ_{AK}	36.5 MPa	36.5 MPa	20.1 MPa
Variable amplitude fatigue strength factor	K_{BK}	1.0	1.0	1.0
Component variable amplitude fatigue strength	σ_{BK}	36.5 MPa	36.5 MPa	20.1 MPa
Local strain factor	K_w	1.0		
Plastic notch factor	K_p	1.0		
Section factor	n_{pl}	1.0		
Weld factor	α_W	0.67	0.67	0.67
Maximum value of the component variable amplitude fatigue strength	$\sigma_{BK,max}$	63.5 MPa	63.5 MPa	63.5 MPa
Temperature factor	$K_{T,D}$	1.0		
Basic safety factor	j_F	1.4		
Load factor	Load factor j_S	1.0		
Total safety factor (fatigue)	j_D	1.4		
Cyclic degree of utilization for individual components	a_{BK}	-0.351	-0.856	-0.011
Combined degree of utilization	$a_{BK,\sigma v}$	0.856		

The following warning messages were recorded for this assessment:

- At least two extrapolation points are in the same element.

Assessment Parameters and Results for "Weld connection 3"

This section starts with the input parameters for this weld, followed by the results of the selected weld nodes.

Weld Parameters

Description	Symbol	Value
Weld type		No or partial penetration
Weld quality		Verified
Residual stresses		High
Thickness factor		B
Plastic notch factor definition method		Manual
Plastic notch factor	K_p	1.0
Surface treatment factor	K_V	1.0
FAT class (perpendicular)	$FAT_\perp$	90.0
FAT class (parallel)	$FAT_\parallel$	90.0
FAT class (shear)	FAT_τ	80.0

Material Parameters

The material "AW-5049.H24/H34 (Zusatz SG-AlMg5)" from the group "Wrought aluminum alloy" was assigned.

Description	Symbol	Value
Component value of tensile strength	R_m	240 MPa
Component value of yield strength	R_p	160 MPa
Elongation at break	A	-
Tensile strength factor	$f_{\sigma,tension}$	1.0
Compression strength factor	$f_{\sigma,compression}$	1.0
Shear fatigue strength factor	$f_{W,\tau}$	0.577
Grey cast iron factor	$K_{NL,E}$	1.0
Lower limit of effective damage sum	$D_{m,min}$	0.5
Softening factor	ρ_{WEZ}	0.79
Weld factor, full penetration or back welded, compression	$\alpha_{W,1}$	1.0
Weld factor, full penetration or back welded, tension, verified	$\alpha_{W,2}$	1.0
Weld factor, full penetration or back welded, tension, not verified	$\alpha_{W,3}$	0.75
Weld factor, full penetration or back welded, shear, verified	$\alpha_{W,4}$	0.59

Description	Symbol	Value
Weld factor, full penetration or back welded, shear, not verified	$\alpha_{W,5}$	0.59
Weld factor, partial penetration or fillet weld	$\alpha_{W,6}$	0.67

Temperature Parameters

Description	Symbol	Value
Temperature	T	23.0 °C
Long-term temperature effect		No
Duration of exposure at temperature		1.0 h

S-N Curve Parameters

Description	Symbol	Value
Number of cycles at first knee point of the S-N curve (type I and II)	$N_{D,\sigma}$	5000000
Number of cycles at second knee point of the S-N curve (type II)	$N_{D,II,\sigma}$	-
First exponent of the S-N curve (type I and II)	k_σ	3.0
Second exponent of the S-N curve (type II)	$k_{II,\sigma}$	-
Number of cycles at first knee point of the S-N curve (type I and II)	$N_{D,\tau}$	100000000
Number of cycles at second knee point of the S-N curve (type II)	$N_{D,II,\tau}$	-
First exponent of the S-N curve (type I and II)	k_τ	5.0
Second exponent of the S-N curve (type II)	$k_{II,\tau}$	-

Safety Parameters

Description	Symbol	Value
Consequences of failure		High
Casting quality		Not verified
Regular inspections		No
Load occurs with high probability		Yes
Manual modification of the total static safety factor		0.0
Manual modification of the total fatigue safety factor		0.0
Basic safety factors set to 1.0		No
Load factor	Load factor j_S	1.0

Assessment Results for "Weld Toe 1"

Assessment Results for Node 4,093

Static strength assessment

The degree of static strength utilized is 39.5 %.

The assessment result details for the critical load combination 2 are listed in the following table.

Description	Symbol	Value
Normal stress, perpendicular	$\sigma_{\perp}$	19.7 MPa
Shear stress, parallel	τ	1.4 MPa
Equivalent stress	σ_{vw}	19.8 MPa
Component value of tensile strength	R_m	240 MPa
Component value of yield strength	R_p	160 MPa
Local strain factor	K_w	1.0
Plastic notch factor	K_p	1.0
Section factor	n_{pl}	1.0
Weld factor	α_W	0.67
Component static strength	$\sigma_{SK,w}$	84.7 MPa
Temperature factor	$K_{T,m}$	1.0
Temperature factor	$K_{T,p}$	1.0
Temperature factor	$K_{T,tm}$	-
Temperature factor	$K_{T,tp}$	-
Basic safety factor for tensile strength	j_m	2.0
Basic safety factor for yield strength	j_p	1.5
Basic safety factor for creep strength	j_{mt}	1.5
Basic safety factor for creep limit	j_{pt}	1.0
Load factor	Load factor j_S	1.0
Total safety factor (static)	j_{ges}	1.695
Degree of utilization for equivalent stress	$a_{SK,w}$	0.395

The following warning messages were recorded for this assessment:

- At least two extrapolation points are in the same element.

Fatigue strength assessment

The degree of fatigue strength utilized is 86 %.

The assessment result details for the critical oscillation between load combination 1 and load combination 2 are listed in the following table.

Description	Symbol	Value for $\sigma_{\perp}$	Value for $\sigma_{\parallel}$	Value for τ
Stress amplitude	σ_a	-8.9 MPa	-22.3 MPa	-0.6 MPa
Mean stress	σ_m	10.8 MPa	27.3 MPa	0.8 MPa
FAT class	FAT	90.0	90.0	80.0
FAT conversion factor	f_{FAT}	0.368	0.368	0.229
Plate thickness for thickness correction	t	1.0		
Thickness factor	f_t	1.1		
Component fatigue limit for completely reversed stresses	σ_{WK}	36.5 MPa	36.5 MPa	20.1 MPa
Mean stress factor	K_{AK}	1.0	1.0	1.0
Component fatigue limit	σ_{AK}	36.5 MPa	36.5 MPa	20.1 MPa
Variable amplitude fatigue strength factor	K_{BK}	1.0	1.0	1.0
Component variable amplitude fatigue strength	σ_{BK}	36.5 MPa	36.5 MPa	20.1 MPa
Local strain factor	K_w	1.0		
Plastic notch factor	K_p	1.0		
Section factor	n_{pl}	1.0		
Weld factor	α_W	0.67	0.67	0.67
Maximum value of the component variable amplitude fatigue strength	$\sigma_{BK,max}$	63.5 MPa	63.5 MPa	63.5 MPa
Temperature factor	$K_{T,D}$	1.0		
Basic safety factor	j_F	1.4		
Load factor	Load factor j_S	1.0		
Total safety factor (fatigue)	j_D	1.4		
Cyclic degree of utilization for individual components	a_{BK}	-0.34	-0.856	-0.045
Combined degree of utilization	$a_{BK,\sigma v}$	0.86		

The following warning messages were recorded for this assessment:

- At least two extrapolation points are in the same element.

Assessment Parameters and Results for "Weld connection 4"

This section starts with the input parameters for this weld, followed by the results of the selected weld nodes.

Weld Parameters

Description	Symbol	Value
Weld type		No or partial penetration
Weld quality		Verified
Residual stresses		High
Thickness factor		B
Plastic notch factor definition method		Manual
Plastic notch factor	K_p	1.0
Surface treatment factor	K_V	1.0
FAT class (perpendicular)	$FAT_{\perp}$	90.0
FAT class (parallel)	$FAT_{\parallel}$	90.0
FAT class (shear)	FAT_{τ}	80.0

Material Parameters

The material "AW-5049.H24/H34 (Zusatz SG-AlMg5)" from the group "Wrought aluminum alloy" was assigned.

Description	Symbol	Value
Component value of tensile strength	R_m	240 MPa
Component value of yield strength	R_p	160 MPa
Elongation at break	A	-
Tensile strength factor	$f_{\sigma,tension}$	1.0
Compression strength factor	$f_{\sigma,compression}$	1.0
Shear fatigue strength factor	$f_{W,\tau}$	0.577
Grey cast iron factor	$K_{NL,E}$	1.0
Lower limit of effective damage sum	$D_{m,min}$	0.5
Softening factor	ρ_{WEZ}	0.79
Weld factor, full penetration or back welded, compression	$\alpha_{W,1}$	1.0
Weld factor, full penetration or back welded, tension, verified	$\alpha_{W,2}$	1.0
Weld factor, full penetration or back welded, tension, not verified	$\alpha_{W,3}$	0.75
Weld factor, full penetration or back welded, shear, verified	$\alpha_{W,4}$	0.59

Description	Symbol	Value
Weld factor, full penetration or back welded, shear, not verified	$\alpha_{W,5}$	0.59
Weld factor, partial penetration or fillet weld	$\alpha_{W,6}$	0.67

Temperature Parameters

Description	Symbol	Value
Temperature	T	23.0 °C
Long-term temperature effect		No
Duration of exposure at temperature		1.0 h

S-N Curve Parameters

Description	Symbol	Value
Number of cycles at first knee point of the S-N curve (type I and II)	$N_{D,\sigma}$	5000000
Number of cycles at second knee point of the S-N curve (type II)	$N_{D,II,\sigma}$	-
First exponent of the S-N curve (type I and II)	k_σ	3.0
Second exponent of the S-N curve (type II)	$k_{II,\sigma}$	-
Number of cycles at first knee point of the S-N curve (type I and II)	$N_{D,\tau}$	100000000
Number of cycles at second knee point of the S-N curve (type II)	$N_{D,II,\tau}$	-
First exponent of the S-N curve (type I and II)	k_τ	5.0
Second exponent of the S-N curve (type II)	$k_{II,\tau}$	-

Safety Parameters

Description	Symbol	Value
Consequences of failure		High
Casting quality		Not verified
Regular inspections		No
Load occurs with high probability		Yes
Manual modification of the total static safety factor		0.0
Manual modification of the total fatigue safety factor		0.0
Basic safety factors set to 1.0		No
Load factor	Load factor j_S	1.0

Assessment Results for "Weld Toe 1"

Assessment Results for Node 9,397

Static strength assessment

The degree of static strength utilized is 39.8 %.

The assessment result details for the critical load combination 2 are listed in the following table.

Description	Symbol	Value
Normal stress, perpendicular	$\sigma_{\perp}$	19.8 MPa
Shear stress, parallel	τ	1.5 MPa
Equivalent stress	σ_{vw}	19.9 MPa
Component value of tensile strength	R_m	240 MPa
Component value of yield strength	R_p	160 MPa
Local strain factor	K_w	1.0
Plastic notch factor	K_p	1.0
Section factor	n_{pl}	1.0
Weld factor	α_W	0.67
Component static strength	$\sigma_{SK,w}$	84.7 MPa
Temperature factor	$K_{T,m}$	1.0
Temperature factor	$K_{T,p}$	1.0
Temperature factor	$K_{T,tm}$	-
Temperature factor	$K_{T,tp}$	-
Basic safety factor for tensile strength	j_m	2.0
Basic safety factor for yield strength	j_p	1.5
Basic safety factor for creep strength	j_{mt}	1.5
Basic safety factor for creep limit	j_{pt}	1.0
Load factor	Load factor j_S	1.0
Total safety factor (static)	j_{ges}	1.695
Degree of utilization for equivalent stress	$a_{SK,w}$	0.398

The following warning messages were recorded for this assessment:

- At least two extrapolation points are in the same element.

Fatigue strength assessment

The degree of fatigue strength utilized is 86.5 %.

The assessment result details for the critical oscillation between load combination 1 and load combination 2 are listed in the following table.

Description	Symbol	Value for $\sigma_\perp$	Value for $\sigma_\parallel$	Value for τ
Stress amplitude	σ_a	-8.9 MPa	-22.4 MPa	-0.7 MPa
Mean stress	σ_m	10.9 MPa	27.4 MPa	0.8 MPa
FAT class	FAT	90.0	90.0	80.0
FAT conversion factor	f_{FAT}	0.368	0.368	0.229
Plate thickness for thickness correction	t	1.0		
Thickness factor	f_t	1.1		
Component fatigue limit for completely reversed stresses	σ_{WK}	36.5 MPa	36.5 MPa	20.1 MPa
Mean stress factor	K_{AK}	1.0	1.0	1.0
Component fatigue limit	σ_{AK}	36.5 MPa	36.5 MPa	20.1 MPa
Variable amplitude fatigue strength factor	K_{BK}	1.0	1.0	1.0
Component variable amplitude fatigue strength	σ_{BK}	36.5 MPa	36.5 MPa	20.1 MPa
Local strain factor	K_w	1.0		
Plastic notch factor	K_p	1.0		
Section factor	n_{pl}	1.0		
Weld factor	α_W	0.67	0.67	0.67
Maximum value of the component variable amplitude fatigue strength	$\sigma_{BK,max}$	63.5 MPa	63.5 MPa	63.5 MPa
Temperature factor	$K_{T,D}$	1.0		
Basic safety factor	j_F	1.4		
Load factor	Load factor j_S	1.0		
Total safety factor (fatigue)	j_D	1.4		
Cyclic degree of utilization for individual components	a_{BK}	-0.342	-0.861	-0.046
Combined degree of utilization	$a_{BK,\sigma v}$	0.865		

The following warning messages were recorded for this assessment:

- At least two extrapolation points are in the same element.

Assessment Parameters and Results for "Weld connection 5"

This section starts with the input parameters for this weld, followed by the results of the selected weld nodes.

Weld Parameters

Description	Symbol	Value
Weld type		No or partial penetration
Weld quality		Verified
Residual stresses		High
Thickness factor		B
Plastic notch factor definition method		Manual
Plastic notch factor	K_p	1.0
Surface treatment factor	K_V	1.0
FAT class (perpendicular)	$FAT_\perp$	90.0
FAT class (parallel)	$FAT_\parallel$	90.0
FAT class (shear)	FAT_τ	80.0

Material Parameters

The material "AW-5049.H24/H34 (Zusatz SG-AlMg5)" from the group "Wrought aluminum alloy" was assigned.

Description	Symbol	Value
Component value of tensile strength	R_m	240 MPa
Component value of yield strength	R_p	160 MPa
Elongation at break	A	-
Tensile strength factor	$f_{\sigma,tension}$	1.0
Compression strength factor	$f_{\sigma,compression}$	1.0
Shear fatigue strength factor	$f_{W,\tau}$	0.577
Grey cast iron factor	$K_{NL,E}$	1.0
Lower limit of effective damage sum	$D_{m,min}$	0.5
Softening factor	ρ_{WEZ}	0.79
Weld factor, full penetration or back welded, compression	$\alpha_{W,1}$	1.0
Weld factor, full penetration or back welded, tension, verified	$\alpha_{W,2}$	1.0
Weld factor, full penetration or back welded, tension, not verified	$\alpha_{W,3}$	0.75
Weld factor, full penetration or back welded, shear, verified	$\alpha_{W,4}$	0.59

Description	Symbol	Value
Weld factor, full penetration or back welded, shear, not verified	$\alpha_{W,5}$	0.59
Weld factor, partial penetration or fillet weld	$\alpha_{W,6}$	0.67

Temperature Parameters

Description	Symbol	Value
Temperature	T	23.0 °C
Long-term temperature effect		No
Duration of exposure at temperature		1.0 h

S-N Curve Parameters

Description	Symbol	Value
Number of cycles at first knee point of the S-N curve (type I and II)	$N_{D,\sigma}$	5000000
Number of cycles at second knee point of the S-N curve (type II)	$N_{D,II,\sigma}$	-
First exponent of the S-N curve (type I and II)	k_σ	3.0
Second exponent of the S-N curve (type II)	$k_{II,\sigma}$	-
Number of cycles at first knee point of the S-N curve (type I and II)	$N_{D,\tau}$	100000000
Number of cycles at second knee point of the S-N curve (type II)	$N_{D,II,\tau}$	-
First exponent of the S-N curve (type I and II)	k_τ	5.0
Second exponent of the S-N curve (type II)	$k_{II,\tau}$	-

Safety Parameters

Description	Symbol	Value
Consequences of failure		High
Casting quality		Not verified
Regular inspections		No
Load occurs with high probability		Yes
Manual modification of the total static safety factor		0.0
Manual modification of the total fatigue safety factor		0.0
Basic safety factors set to 1.0		No
Load factor	Load factor j_S	1.0

Assessment Results for "Weld Toe 1"

Assessment Results for Node 34,429

Static strength assessment

The degree of static strength utilized is 39 %.

The assessment result details for the critical load combination 2 are listed in the following table.

Description	Symbol	Value
Normal stress, perpendicular	$\sigma_{\perp}$	19.4 MPa
Shear stress, parallel	τ	1.5 MPa
Equivalent stress	σ_{vw}	19.5 MPa
Component value of tensile strength	R_m	240 MPa
Component value of yield strength	R_p	160 MPa
Local strain factor	K_w	1.0
Plastic notch factor	K_p	1.0
Section factor	n_{pl}	1.0
Weld factor	α_W	0.67
Component static strength	$\sigma_{SK,w}$	84.7 MPa
Temperature factor	$K_{T,m}$	1.0
Temperature factor	$K_{T,p}$	1.0
Temperature factor	$K_{T,tm}$	-
Temperature factor	$K_{T,tp}$	-
Basic safety factor for tensile strength	j_m	2.0
Basic safety factor for yield strength	j_p	1.5
Basic safety factor for creep strength	j_{mt}	1.5
Basic safety factor for creep limit	j_{pt}	1.0
Load factor	Load factor j_S	1.0
Total safety factor (static)	j_{ges}	1.695
Degree of utilization for equivalent stress	$a_{SK,w}$	0.39

The following warning messages were recorded for this assessment:

- At least two extrapolation points are in the same element.

Fatigue strength assessment

The degree of fatigue strength utilized is 86.7 %.

The assessment result details for the critical oscillation between load combination 1 and load combination 2 are listed in the following table.

Description	Symbol	Value for $\sigma_{\perp}$	Value for $\sigma_{\parallel}$	Value for τ
Stress amplitude	σ_a	-8.7 MPa	-22.5 MPa	-0.7 MPa
Mean stress	σ_m	10.7 MPa	27.5 MPa	0.8 MPa
FAT class	FAT	90.0	90.0	80.0
FAT conversion factor	f_{FAT}	0.368	0.368	0.229
Plate thickness for thickness correction	t	1.0		
Thickness factor	f_t	1.1		
Component fatigue limit for completely reversed stresses	σ_{WK}	36.5 MPa	36.5 MPa	20.1 MPa
Mean stress factor	K_{AK}	1.0	1.0	1.0
Component fatigue limit	σ_{AK}	36.5 MPa	36.5 MPa	20.1 MPa
Variable amplitude fatigue strength factor	K_{BK}	1.0	1.0	1.0
Component variable amplitude fatigue strength	σ_{BK}	36.5 MPa	36.5 MPa	20.1 MPa
Local strain factor	K_w	1.0		
Plastic notch factor	K_p	1.0		
Section factor	n_{pl}	1.0		
Weld factor	α_W	0.67	0.67	0.67
Maximum value of the component variable amplitude fatigue strength	$\sigma_{BK,max}$	63.5 MPa	63.5 MPa	63.5 MPa
Temperature factor	$K_{T,D}$	1.0		
Basic safety factor	j_F	1.4		
Load factor	Load factor j_S	1.0		
Total safety factor (fatigue)	j_D	1.4		
Cyclic degree of utilization for individual components	a_{BK}	-0.335	-0.863	-0.046
Combined degree of utilization	$a_{BK,\sigma v}$	0.867		

The following warning messages were recorded for this assessment:

- At least two extrapolation points are in the same element.

Assessment Parameters and Results for "Weld connection 6"

This section starts with the input parameters for this weld, followed by the results of the selected weld nodes.

Weld Parameters

Description	Symbol	Value
Weld type		No or partial penetration
Weld quality		Verified
Residual stresses		High
Thickness factor		B
Plastic notch factor definition method		Manual
Plastic notch factor	K_p	1.0
Surface treatment factor	K_V	1.0
FAT class (perpendicular)	$FAT_\perp$	90.0
FAT class (parallel)	$FAT_\parallel$	90.0
FAT class (shear)	FAT_τ	80.0

Material Parameters

The material "AW-5049.H24/H34 (Zusatz SG-AlMg5)" from the group "Wrought aluminum alloy" was assigned.

Description	Symbol	Value
Component value of tensile strength	R_m	240 MPa
Component value of yield strength	R_p	160 MPa
Elongation at break	A	-
Tensile strength factor	$f_{\sigma,tension}$	1.0
Compression strength factor	$f_{\sigma,compression}$	1.0
Shear fatigue strength factor	$f_{W,\tau}$	0.577
Grey cast iron factor	$K_{NL,E}$	1.0
Lower limit of effective damage sum	$D_{m,min}$	0.5
Softening factor	ρ_{WEZ}	0.79
Weld factor, full penetration or back welded, compression	$\alpha_{W,1}$	1.0
Weld factor, full penetration or back welded, tension, verified	$\alpha_{W,2}$	1.0
Weld factor, full penetration or back welded, tension, not verified	$\alpha_{W,3}$	0.75
Weld factor, full penetration or back welded, shear, verified	$\alpha_{W,4}$	0.59

Description	Symbol	Value
Weld factor, full penetration or back welded, shear, not verified	$\alpha_{W,5}$	0.59
Weld factor, partial penetration or fillet weld	$\alpha_{W,6}$	0.67

Temperature Parameters

Description	Symbol	Value
Temperature	T	23.0 °C
Long-term temperature effect		No
Duration of exposure at temperature		1.0 h

S-N Curve Parameters

Description	Symbol	Value
Number of cycles at first knee point of the S-N curve (type I and II)	$N_{D,\sigma}$	5000000
Number of cycles at second knee point of the S-N curve (type II)	$N_{D,II,\sigma}$	-
First exponent of the S-N curve (type I and II)	k_σ	3.0
Second exponent of the S-N curve (type II)	$k_{II,\sigma}$	-
Number of cycles at first knee point of the S-N curve (type I and II)	$N_{D,\tau}$	100000000
Number of cycles at second knee point of the S-N curve (type II)	$N_{D,II,\tau}$	-
First exponent of the S-N curve (type I and II)	k_τ	5.0
Second exponent of the S-N curve (type II)	$k_{II,\tau}$	-

Safety Parameters

Description	Symbol	Value
Consequences of failure		High
Casting quality		Not verified
Regular inspections		No
Load occurs with high probability		Yes
Manual modification of the total static safety factor		0.0
Manual modification of the total fatigue safety factor		0.0
Basic safety factors set to 1.0		No
Load factor	Load factor j_S	1.0

Assessment Results for "Weld Toe 1"

Assessment Results for Node 964

Static strength assessment

The degree of static strength utilized is 43.4 %.

The assessment result details for the critical load combination 2 are listed in the following table.

Description	Symbol	Value
Normal stress, perpendicular	$\sigma_{\perp}$	21.5 MPa
Shear stress, parallel	τ	3 MPa
Equivalent stress	σ_{vw}	21.7 MPa
Component value of tensile strength	R_m	240 MPa
Component value of yield strength	R_p	160 MPa
Local strain factor	K_w	1.0
Plastic notch factor	K_p	1.0
Section factor	n_{pl}	1.0
Weld factor	α_W	0.67
Component static strength	$\sigma_{SK,w}$	84.7 MPa
Temperature factor	$K_{T,m}$	1.0
Temperature factor	$K_{T,p}$	1.0
Temperature factor	$K_{T,tm}$	-
Temperature factor	$K_{T,tp}$	-
Basic safety factor for tensile strength	j_m	2.0
Basic safety factor for yield strength	j_p	1.5
Basic safety factor for creep strength	j_{mt}	1.5
Basic safety factor for creep limit	j_{pt}	1.0
Load factor	Load factor j_S	1.0
Total safety factor (static)	j_{ges}	1.695
Degree of utilization for equivalent stress	$a_{SK,w}$	0.434

The following warning messages were recorded for this assessment:

- At least two extrapolation points are in the same element.

Fatigue strength assessment

The degree of fatigue strength utilized is 90.7 %.

The assessment result details for the critical oscillation between load combination 1 and load combination 2 are listed in the following table.

Description	Symbol	Value for $\sigma_{\perp}$	Value for $\sigma_{\parallel}$	Value for τ
Stress amplitude	σ_a	-9.7 MPa	-23.2 MPa	-1.3 MPa
Mean stress	σ_m	11.8 MPa	28.4 MPa	1.6 MPa
FAT class	FAT	90.0	90.0	80.0
FAT conversion factor	f_{FAT}	0.368	0.368	0.229
Plate thickness for thickness correction	t	1.0		
Thickness factor	f_t	1.1		
Component fatigue limit for completely reversed stresses	σ_{WK}	36.5 MPa	36.5 MPa	20.1 MPa
Mean stress factor	K_{AK}	1.0	1.0	1.0
Component fatigue limit	σ_{AK}	36.5 MPa	36.5 MPa	20.1 MPa
Variable amplitude fatigue strength factor	K_{BK}	1.0	1.0	1.0
Component variable amplitude fatigue strength	σ_{BK}	36.5 MPa	36.5 MPa	20.1 MPa
Local strain factor	K_w	1.0		
Plastic notch factor	K_p	1.0		
Section factor	n_{pl}	1.0		
Weld factor	α_W	0.67	0.67	0.67
Maximum value of the component variable amplitude fatigue strength	$\sigma_{BK,max}$	63.5 MPa	63.5 MPa	63.5 MPa
Temperature factor	$K_{T,D}$	1.0		
Basic safety factor	j_F	1.4		
Load factor	Load factor j_S	1.0		
Total safety factor (fatigue)	j_D	1.4		
Cyclic degree of utilization for individual components	a_{BK}	-0.371	-0.891	-0.093
Combined degree of utilization	$a_{BK,\sigma v}$	0.907		

The following warning messages were recorded for this assessment:

- At least two extrapolation points are in the same element.

Assessment Parameters and Results for "Weld connection 7"

This section starts with the input parameters for this weld, followed by the results of the selected weld nodes.

Weld Parameters

Description	Symbol	Value
Weld type		No or partial penetration
Weld quality		Verified
Residual stresses		High
Thickness factor		B
Plastic notch factor definition method		Manual
Plastic notch factor	K_p	1.0
Surface treatment factor	K_V	1.0
FAT class (perpendicular)	$FAT_\perp$	90.0
FAT class (parallel)	$FAT_\parallel$	90.0
FAT class (shear)	FAT_τ	80.0

Material Parameters

The material "AW-5049.H24/H34 (Zusatz SG-AlMg5)" from the group "Wrought aluminum alloy" was assigned.

Description	Symbol	Value
Component value of tensile strength	R_m	240 MPa
Component value of yield strength	R_p	160 MPa
Elongation at break	A	-
Tensile strength factor	$f_{\sigma,tension}$	1.0
Compression strength factor	$f_{\sigma,compression}$	1.0
Shear fatigue strength factor	$f_{W,\tau}$	0.577
Grey cast iron factor	$K_{NL,E}$	1.0
Lower limit of effective damage sum	$D_{m,min}$	0.5
Softening factor	ρ_{WEZ}	0.79
Weld factor, full penetration or back welded, compression	$\alpha_{W,1}$	1.0
Weld factor, full penetration or back welded, tension, verified	$\alpha_{W,2}$	1.0
Weld factor, full penetration or back welded, tension, not verified	$\alpha_{W,3}$	0.75
Weld factor, full penetration or back welded, shear, verified	$\alpha_{W,4}$	0.59

Description	Symbol	Value
Weld factor, full penetration or back welded, shear, not verified	$\alpha_{W,5}$	0.59
Weld factor, partial penetration or fillet weld	$\alpha_{W,6}$	0.67

Temperature Parameters

Description	Symbol	Value
Temperature	T	23.0 °C
Long-term temperature effect		No
Duration of exposure at temperature		1.0 h

S-N Curve Parameters

Description	Symbol	Value
Number of cycles at first knee point of the S-N curve (type I and II)	$N_{D,\sigma}$	5000000
Number of cycles at second knee point of the S-N curve (type II)	$N_{D,II,\sigma}$	-
First exponent of the S-N curve (type I and II)	k_{σ}	3.0
Second exponent of the S-N curve (type II)	$k_{II,\sigma}$	-
Number of cycles at first knee point of the S-N curve (type I and II)	$N_{D,\tau}$	100000000
Number of cycles at second knee point of the S-N curve (type II)	$N_{D,II,\tau}$	-
First exponent of the S-N curve (type I and II)	k_{τ}	5.0
Second exponent of the S-N curve (type II)	$k_{II,\tau}$	-

Safety Parameters

Description	Symbol	Value
Consequences of failure		High
Casting quality		Not verified
Regular inspections		No
Load occurs with high probability		Yes
Manual modification of the total static safety factor		0.0
Manual modification of the total fatigue safety factor		0.0
Basic safety factors set to 1.0		No
Load factor	Load factor j_S	1.0

Assessment Results for "Weld Toe 1"

Assessment Results for Node 7,222

Static strength assessment

The degree of static strength utilized is 38.9 %.

The assessment result details for the critical load combination 2 are listed in the following table.

Description	Symbol	Value
Normal stress, perpendicular	$\sigma_{\perp}$	19.4 MPa
Shear stress, parallel	τ	1.5 MPa
Equivalent stress	σ_{vw}	19.4 MPa
Component value of tensile strength	R_m	240 MPa
Component value of yield strength	R_p	160 MPa
Local strain factor	K_w	1.0
Plastic notch factor	K_p	1.0
Section factor	n_{pl}	1.0
Weld factor	α_W	0.67
Component static strength	$\sigma_{SK,w}$	84.7 MPa
Temperature factor	$K_{T,m}$	1.0
Temperature factor	$K_{T,p}$	1.0
Temperature factor	$K_{T,tm}$	-
Temperature factor	$K_{T,tp}$	-
Basic safety factor for tensile strength	j_m	2.0
Basic safety factor for yield strength	j_p	1.5
Basic safety factor for creep strength	j_{mt}	1.5
Basic safety factor for creep limit	j_{pt}	1.0
Load factor	Load factor j_S	1.0
Total safety factor (static)	j_{ges}	1.695
Degree of utilization for equivalent stress	$a_{SK,w}$	0.389

The following warning messages were recorded for this assessment:

- At least two extrapolation points are in the same element.

Fatigue strength assessment

The degree of fatigue strength utilized is 86.5 %.

The assessment result details for the critical oscillation between load combination 1 and load combination 2 are listed in the following table.

Description	Symbol	Value for $\sigma_{\perp}$	Value for $\sigma_{\parallel}$	Value for τ
Stress amplitude	σ_a	-8.7 MPa	-22.4 MPa	-0.7 MPa
Mean stress	σ_m	10.7 MPa	27.4 MPa	0.8 MPa
FAT class	FAT	90.0	90.0	80.0
FAT conversion factor	f_{FAT}	0.368	0.368	0.229
Plate thickness for thickness correction	t	1.0		
Thickness factor	f_t	1.1		
Component fatigue limit for completely reversed stresses	σ_{WK}	36.5 MPa	36.5 MPa	20.1 MPa
Mean stress factor	K_{AK}	1.0	1.0	1.0
Component fatigue limit	σ_{AK}	36.5 MPa	36.5 MPa	20.1 MPa
Variable amplitude fatigue strength factor	K_{BK}	1.0	1.0	1.0
Component variable amplitude fatigue strength	σ_{BK}	36.5 MPa	36.5 MPa	20.1 MPa
Local strain factor	K_w	1.0		
Plastic notch factor	K_p	1.0		
Section factor	n_{pl}	1.0		
Weld factor	α_W	0.67	0.67	0.67
Maximum value of the component variable amplitude fatigue strength	$\sigma_{BK,max}$	63.5 MPa	63.5 MPa	63.5 MPa
Temperature factor	$K_{T,D}$	1.0		
Basic safety factor	j_F	1.4		
Load factor	Load factor j_S	1.0		
Total safety factor (fatigue)	j_D	1.4		
Cyclic degree of utilization for individual components	a_{BK}	-0.335	-0.861	-0.047
Combined degree of utilization	$a_{BK,\sigma v}$	0.865		

The following warning messages were recorded for this assessment:

- At least two extrapolation points are in the same element.

Assessment Parameters and Results for "Weld connection 8"

This section starts with the input parameters for this weld, followed by the results of the selected weld nodes.

Weld Parameters

Description	Symbol	Value
Weld type		No or partial penetration
Weld quality		Verified
Residual stresses		High
Thickness factor		B
Plastic notch factor definition method		Manual
Plastic notch factor	K_p	1.0
Surface treatment factor	K_V	1.0
FAT class (perpendicular)	$FAT_\perp$	90.0
FAT class (parallel)	$FAT_\parallel$	90.0
FAT class (shear)	FAT_τ	80.0

Material Parameters

The material "AW-5049.H24/H34 (Zusatz SG-AlMg5)" from the group "Wrought aluminum alloy" was assigned.

Description	Symbol	Value
Component value of tensile strength	R_m	240 MPa
Component value of yield strength	R_p	160 MPa
Elongation at break	A	-
Tensile strength factor	$f_{\sigma,tension}$	1.0
Compression strength factor	$f_{\sigma,compression}$	1.0
Shear fatigue strength factor	$f_{W,\tau}$	0.577
Grey cast iron factor	$K_{NL,E}$	1.0
Lower limit of effective damage sum	$D_{m,min}$	0.5
Softening factor	ρ_{WEZ}	0.79
Weld factor, full penetration or back welded, compression	$\alpha_{W,1}$	1.0
Weld factor, full penetration or back welded, tension, verified	$\alpha_{W,2}$	1.0
Weld factor, full penetration or back welded, tension, not verified	$\alpha_{W,3}$	0.75
Weld factor, full penetration or back welded, shear, verified	$\alpha_{W,4}$	0.59

Description	Symbol	Value
Weld factor, full penetration or back welded, shear, not verified	$\alpha_{W,5}$	0.59
Weld factor, partial penetration or fillet weld	$\alpha_{W,6}$	0.67

Temperature Parameters

Description	Symbol	Value
Temperature	T	23.0 °C
Long-term temperature effect		No
Duration of exposure at temperature		1.0 h

S-N Curve Parameters

Description	Symbol	Value
Number of cycles at first knee point of the S-N curve (type I and II)	$N_{D,\sigma}$	5000000
Number of cycles at second knee point of the S-N curve (type II)	$N_{D,II,\sigma}$	-
First exponent of the S-N curve (type I and II)	k_σ	3.0
Second exponent of the S-N curve (type II)	$k_{II,\sigma}$	-
Number of cycles at first knee point of the S-N curve (type I and II)	$N_{D,\tau}$	100000000
Number of cycles at second knee point of the S-N curve (type II)	$N_{D,II,\tau}$	-
First exponent of the S-N curve (type I and II)	k_τ	5.0
Second exponent of the S-N curve (type II)	$k_{II,\tau}$	-

Safety Parameters

Description	Symbol	Value
Consequences of failure		High
Casting quality		Not verified
Regular inspections		No
Load occurs with high probability		Yes
Manual modification of the total static safety factor		0.0
Manual modification of the total fatigue safety factor		0.0
Basic safety factors set to 1.0		No
Load factor	Load factor j_S	1.0

Assessment Results for "Weld Toe 1"

Assessment Results for Node 27,931

Static strength assessment

The degree of static strength utilized is 43.9 %.

The assessment result details for the critical load combination 2 are listed in the following table.

Description	Symbol	Value
Normal stress, perpendicular	$\sigma_{\perp}$	21.7 MPa
Shear stress, parallel	τ	3 MPa
Equivalent stress	σ_{vw}	21.9 MPa
Component value of tensile strength	R_m	240 MPa
Component value of yield strength	R_p	160 MPa
Local strain factor	K_w	1.0
Plastic notch factor	K_p	1.0
Section factor	n_{pl}	1.0
Weld factor	α_W	0.67
Component static strength	$\sigma_{SK,w}$	84.7 MPa
Temperature factor	$K_{T,m}$	1.0
Temperature factor	$K_{T,p}$	1.0
Temperature factor	$K_{T,tm}$	-
Temperature factor	$K_{T,tp}$	-
Basic safety factor for tensile strength	j_m	2.0
Basic safety factor for yield strength	j_p	1.5
Basic safety factor for creep strength	j_{mt}	1.5
Basic safety factor for creep limit	j_{pt}	1.0
Load factor	Load factor j_S	1.0
Total safety factor (static)	j_{ges}	1.695
Degree of utilization for equivalent stress	$a_{SK,w}$	0.439

The following warning messages were recorded for this assessment:

- At least two extrapolation points are in the same element.

Fatigue strength assessment

The degree of fatigue strength utilized is 91.9 %. The assessment result details for the critical oscillation between load combination 1 and load combination 2 are listed in the following table.

Description	Symbol	Value for $\sigma_{\perp}$	Value for $\sigma_{\parallel}$	Value for τ
Stress amplitude	σ_a	-9.8 MPa	-23.5 MPa	-1.4 MPa
Mean stress	σ_m	11.9 MPa	28.7 MPa	1.7 MPa
FAT class	FAT	90.0	90.0	80.0
FAT conversion factor	f_{FAT}	0.368	0.368	0.229
Plate thickness for thickness correction	t	1.0		
Thickness factor	f_t	1.1		
Component fatigue limit for completely reversed stresses	σ_{WK}	36.5 MPa	36.5 MPa	20.1 MPa
Mean stress factor	K_{AK}	1.0	1.0	1.0
Component fatigue limit	σ_{AK}	36.5 MPa	36.5 MPa	20.1 MPa
Variable amplitude fatigue strength factor	K_{BK}	1.0	1.0	1.0
Component variable amplitude fatigue strength	σ_{BK}	36.5 MPa	36.5 MPa	20.1 MPa
Local strain factor	K_w	1.0		
Plastic notch factor	K_p	1.0		
Section factor	n_{pl}	1.0		
Weld factor	α_W	0.67	0.67	0.67
Maximum value of the component variable amplitude fatigue strength	$\sigma_{BK,max}$	63.5 MPa	63.5 MPa	63.5 MPa
Temperature factor	$K_{T,D}$	1.0		
Basic safety factor	j_F	1.4		
Load factor	Load factor j_S	1.0		
Total safety factor (fatigue)	j_D	1.4		
Cyclic degree of utilization for individual components	a_{BK}	-0.375	-0.902	-0.095
Combined degree of utilization	$a_{BK,\sigma v}$	0.919		

The following warning messages were recorded for this assessment:

- At least two extrapolation points are in the same element.

Образац 5.

Изјава о ауторству

Име и презиме аутора Абулгасим Муса Саид Сгајер

Број индекса D40/2013

Изјављујем

да је докторска дисертација под насловом

ПРОЦЕНА ЗАМОРНОГ ВЕКА ОШТЕЋЕНИХ ИНТЕГРАЛНИХ ОПЛАТА-УЗДУЖНИЦИ ПАНЕЛА

(FATIGUE LIFE ASSESSMENT OF DAMAGED INTEGRAL SKIN –STRINGER PANELS)

- резултат сопственог истраживачког рада;
- да дисертација у целини ни у деловима није била предложена за стицање друге дипломе према студијским програмима других високошколских установа;
- да су резултати коректно наведени и
- да нисам кршио/ла ауторска права и користио/ла интелектуалну својину других лица.

Потпис аутора

У Београду, 01.05.2018.

Образац 6.

Изјава о истоветности штампане и електронске верзије докторског рада

Име и презиме аутора Абулгасим Муса Саид Сгајер

Број индекса D40/2013

Студијски програм докторске студије

Наслов рада ПРОЦЕНА ЗАМОРНОГ ВЕКА ОШТЕЋЕНИХ ИНТЕГРАЛНИХ ОПЛАТА-УЗДУЖНИЦИ ПАНЕЛА (FATIGUE LIFE ASSESSMENT OF DAMAGED INTEGRAL SKIN – STRINGER PANELS)

Ментор Проф. др Александар Грбовић

Изјављујем да је штампана верзија мог докторског рада истоветна електронској верзији коју сам предао/ла ради похрањена у **Дигиталном репозиторијуму Универзитета у Београду.**

Дозвољавам да се објаве моји лични подаци везани за добијање академског назива доктора наука, као што су име и презиме, година и место рођења и датум одбране рада.

Ови лични подаци могу се објавити на мрежним страницама дигиталне библиотеке, у електронском каталогу и у публикацијама Универзитета у Београду.

Потпис аутора

У Београду, 01.05.2018.

Образац 7.

Изјава о коришћењу

Овлашћујем Универзитетску библиотеку „Светозар Марковић“ да у Дигитални репозиторијум Универзитета у Београду унесе моју докторску дисертацију под насловом:

ПРОЦЕНА ЗАМОРНОГ ВЕКА ОШТЕЋЕНИХ ИНТЕГРАЛНИХ ОПЛАТА-УЗДУЖНИЦИ ПАНЕЛА

(FATIGUE LIFE ASSESSMENT OF DAMAGED INTEGRAL SKIN –STRINGER PANELS)

која је моје ауторско дело.

Дисертацију са свим прилозима предао/ла сам у електронском формату погодном за трајно архивирање.

Моју докторску дисертацију похрањену у Дигиталном репозиторијуму Универзитета у Београду и доступну у отвореном приступу могу да користе сви који поштују одредбе садржане у одабраном типу лиценце Креативне заједнице (Creative Commons) за коју сам се одлучио/ла.

1. Ауторство (CC BY)

2. Ауторство – некомерцијално (CC BY-NC)

3. Ауторство – некомерцијално – без прерада (CC BY-NC-ND)

4. Ауторство – некомерцијално – делити под истим условима (CC BY-NC-SA)

5. Ауторство – без прерада (CC BY-ND)

6. Ауторство – делити под истим условима (CC BY-SA)

(Молимо да заокружите само једну од шест понуђених лиценци.
Кратак опис лиценци је саставни део ове изјаве).

Потпис аутора

У Београду, 01.05.2018.

1. **Ауторство**. Дозвољавате умножавање, дистрибуцију и јавно саопштавање дела, и прераде, ако се наведе име аутора на начин одређен од стране аутора или даваоца лиценце, чак и у комерцијалне сврхе. Ово је најслободнија од свих лиценци.

2. **Ауторство – некомерцијално**. Дозвољавате умножавање, дистрибуцију и јавно саопштавање дела, и прераде, ако се наведе име аутора на начин одређен од стране аутора или даваоца лиценце. Ова лиценца не дозвољава комерцијалну употребу дела.

3. **Ауторство – некомерцијално – без прерада**. Дозвољавате умножавање, дистрибуцију и јавно саопштавање дела, без промена, преобликовања или употребе дела у свом делу, ако се наведе име аутора на начин одређен од стране аутора или даваоца лиценце. Ова лиценца не дозвољава комерцијалну употребу дела. У односу на све остале лиценце, овом лиценцом се ограничава највећи обим права коришћења дела.

4. **Ауторство – некомерцијално – делити под истим условима**. Дозвољавате умножавање, дистрибуцију и јавно саопштавање дела, и прераде, ако се наведе име аутора на начин одређен од стране аутора или даваоца лиценце и ако се прерада дистрибуира под истом или сличном лиценцом. Ова лиценца не дозвољава комерцијалну употребу дела и прерада.

5. **Ауторство – без прерада**. Дозвољавате умножавање, дистрибуцију и јавно саопштавање дела, без промена, преобликовања или употребе дела у свом делу, ако се наведе име аутора на начин одређен од стране аутора или даваоца лиценце. Ова лиценца дозвољава комерцијалну употребу дела.

6. **Ауторство – делити под истим условима**. Дозвољавате умножавање, дистрибуцију и јавно саопштавање дела, и прераде, ако се наведе име аутора на начин одређен од стране аутора или даваоца лиценце и ако се прерада дистрибуира под истом или сличном лиценцом. Ова лиценца дозвољава комерцијалну употребу дела и прерада. Слична је софтверским лиценцама, односно лиценцама отвореног кода.